6300Å (OI) AIRGLOW AT HIGHER MIDLATITUDES DURING SOLAR MAXIMUM

by: D. G. Nichol

A thesis submitted in fulfilment of the requirements for the degree of Doctor of Philosophy in the University of Tasmania

Hobart
February, 1971

TABLE OF CONTENTS

Chapter 1: INTRODUCTION

This thesis describes work carried out at Hobart (42.9^{o}S, 147.3^{o}E) during the 1968 - 1970 solar/auroral maximum on the airglow emissions of atomic oxygen particularly the red 6300Å line. (This 'line' is actually a doublet : see chapter two). Both the red and the green 5577Å lines originate from forbidden transitions of OI; these are the ($^{3}P - {}^{1}D$) and the ($^{1}D - {}^{1}S$) transitions respectively. Until recently the green line was much more studied than the 6300Å line, partly because it is usually stronger in the normal night airglow and also because photo-electron detectors are more sensitive in its spectral range. It is really only during the last fifteen years or so that adequately red sensitive detectors have become available to study the weak night airglow. Thus although these OI lines have been known to exist in auroras for over a century (Angstrom 1868, Zollner 1870) the recent solar maximum is only the second available for detailed study of the weak red night emissions. The previous maximum of 1957 - 1959 proved very fruitful for airglow/auroral studies so it was hoped that the recent maximum would be the same. However this maximum was considerably weaker

and few opportunities were available to study such novel auroral features as the 'mantel aurora' (Sandford 1964) or the Stable Auroral Red Arc (SAR-arc) (Barbier 1959, Cole 1965a) both originally detected during the previous maximum. Furthermore the normal night airglow appeared to be less intense by a factor of five during the 1968 - 1970 maximum than during the previous one. This is rather puzzling and would not be expected in terms of the solar flux or ionospheric content differences. Possible explanations are examined in various chapters of this thesis.

From the Table of Contents it can be seen that because of the absence of much auroral activity this study has been confined to the quiet airglow behaviour and particularly the regular red airglow enhancements. The first of these was found to occur in summer near local midnight; it was only small but very regular and had not been detected before at such high latitudes. The second enhancement studied is one which has been widely examined recently; the pre-dawn enhancement of 6300Å airglow. This is of interest particularly because of its probable association with magnetic conjugate point photo-electron emissions (Cole 1965b). One aspect which has aroused controversy

is a possible latitude cut-off in this line. Hobart is well situated for a study of this effect.

Also because of Hobart's situation it is well placed for a study of airglow intensity inside the mid-latitude ionospheric trough (Muldrew 1965). This unusual feature is a quasi-permanent field aligned depletion of the F-region which is up to 15^{o} in latitude wide and centred near 60^{o} invarient geomagnetic latitude. It has only been recognised as a distinctive phenomenon since the introduction of topside ionospheric sounders such as Alouette. Its origin is unknown but it was hoped that airglow observations would give information on its formation.

Below is given a brief abstract of the thesis contents. For convenience the observations have been split into seasonal groups and a theoretical discussion of these ob servations has been separated from the observations themselves. This is basically because some of the theoretical discussion overlaps different groups of data.

Except where acknowledged in the text and in the final acknowledgments all the work discussed herein has been carried out by the author. Some of the material has been already published in the

following papers, copies of which are to be found inside the back cover of the thesis.

(D. G. Nichol, February, 1971).

1. D. G. Nichol, 'A Summertime Midnight Enhancement of 6300Å Airglow', Aust. J. Phys. 23: 109, 1970
2. D. G. Nichol, 'The Pre-dawn Enhancement of 6300Å Airglow at Higher Midlatitudes', Planet Space Sci., 18: 1335, 1970
3. D. G. Nichol, 'The Excitation of 6300Å Airglow by Soft Electron Fluxes', Nature, (Phys. Sci.,), January, 1971.
4. D. G. Nichol, '6300Å OI Airglow in the Midlatitude Ionospheric Trough', submitted to Planetary and Space Science, 1971.

Thesis Outline

Chapter One: Introduction:

Chapter Two: The Production of OI Airglow:

This describes the major mechanisms for exciting the OI lines. These include dissociative recombination, soft electron excitation and thermal excitation.

Chapter Three: Experimental Technique:

The electronic, optical and mechanical equipment designed and built for this experiment is described.

Chapter Four: Data Analysis:

This includes the methods of calibration; correction of systematic and random errors; and estimates of the accuracy of the measurements.

Chapter Five: The Midlatitude Ionospheric Trough (I):

This discusses the current knowledge of the trough and describes the airglow observations in the trough. Basically the 6300Å airglow seems to be enhanced inside the trough.

Chapter Six: The Midlatitude Ionospheric Trough (II):

The airglow observations of the previous chapter are discussed. A mechanism is proposed to explain both the airglow levels inside the trough and the existence of the trough itself.

Chapter Seven: 6300Å Airglow - Summer observations:

The midnight summer enhancement is described and it is found to be caused by increased dissociative recombination due to a fall in the F-region.

Chapter Eight: 6300Å Airglow - Winter observations:

It is shown that the pre-dawn enhancement is more complex than previously imagined. Dissociative recombination and conjugate point electrons both seem to play a part.

Chapter Nine: Photo-electrons, Neutral Winds and the 6300Å Airglow:

Both the summer and winter observations of airglow enhancements can be partly explained by neutral winds in the upper atmosphere. These cause regular rises and falls in the F-region. In the winter and the equinoxes the effect of conjugate fluxes is also important.

Chapter Ten: Concluding Remarks:

Chapter 2 PRODUCTION OF OI AIRGLOW

2.1 Introduction

The green 5577Å airglow arises from the $(^1D - ^1S)$ transition of atomic oxygen O I and the red doublet, (usually referred to as a 'line') 6300Å and 6364Å air - glow, from the $(^3P - ^1D)$ transition. As the vast majority of O I atoms in the earth's atmosphere are in the ground (^3P) state the basic problem of airglow physics is to deduce how the observed excitations to $O(^1S)$ and $O(^1D)$ occur. Fig. 2.1 shows the low energy end of the O I energy scheme. Also shown are the Einstein transition coefficients A_λ (Garstang 1951) for each line of wavelength λ .

To excite the $O(^1S)$ state 4.19 eV of energy is needed and the $(^1D - ^1S)$ transition is the only one of significance for this state. The lifetime of this state is 0.74 seconds which is two orders of magnitude lower than that of the $O(^1D)$ state. This and the fact that the $O(^1D)$ state requires only 1.97 eV of energy to excite it leads to a totally different behaviour of the red and green airglow. The red airglow only occurs above about 200 km because the long lifetime $O(^1D)$ state is easily deactivated by molecular collisions. However, at this height the green line is weak; basically because of its higher excitation potential. Below 200 km the green-line is strong but arises from quite different mechanisms to

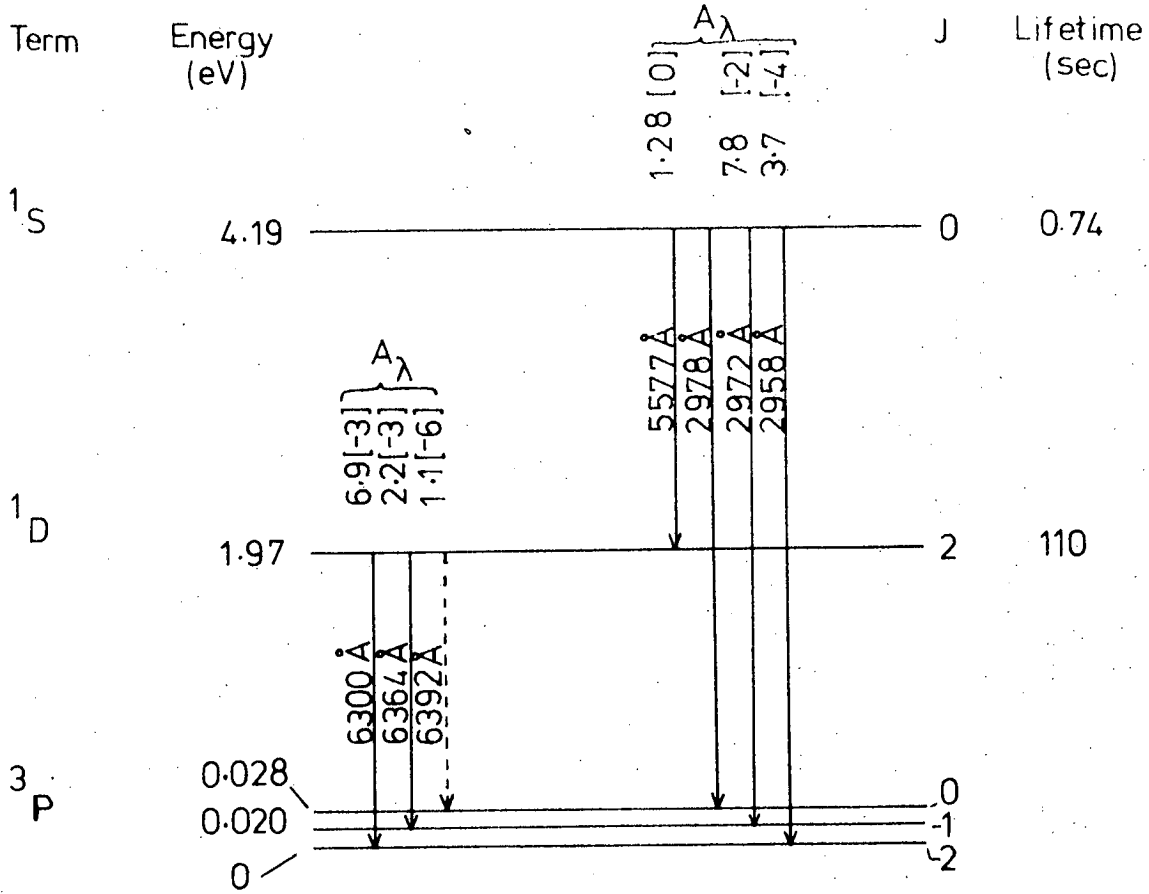

Fig. 2.1 Low energy end of OI energy scheme

those causing O I airglow at greater heights. Because this thesis is essentially concerned with the F-region these E-region processes will not be examined here.

The major processes causing O I airglow at F-region heights are : dissociative recombination of O_2^+ ions; production of ^1D and ^1S atoms by thermal collisions and their direct excitation by non-ionospheric precipitating electrons. A number of other mechanisms such as resonance scattering and ultraviolet dissociation are important in the dayglow (Dalgarno and Walker 1964) and twilight airglow (Chamberlain 1960 ; Deehr 1969 a) but will not be discussed here.

2.2.1 Dissociative recombination

The treatment used here is essentially that of Peterson, Vanzandt and Norton (1966) with only minor exceptions. These include that of assuming $O(^1D)$ and $O(^1S)$ arise from O_2^+ recombination only and not from NO^+; as well emphasis is placed on determining the emission rate of 6300Å and 5577Å photons as a function of molecular and electron height profiles, either as measured or derived from atmospheric models, rather than using approximate analytic expressions for these profiles; also it is assumed that N_2 is the deactivating species; and finally more recent rate coefficients and their temperature dependences are used where applicable.

Now if the concentration of the i th state is $[i]$ and A_λ is the transition coefficient for the $i \rightarrow j$ transition which yields a photon of wavelength λ then the number of photons emitted per unit volume . unit time is:

$$E_\lambda = A_\lambda [i] \qquad 2.1$$

The continuity equation for the i th state is:

$$\frac{\partial [i]}{\partial t}(h) = P_i(h) - L_i(h) - \text{div}([i]\,\underline{v}_i) \qquad 2.2$$

where $P_i(h)$, $L_i(h)$ are the rates of production and loss respectively (cm^{-3} sec^{-1}) of the i th state at height h; $\underline{v}_i$ is the velocity of atoms in state i.

Now ground observations of airglow measure the height integrated emission rate Q of a vertical column of unit area. The unit involved (see next chapter) is the rayleigh which is equivalent to 10^6 photons cm^{-2} (column) sec^{-1}. Thus

$$Q(\lambda) = 10^{-6} \int_0^\infty E(h)\, dh$$
$$= 10^{-6} A_\lambda \int_0^\infty [i]\, dh \qquad 2.3$$

Thus to obtain a theoretical estimate of the amount of photon emission from the i th state it is necessary to obtain the height - profile of the population of that state i.e. the continuity equation 2.2 must be solved for the $O(^1D)$ and $O(^1S)$ populations.

2.2.2 Loss terms

Because of its short lifetime the only significant loss mechanism for the $O(^1S)$ population are the $(^1D - {}^1S)$ and $(^3P - {}^1S)$ transitions. Thus:

$$L_s = A_s [{}^1S] \qquad 2.4$$

Now the $O(^1D)$ state can be deactivated by collisions. The actual mechanism involved is uncertain (Seaton 1958, DeMore and Raper 1964) but there is little doubt that the deactivating species are O_2 and /or N_2 ; with N_2 the currently accepted choice (Noxon 1970). Peterson et al. 1966 define d_D as the deactivating coefficient such that $d_D [{}^1D]$ is the loss rate per unit volume due to collisional deactivation. If the deactivating species is N_2 then a specific deactivation coefficient S_D may be defined such that $d_D = S_D [N_2]$. Then:

$$L_D = (A_D + d_D) [{}^1D] \qquad 2.5$$

2.2.3 Production terms

At E and F region heights the only significant recombination is by:

α_1 : $O_2^+ + e \rightarrow O + O + 6.96$ eV 2.6

α_2 : $NO^+ + e \rightarrow N + O + 2.76$ eV 2.7

where the α's are the rate coefficients. $O(^1D)$ excitations may arise from 2.6 only because of spin conservation (Dalgarno and Walker 1964). 2.6 is also energetically capable of exciting the $O(^1S)$ state.

If the number of excitations of ^1D atoms per recombination of O_2^+ is k_D and the number of ^1S excitations is k_S where,

$$0 \leq k_S \leq 1$$

$$0 \leq k_D \leq k_D + k_S \leq 2 \quad ,$$

then the production rate of $O(^1S)$ is:

$$P_S = k_S \alpha_1 \left[O_2^+ \right] n \qquad 2.8$$

where n is the electron density, and the production rate of $O(^1D)$ is:

$$P_D = k_D \alpha_1 \left[O_2^+ \right] n + A_{5577} \left[^1S \right] \qquad 2.9$$

The second term in 2.9 arises because of cascading from the $(^1D - ^1S)$ transition.

Now Peterson et al (1966) shows that the time - derivative and divergence terms of (2.2) may be ignored for F-region heights i.e. 2.2 reduces to:

$$P_i(h) = L_i(h) \qquad 2.10$$

Using 2.4, 2.5, 2.8, 2.9 and 2.10 yields:

$$\left[^1S \right] = \frac{k_S}{A_S} \alpha_1 \left[O_2^+ \right] n \qquad 2.11$$

$$\left[^1D \right] = \left(k_D + \frac{A_{5577}}{A_S} k_S \right) \frac{\alpha_1 \left[O_2^+ \right] n}{A_D + d_D}$$

i.e. $$\left[^1D \right] = \alpha_1 K'_D \frac{\left[O_2^+ \right] n}{A_D + d_D} \qquad 2.12$$

where $$K'_D = k_D + \frac{A_{5577}}{A_S} K_S$$

2.2.4 Ion concentrations

To eliminate the ion concentration terms from 2.11 and 2.12 the continuity equations for O_2^+ and NO^+ must be solved. The molecular ions mainly originate from;

$$\gamma_1 : O^+ + O_2 \rightarrow O_2^+ + O + 1.53 \text{ eV} \qquad 2.13$$

$$\gamma_2 : O^+ + N_2 \rightarrow NO^+ + N + 1.09 \text{ eV} \qquad 2.14$$

(the γs are the rate coefficients) O^+ being the dominant ion at F-region heights. The continuity equations are therefore from 2.6, 2.7, 2.13 and 2.14.

$$\frac{\partial [O_2^+]}{\partial t} = \gamma_1 [O_2][O^+] - \alpha_1 n [O_2^+] - \text{div}\,[O_2^+]\,\underline{v}\,(O_2^+) \qquad 2.15$$

$$\frac{\partial [NO^+]}{\partial t} = \gamma_2 [N_2][O^+] - \alpha_2 n [NO^+] - \text{div}\,[NO^+]\,\underline{v}\,(NO^+) \qquad 2.16$$

As before the time derivative and divergence terms may be ignored then equations 2.15 and 2.16 together with the charge conservation equation,

$$n = [O^+] + [O_2^+] + [NO^+] \qquad 2.17$$

give:

$$[O_2^+] = \frac{\gamma_1}{\alpha_1}[O_2] \frac{1}{1 + \frac{\gamma_1 [O_2]}{\alpha_1 n} + \frac{\gamma_2 [N_2]}{\alpha_2 n}} \qquad 2.18$$

and

$$[NO^+] = \frac{\gamma_2}{\alpha_2}[N_2] \frac{1}{1 + \frac{\gamma_1 [O_2]}{\alpha_1 n} + \frac{\gamma_2 [N_2]}{\alpha_2 n}} \qquad 2.19$$

Substituting these expressions in 2.11 and 2.12 yields

$$\left[{}^1S\right] = \frac{k_S}{A_S} \frac{\left[O_2\right]_n}{1 + \frac{\gamma_1[O_2]}{\alpha_1 n}\left(1 + \frac{\gamma_2[N_2]}{\gamma_1[O_2]}\frac{\alpha_1}{\alpha_2}\right)} \qquad 2.20$$

$$\left[{}^1D\right] = \frac{k_D}{A_D} \frac{\left[O_2\right]_n}{1 + \frac{\gamma_1[O_2]}{\alpha_1 n}\left(1 + \frac{\gamma_2[N_2]}{\gamma_1[O_2]}\frac{\alpha_1}{\alpha_2}\right)} \frac{1}{1 + \frac{d_D}{A_D}} \qquad 2.21$$

Now the values of A_S, A_D, k_S, k_D are known & the γ's and α's are dependent only on temperature $\left(\propto T^{-\frac{1}{2}}\right)$.

For a discussion of d_D see Wallace and Chamberlain (1965); Dalgarno and Walker (1964); Zipf (1965); Wallace and McElroy (1966), Peterson and Van Zandt (1968) and Noxon 1970. Equation 2.20 and 2.21 may then be solved if:

(a) The electron profile is known. This can be obtained from ionograms or else an appropriate model may be used.

(b) The N_2 and O_2 height profiles are known, several suitable model atmospheres are available (e.g. Jacchia 1965, CIRA 1965).

2.2.5 Other 6300Å formulae

Since the original ideas of Bates (1946) on the dissociative recombination theory of 6300Å airglow, several attempts have been made to derive formulae for 6300Å airglow intensity in terms of ionospheric parameters such as virtual height h'f and the F-region peak

critical frequency foF2 (Barbier 1959; Barbier and Glaume 1962, Kamiyama 1962). Peterson (1968) has shown how these semi-empirical 'Barbier formulae' may be derived from the recombination theory of Peterson et al (1966) outlined in the previous section. These formulae are of the form:

$$Q_{63} = B\ (foF2)^2 \exp - \frac{h'f - 200}{H_{32}} \qquad 2.22$$

The parameter h'f and foF2 are easily read from ionograms but the 'constants' B and H_{32} must be evaluated on each night. H_{32} is in fact the scale height of O_2 given in diffusive equilibrium by:

$$H_{32} = \frac{k\ T}{M_{32}\ g}\ 10^{-5}\ (km) \qquad 2.23$$

where T is the neutral temperature of the emitting region and M_{32} is the mass of the O_2 molecule. The temperature T can be obtained from the various ionospheric models although both B and H_{32} are usually obtained by a process of maximising the correlation coefficient between the calculated intensity Q_{63} and the measured intensity I(6300) (Barbier et al.1962). Formulae of the type 2.22 have proved fairly accurate in computing changes in the red airglow intensity but less well in computing <u>total</u> intensities (Peterson and Steiger 1966; Carmen and Kilfoyle 1963), but this accuracy does not hold at middle to high latitudes. At Hobart for example it

seems that B and H_{32} vary from hour to hour not just from day to day. The reason for this breakdown at higher latitudes is not really understood although Barbier 1959 and others have suggested it may be due to non-recombination sources of ^1D atoms. In chapters 5 and 6 however it is shown that a more probable reason is the result of increased neutral temperatures in the cisauroral region.

2.3 Thermal and direct excitation

2.3.1 Introduction

Seaton (1953, 1955 a and b) suggested that the excitation of the meta-stable ^1S and ^1D states of OI may be due to electron impact in the upper atmosphere. The only distinction between 'thermal' and 'direct' excitation is in the velocity distribution of the exciting electrons. In the former case the ambient electrons in the F-region are at a sufficient temperature ($> 2000^oK$) to have a sufficient population in the E 4 eV tail to be able to excite the ^1D state at least. In this thesis only low geomagnetic activity times are studied in detail and little 'thermal airglow' can be generated because ionospheric electron temperatures do not reach the necessary level. However, some evidence was found to suggest that south of Hobart the ionosphere may be more or less permanently hot enough to maintain the required temperature.

The 'direct' excitation is usually thought of as arising from a non-local ionospheric source of non-thermal electrons. For example it is thought that photoelectrons can travel along a field line and contribute to the pre-dawn enhancement by impact excitation. Any precipitation of low energy trapped electrons would also excite $O(^1D)$ directly; both these mechanisms have to compete with coulomb losses.

2.3.2. Outline of theory

Consider an atmosphere of OI atoms of density $[O]$. Suppose electrons of density n are moving through this region and their speed distribution is f(v) such that the fraction of electrons with speeds in the range v to v + dv is f(v) dv. If the cross section for the $(^3P - {}^1D)$ transition is Q_{PD}, then the number of transitions occurring (cm^{-3} sec^{-1}) is:

$$F_{PD} = [O]\, n \int_0^\infty Q_{PD}(v)\, v\, f(v)\, dv \qquad 2.24$$

Values of Q_{PD} (and cross-sections for the $^3P - {}^1S$ transition) have been evaluated by Seaton (1955 b) and more recently by Smith, Henry and Burke (1966 and 1967). Figs. 2.2 and 2.3 are taken from Smith et al (1967).

For thermal excitation it is usually assumed that the electrons are in a Maxwell distribution

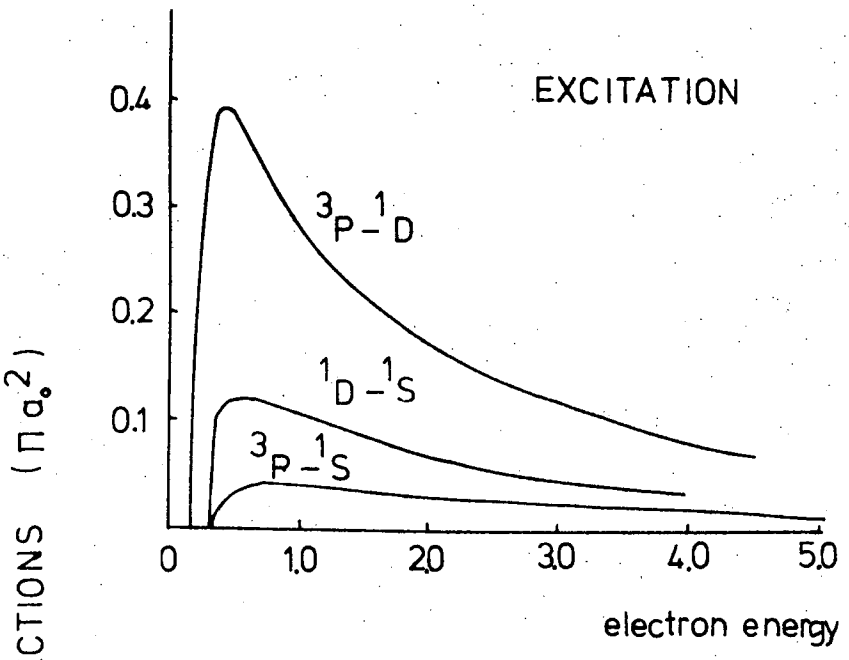

2.2

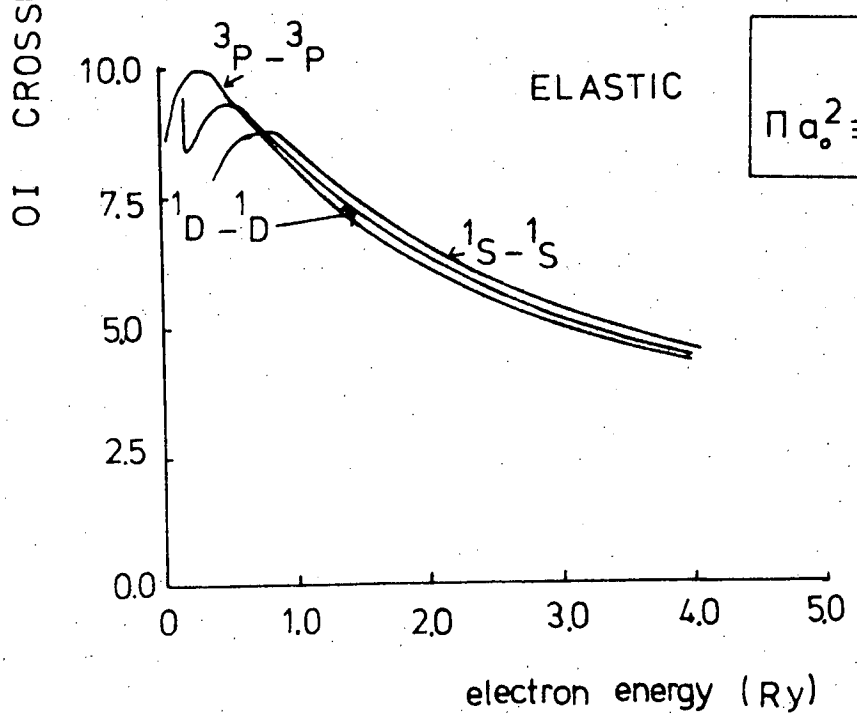

1 Ry ≡ 13.6 eV

$\Pi a_o^2 \equiv 8.8\ 10^{-17} cm^2$

2.3

i.e.

$$f(v)\,dv = 4\pi\left(\frac{m}{2\pi\,kTe}\right)^{3/2} v^2\, e^{-m v^2/2\,kTe}\,dv \qquad 2.25$$

Where m is the electron mass, Te is electron temperature and k is Boltzmann's constant, thus

$$F_{PD} = [O]\,n\quad A(Te)$$

where $A(Te) = \int_0^\infty 4\pi\left(\frac{m}{2\pi\,kTe}\right)^{3/2} v^3\, e^{-mv^2/2\,kTe}\, Q_{PD}(v)dv$ 2.26

The integral for A(Te) can be easily solved numerically.

The quantity which is measured is I(6300) the column integrated emission rate. The component of I(6300) due to thermal emission $I^*(6300)$ is given by:

$$I^*(6300) = \int_0^\infty F_{PD}\,dz$$

$$= \int_0^\infty n\,[O]\,A(Te)\,dz \qquad 2.27$$

where z is the height of emission. Strictly a term for collisional deactivation should be included in 2.27 but this is usually dis-regarded because thermal emission arises at much greater heights than dissociative recombination emission and this loss mechanism is usually negligible. Note that for direct electron excitation by a flux of electrons the 'n' of equation 2.24 refers to the flux density and not to the ambient density.

Chapter 3 EXPERIMENTAL TECHNIQUE

3.1 Introduction

The main experimental problems arising out of 6300Å airglow studies are measuring a rather weak line-emission against a strong continuum and in a region of the spectrum in which photo-electron detectors are not particularly sensitive. The technique used to overcome the first problem is to isolate the line by the use of narrow band interference filters and then to remove the background by comparing the intensity at 6300Å with a nearby control spectral region which does not contain any significant airglow emissions. For the second problem the technique is to minimise the noise generated in the electronics and especially the photo-multiplier itself. The actual techniques used in the present work are described herein. A description of observational equipment, all of which was specially designed and built for the project is also given. As many of the techniques used are standard procedures only brief outlines of much of the electronics are given; only new techniques, such as the simple all-sky sweeping system are described in detail.

3.2 Optical design

3.2.1 Airglow detection

The red air-glow emitting region is the F-region between 200 km and up to 400 km. It is usually thought of as having little horizontal structure so that the emissions within the 2^{o} to 5^{o} photometer's field of view are uniformly diffused. If this is so then it is clear that, provided the emitting source is uniform and broad, then the same number of photons will enter the photometer no matter what the source-photometer distance is. Because the emitting region is a layer, however, then obviously airglow originating near the horizon will appear brighter than the same intensity emission from near the zenith simply because a thicker emitting region is being observed. Corrections for this "Van Rhijn effect" are discussed in the next chapter.

Suppose that the emission rate of the line is $E(z)$ cm^{-3} sec^{-1} where z is the distance from the observer. Suppose the airglow is observed with a photometer with an entry pupil of area A cm^{2} and field of view Ω steradians

(v. fig. 3.1). If the airglow is emitted isotropically then the number of photons entering the photometer from unit volume is $\Gamma E(z)/4\pi$ where Γ is the solid angle subtended by the entry pupil from the airglow source. If Ω is sufficiently small and z sufficiently large then all the photons emitted can be considered to travel normal to the photometer; then $\Gamma = A / z^2$.

The total number of photons entering the photometer from distance z to z + dz is then:

$dN = dz \; z^2 \Omega \, (E(z) / 4\pi) \; A/z^2$; and the total number is:

$$N = \frac{\Omega A}{4\pi} \int_0^\infty E(z) \; dz \qquad 3.1$$

Thus by counting N and knowing Ω and A it is possible to obtain the integrated (apparent) emission rate of the line, $I(\lambda)$, where

$$I\lambda = \int_0^\infty E(z) \; dz = \frac{4\pi \; N}{\Omega \; A} \qquad 3.2$$

I is often called the <u>intensity</u> of the airglow. To obtain $I(\lambda)$ in the airglow unit of the rayleigh the integrated emission rate is multiplied by 10^{-6}.

Note that from 3.1 above an obvious way to

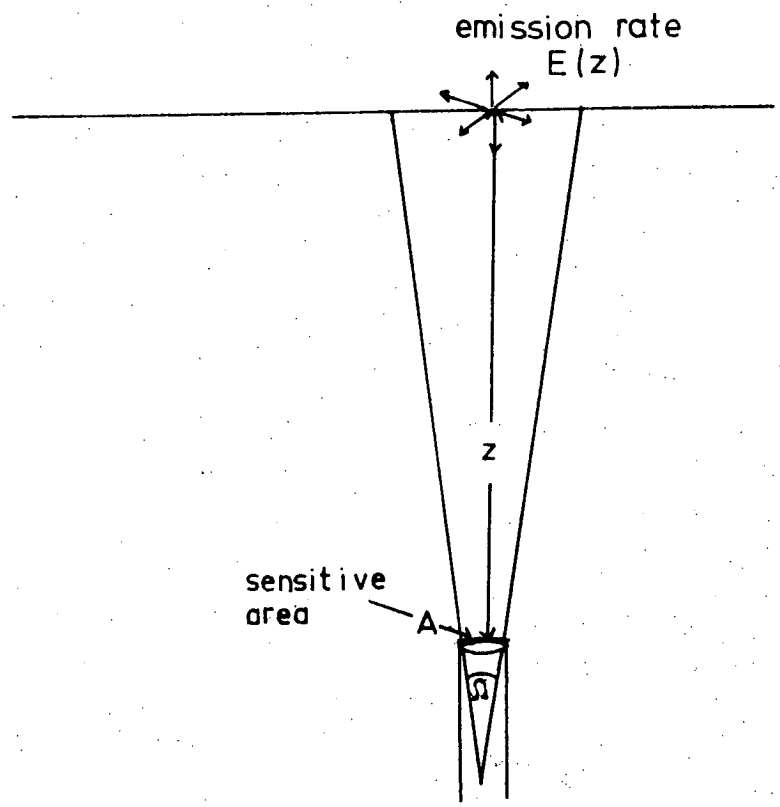

Fig. 3.1 Airglow observation

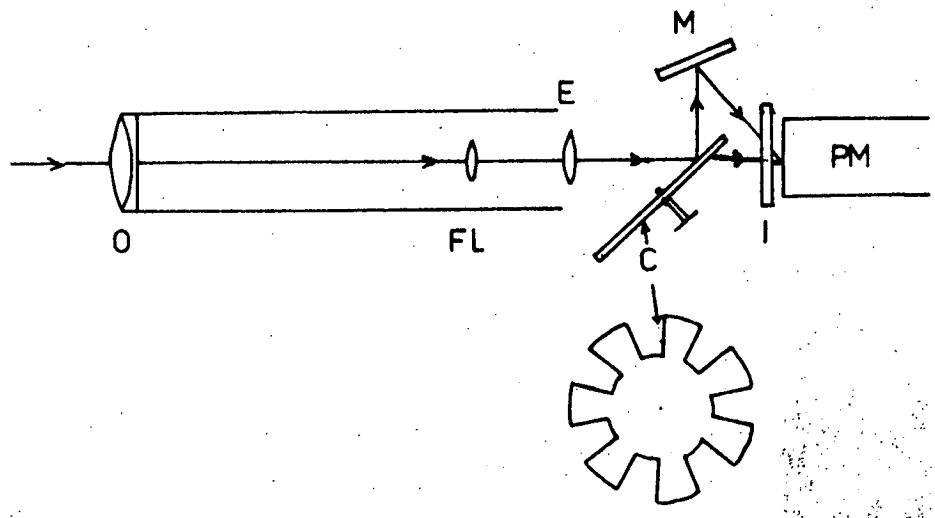

Fig. 3.2 The 11 T R 1 photometer

increase the signal to noise ratio of the photomultiplier detector is to increase the angle of view Ω and/or the sensitive area A. There are dangers in increasing however. Firstly if Ω is large enough then even broad structure in the airglow may be integrated out. Secondly for the type of photometer which has an interference filter behind the objective lens's focal plane then the increase in bandwidth caused by the increased entry cone angle will tend to decrease the signal to noise ratio (S/N). So in this experiment when it was decided to increase the sensitivity of the equipment (March 1969) the objective lens was increased in diameter from 3" to 4" which theoretically increased the S/N rates by 9 : 16.

3.2.2 The IITRI photometer

A number of types of so called continuum compensating photometers have been designed. These include the polarizing type (Dunn and Manning 1956), the wedge filter type (Hunter et al 1964), the tilting filter type (Eather and Jacka 1967) and the IITRI beam-splitting type (Filosofo et al, 1965). The photometer built for this project is the IITRI

type. The main reasons for this choice are that it is simpler than the polarizing or wedge filter type and has a better time resolution than the tilting filter photometer. However, it is more difficult to compensate for the troublesome O H emission with the IITRI type than the tilting filter type (see chapter 4). All-sky sweeping was desired for the project however and the good time resolution of the IITRI type made it ideal for this purpose.

Fig 3.2; shows the principle on which the IITRI photometer works. The incoming beam is collimated by the eye-piece E and the resultant parallel beam is then split by the rotating mirror chopper C which alternately transmits and reflects the beam. The transmitted beam passes directly through the interference filter I and the reflected beam is reflected off the fixed mirror M so as to enter the interference filter at an angle α. Now if an interference filter is tilted to a beam of light then the wavelength of peak transmission becomes less and the bandwidth is widened (Vasirek 1960). Also the transmission efficiency becomes less but for a white light source the total

integrated photon count is similar for the normal and oblique beam. The resultant effect of the arrangement of fig. 3.2 is to pass into the photo-multiplier (P M) alternate beams of light which pass through different filtering paths. If the integrated response of both channels is made the same then the output of the photomultiplier will not change for a white light source no matter what the position of the chopper. In the IITRI photo-meter it is assumed that the spectral region of the oblique beam contains a similar continuum to the spectral region containing the required line, thus if the oblique pass-band contains no significant line emission then, after both responses have been equalised for white light, any A.C. signal from the photo-multiplier will be a measure of the intensity of the required line.

Unfortunately the 6300Å region of the spectrum is contaminated by the [5 , 0] and [9 , 3] hydroxyl bands and the assumption of a 'level' continuum from 6200Å to 6300Å may not apply. In an attempt to allow for this both A.C. (red air-glow) and D.C. (continuum) signals were recorded

in this region. The [7 , 1] OH band contamination of 5577Å is much less severe, largely because of the strength of the green line, but the D.C. level was still recorded (see fig. 4.2.).

3.2.3 The filters

The two narrow band interference filters had the following characteristics:

Table 3.1

diameter	peak wavelength	peak transmissivity	bandwidth
2"	5577.2Å	73.8%	8.0Å
2"	6301.1Å	67.3%	8.4Å

As mentioned above the finite angle of view of the photometer means that some broadening of the bandwidth occurs. This of course depends on the angle of view but for the 2° total field of view usually used in this experiment the effective bandwidth rose to between 10 and 13 Å. Fig. 3.4 shows the responses of the photometer system used in the project with the above filters. This has been obtained using a 1 Å monochrometer and a low intensity standard lamp. This lamp has been calibrated by the Australian Defence Standards Laboratories so the luminance at any particular spectral interval is known. Fig.3.4

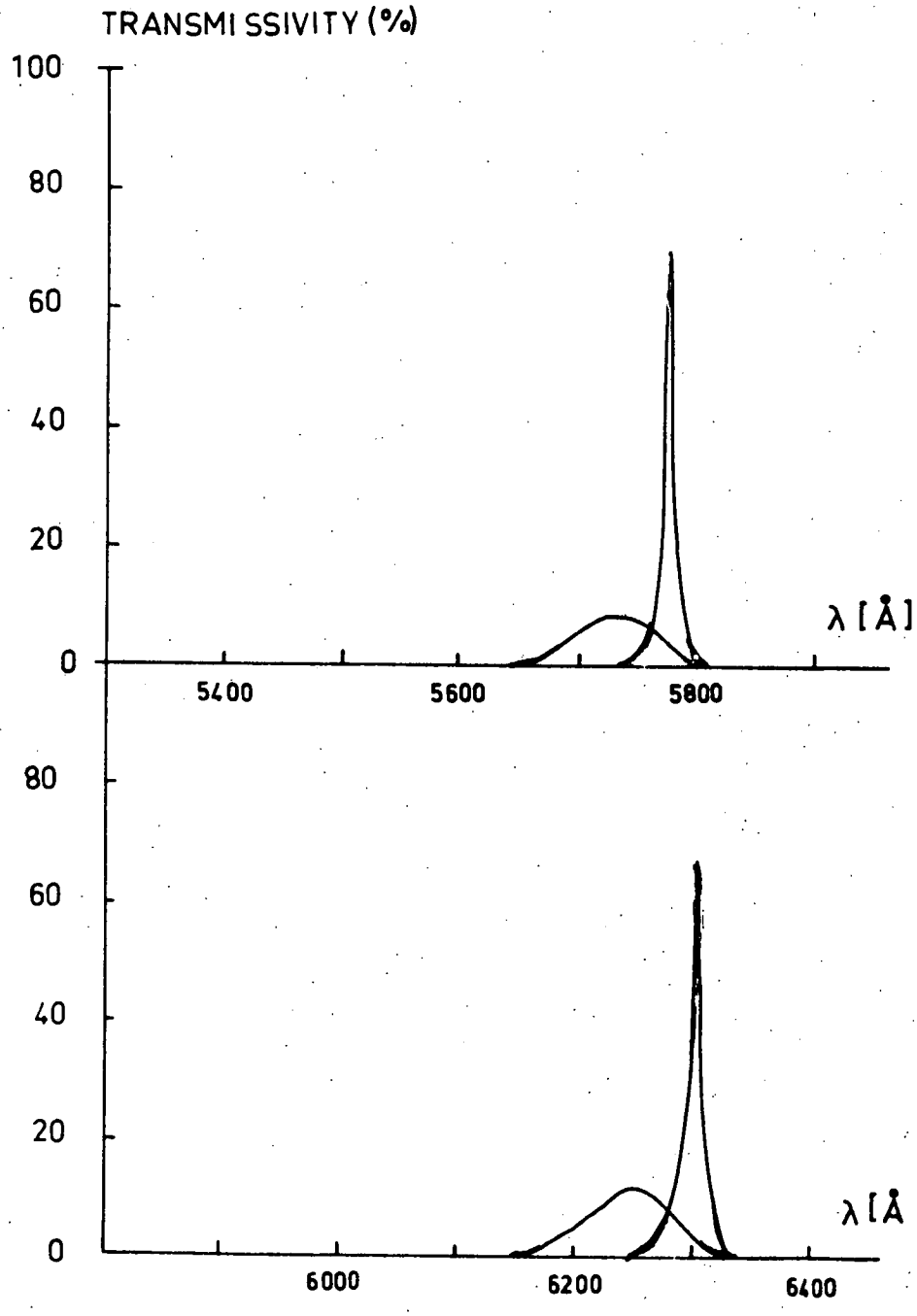

Fig. 3.4 Passbands for filter used in this experiment.

has thus been normalised for a white light source. From the integrated responses of the curves in fig 3.4 it is seen that the normal beam for the red filter is transmitted 25% more efficiently than the oblique beam; for the green filter the difference was 15%. To overcome this, neutral filters of the required strength were placed in the path of the normal beam. These changed position automatically when the interference filters did and the photometer thus did not respond to white light.

3.2.4 Lens system

The lens system consisted of an achromatic doublet objective; a field lens at the focal plane of the objective, behind which was a variable aperture to change the field of view; and a simple eyepiece lens. In the final system used the lenses' parameters were

Table 3.2

Lens	diameter (cm)	focal length (cm)	f/-
objective	10.2	40 cm	4
field	variable	5 cm	-
eyepiece	3.3	10 cm	3

3.2.5 The photomultiplier

Because of their good red sensitivity EMI 9558 detectors were used. These were used for two weeks and then 'rested' in the dark because of the tendency for sensitivity to drop off with extended use. This practice necessitated frequent calibration of the system which was rather tedious. Details are given in chapter 4. Now to improve the signal to noise ratio of the detection system in the most important place, the front end, the photomultiplier is often cooled (e.g. by liquid N_2) to remove thermal noise. This was only done for a short time at Hobart but to keep the photomultiplier characteristics constant the whole photometric system was kept in a constant temperature chamber ($\sim 1\ ^{o}$ C). This had the added advantage of keeping the interference filters at a constant temperature which is important because their transmission characteristics are temperature sensitive.

3.2 Mechanical systems

3.2.1 The photometer

Fig 3.5 shows a photograph of the photometer with the outer constant temperature chamber removed. Behind the chopper C is a second similar but smaller thin aluminium chopper which passed through the jaws of a magnetic sensing head (MH).

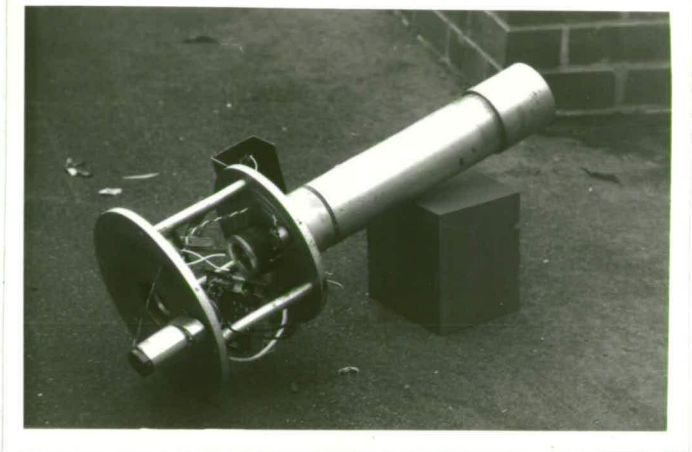

Fig. 3.5 Photometer with cover removed.

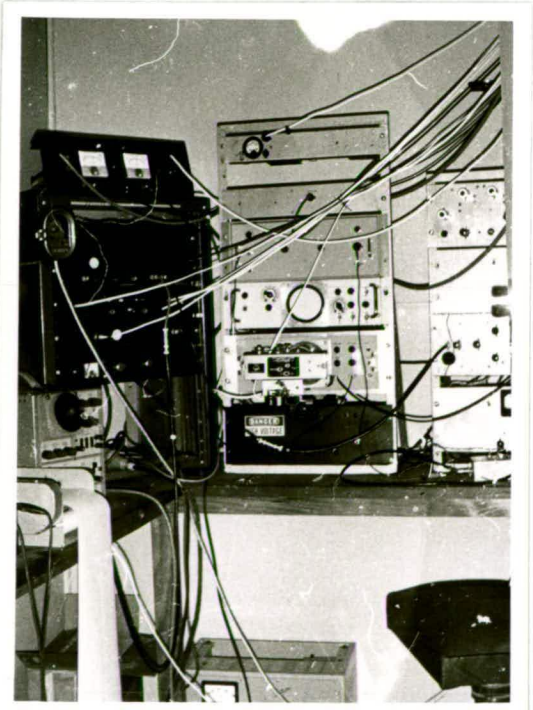

Fig. 3.6 the master control panel in the observing hut

This provided a square wave reference signal for the phase sensitive detector (see section 3.3). The rotating filter turret (FT) can be seen immediately in front of photomultiplier. This was driven by a small synchronous motor mounted on the base plate of the photometer. For clarity the blocking-off screen mechanism, which was used to protect the photometer in daylight and which was switched on (by solenoid) whenever internal calibrations were being made, has been removed;but it was situated on the top plate behind the eyepiece E. The whole photometer was fixed on a mounting, pointing at 15° away from the zenith. It was then mounted on a small tower, enclosed in an observing chamber and fed by a two mirror all sky-sweeping system (fig. 3.7).

3.3.1 Sweeping system

Fig. 3.8 shows a photograph of the mirror sweeping system. This was designed to be as simple as possible but to be versatile. The principle it works on is shown in fig. 3.9 . The mirror M is rotated on the threaded shaft TS which passes through the threaded plate TP. The mirror M thus sweeps through 360° in azimuth but if the plate TP is constrained from rotating then this plate will move up the shaft TS; this has

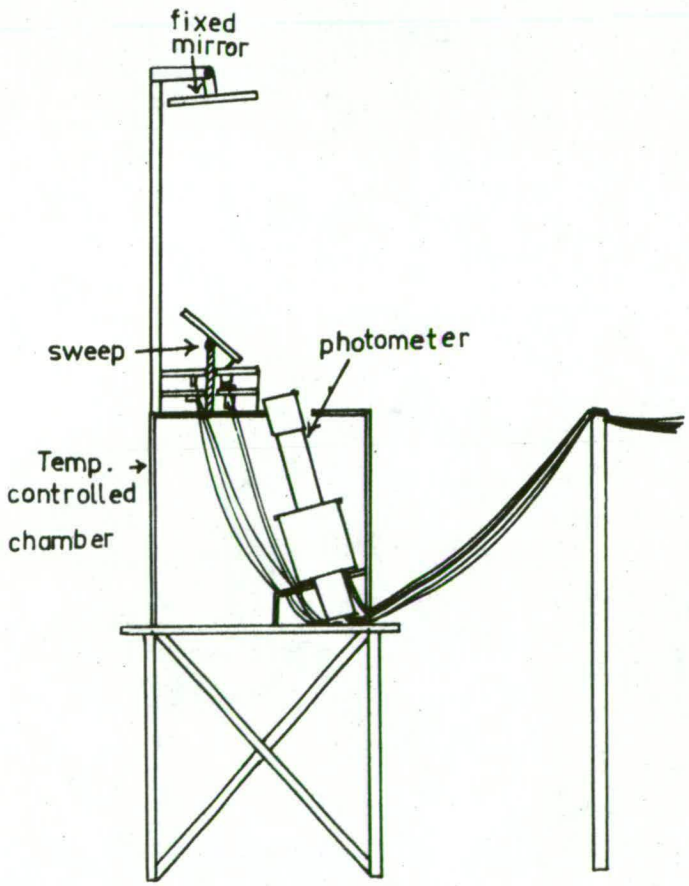

Fig. 3.7 Observing method.

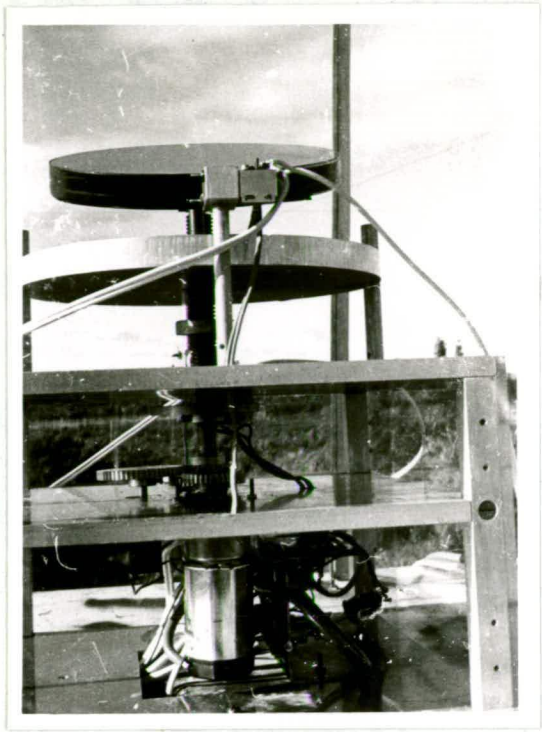

Fig. 3.8 Sweeping system.

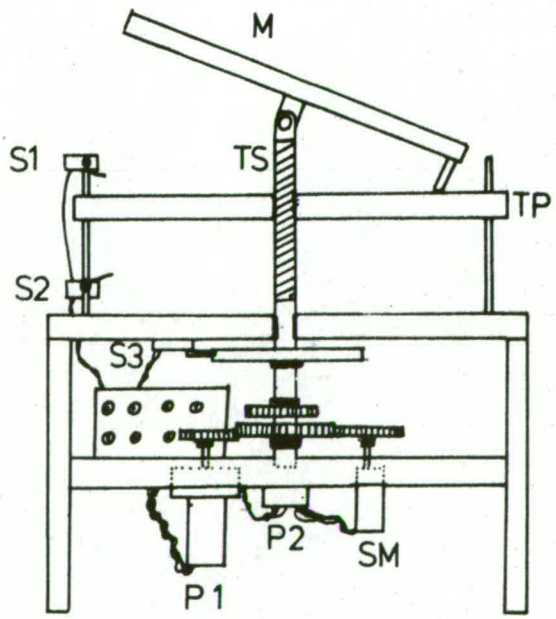

Fig. 3.9 If plate TP is fixed then zenith angle changes for each rotation.

the effect of changing the zenith angle of observation and by this means the whole sky may be observed in a spiral sweep. Once the plate TP reaches the top of the shaft it operates two micro-switches, one of which reverses the direction of rotation of the driving synchronous motor and the other changes the filter in the filter turret. In this way the sky is alternately recorded in 6300Å and 5577Å light. Unfortunately the spiral is not linear in the sense that the change in zenith angle per rotation is greater near the horizon than near the zenith. The sweeping system was designed so that this effect was minimised. Also it is impossible to observe closer to the zenith than 5°, but in view of the weak horizontal structure of 6300Å airglow this is not important.

Direct information on where the photometer is pointing is given by two potentiometers visible in fig. 3.8. One of these was a 15 - turn pot which gave zenith angle position and the other a 360° one for the azimuth angle. Both voltages were visible on the master control panel in the observing hut (fig. 3.6). From this panel it was possible to reverse the direction of

sweeping and to override the automatic filter changing. The voltage from the 360° pot was also used for moving a spot on a cathode-ray tube in the y-direction; the phase-detected photomultiplier signal was applied to the x - plate and the resulting trace recorded on an oscilloscope camera. The 360° pot was so arranged that 0 Volts corresponded to (magnetic) north. As soon as the sweep reached this position the camera motor switched on and moved the 35 mm film along a few millimetres. In this way a record of airglow intensities from all over the sky was built-up in a very compact form (fig. 3.10a). Calibrations were automatically given every complete sweep and zeros every rotation. The data was also recorded on chart (fig. 3.10b) but this had only a low spatial resolution.

The number of rotations from the 80° zenith angle to the 5° zenith angle was varied by changing the threaded plate and shaft. The best results were obtained for 10 rotations per complete sweep and the most convenient sweeping time was 7 minutes. With the integration time of the phase sensitive detection system taken into account the azimuth angular resolution is 8° for the sweeping time listed above. This is about the same as the altitude resolution.

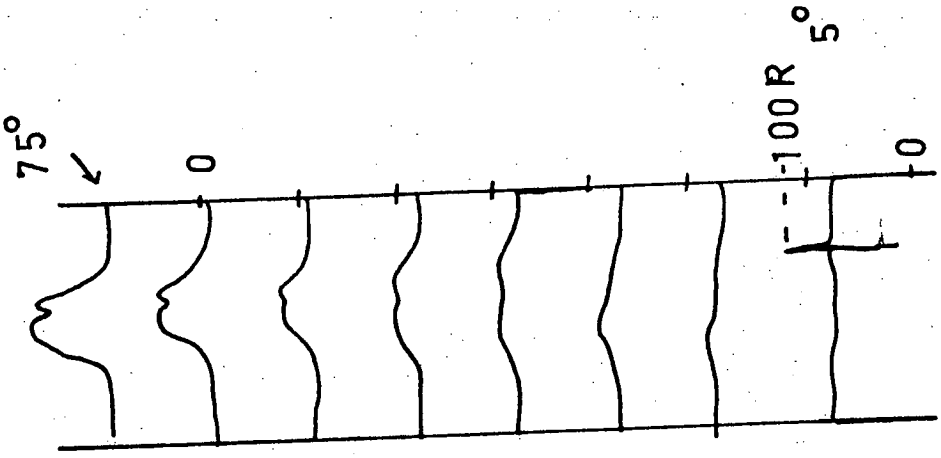

Fig. 3.10(a) Typical film record.

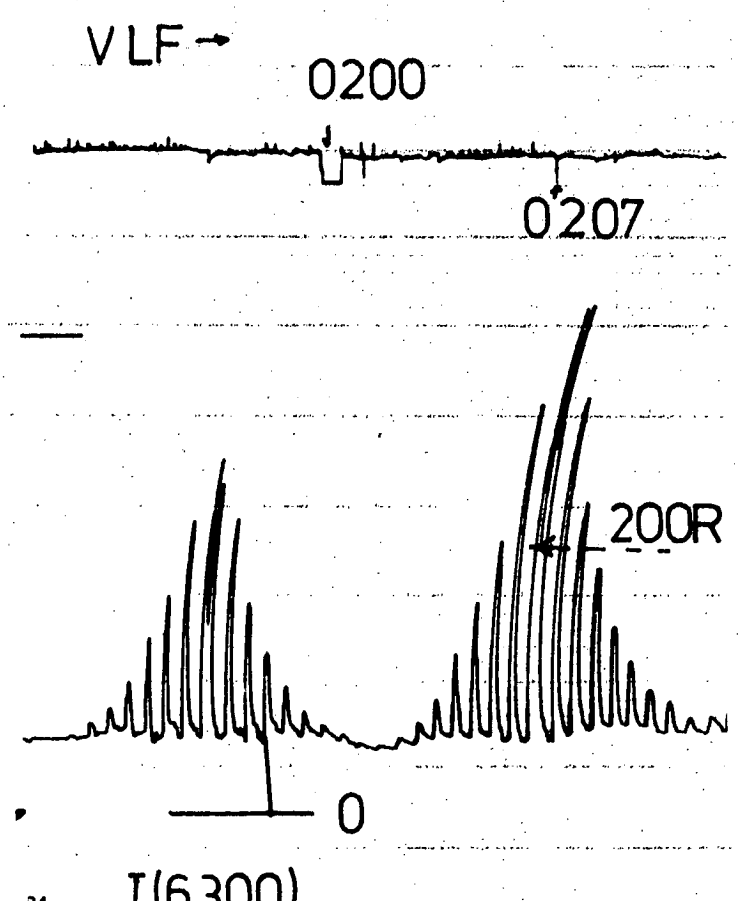

Fig. 3.10(b) Low resolution chart

3.4 Electronics systems

3.4.1 General

A block diagram of the electronics system is shown in fig. 3.11. After the light has been converted into an electrical signal the A.C. and D.C. components of this are separated. The D.C. signal is recorded, after amplification, on a pen chart. The A.C. signal passes through a high input impedance narrow band amplifier and then into the phase sensitive detector. The reference signal is fed into a phase splitting network which produces two square waves, 180° out of phase, whose phase may be arbitrarily changed. These two reference signals are fed into the phase-sensitive detector which is of the full wave rectifier type. The D.C. output is then recorded on the y-plates of the oscilloscope as described above. Part of this output is however amplified by a D.C. amplifier and recorded on a pen-chart.

3.4.2 Amplification

Because of the high output impedance ($\sim \frac{1}{2}$ MΩ) of the photomultiplier high impedance A.C. and D.C. amplifiers were needed to record the signal.

This had a MOS - FET front end followed by a broad band amplifier based on μ A709's integrated circuits.

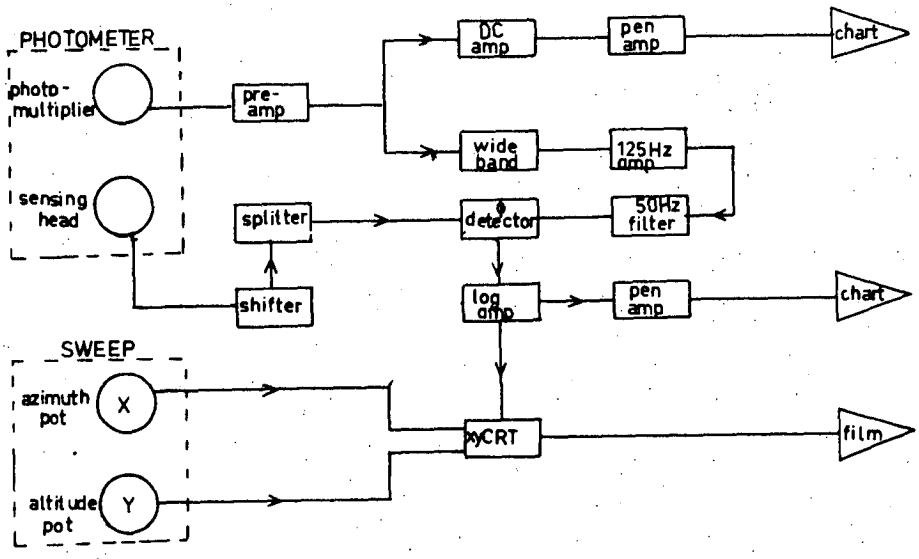

Fig. 3.11 The electronics system.

The signal from this was fed via a resistor chain into the narrow band amplifier which was also based on μA709's. The resistors in the input circuit could be changed automatically, as the signal strength increased, to keep the final output in the recording limits. An overlap on this system prevents range 'hunting'. The narrow band amplifier had a variable bandwidth of between 5 and 1 Hz centered on 125 Hz. The narrower bandwidths improved the S/N ratio but also increased frequency drift problems which affected the phase sensitive detector output. Satisfactory results were obtained using a bandwidth of 2.5 Hz. The output A.C. signal was then fed into the phase sensitive detector where after rectification part of the D.C. output went into the cathode ray tube recording system and part into a logarithmic amplifier (Gile 1967) in order to increase the dynamic range of the pen-recording system.

The gain of the whole system could be changed in several ways. These were, together with the approximate gain changes:

(i) change in narrow band amplifier input (20:1)

(ii) change in anode resistors (10:1)

(iii) change in photo-multiplier supply voltage (80:1)

(iv) change in phase sensitive detector gain (10:1)

In practice none of these was done unless absolutely necessary because of the new calibration required after each change.

Chapter 4: DATA ANALYSIS

4.1 Introduction

This chapter outlines the data reduction techniques employed to obtain all-sky plots of airglow intensity contours ('isophotes') from the raw photometer output data. These include correcting for atmospheric effects such as scattering, the Van Rhijn effect, and airglow contamination by OH bands. An estimate is made of errors involved in these processes.

4.2 Calibration

4.2.1 General

Suppose it is required to measure the intensity of the airglow line of wavelength λ. The IITRI photometer splits the incoming collimated beam into two components, one of which enters the filter normally and the other at an angle of about 12^{o}. The transmission properties of both light paths can be described as functions of wavelengths by:

$$T_i(\lambda) = d N_i'(\lambda) \quad / \quad d N_i(\lambda) \qquad 4.1$$

where $d N_i(\lambda)$ is the number of photons entering the filter from path i and $d N_i(\lambda)$ is the number passing through. Here i = 1 for the normal beam and i = 2 for the oblique beam.

Now if the intensity of a broad diffuse isotropic source is defined by $L(\lambda)$ Rayleighs per Angstrom then from section 3.2 the total number of

photons entering the photometer in the region λ to $\lambda + d\lambda$ is:

$$d N_o (\lambda) = 10^6 \times \frac{\Omega \ A}{4 \pi} . L (\lambda) . d\lambda \qquad 4.2$$

where Ω (steradeb) is the angle of view and A (cm^2) the entry pupil area; then the number of photons passing through the filter by the i th path is from 4.1 and 4.2:

$$d N_i' (\lambda) = 10^6 \ \alpha i \ \frac{\Omega \ A}{4 \pi} \ L (\lambda) . d\lambda . T_i (\lambda) \qquad 4.3$$

where α_i is the fraction of light remaining after passage through the mirror and lens systems. This factor is different from both paths because of the neutral compensating filter for the normal path; however, it is assumed that over the region of interest the α's are independent of λ.

The output voltage V_i of the photo-multiplier / amplifier / detector system is related to the incoming photon count by the response function R (λ) which is defined by:

$$d V_i (\lambda) = 10^{-6} R (\lambda) \ d N_i' (\lambda) \qquad 4.4$$

which from 4.3 gives:

$$d V_i (\lambda) = \alpha_i \ \frac{\Omega \ A}{4 \pi} \ L (\lambda) \ T_i (\lambda) \ R (\lambda) \qquad 4.5$$

The total output is thus:

$$Vi = \alpha_i \ \frac{\Omega \ A}{4 \pi} \int_0^\infty L (\lambda) \ T_i (\lambda) \ R (\lambda) \ d\lambda \qquad 4.6$$

The integral in 4.6 vanishes outside the filter passband, (i.e. where $T_i(\lambda) = 0$).

If the oblique beam is blocked-off then the voltage output from a standard source of intensity $S(\lambda)$ is then:

$$V_s = \alpha_i \frac{\Omega A}{4\pi} \int_0^\infty S(\lambda)\, T_1(\lambda)\, R(\lambda)\, d\lambda \qquad 4.7$$

Suppose it is required to measure a line of wavelength λ_o and intensity E_o, then an observation with the oblique beam blocked off would include the continuum emissions of intensity $E_c(\lambda)$; the output voltage would be:

$$V_1 = \alpha_1 \frac{\Omega A}{4\pi} E_o\, T_1(\lambda_o)\, R(\lambda_o) + 1 \frac{\Omega A}{4\pi} \int_0^\infty E_c(\lambda)\, T_1(\lambda)\, R(\lambda)\, d\lambda \qquad 4.8$$

and an observation with the normal beam blocked-off would yield a voltage:

$$V_2 = \alpha_2 \frac{\Omega A}{4\pi} \int_0^\infty E_c(\lambda)\, T_2(\lambda)\, R(\lambda)\, d\lambda \qquad 4.9$$

It has been assumed, however (section 3.3), that $E_c(\lambda)$ is constant over the passbands of both filters and the α's have been thus adjusted so that

$$\alpha_1 \frac{\Omega A}{4\pi} \int_0^\infty E_c(\lambda)\, T_1(\lambda)\, R(\lambda)\, d\lambda = \alpha_2 \frac{\Omega A}{4\pi} \int_0^\infty E_c(\lambda)\, T_2(\lambda)\, R(\lambda)\, d\lambda \qquad 4.10$$

The quantity measured by the photometer with both paths open is $(V_1 - V_2)$ which from 4.8, 4.9 and 4.10 is:

$$\Delta V = V_1 - V_2 = \alpha_1 \frac{\Omega A}{4\pi} E_o T_1 (\lambda_c) R (\lambda_o) \quad 4.11$$

In 4.7 the voltage V_s is measured with only the narrow band pass, centered at $\lambda = \lambda_o$ open ; it is possible then to rewrite the integral in terms of functional values at λ_o and the 'effective' bandwidth $\Delta\lambda_o$ thus:

$$V_2 = \Delta\lambda_o \alpha_1 \frac{\Omega A}{4\pi} S (\lambda_c) T_1 (\lambda_c) R(\lambda_c) \quad 4.12$$

Thus from 4.11 and 4.12 it is possible to obtain the desired line intensity in terms of measurable parameters:

$$E_o = \frac{\Delta V}{V_s} S (\lambda_c) \Delta \lambda_o \quad 4.13$$

Hence if a standard source of $S(\lambda)$ R/Å is used and the output voltage V_s measured, then knowing $\Delta\lambda_o$ the line intensity at λ_o is given from 4.13 simply by inserting the measured output voltage

4.2.2 Calibration errors

As mentioned earlier the standard lamps in calibrating the photometer had been accurately ($\pm$ 2%) calibrated by the Defence Standards Laboratories. The whole photometric system was calibrated before and after each change of photomultiplier.

This was a tedious job because all the optical and electronic equipment had to be brought back to the laboratory from the field-station. In the field a regular hourly calibration was given by a secondary internal source. Over a night's observations the photometer's response changed by less than 3% and over a month by less than 10%. The output data was corrected accordingly.

The standard calibrating technique is shown in fig. 4.1. It involves using a standard source to illuminate an isotropic (back) scattering surface of known albedo (usually magnesium oxide). This surface then represents the broad diffuse source required for calibration. Its intensity may be changed by either moving the lamp further away, or, as in this case, attenuating the source by neutral filters of accurately known strengths. The photometer was set up and pointed at this source via the two mirrors used in sweeping the sky and measurements of output voltage recorded for various anode resistors, photomultiplier voltages and detector gains: the source intensity was varied to give similar output voltages to those obtained in the field.

Thus from equation 4.13 above various values of the factor $Q = S(\lambda_c)\ \Delta\ \lambda_o / V_s$ were obtained.

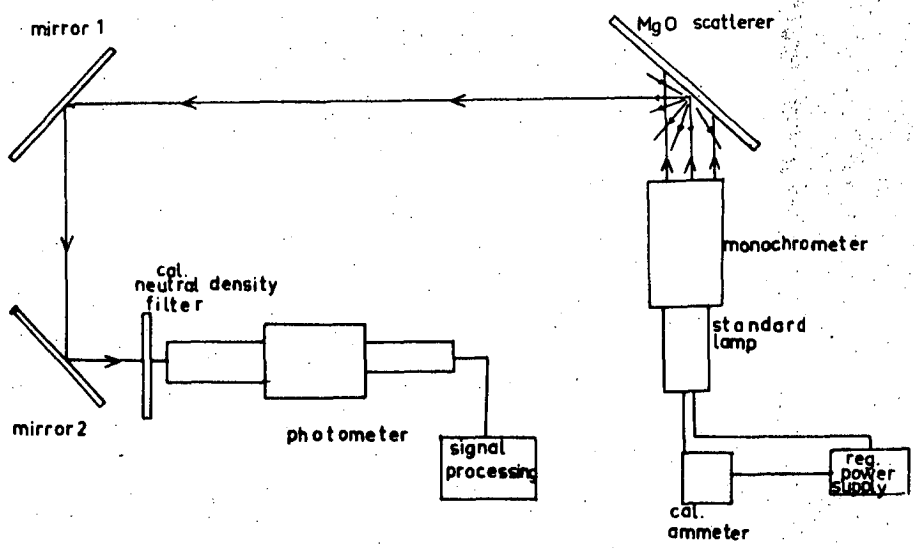

Fig. 4.1 Calibrating system.

The apparent airglow intensity is then obtained from the output voltage ΔV by multiplying by the appropriate Q.

This apparent intensity must be corrected for atmospheric effects but the major error in this intensity comes from the approximations used in obtaining 4.12 and 4.13 above. This approximation is the replacement of the integral in 4.11 by a multiplicative expression. As Blacker and Gadsen (1966) point out, this error becomes less as the filter bandwidth is decreased.

The integral to be approximated is:

$$\Psi = \int_0^\infty T_1(\lambda)\, R(\lambda)\, S(\lambda)\, d\lambda \qquad 4.14$$

Now, as λ_o is the centre of the region of integration then provided $R(\lambda)$ and $T(\lambda)$'s slopes remain constant across the pass band, then Ψ can be accurately rewritten as:

$$\Psi = R(\lambda_o)\, S(\lambda_o) \int_0^\infty T_1(\lambda)\, d\lambda \qquad 4.15$$

To determine $T_1(\lambda)$ it is necessary to use a monochromator and measure the photometer's response with and without the filter in position over the spectral range of interest. Once this has been done the effective bandwidth can be determined by:

$$\Delta\lambda_o = \frac{\int_0^\infty T_1(\lambda)\, d\lambda}{T_1(\lambda_o)} \qquad 4.16$$

The order of magnitude error involved in this is ± 5% and with errors of ± 2% in S (λ_o) and ± 1% in V_s and (Ω.A) this gives an error of O (10%) in determining the apparent airglow intensity.

Another source of error discussed by Blacker and Gadsen (1966) is the existence of secondary pass bands in interference filter. For the 6300Å filter used in this experiment these bands were efficiently blocked beyond 6320Å to 8000Å. It is estimated that only about 2% overall error would arise from them for the 2040°K standard lamp.

Thus the total errors in calibration are O (12½%) but this does not include any errors due to the assumptions about the airglow continuum. These are discussed below.

4.3 Continumm and Atmospheric corrections

4.3.1 OH Contamination

The contamination of OI airglow emissions by the OH Meinel bands is potentially very serious. Fig. 4.2 shows the positions of the contaminating bands; the [9,3] band is especially badly placed near the 6300Å - 6364Å doublet. Unfortunately the diurnal, seasonal and latitude variation of the bands have not been adequately measured nor do theoretical predictions of intensities agree well with observed intensities (Hunt, 1966, Gattinger 1969). It is thought

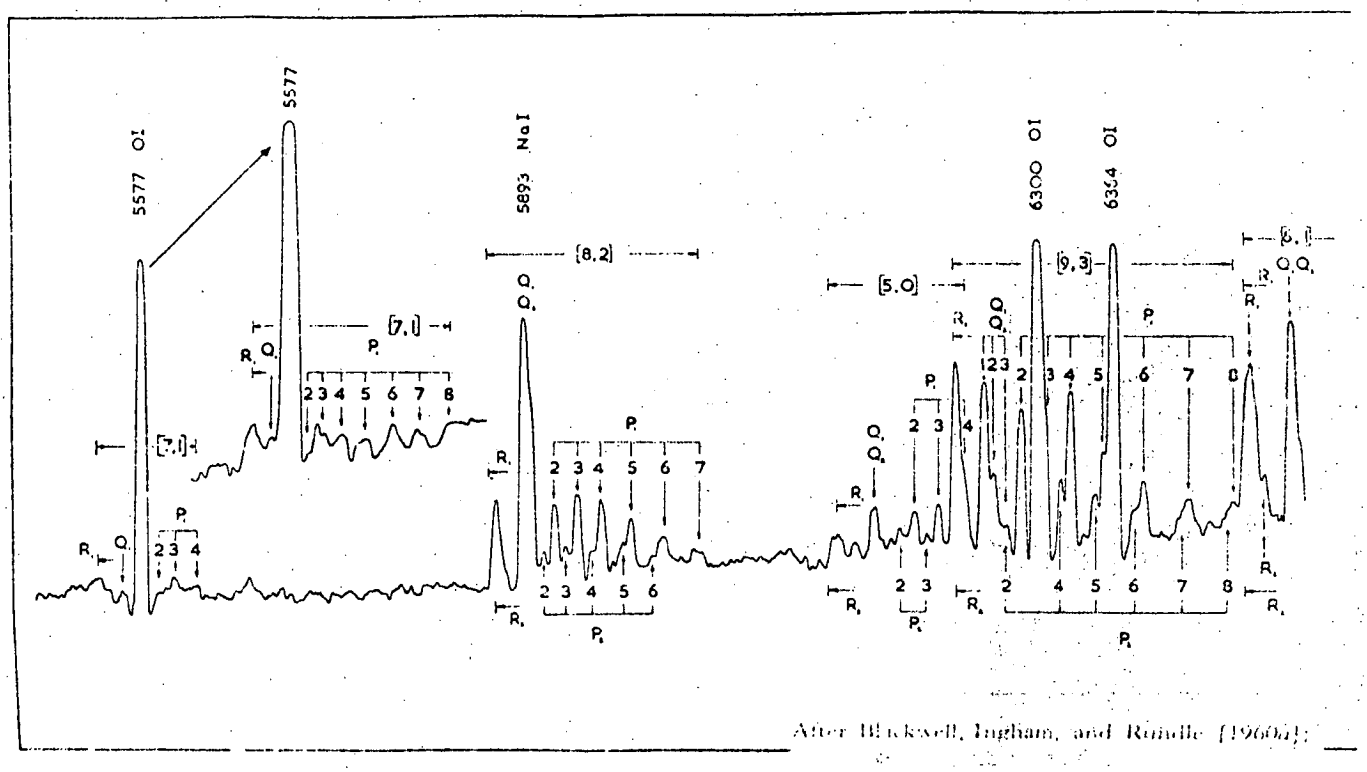

After Blackwell, Ingham, and Rundle [1960a].

Fig. 4.2 The OH Meinel Bands. (from Chamberlain 1961)

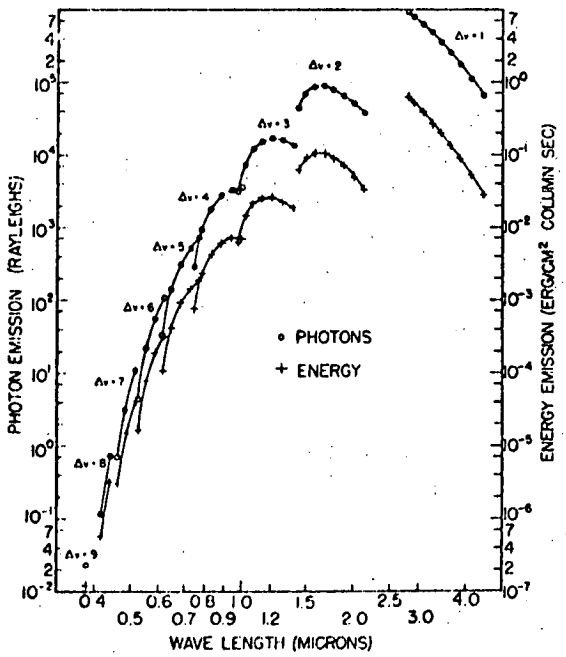

From Chamberlain and Smith [1959a].

Fig. 4.3 OH emission strengths

that the OH emissions arise from atomic hydrogen and ozone interactions and that the emitting layer is near 85 km (Barbier 1964). This low height of emmission means that the radius of observation for an all-sky sweeping photometer is much smaller for the OH bands than it is for the 6300Å airglow (400 km cf. 1100 km) and also that more Van Rhijn correction is needed for high zenith angle observations for OH airglow than for corresponding observations of 6300Å airglow (see section 4.3.2). There does not appear to be any way of completely eliminating OH contamination from the 6300Å data but the technique outlined below has proved satisfactory, at least with average data.

The technique relies on the fact that any airglow emitted in a finitely thick layer, and at a finite height, will increase in intensity towards the horizon (the 'Van Rhijn effect'). It was stated in the previous chapter that the 'continuum level' from the photometer is recorded as well as the line intensity. Essentially this 'D.C. level' is the intensity of light passing through the oblique path. As can be seen from fig. 4.2 this band pass, for the red-filter, contains the [5,0] Meinel band as well as part of the [9,3] band. The continuum also contains

an astronomical component but unlike the airglow component this is not subject to the Van Rhijn effect (it is subject to scattering and extinction however; but these were ignored in view of the approximate nature of the OH correction). The technique then involves estimating the OH component in the oblique band by calculating the amount of the continuum which is subject to the Van Rhijn effect. Thus if the total intensity of the continuum at a zenith angle of θ° is $E_2(\theta)$ then:

$$E_2(0) = E_A(0) + E_{OH}(0) \qquad 4.17$$

where E_A is the astronomical component and E_{OH} the airglow component also:

$$E_2(75) = E_A(75) + E_{OH}(75) \qquad 4.18$$

Now if the OH airglow is uniform then:

$$E_{OH}(75) = Z(75)\, E_{OH}(0) \qquad 4.19$$

where $Z(\theta)$ is the Van Rhijn factor; and if it is assumed that:

$$E_A(75) = E_A(0) \qquad 4.20$$

then, from 4.17 to 4.20:

$$E_{OH}(0) = \frac{E_2(75) - E_2(0)}{(Z - 1)} \qquad 4.21$$

This gives the OH contamination of the

oblique beam. Now there are published plots of relative photon emissions (R /Å) for the OH bands (Chamberlain and Smith 1959, Krassowsky et al 1961) and using these the relative amounts of OH passing through the oblique and normal pass bands can be estimated (fig. 4.3) thus using 4.21 above, and the relevant factor, an estimate of the OH contamination of the airglow line intensity is possible which can be subtracted from the line intensity. Usually this correction is less than 12 R which is only half that expected from fig. 4.3; this may be due to the different intensities of the past two solar cycles.

4.3.2 Van Rhijn correction

If the airglow is emitted in a thin homogeneous layer which is parallel to the earth's surface, then the correction necessary to reduce intensity observations to zenith values was first given by Van Rhijn (1921). Fig. 4.4 shows the geometry of the situation where R_E is the radius of the earth, z the emission height and θ the zenith angle. The intensity of the airglow is proportional to $\sec\phi$ (see fig. 4.4) and clearly

$$\sin \phi = \frac{R_E}{R_E + z} \sin \theta \qquad 4.22$$

If the intensity of the airglow at angle θ° is

Fig. 4.4 The Van Rhijn effect

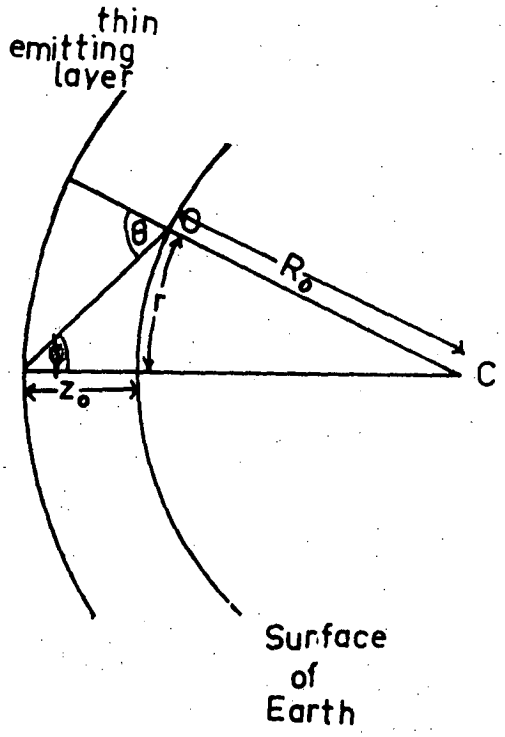

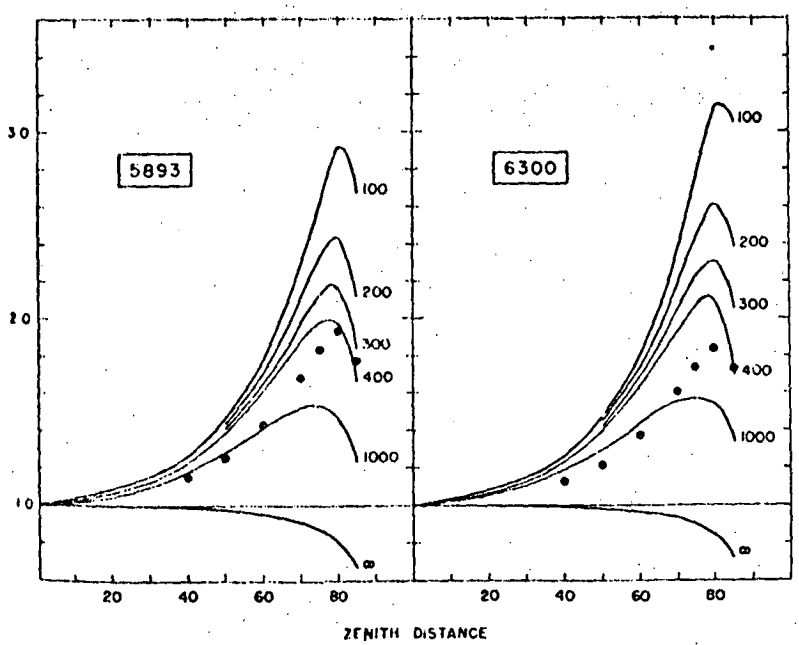

From Roach and Meinel [1955a]

Fig. 4.5 Modified Van Rhijn correction

I (θ) then

$$I(\theta) = I(o)\ Z(\theta, z) \qquad 4.23$$

where $Z(\theta, z)$ is the Van Rhijn function given by:

$$Z(\theta, z) = \frac{1}{(1 - [R_E / (R_E + z)]^2 \sin^2\theta)^{\frac{1}{2}}} \qquad 4.24$$

Tables of Z for various z's and θ's are given in Chamberlain (1961).

4.3.3 Scattering and extinction

For observations near the horizon light may be absorbed or scattered by the troposphere. For a point source, such as a star all scattered light is lost and the star appears to grow dimmer as it approaches the horizon. This is known as 'extinction'. For a broad source, such as the airglow, some light is scattered back into the line of sight. The theoretical treatment of the various types of scattering and other loss mechanisms is complex and will not be reviewed here. (An extensive review is given in Chamberlain 1961, chapter 2). The effect of these mechanisms is to reduce the Van Rhijn factors, especially near the horizon. Fig. 4.5 taken from Chamberlain (1961), page 489, are the modified Van Rhijn coefficients Z which were used in this study.

4.3.4 Summary

Thus from the raw output data the final airglow intensity is estimated by:

$$I(\lambda_c) = Z_{\lambda}'(\theta)\left[\frac{\Delta V.S(\lambda_o)\Delta(\lambda_o)}{V_s}\right] - Z_{OH}'(\theta)\, E_{OH}'(\theta) \qquad 4.25$$

where ΔV, $S(\lambda_o)$, $\Delta\lambda_o$ and V_s mean the same as in section 4.3.5. $E_{OH}'(0)$ is the estimated zenith OH contamination of the normal beam; and $Z_{\lambda}'(\theta)$ and $Z_{OH}'(\theta)$ are the Van Rhijn coefficients for the airglow line and OH band respectively. In practice to obtain $I(\lambda_o)$ it is only necessary to feed values of V and $E_{OH}(\ )$ into the computer and specify the and $Q\ (= \frac{S(\lambda)\ \Delta\lambda_o}{V_s}\ )$ required

4.4 All-sky charts

Fig. 4.6(a) shows the relationship between zenith angle and the distance from the observer to the projection on to the earth's surface of the emitting region. The assumed emission height for 6300Å airglow is 300 km and for 5577Å airglow it is 120 km The geometry involved is shown in fig. 4.6(b). The airglow was plotted on to an azimuth - 'real range' grid using fig. 4.6(a) to convert zenith angles to distance. Of course different emission heights exist in the field of view but the errors involved are not

Fig. 4.6(a) Zenith angle and actual distance of observation.

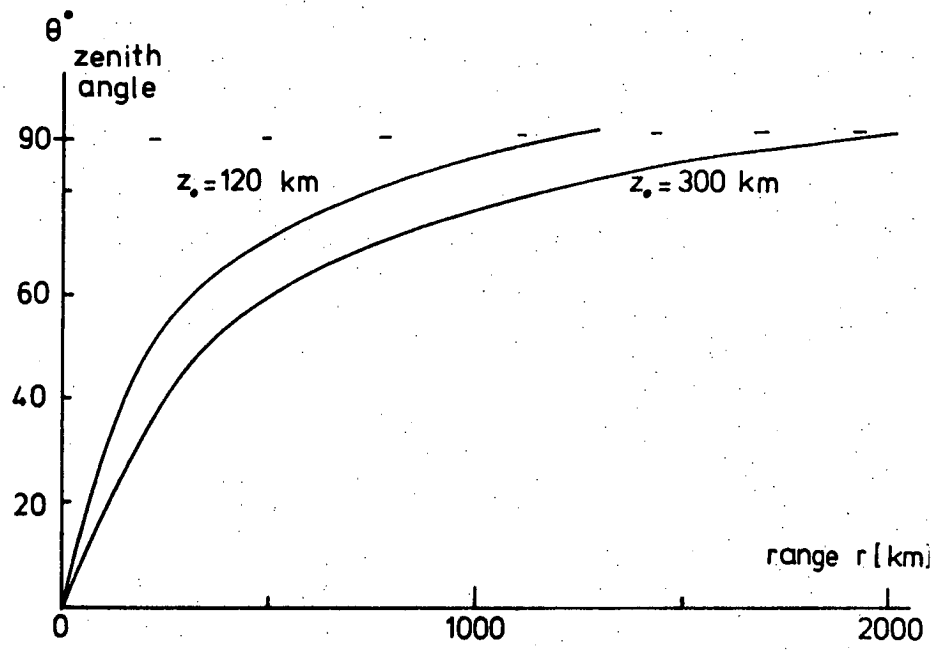

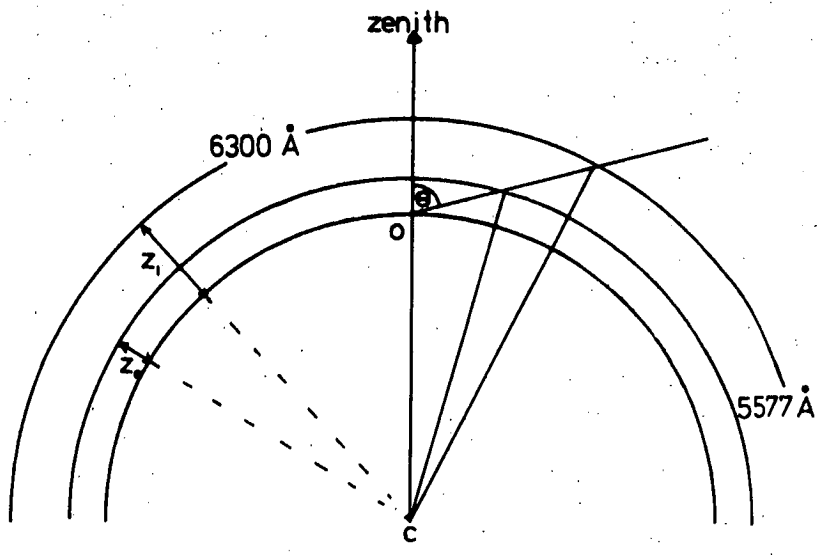

Fig. 4.6(b)

great.

Contour maps based on this display were plotted either by hand or by computer; the latter was not always satisfactory near the zenith where gradients in intensity were small.

Chapter 5 OI AIRGLOW AND THE MIDLATITUDE IONOSPHERIC TROUGH

PART I

5.1 Introduction

One of the most significant ionospheric features to be discovered since the introduction of topside sounding satellites is the midlatitude ionospheric trough. This is a rather severe depletion of the ionospheric F-region which on a north-south transit appears as a sharp dip, then rise, in an electron density (or total content) versus latitude display. The drop in electron density can be up to an order of magnitude at all heights over only a few degrees of latitude; at 1000KM the fall in light ion density can be even more dramatic. The trough is aligned east-west magnetically and appears only in the non-sunlit part of the hemisphere; it moves in a regular way on a local time-magnetic latitude display. It appears to be most prominent on early winter mornings. The trough was first detected from topside soundings but a number of workers have shown that it can be observed from ground-based ionosondes and that the trough extends below the F-region peak. One of the reasons why the trough had not been detected earlier appears

to be that the ionosondes had a very poor spatial resolution; also they were not sensitive enough at low frequencies. Some work on the trough has been done by ground based monitoring of beacon satellite signals but this also suffers from latitude resolution difficulties.

In spite of the extensive observations of the trough there seems to have been little progress in explaining its formation. Generally it is thought that the quiet-time trough represents a region at midlatitudes which is between the auroral zone, where night-time ionization is always occurring, and the equatorial ionospheric mass. However, the temporal morphology and the sharpness of the trough's edges are not easily explained. The purpose of the present study is to obtain data on the recombination rates inside, and equatorwards of the trough. This is possible because during the early morning Hobart is usually underneath the trough whereas Canberra is very rarely so. Now there are ionosondes at both these stations and Canberra lies within the field of view of 6300Å observations from Hobart. Both types of data yield independent information on recombination rates.

Firstly it is shown how the trough's formation may be studied from published ionospheric data (I.P.S. Series D) as well as from the ionograms themselves. The general morphology is found to be similar to that deduced from total content observations in the northern hemisphere. Having established this, an estimate using model ionospheres and neutral atmospheres of the recombination rates within the trough is made. It is then found that this estimate is clearly too low to explain the observed 6300Å levels within the trough if recombination is the sole cause of the airglow. The implications of this are discussed in part II (Chapter 6) of this study and it is shown that none of the current ideas on trough formation appears to be adequate to explain these observations. A more adequate theory is postulated.

5.2. The Midlatitude Ionospheric Trough - A Review

5.2.1. Topside observations

Thomas and Sadar (1964) and Muldrew (1965) appear to be amongst the first observers to report the existence of persistent troughs in the mid-to-high latitude ionosphere. Their results are from the topside sounder Alouette I

which measured the x-mode penetration frequency of the F2 layer, fxF2 at intervals of 1^{o} of latitude. This resolution enabled Muldrew to show that fxF2 had a very pronounced minimum at midlatitudes and several more minima at higher latitudes. Upon moving into this midlatitude minimum or 'trough' fxF2 could change from 6MHz to 2MHz (an electron density drop of 9.1) over 2^{o} of latitude. Muldrew's high latitude troughs were not as deep but narrower; however they were not as regular or as persistent as the midlatitude or 'main' trough. Sharp (1966) measured ion density in situ using an ion trap on a polar orbiting satellite at various heights above and below the F-region peak. The ion concentration could change very rapidly with latitude at all heights particularly at the polewards edge of the trough. Fig. 5.1. taken from Sharp (1966) shows a trough in which the concentration changed by a ratio of 47.1 over 170KM. Several workers report that at certain times the fall in light ion concentration (He^{+}, H^{+}) can be very severe in the high ionosphere, e.g. Colin et al. (1969); Taylor et al (1968)

The topside sounders can only give electron density profiles down to the F-region peak. From

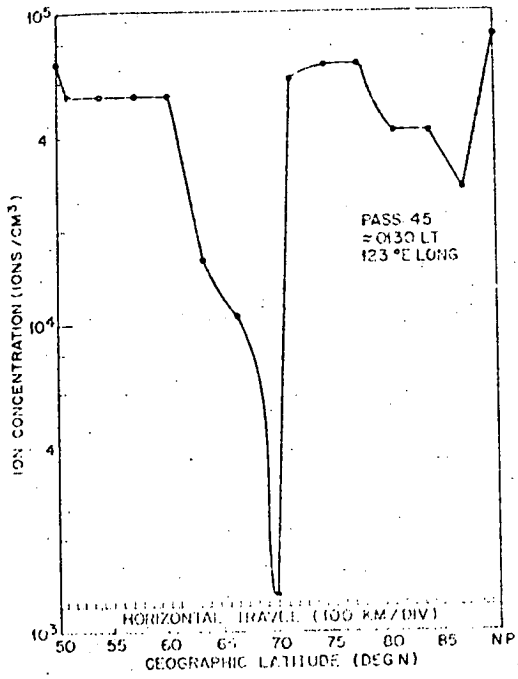

Fig. 5.1 A deep ion trough from Sharp (1966).

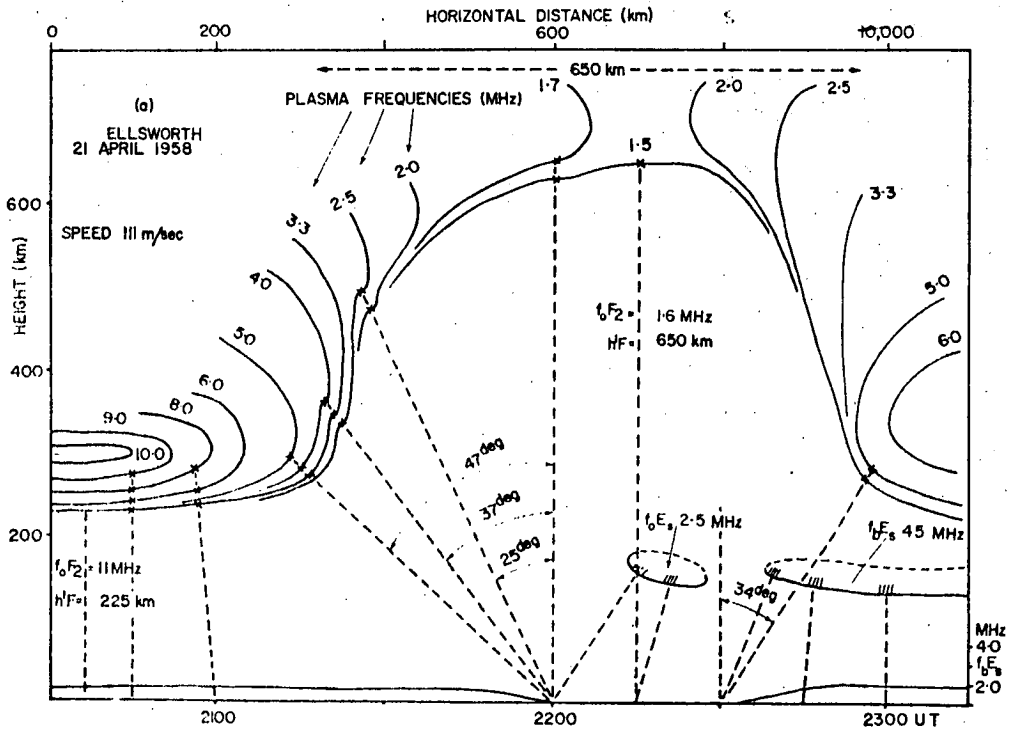

DISTRIBUTION OF IONIZATION FOR BOTTOMSIDE TROUGH ON 21 APRIL, 1958.

Fig. 5.2 Bottomside trough from Bowman (1969).

the work of Nelms (1964), Thomas et al (1966) Chan and Colin 1969) and similar reports it seems that the effects of the trough are more or less uniform from the F-region peak up to the 1200KM level. Of more significance for recombination and thus 6300Å airglow aspects is that the trough effect is equally intense below the F-region peak. This has been shown from ground-based observations.

5.2.2 Ground-based Observations

Some workers operating ionosondes in the region of the auroral zone have found that as well as the normal night-time F-region echoes there often occurs a second echo (sometimes called an 'oblique echo'). This second echo (Anzari 1963, Bellchambers et al 1962) has a higher critical frequency, suggesting it is being reflected off a region of higher electron density, and has as well a large but very variable critical range. Stanley (1966) from observations made at College (L = 5.4, $\Lambda = 64^{\circ}N$) during 1964 - 1966 showed that oblique echo is probably caused by the reflection of the broad band ionosonde signal off the pole-wards edge of the trough. Stanley shows that the 'normal' F-region had at this time, a very low critical frequency (< 1 MHz) which was below the usual limit

of sensitivity of the ionosondes generally in use (~ 1.5 MHz). He suggests that many auroral zone ionograms are routinely measured incorrectly because of this, the measured values of foF2 being for the oblique rather than the (invisible) normal echo. The general morphology of this 'ionization cliff' which causes the second echo was found to be very similar to the midlatitude trough of Muldrew (1965) and presumably it was the sub-peak continuation of the sharp polewards edge of the trough. The equatorial edge and the ionization contour of the sub-peak trough have been observed from the ground by Bowman (1969). He was able to do this because the stations he used in this analysis (mainly Ellesworth 62.6°S geomagnetic) were situated on the Filchner Ice Shelf and interference effects from this enabled directional information to be drawn from the ionograms. Fig. 5.2 shows one of his troughs. Note the extremely high values of h'(f) within the trough. These are rather puzzling and do not agree with the values of h'f obtained by Stanley (1966). However, these sub-peak troughs behaved exactly like the topside troughs and it is generally accepted that both are

different aspects of a depletion at all heights of the F-region. It has even been suggested Muldrew (1965) that this depletion extends into the exosphere where it is known that a fairly sharp drop in electron density occurs at a distance of 3.5 earth radii on the night side (Carpenter 1963). This 'knee' or 'plasma-pause' moves in a similar fashion in local time to the trough although some aspects of its morphology are quite different according to Liszka (1967). The exact relationship of the two phenomena is, however, by no means certain.

5.2.3 Local time movement

All workers agree that from 1400LMT to 0000LMT the trough moves from near $\Lambda = 80^{\circ}$ down to $\Lambda = 56^{\circ}$. It is generally accepted that at time of high Kp the trough moves even closer to the equator ($\Lambda = 50^{\circ}$S) which for a 20° wide trough would imply that most of midlatitude region is under the trough. All this is similar to the movement of the auroral oval.

During the early morning the trough drifts back slowly in latitude as can be seen from figs. 5.3 and 5.4. These figures are taken from Bowman (1969) and are based on Muldrew's (1965) results.

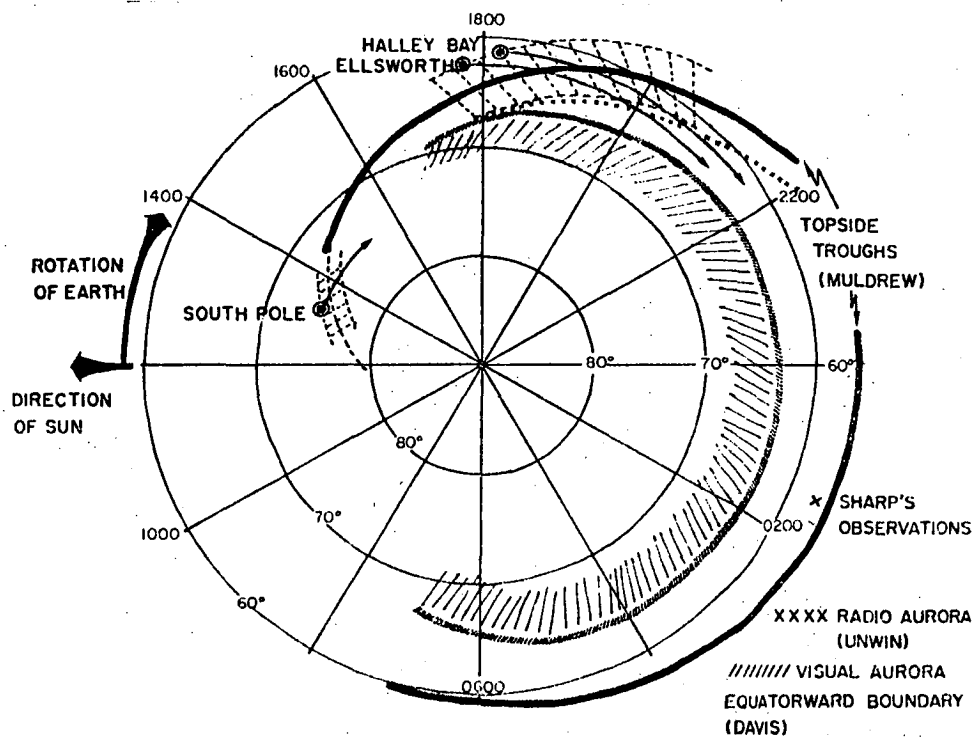

Fig. 5.3 Diurnal movement of the trough (low k_p)

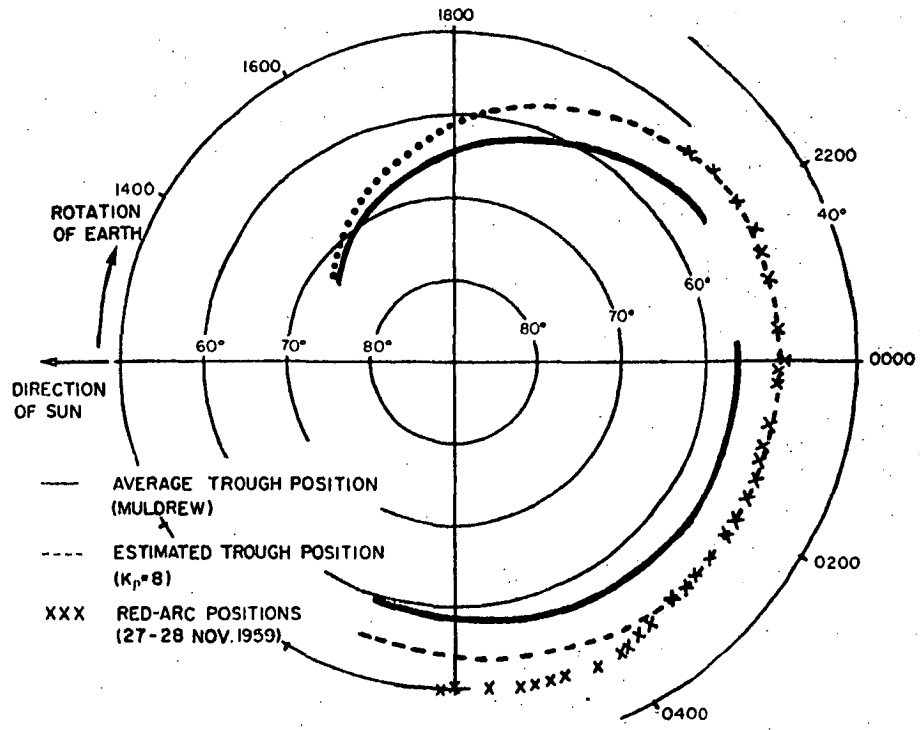

Fig. 5.4 Diurnal movement of the trough (high K_p)

It is quite clear from them that Hobart at $\Lambda = 54^{o}$ will be underneath or on the edge of the trough on even quiet nights. Because of the wide field of view for 6300Å observations the whole of the trough can be observed from Hobart.

5.2.4 Trough width

The width of the trough can vary greatly. Sharp (1966) defined the 'half-width' as being the distance between the two points, one on each side of the trough, whose 'depth' is one half of the maximum depth of the trough. He found this could vary from 3^{o} to 20^{o} even over a few hours. When the trough does narrow it does so by moving in towards the centre. Sharp says that the width is inversely proportional to the particle energy precipitated into the auroral zone.

5.2.5 Seasonal variations

The echoes reported by Stanley (1966) showed a very marked seasonal variation. During December and January the echoes occurred on nearly 100% of all nights whereas in June and July they only occurred on 5% of the nights. This could be interpreted as due to the trough's vanishing in summer. A more detailed view was obtained by

Liszka (1967) observing signals from the beacon satellite S66 from Kiruna (Λ = 67°N). He published mean total-content contour maps in latitude/local time for each season. These are shown here as figs. 5.5 and 5.6. Because of the inevitable latitude integrating effect of such measurements the troughs shown here do not have very sharp edges. However, the trough is clearly visible at all seasons except for summer. The trough is widest and most longitude extensive in winter. It is furthest south between midnight and 0300LMT The absence of the trough in summer is not generally agreed for some topside results e.g. Chan & Colin (1969) appear to show a trough in the summer hemisphere, but this is weaker than the winter one. This point is by no means settled however and it seems possible that the situation is different at differing longitudes.

5.3 Observations: (1) Ionospheric

5.3.1 Solar cycle and seasonal variations

Fig. 5.7 is taken from Ellis and Hamilton (1965) and shows the frequency fxF2 (x-mode critical frequency of the F-region) from several topside passes near the longitude of Hobart. The

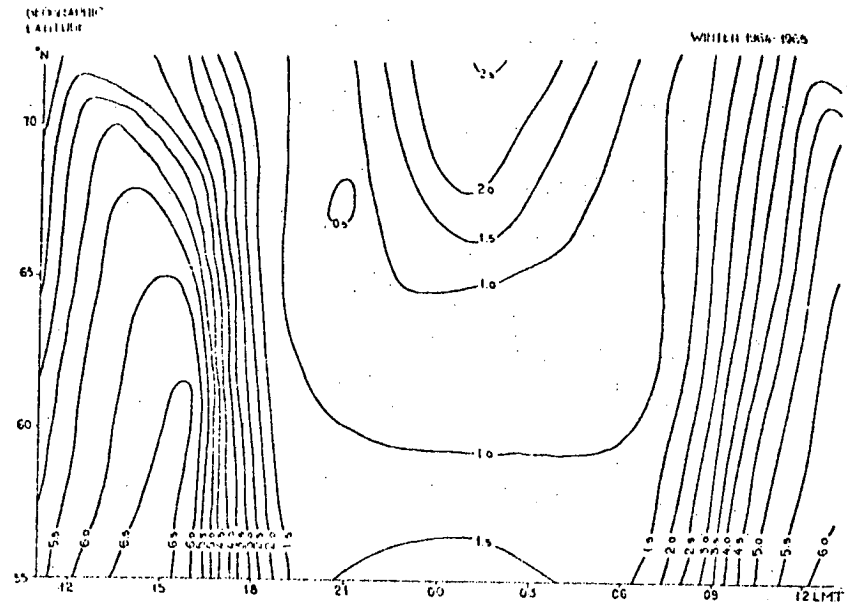

Fig. 3. Contours of ionospheric electron content (in 10^{-16} electrons/m^2) during winter 1964-65.

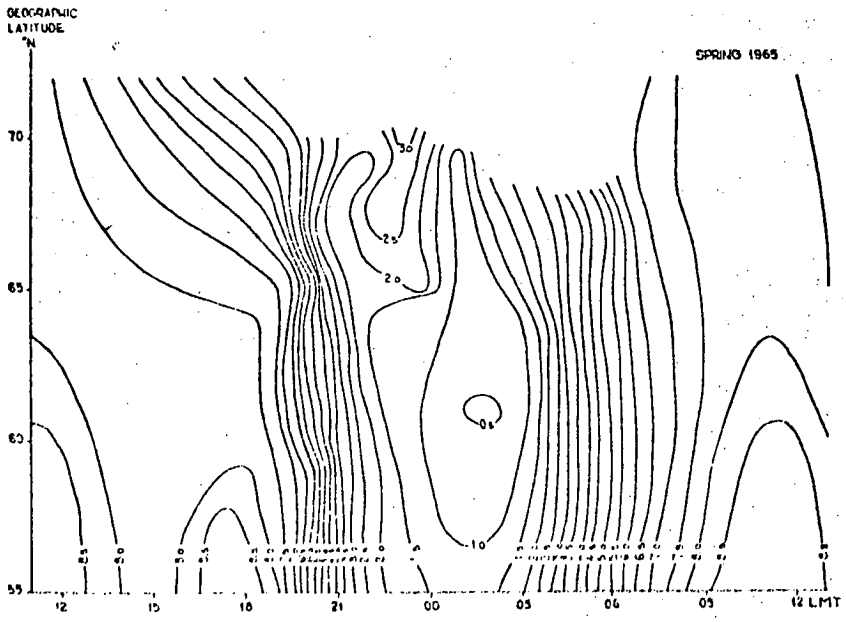

Fig. 4. Contours of ionospheric electron content (in 10^{-16} electrons/m^2) during spring 1965.

Fig. 5.5 Total content observations of the trough - from Liszka (1967).

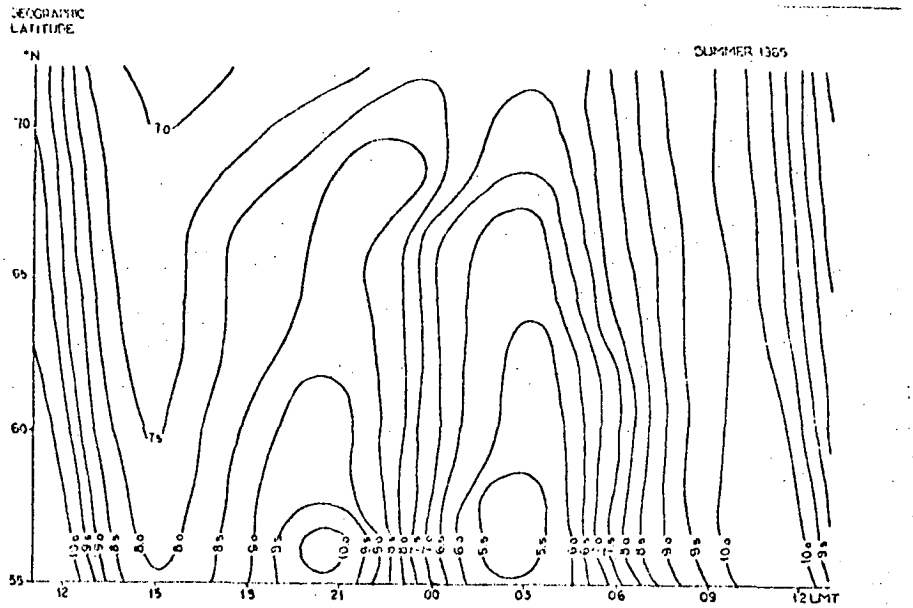

Fig. 5. Contours of ionospheric electron content (in 10^{-16} electrons/m^2) during summer 1965.

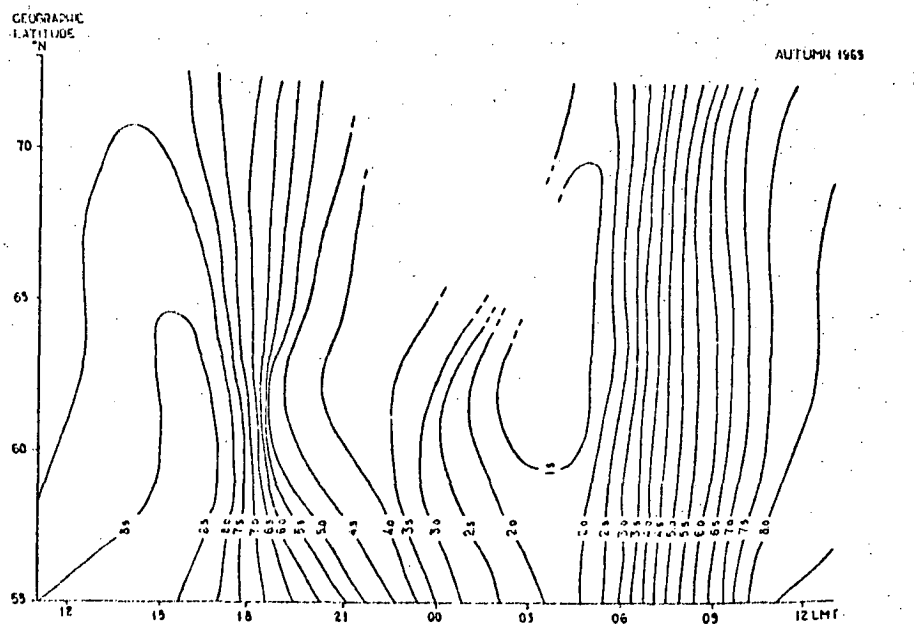

Fig. 6. Contours of ionospheric electron content (in 10^{-16} electrons/m^2) during autumn 1965.

Fig. 5.6 Total content observations of the trough - from Liszka (1967).

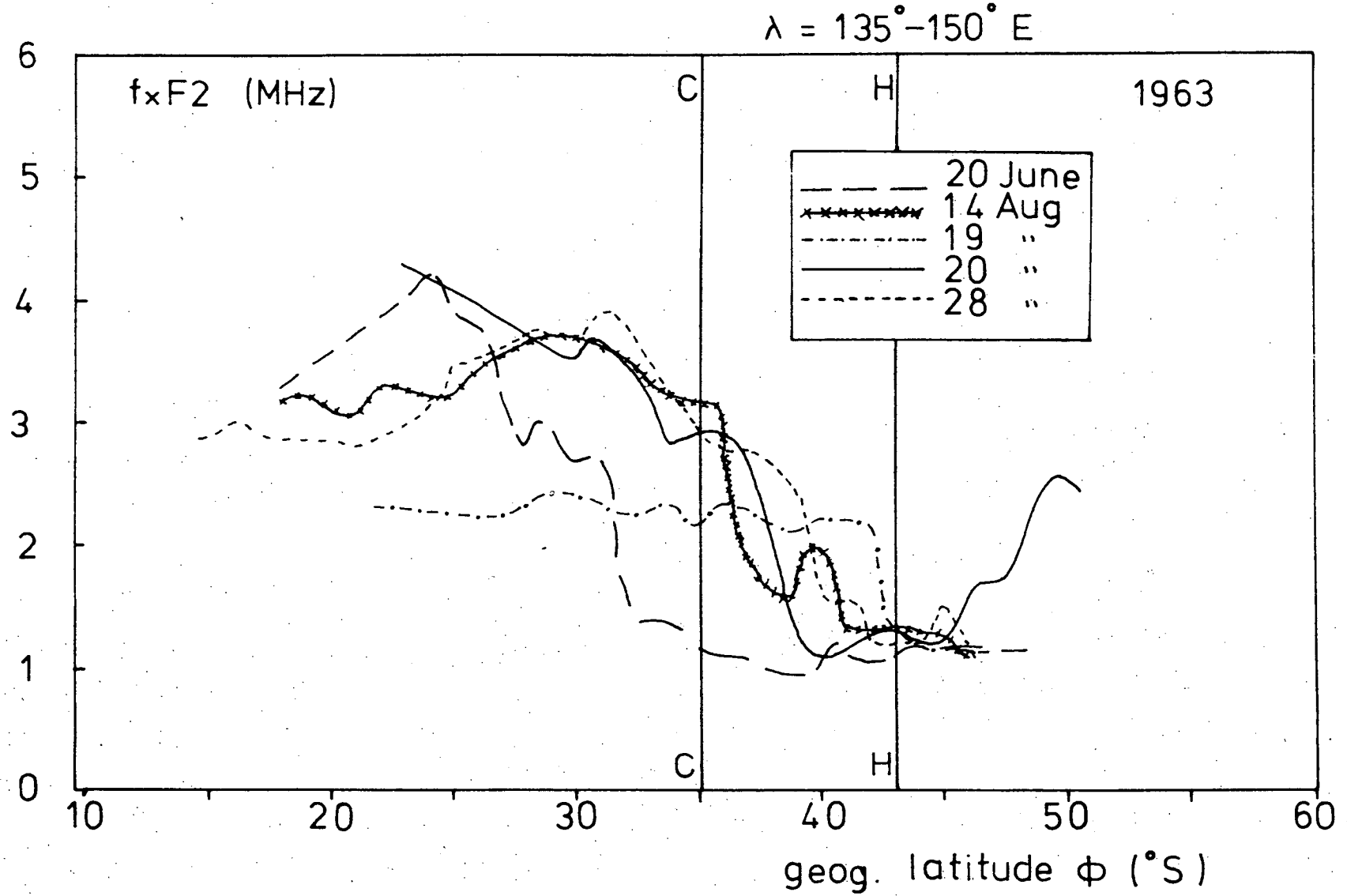

Fig. 5.7 The trough near Hobart (Ellis & Ham. Ito. 1966)

transits are all early morning ones in winter and, as might have been expected from section 5.2, they thus show the northern part of well developed troughs. The depth is about 10.1 (in peak density) and their width is at least 15^{o}. Clearly Canberra is not usually under the trough but Hobart is. It appears then that ground-based observations of foF2 should show quite different behaviour at this time at the two stations. Some measure of the 'depth' of the trough should be obtainable by comparing values of foF2 obtained at the same time by the two stations. Now the peak electron density Ne is related to foF2 by:

$$Ne = \pi m_e (foF2)^2 e^{-2} \qquad 5.1$$

where m_e and e are the electron mass and charge in c.g.s. units. The ratio of the peak density at Canberra, Ne(C), to that at Hobart, Ne(H), is expressed as a percentage:

$$F_{HC} = 100 Ne(H) / Ne(C)$$
$$= 100 \left[foF2(H)\right]^2 / \left[foF2(C)\right]^2 \qquad 5.2$$

This ratio F_{HC} can then be obtained from published hourly values of foF2 (I.P.S. series D). Fig. (5.8) shows how F_{HC} varies during the day for each month in the year 1964 and 1968. Obviously

Fig. 5.8 The night-time depletion of the ionosphere at Hobart, is very regular and greatest in winter and solar minimum.

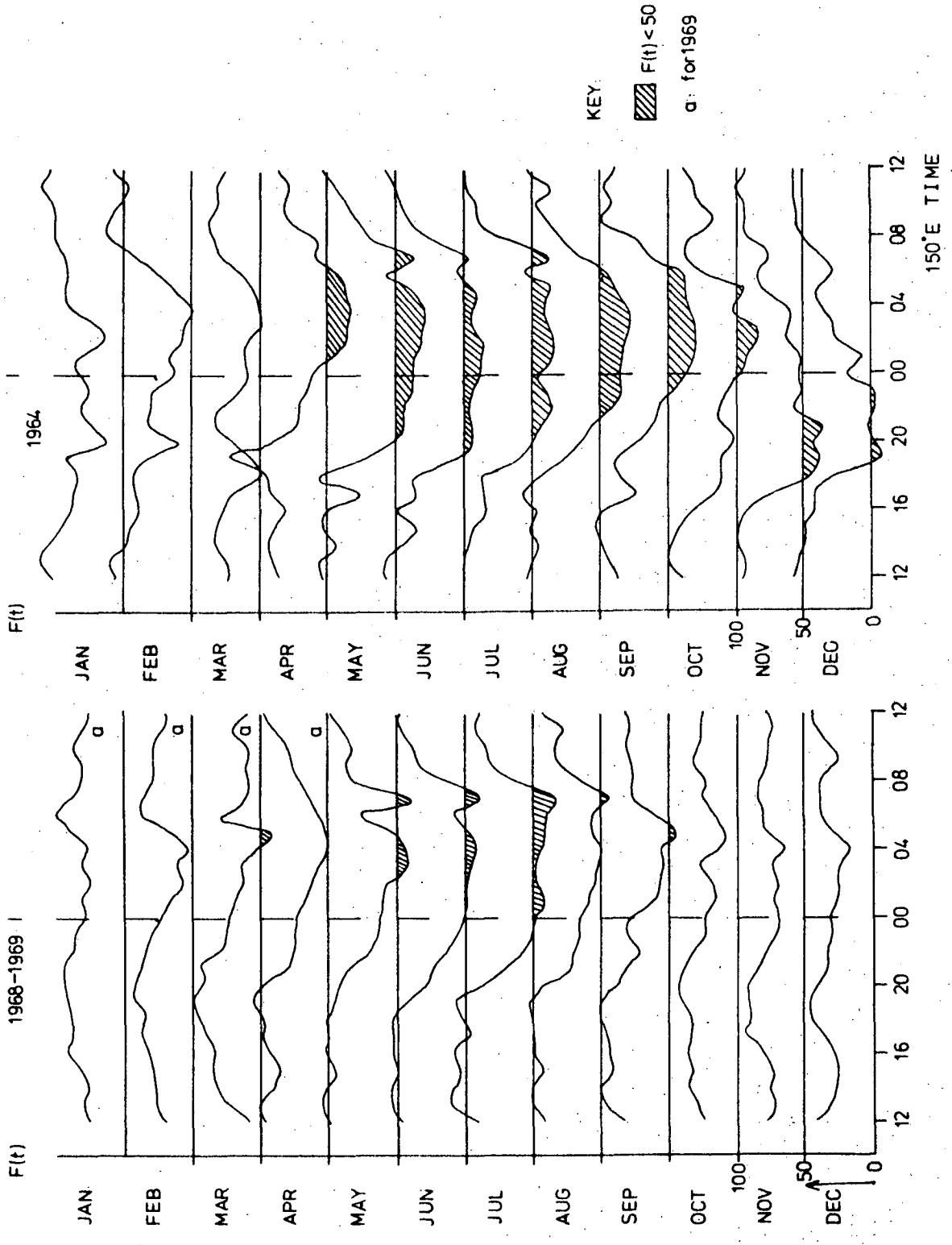

values of F_{HC} less than 100 implies that the peak density at Hobart is less than at Canberra. During the night on these monthly median data this is always so. It should be emphasised that the same statement holds for every individual night examined i.e. at each hour of all nights in all seasons the peak density at Hobart is less than (or equal to) the peak density at Canberra. This is rather remarkable for the same is not true of the daytime densities. Note that in many months the density at Hobart is less than half that at Canberra. The main features of fig. 5.8 are:

1. At both extremes of the solar cycle there is only a significant difference in daytime peak densities in summer.
2. In the winter and the equinoxes the density at Hobart is less than half that at Canberra at night.

   This comparative depletion begins earlier nearer the winter solstice.
3. At solar minimum (1964) the depletion begins earlier than at maximum and is more severe. Intervening years (not shown here) are intermediate in behaviour.

4. Some months (e.g. May) show a second sharp minimum of F_{HC}. This is probably due to the earlier sunrise at Canberra and is thus unrelated to the presence of the trough.

This shows that at night in the winter and equinoxes there is a strong decrease in peak electron density from $\Lambda = 45^{\circ}$ to $\Lambda = 55^{\circ}S$. This gradient is not present during the day and it seems probable that it is due to the trough formation. If this is so then it seems that the trough is more marked at solar minimum. In the next section it will be shown that the formation of the trough is due as much to lack of maintenance as to increased recombination.

5.3.2 Formation of the trough

Figs. 5.9, 5.10, 5.11 and 5.12 show contour maps of Ne_m obtained from the published values of foF2 for I.P.S. stations situated near the $150^{\circ}E$ meridian. These stations are listed in Appendix 'A' and it is unfortunate that no station operates further south (say at Macquarie Island). However, these figures do show how the equatorwards edge of the trough forms and the seasonal and solar cycle variations in this formation.

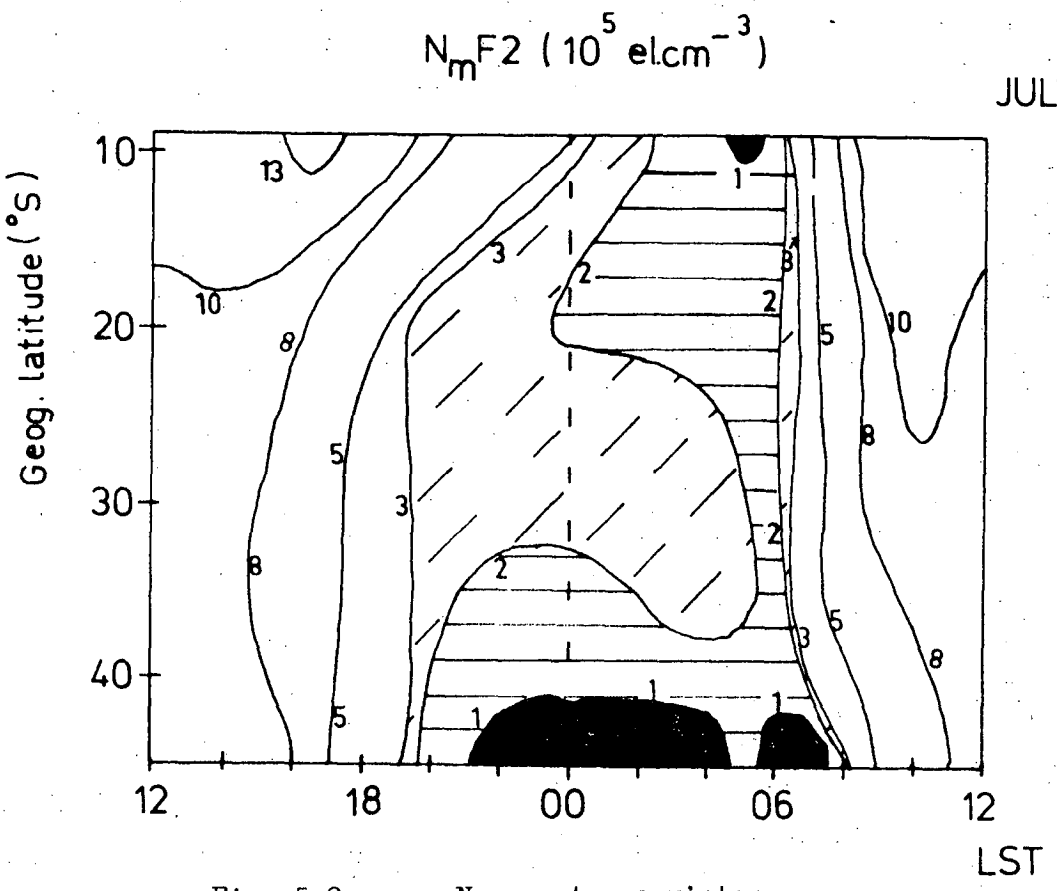

Fig. 5.9 Ne_m contours winter

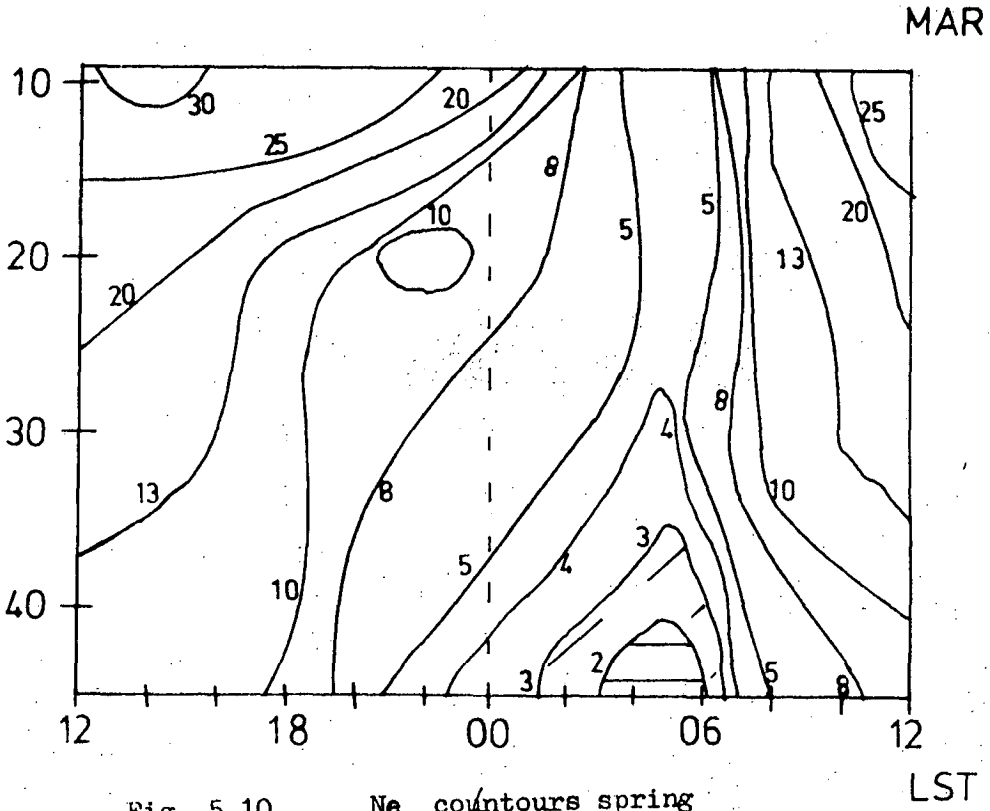

Fig. 5.10 Ne_m countours spring

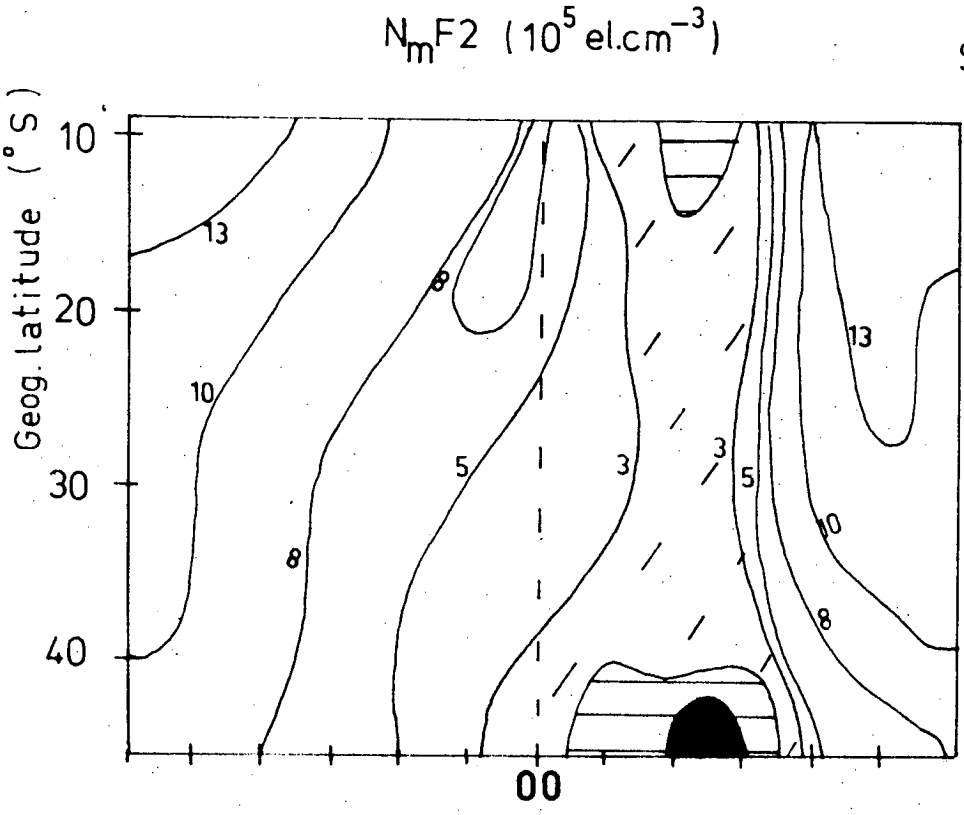

Fig. 5.11 Ne_m contours autumn

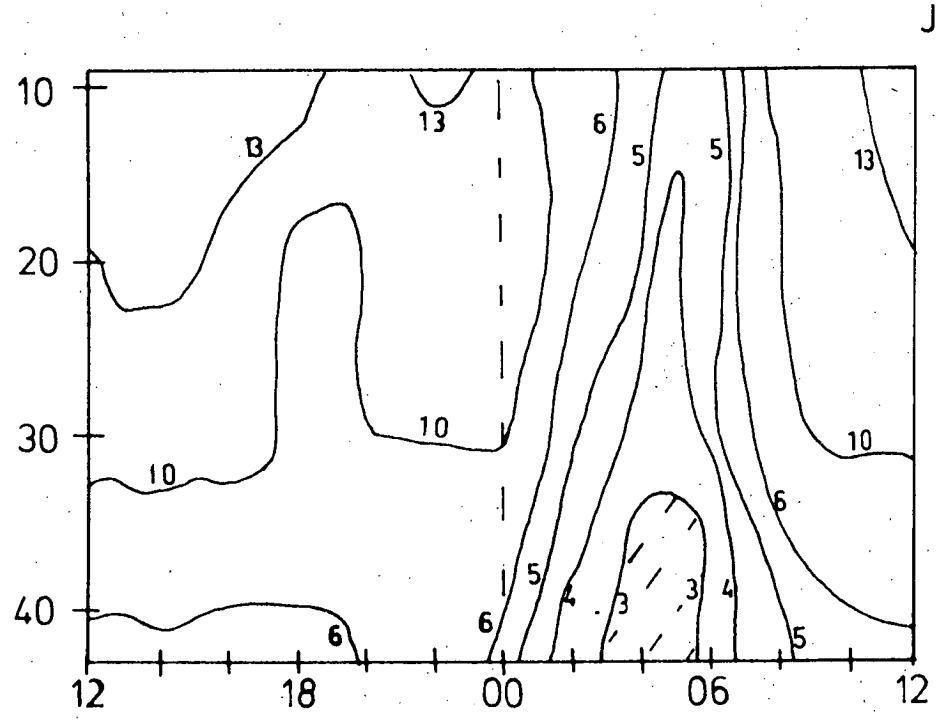

Fig. 5.12 Ne_m contours summer

The main features of the trough formation are:

A. Winter

From fig. 5.9 it seems that southwards of 25°S (geog.) there is little difference in daytime peak densities. However, between 2000 and 2200LMT a steep gradient in electron density forms south of about 40°S which persists until sunrise. This gradient forms about two hours earlier at solar minimum than at solar maximum. Northward of about 25°S the peak electron density decays monotonically all night. Southward of this there is an increase in Ne_m in the early morning. This increase is greatest near 30°S. Because of this effect the gradient near 40°S is greatest near this time. The increase is relatively stronger at solar minimum. It appears from this that the equatorwards edge of the trough forms because the region south of it is poorly maintained compared with the region to the north.

B. Equinox

Figs. 5.10 and 5.11 show contours of Ne_m for the equinoctial months of March and September. March is similar to fig. 5.12, a summer month, whereas September is more like the winter months.

This suggests that the change from winter to summer behaviour is very rapid. However, both months do show a step gradient beyond 40°S in the early morning. This forms about four hours after the gradient in fig. 5.9. It appears to rise from the same basic cause as the winter gradient i.e. lack of maintenance south of 40°S.

C. Summer

This is the only month which shows a distinct daytime gradient in peak density. This is of course what would be expected from the classical theory of the formation of the ionosphere Chapman (1945), Ratcliff (1951). However, note that an increase of Ne_m occurs at local sunset although only weak south of 40°S. This has the effect of increasing the strength of the gradient during the night.

The above descriptions are very similar to Liszka's (1967) total content work. The origin of the trough seems to be largely due to the fact that the night-time maintenance of the F-region is latitude (and seasonally) dependent. That the drop in electron density between Canberra and Hobart is very sharp on winter mornings (i.e. it would appear as a trough wall on a topside transit)

is shown from spread-F data in the next section.

5.3.3 Reflections from the trough

Night-time ionograms obtained at Hobart are usually unsatisfactory for real-height analysis. This situation is worst at those times when the trough is overhead and this, it is believed, is no coincidence. Firstly sporadic-E is often present at these times and according to Bowman (1969) the troughs at Ellesworth were always preceeded by sporadic-E. More persisent and regular, however, was the occurrence of spread-F. Fig. 5.13(a) shows a typical ionogram showing the usual type of spread-F which occurs at Hobart. This is known as 'frequency spread-F' and according to King (1970) is caused by echoes reflecting off steep ionization density contours as shown in fig. 5.13 (b). It seems possible, thus, that the spread-F results from echoes off the equatorwards edge of the trough. This is supported by the onset times of the spread-F. Fig. 5.14 shows histograms for three representative months in 1969 of the number of times in a given month spread-F is present at a particular hour. By comparing this figure with figs. 5.10-

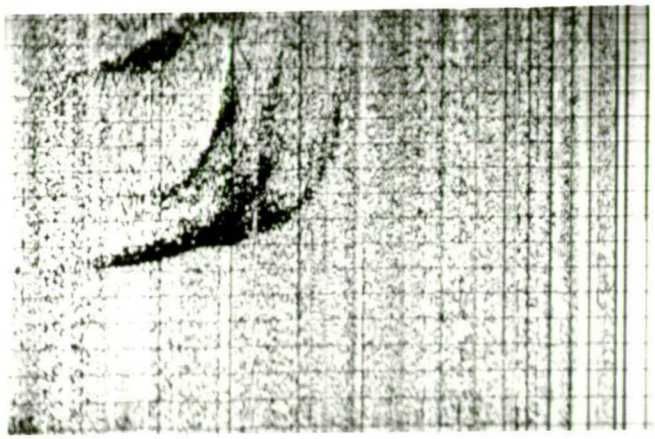

Fig. 5.13(a) Frequency spread - F at Hobart.

From G. A. M. KING (1970)

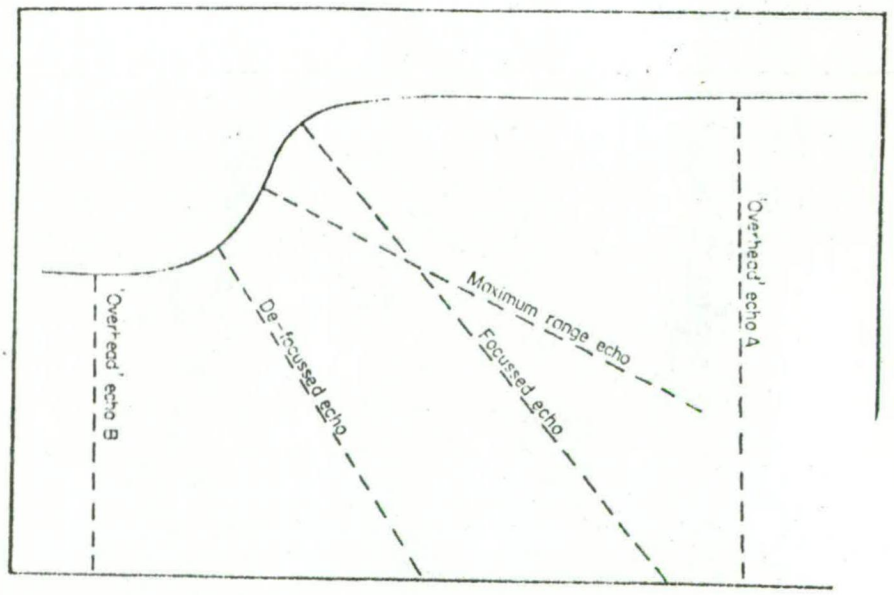

Sketch showing the geometry of reflection from a 'step'.

Fig. 5.13(b) Probable cause of frequency spread F.

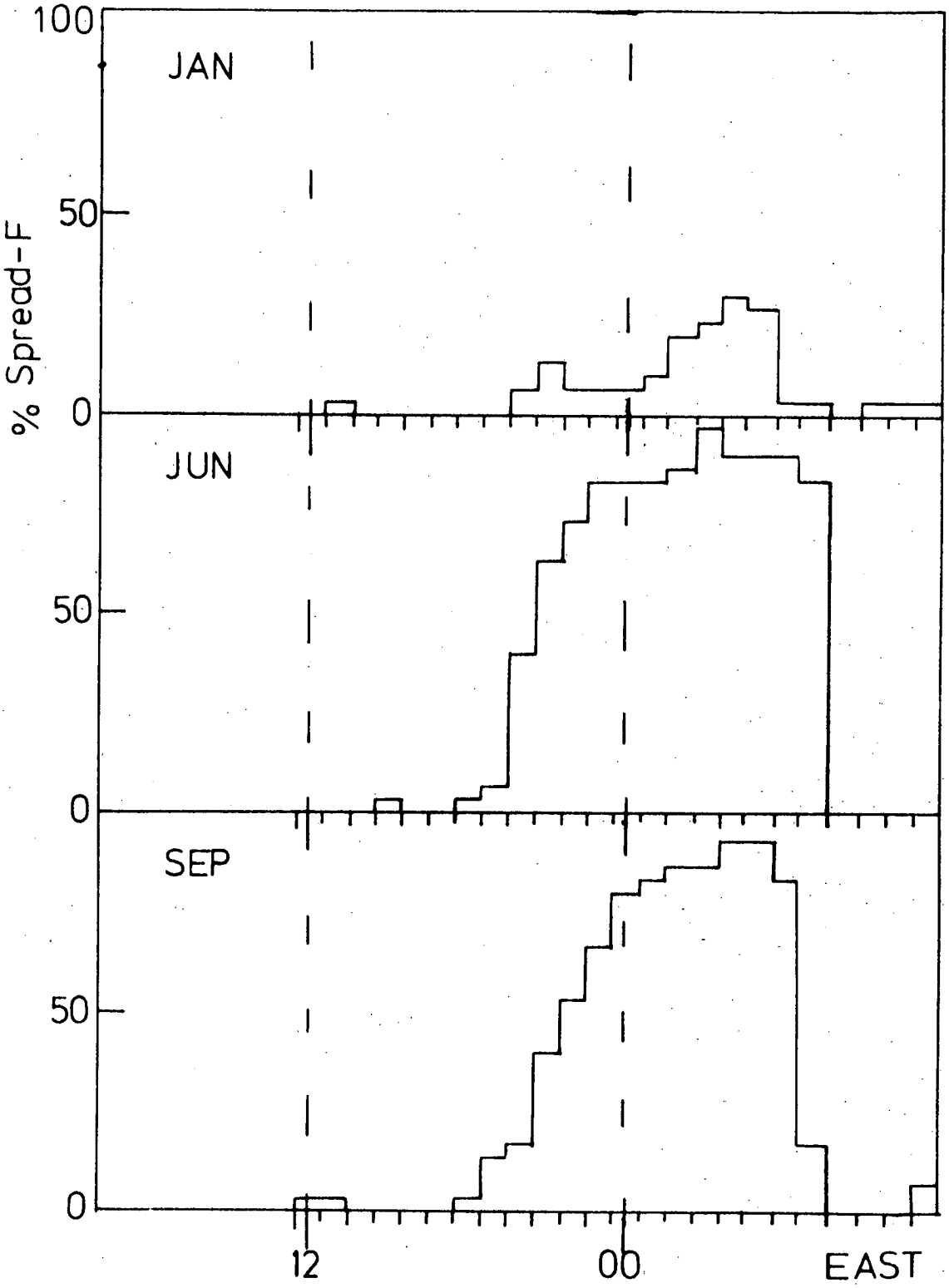

Fig. 5.14 Percentage of time during months when spread - F occurs.

5.12, it is quite clear that spread-F occurs when the electron density gradient is strongest south of 40°S. During the day-time spread-F hardly ever occurs, showing that even in summer the gradient is only gradual. It is also rare at Canberra even at night. To get these sorts of echoes at night there must be a sharp drop in electron density somewhere between Canberra and Hobart i.e. the equatorwards edge of the trough is quite steep even on normal nights. This is consistent with the topside troughs of fig. 5.6.

5.3.4 F-region heights within the trough:

The importance of the height of the F-region in determining the amount of recombination has been emphasised in Chapter 2. Fig 5.15 shows hm F2 differences between Canberra and Hobart for various months in 1969. The values of h_mF2 have been obtained by Shimazaki's (1955) formula:

$$h_mF2 = \frac{1490}{MUF} - 176 \qquad 5.3$$

where h_mF2 is in kilometres and MUF is the published (I.P.S. series D) monthly median of the M (3000) F2 parameter (see for example I.P.S. series H, 66, 1969). This forumla is only accurate to about ± 13 KM (Wright and McDuffie 1960), a range which

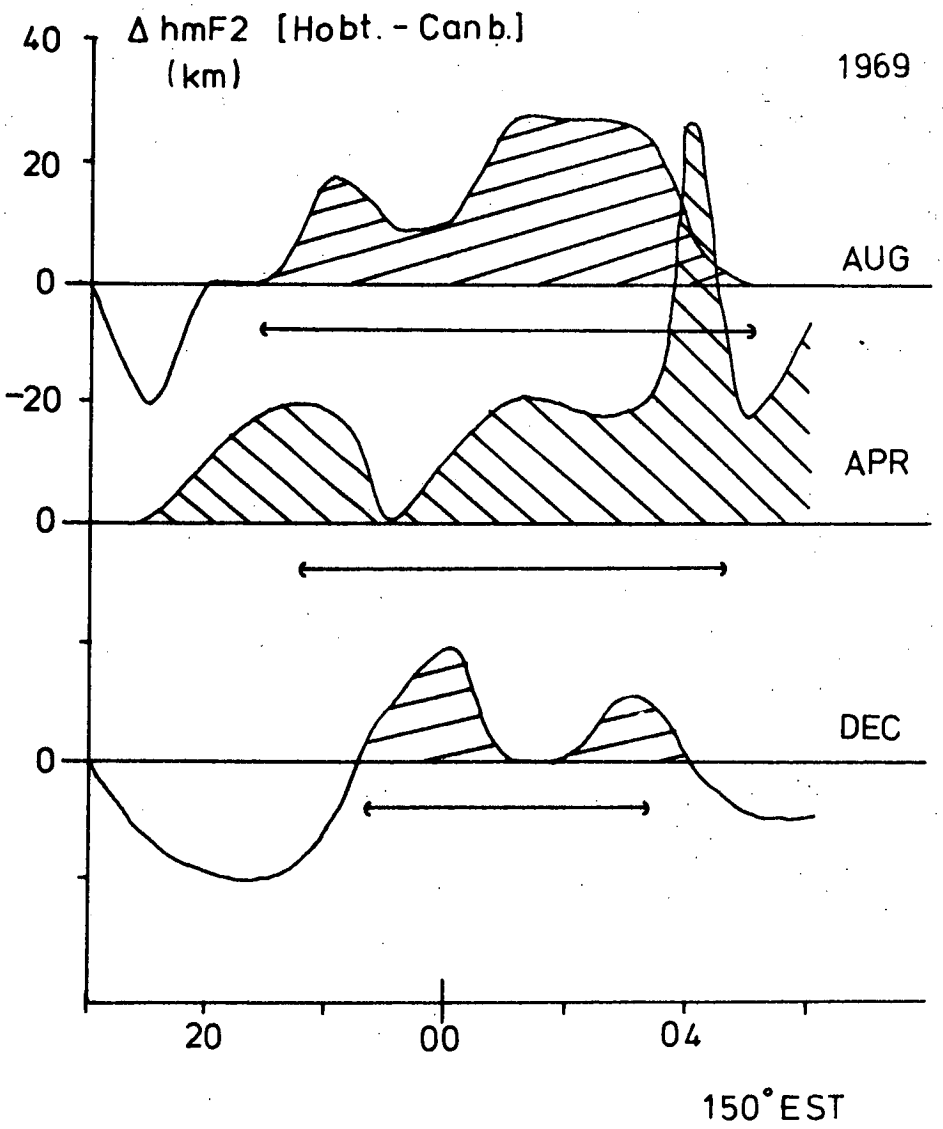

Fig. 5.15 Height of F-region peak at 150°E.

can mean an enormous difference in recombination values. However, the general trend is obvious from fig. 5.15 i.e. on the median nights the ionosphere is higher at $\Lambda = 55^{\circ}S$ than at $\Lambda = 45^{\circ}S$ at 0000 LMT in all seasons. This is consistent with northern hemisphere results (Wright 1960). It should be noted that on individual nights the same situation nearly always occurs in the early morning. However, it is only on extremely disturbed nights that ionospheric heights reach those reported by Bowman (1969). Thus even when, from electron density data, it is believed Hobart is under the trough, the heights h'f and h_mF2 are only slightly higher inside than outside the trough. This tends to support the findings of Stanley (1966) at College. However, combined with the great decrease in electron density this small increase in height should lead to a large decrease in recombination from $\Lambda = 45^{\circ}$ to $\Lambda = 55^{\circ}$ during the trough's presence.

5.4 Recombination - latitude variation:

5.4.1 Neutral temperature and atmospheric density

Based on satellite drag results the semi-empirical static diffusion models of Jacchia

(1965 a and b) and Jacchia and Slowey (1967) are usually used in estimating latitude variations in the exospheric (neutral) temperature T_∞ . In these and similar models (e.g. CIRA 1965) the atomic/molecular height profiles depend entirely on the exospheric temperature because the lower boundary (120 KM) conditions are fixed. A closer examination of this is made in the next chapter but the important point here is that the molecular concentrations of O_2 and N_2, at a given height, increase as T_∞ does. Now Jacchia (1965) provided for an increase in T_∞ with latitude which implies an increase in $[O_2]$ and $[N_2]$ at a given height with latitude. Thus Hobart will have a more dense neutral atmosphere than Canberra which will tend to lead to more recombination at Hobart. The magnitude of this gradient in density varies with local time, solar declinations and solar activity. The relation used by Jacchia (1965) is:

$$T = T_o \frac{(1 + R \sin^m \theta)}{(1 + R \cos^m \eta - \sin^m \theta, \cos^n \frac{\tau}{2})} \qquad 5.4$$
$$(1 + R \sin^m \theta)$$

where T_o is the lowest value of T_∞ anywhere on the globe (this can be calculated from the 10.7 cm solar flux) and R is a factor such that RT_o is the highest temperature on the globe; m and n are constants, τ is a measure of local time containing a lag factor); and η and θ are found by:

$$\eta = \tfrac{1}{2}(\phi - \delta) \qquad 5.5$$

$$\theta = \tfrac{1}{2}(\phi + \delta) \qquad 5.6$$

where ϕ is geographic latitude and δ solar declination. To obtain an estimate of the molecular concentration latitude gradient between Hobart and Canberra three months in 1969; January (summer), July (winter and September (equinox); are considered. Using the mean 10.7 cm (Ottawa) levels for these months R, and T_o have been obtained from Jacchia's (1965) data. Using 5.4 above with the relevant values of ϕ & δ values of minimum T_∞ at Hobart (H) and Canberra (C) can be calculated thus:

Table 5.1

	$\bar{F}(10.7)$ 10^{-22} $Wm^{-2}(Hz)^{-1}$	H ^oK	C ^oK	HC ^oK
JAN	147.8	1030	1010	20
JULY	141.1	918	910	8
SEP	134.7	956	941	15

The difference between the neutral exospheric temperatures is greatest in summer and least in winter. This implies that density (and thus recombination differences are also greatest in summer and least in winter. To estimate this effect the diffusive separation equations were numerically integrated using the temperature's T_∞ given above and the Harris and Priester (1964) temperature profiles. An outline of this procedure is given in the Introduction (section 5) to the CIRA 1965 models and will not be amplified here. Fig. 5.16 shows the mean neutral temperature and O_2 and N_2 height profiles for January, 1969 at 0200 LMT for Hobart and Canberra. However, if the mean height h_mF2 is calculated from 5.3 above for the three months listed in Table 5.2 then it is clear that the difference in molecular density at a given height between the two stations is more than made up by the higher F-region at Hobart. Thus at the F-region peak at 0000 LMT the following values of $[N_2]$ and $[O_2]$ occur:

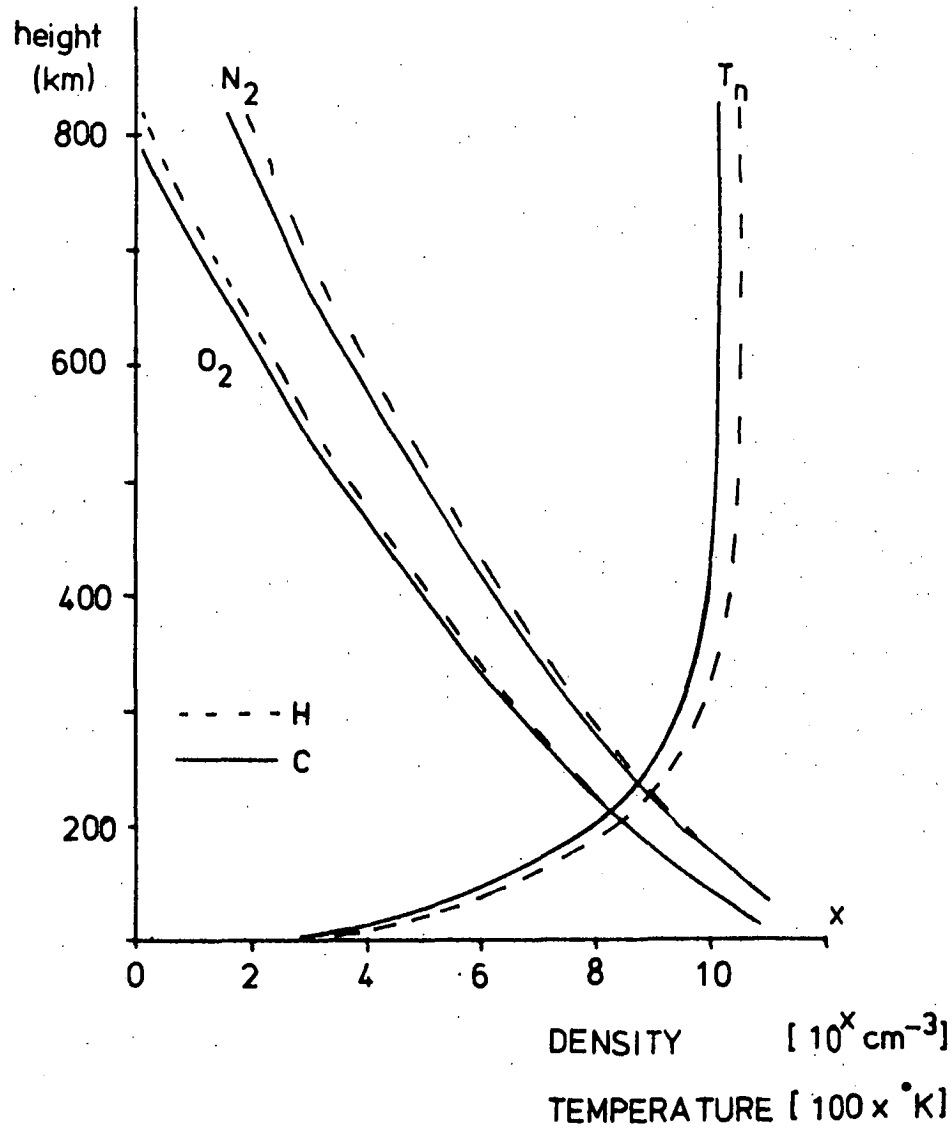

Fig. 5.16 Neutral temperature, N_2 and O_2 profiles for January 1969.

Table 5.2

	10^{-7} x N_2 (cm^{-3})		10^{-6} x O_2 (cm^{-3})	
	H	C	H	C
JAN	1.823	2.842	0.955	1.799
JULY	2.182	4.287	1.204	2.511
SEP	1.701	3.160	0.898	1.772

The median values of h_mF2 and peak electron density Ne at 0000 LMT during these months are:

Table 5.3

	10^{-5} x Ne (cm^{-3})		h_mF2 (KM)	
	H	C	H	C
JAN	5.24	6.80	369	347
JULY	0.84	1.87	338	321
SEP	2.51	3.35	359	338

As dissociative recombination depends strongly on both electron and molecular density it is clear from Tables 5.2 and 5.3, that the amount of recombination occurring at Hobart's F-region's peak is far less than at Canberra's, even in summer. It should be noted that the three months used above are in no way unusual or anomolous.

To obtain an exact estimate of the ratio of recombination between the two stations it is necessary to solve the F-region continuity equation.

5.4.2 Night-time recombination

To obtain an estimate of recombination occurring at F-region heights only the following production and loss mechanisms are assumed to occur at night:

$$O^+ + O_2 \rightarrow O_2^+ + O \qquad \gamma_1$$

$$O_2^+ + e \rightarrow O + O + 6.96 \text{ eV} \qquad \alpha_1$$

$$O^+ + N_2 \rightarrow NO^+ + N \qquad \gamma_2$$

$$NO^+ + e \rightarrow N + O + 2.76 \text{ eV} \qquad \alpha_2$$

The γ's and the α's are the respective reaction coefficients.

The continuity equations yield:

$$\frac{\partial [O_2^+]}{\partial t} = \gamma_1 [O_2][O^+] - \alpha_1 n [O_2^+] - \text{div}\,[O_2^+]\ \underline{V}\ (O_2^+)$$

and

$$\frac{\partial [NO^+]}{\partial t} = \gamma_2 [N_2][O^+] - \alpha_2 n [NO^+] - \text{div}\,[NO^+]\ \underline{V}\ (NO^+)$$

where the $\underline{V}$'s are the ion velocities

Assuming as in chapter 2 and Peterson et al (1966) that both time derivative and divergence terms vanish then these equations reduce to:

$$\alpha_1 \; n[O_2^+] = \gamma_1 [O_2][O^+] \qquad 5.7$$

and

$$\alpha_2 \; n[NO^+] = \gamma_2 [N_2][O^+] \qquad 5.8$$

for charge conservation:

$$n = [O^+] + [NO^+] + [O_2^+] \qquad 5.9$$

The electron loss rate ($cm^{-3}\ sec^{-1}$) is:

$$L_n = -\alpha_1[O_2^+] \; -\alpha_2 [NO^+]n \qquad 5.10$$

Using 5.7, 5.8, 5.9 and 5.10 to remove the ion densities, this yields:

$$L_n = \frac{(\gamma_1[O_2] + \gamma_2 [N_2])n^2}{\frac{\gamma_2}{\alpha_2}[N_2] + \frac{\gamma_1}{\alpha_1}[O_2] + n} \qquad 5.11$$

Using Donahue's (1964) α's and γ's this reduces to:

$$L_n = \frac{n^2 \; 4 \times 10^{-11}[O_2] + 4 \times 10^{-12}[N_2]}{7.7 \times 10^{-6}[N_2] + 3.34 \times 10^{-4}[O_2] + n} \qquad 5.12$$

Using 5.12 an estimate of relative recombination for the median data of Tables 5.2 and 5.3 may be obtained at the F-region peak:

Table 5.4

0000 LMT 1969	$L_n(H)$	$L_n(C)$	R_{HC}
JAN	58.00	111.8	1.93
JULY	11.41	50.8	4.38
SEPT	28.41	66.0	2.32

Where (H) and (C) refer to Hobart and Canberra respectively, R_{HC} is the ratio L_n (C) : L_n (H). Thus for the months shown the recombination occurring in the early morning in Canberra's F-region is always greater than at Hobart. The same result holds for all months during the 1958 - 1969 solar cycle. The ratio is least in summer and greatest in winter. Assuming that the electron height profiles at both stations are similar then the total amount of recombination (not just at the peak) occurring at both stations will be similarly related. Although allowances must be made for quenching it is quite clear that the 6300Å airglow which results from this recombination should be higher at Canberra by the ratio the order of R_{HC} in Table 5.4. In fact this is not so; on 98% of nights the red airglow at Hobart is greater than that at Canberra.

5.5 6300Å Airglow in the trough

5.5.1 Quiet nights

Fig. 5.17 shows all-sky isophote charts for four different quiet ($K_p < 2-$) nights at 0000 LMT. The airglow is weaker to the north

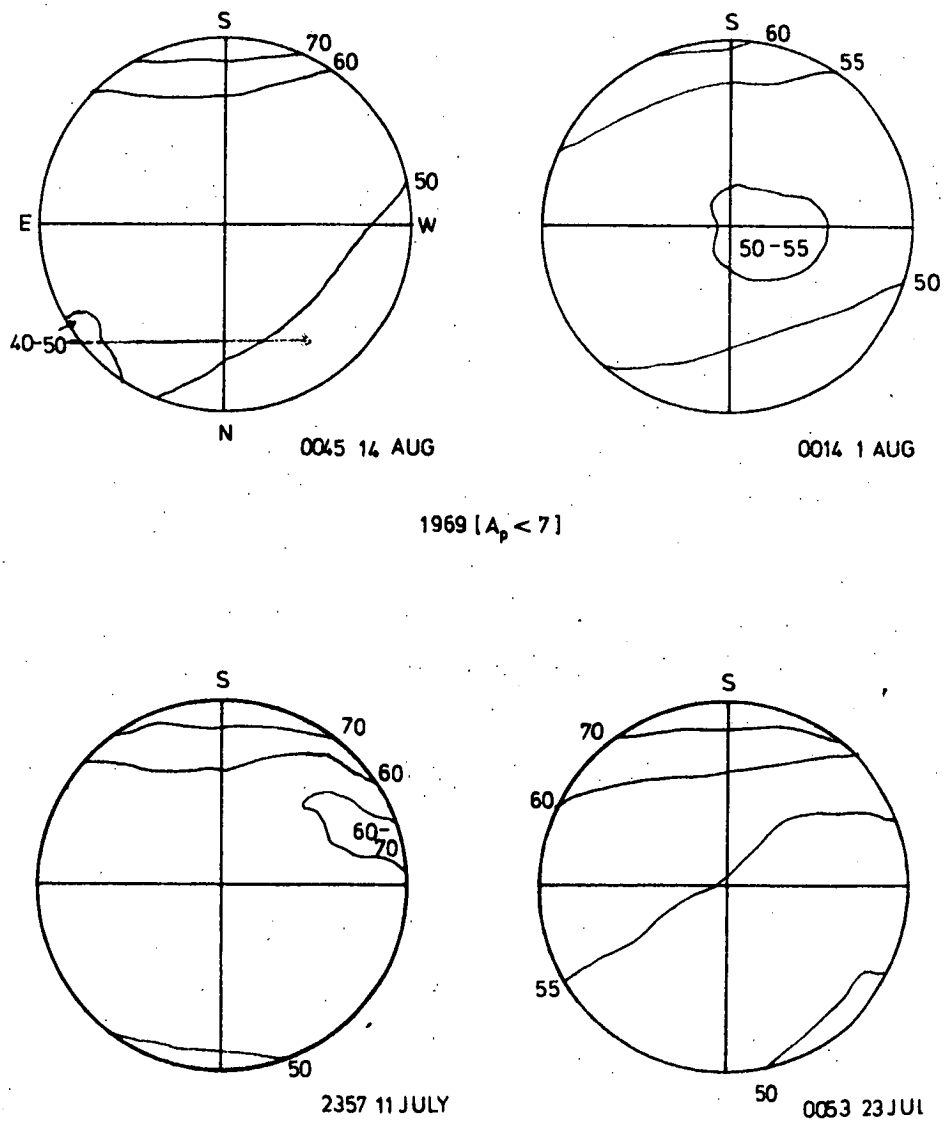

Fig. 5.17 All-sky charts for four quiet winter/equinox nights.

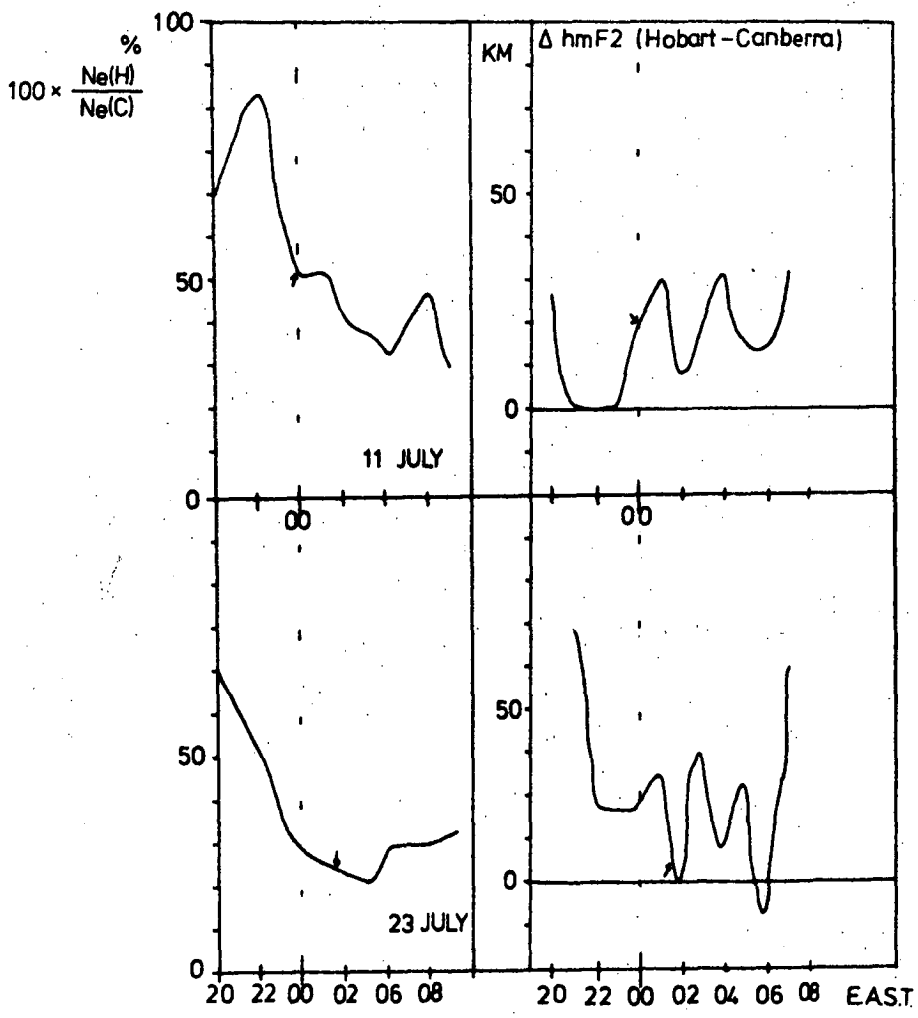

Fig. 5.18 Electron density and F-region heights for nights of fig. 5.17.

(i.e. Canberra) than to the zenith. As always the south showed an enhancement (the southern enhancement) which is rather stable for low K_p. These nights are typical of the usual quiet-night airglow distribution yet the ionospheric data (fig. 5.18 a and b) suggest that from between two and four times as much recombination should be occurring to the north in fig. 5.17 than at the zenith.

Note that on three of these nights the trough is overhead at Hobart (in July and September) and from the spread-F evidence it appears to have a sharp polewards edge yet no sudden discontinuity occurs in I (6300) at the trough's edge. (Such sudden discontinuities are known to occur in the tropics; see King 1970). This smooth transition suggests that the mechanism which must be producing excess 6300Å photons in the trough is also responsible for the trough's formation. This is obviously what would occur if recombination were occurring much more rapidly in the trough. However, this would imply a breakdown of Jacchia and Slowey's (1967) atmospheric model in

the trough region; this possibility will be examined in Chapter 6.

Using all-sky data for all quiet days in January, July and September 1969 the following table of mean intensities to the north (N), south (S) and to the zenith (z) is derived.
Both N and S values are obtained for points where the NS meridian intersects the 75^{o} zenith angle sweep. The number of days used is indicated in parentheses; the standard deviations are also shown. The times for the measurements are between 0000 LMT and 0100 LMT (depending on cloud cover) and all days where $K_p < 3_o$ at all times are included in the mean.

Table 5.5

	I_N R	σ	I_z R	σ	I_s R	σ
JAN (7)	30.2	4.6	33.8	4.7	42.1	8.1
JULY(8)	23.7	3.4	27.2	3.2	40.0	4.1
SEP (8)	27.0	4.7	30.6	4.9	38.3	9.6

The ratio between I_z and I_N are completely unlike those predicted from the recombination estimates of Table 5.4. In general $I_N \leq I_z \leq I_s$ which is just the reverse of that expected from

Table 5.4. This polewards increase in I (6300) is known to occur at other longitudes (Sandford 1964 in New Zealand, and Eather 1968 over North America) although the corresponding ionospheric data has not been published.

5.5.2 Disturbed nights

The general 6300Å distribution on disturbed nights is similar to that on quiet nights but the southern enhancement (N.B. this is really just the southern extension of the polewards gradient mentioned above) is more intense and the zenith intensities fluctuate rather erratically. This can be seen from fig. (5.19) which shows how in a matter of minutes the whole region south of about $\Lambda = 50^{\circ}S$ (i.e. the trough zone) may become enhanced. Note as well that the N - S 6300Å gradient is much stronger on this night (as on all disturbed nights) but the ionosphere at Hobart appears to be very depleted (fig. 5.20).

Fig. (5.21) is taken from Sandford (1964) and shows how the latitude airglow gradient varied with local K index during 1957 - 1958. A similar variation occurred at Hobart for 1968 - 1970 but the absolute values of I (6300) were less

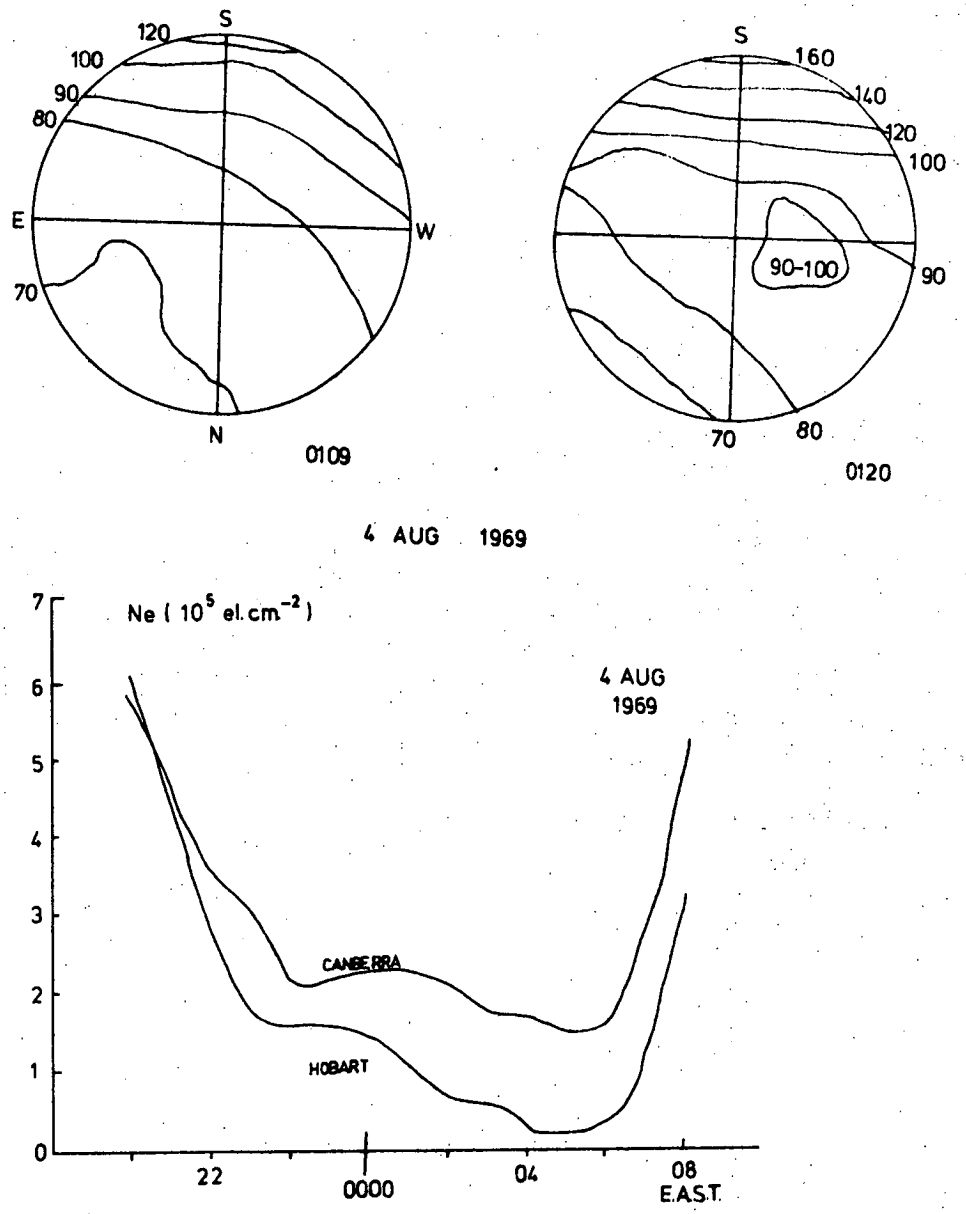

Fig. 5.19,20 Typical example of sudden increase in southern enhancement.

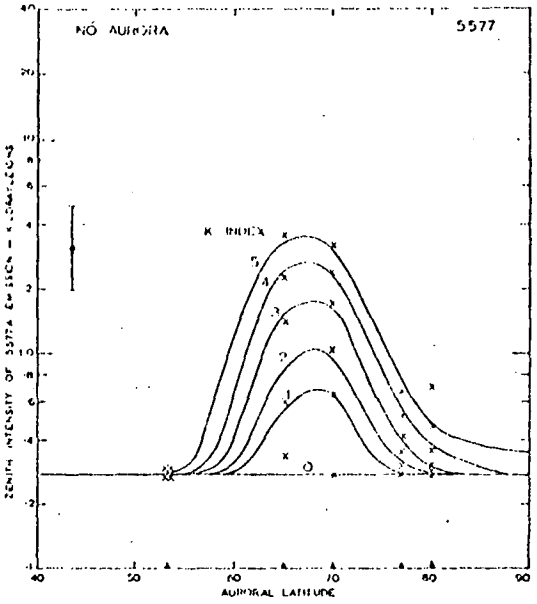

. The mean zenith intensity of 5577 Å emission as a function of auroral latitude for each local K-index from observations made only on clear moonless nights in the absence of discrete visual aurora.

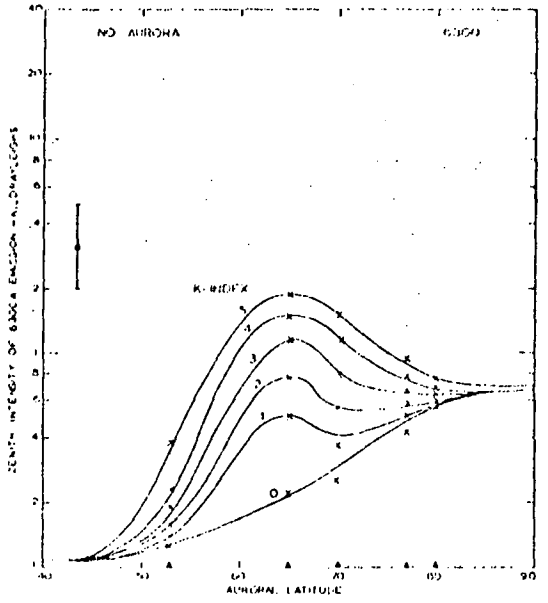

The mean zenith intensity of 6300 Å emission as a function of auroral latitude for each local K-index from observations made only on clear moonless nights in the absence of discrete visual aurora.

Fig. 5.21 Variation of airglow gradient with K index - after Sandford (1964).

than half those observed by Sandford. Presumably this reflects the difference in strengths of the two solar maxima.

Chapter 6 THE 6300Å AIRGLOW AND THE MIDLATITUDE IONOSPHERIC TROUGH - PART II

6.1 Introduction

The observations described in the previous chapter raise several important questions such as:

What controls the formation of the trough?

Why are its edges so sharp?

Why are its diurnal and seasonal motions so regular?

Why does the 6300Å airglow not drop across the trough?

It is believed that a fundamental point raised in chapter 5 is the apparent close link between the trough depleting mechanism and the 6300Å intensity 'maintenance' mechanism which must be operating in the trough. In this chapter an examination of possible mechanisms is made. Two separate mechanisms are found which fulfil the above criterion; i.e. they lead to a relative depletion of the F-region but tend to maintain 6300Å intensities. It is shown that both mechanisms are not incompatible with any other experimental evidence and that both may be operating simultaneously.

6.2 Latitude gradient in T_e

6.2.1 Topside observations

There have been many attempts to obtain

simultaneous measurements using satellites, of electron/ion temperatures and concentrations in the topside ionosphere. These have largely come from the Ariel, the Explorer and the OGO series (Bowen et al 1964, Brace and Reddy 1965; Brace et al 1967; Serbu and Maier 1966; Mahajan and Brace 1969; Chandra et al 1970; and Serbu and Maier 1970). Figs. 6.1 and 6.2 are based on data published in Brace and Reddy 1965. They show the day and night latitude variations of electron temperature T_e and electron density n during the November and December period of 1964. Fig. 6.1 shows that on the meridian near to Hobart the electron temperature increases sharply from $1000^{o}K$ at $\Lambda = 40^{o}S$ to $2500^{o}K$ at $\Lambda = 58^{o}S$ at a height of 1000 km. In the winter hemisphere the increase along the $100^{o}W$ longitude is from $1000^{o}K$ at $\Lambda = 40^{o}N$ to $2700^{o}K$ at $\Lambda = 58^{o}N$. It is thought that this latter longitude is more typical of winter conditions near to Hobart than those observed on the northern half of the $150^{o}E$ longitude. This is because of a similar displacement of the geographic and geomagnetic field for $100^{o}W$ (north) and $150^{o}E$ (south). The daytime results also show maximum electron temperatures near $60^{o}N$ and S but the maxima are less distinctive than at night. From the plot of n shown in fig. 6.2 it is seen that the sharp drop in density

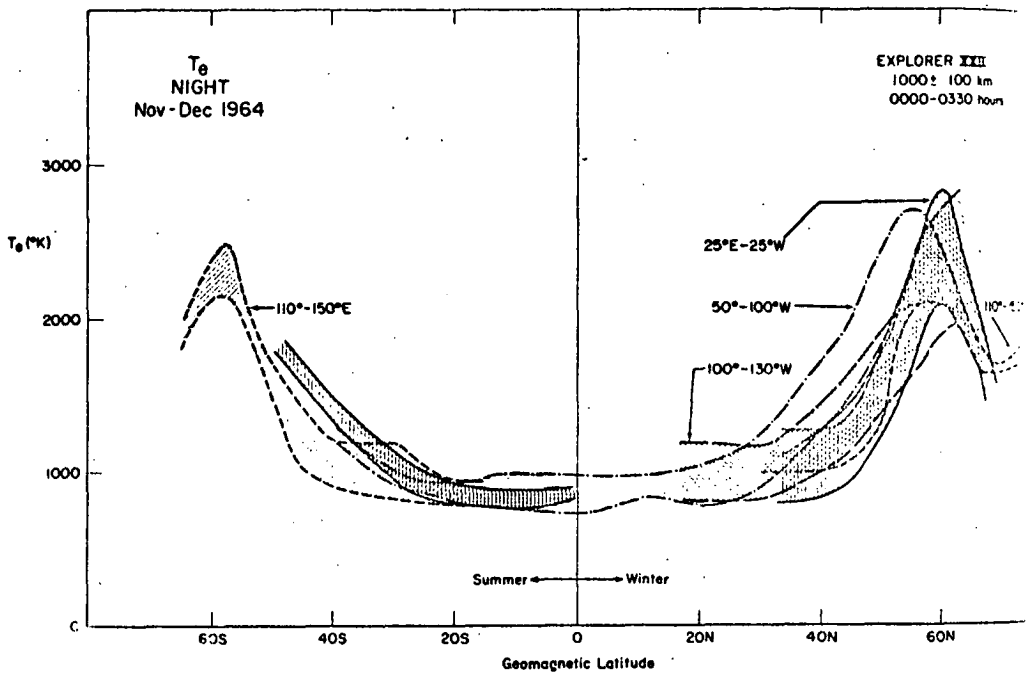

Fig. 6.1 Electron temperature variation with latitude (From Brace and Reddy, 1967 data).

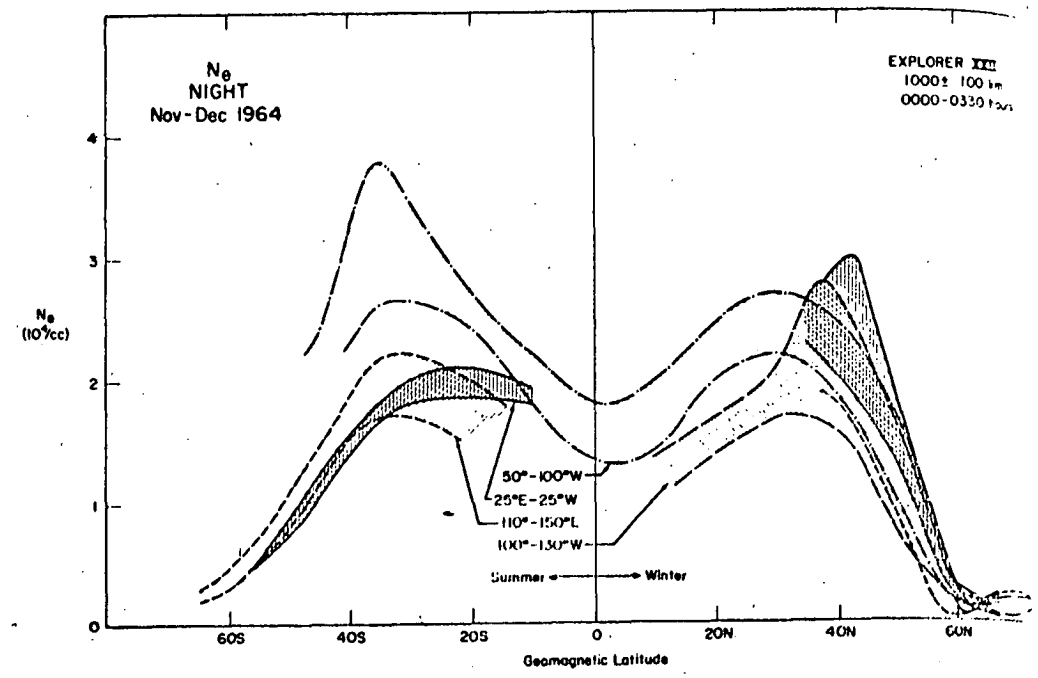

Fig. 6.2 Night-time electron density variation with latitude.

which corresponds to the midlatitude trough is also a region of high electron temperature. If this is so it appears that as well as having a 6300Å intensity maintenance mechanism another mechanism, to maintain T_e near its daytime values, must also be operating in the trough. Note that on this data display it seems that the trough exists in both hemispheres simultaneously. Both troughs are regions of high electron temperature and whilst for some longitudes (e.g. 100°W in the southern hemisphere) this may, in summer, be due to the direct action of sunlight there are times (fig. 6.3) at the equinox when both ends of the $\Lambda = 58^{\circ}$ field line are in shadow (to 900 km) yet high electron temperatures extend down to at least 700 km. The ion concentrations are also shown for the same pass but in view of the changing satellite heights they do not show well where the trough begins. However, in view of the great depth of the light ion trough (Taylor et al 1968), the fall-off in $[H^+]$ near 42°S (which is in spite of the drop in satellite height) may be interpreted as the beginning of the trough. Now the electron temperature T_e has been found to be more or less constant above 450 km (e.g. Evans 1965 a) so if the topside electron temperature is of the order of 2500°K then there is a distinct possibility that significant 6300Å airglow can be generated thermally in

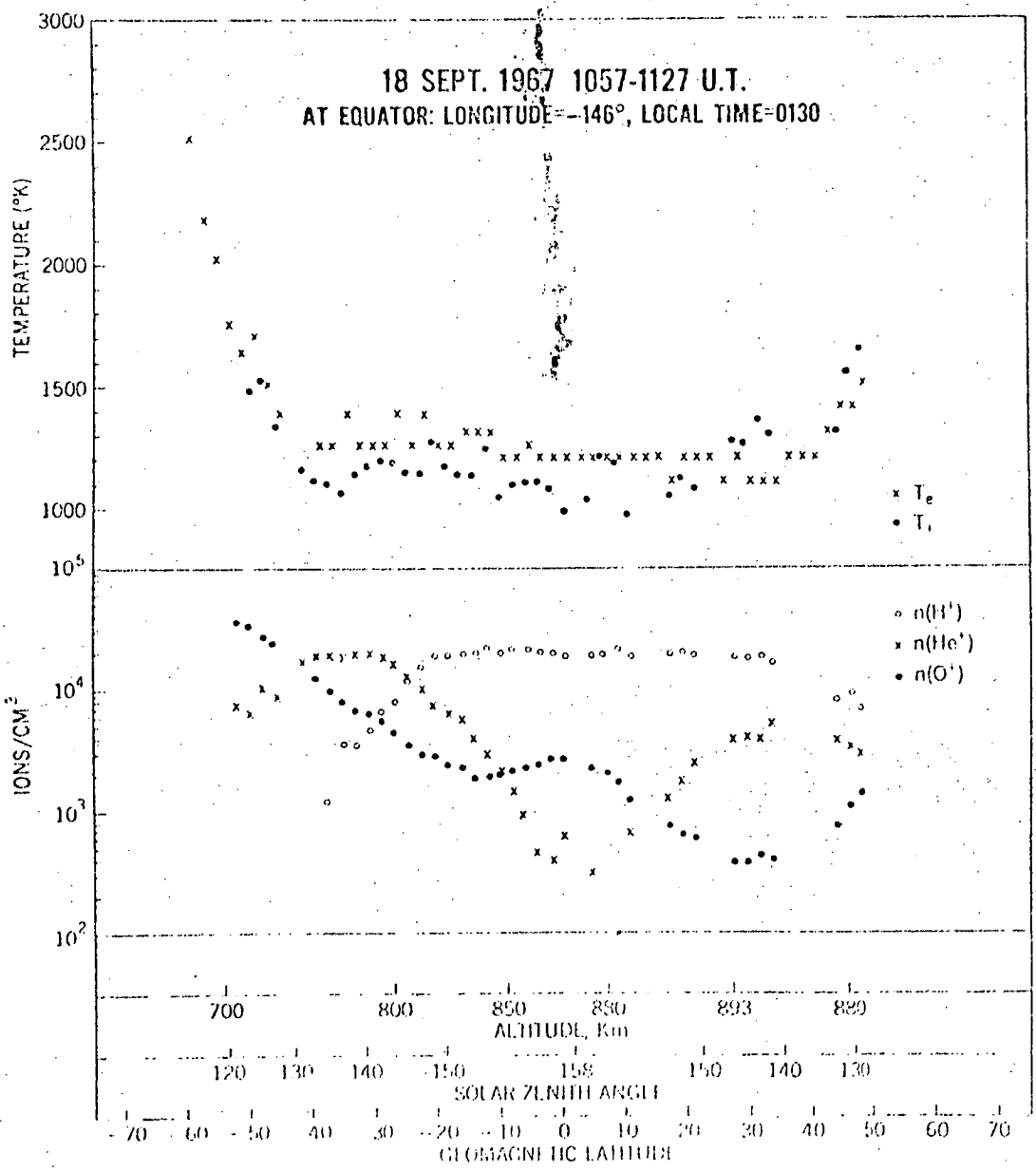

Latitudinal variation in electron and ion temperatures and ion composition for a nighttime apogee pass through the equator. The temperatures and ion densities are plotted against the common scales of altitude, solar zenith angle, and geomagnetic latitude.

Fig. 6.3 Night-time ion concentrations and their latitude variation. This is an equinox pass based on Chandra et al 1970.

the trough. This will of course tend to counteract the effects of reduced O_2^+ recombination on the 6300Å intensities.

6.2.2 Thermal production of $O(^1D)$

It will be remembered from chapter 2 that an expression for the rate co-efficient of thermal excitation of the $(^3P - {}^1D)$ transition was obtained in terms of the OI - electron excitation collision cross-section Q_{PD}. In Seaton's (1955) treatment he replaces this by the parameter Ω_{PD} known as the 'collision strength' and given by:-

$$\Omega_{PD} = \frac{4\pi m^2 v^2 \omega}{h^2} Q_{PD}$$

$$= \frac{v^2}{4.17} Q_{PD} \qquad 6.1$$

where v is the electron velocity; ω the statistical weight of the ^3P configuration; m is the electron mass and h is Planck's constant.

Now the rate coefficient of a collision process may be defined, as in chapter 2, by:

$$S_{PD} = \int_0^\infty Q_{PD}(v)\, v\, f(v)\, dv \qquad 6.2$$

where f(v) is the distribution function of the electon velocity. For a Maxwellian distribution this equation becomes:

$$S_{PD} = 8.54 \times 10^{-6} \int \frac{Q_{PD}(v)\, e^{\frac{-mv^2}{2kTe}}}{\omega\, Te^{\frac{1}{2}}} d\left(\frac{mv^2}{2kTe}\right) \qquad 6.3$$

where Te is electron temperature and k is Boltzmann's

constant. Seaton's (1955) and Smith et al's (1967) values for Ω_{PD} are shown in fig. 6.4. Beyond the excitation level of the ^1D state (1.97 eV) Ω_{PD} does not change rapidly and it is often removed outside the integral of 6.3 and given some constant value $= \Omega'$. If this is done then the integral is soluble; this 6.3 becomes:

$$S_{PD} = \frac{8.54 \times 10^{-6}}{Te^{\frac{1}{2}}\,\omega} \exp\left(\frac{-mv_o^2}{2kTe}\right)\Omega'_{PD} \qquad 6.4$$

where $(\frac{1}{2} mv_o^2)$ is the minimum energy needed to excite the ^1D state. Putting $\Omega'_{PD} = 1$ values of S_{PD} versus Te are shown in figure 6.5.

Now if deactivation of the ^1D state and cascading from the ^1S state are ignored the height integrated intensity of the 6300Å ariglow due to this cause is:

$$Q(6300) = 0.75 \int_o^\infty S_{PD}\, n[O]\, dz \qquad 6.5$$

where z is the height above ground and [O] is the OI density.

Now assuming that the electron temperature is constant above a height $z = z_o$ then 6.5 becomes:

$$Q(6300) = 0.75\ S_{PD}(Te) \int_o^\infty n[O]\, dz \qquad 6.6$$

where contributions to Q from heights less than z_o is ignored.

If z_o = 420 km then using the three ionospheres given in Appendix C the variation of Q(6300)

Fig. 6.4 Collision strengths of the 3p - ^1D transition.

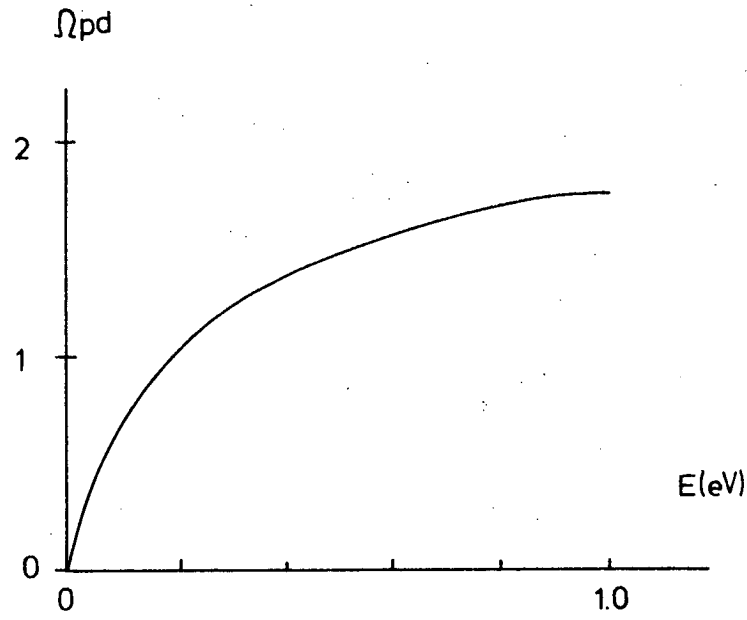

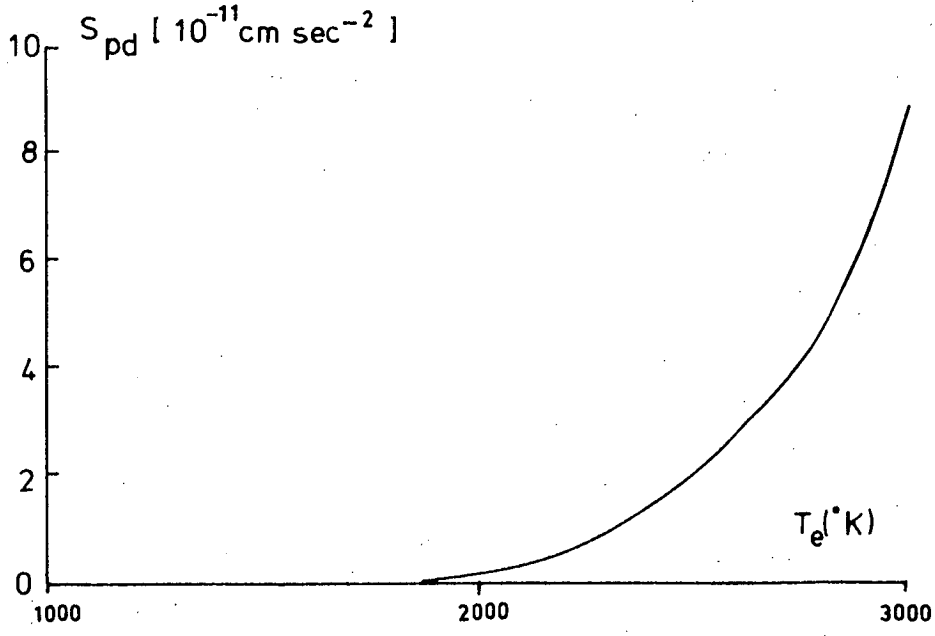

Fig. 6.5 S_{pD} as a function of electron temperature.

with Te is as shown in fig. 6.6. The CIRA 1965 model 5, which is appropriate to the solar radiation levels for these ionospheres, was used for the oxygen (OI) densities of 6.6.

From fig. 6.6 it is clear that if the ionosphere above 400 km is hotter than about 2500°K then significant 6300Å emissions will occur in this region. Thus if the temperature latitude gradients shown in figs. 6.1 - 6.3 are similar at 400 km then less than 1R of 6300Å radiation will be produced thermally at Λ = 45°S & about 10-20 R will be produced at Λ = 55°S This is sufficient to maintain the total 6300Å intensity I(6300) across the depleted region (see section 5.3.2) where the recombination contribution to I(6300) appears to drop severely.

Now it is known from Evans's (1964, 1965 a and b) work that Te is greatest at night in winter and least in summer. His electron temperature height profiles for solar minimum at Millstone Hill (Λ = 55°N) show that only on winter nights does Te appear high enough to produce significant 6300Å photons thermally. This of course is the period when trough depletion is most severe. Unfortunately little data for solar maximum has been published and theoretical predictions of Te variation with the solar cycle appear not to agree very well with the measured temperatures

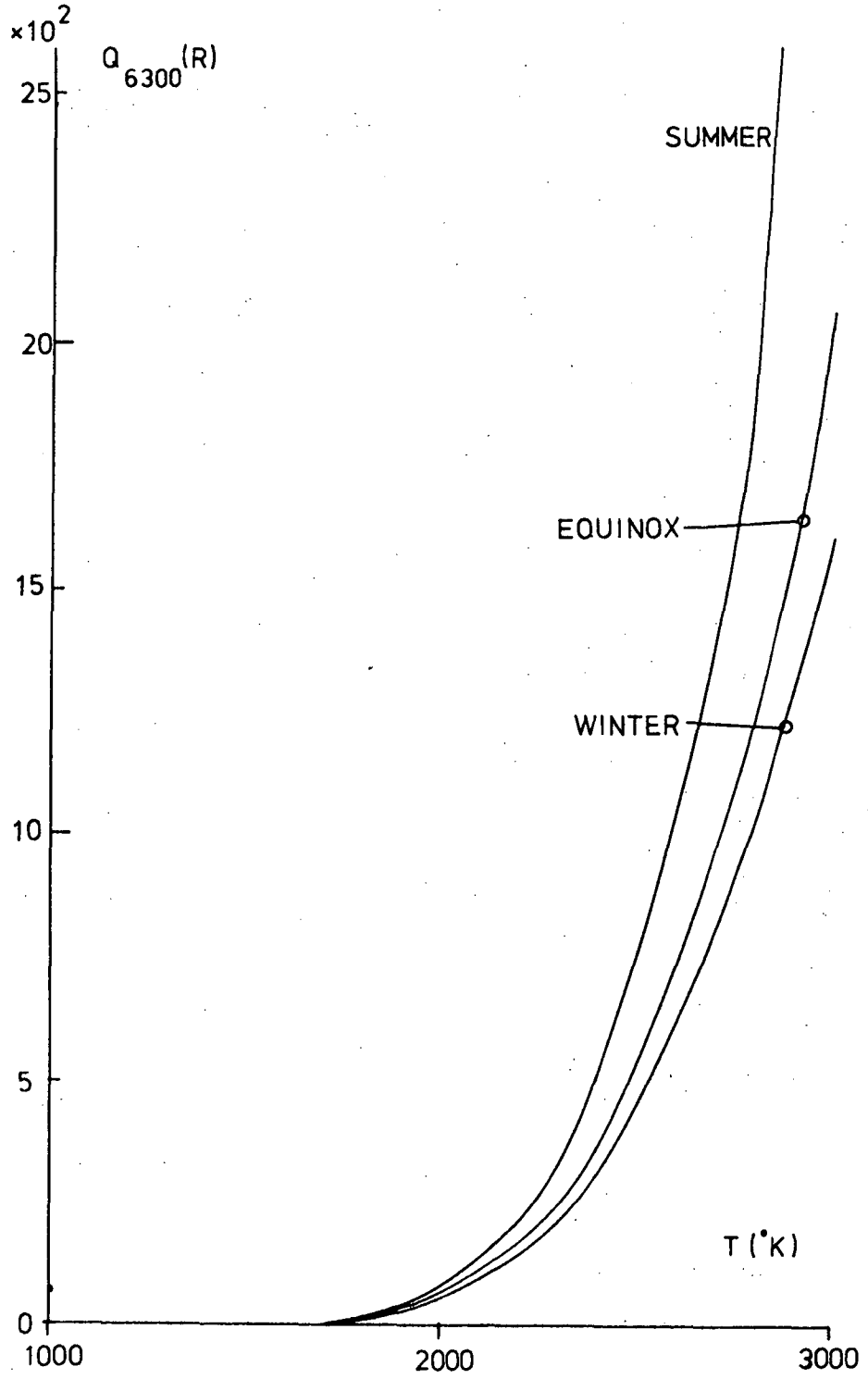

Fig. 6.6 Q(6300) as a function of electron temperature for three ionospheric models.

(Dalgarno et al 1967, Dalgarno and Degges 1968, Herman and Chandra 1969). Present indications are, however, that Te is not quite high enough at $\Lambda = 55^{\circ}$S at night to excite 6300Å airglow thermally during quiet conditions. During disturbed conditions, however, it seems likely that Te rises sufficiently to do so (Reddy et al 1967, Findlay et al 1970). Cole's (1965, 1970) theory of SAR-arcs invokes this mechanism to explain the high degree of monochromacity observed in the arcs. The question of thermal excitation at midlatitudes is by no means settled however, and a final solution must await the publication of Te data for 1968-1970.

6.2.3 Te gradient and ionospheric maintenance

It is well known that at midlatitudes an influx of ionization into the ionosphere occurs during the night (Allen 1953, Rostogi 1960, Arendt and Soicher 1964). The effect is most marked in winter between $\Lambda = 25^{\circ}$ and $\Lambda = 40^{\circ}$. The important point for present purposes is that the magnitude of the increase varies directly with the degree of cooling of the upper ionosphere. It has already been shown (6.2.1) that near Hobart's geomagnetic latitude there is little difference between the day and night-time values of Te whereas near Canberra the difference is large. This means that the influx is much weaker at

Λ = 55°S than at Λ = 45°S. This is consistent with the plots of peak electron density, Ne_m, shown in figs. 5.9 - 5.12. According to Titheridge (1968) the influx increase with sun-spot number R_z and at times of magnetic activity. Fig. 6.7 is based on Titheridge's results but has been extrapolated to higher latitudes. It shows the latitude variation of the total influx at the various seasons and for a level of solar activity consistant with 1969 levels (R_z = 120). It is quite clear that at least part of the trough's formation is due to this latitude effect. Titheridge found that the influx occurred at different local times at different latitudes and different seasons. Thus:

Table 6.1

	Range of Influx (Λ)	Local time
Summer	15 - 40°S	21.30 - 00.00
Equinox	20 - 45°S	22.30 - 01.00
Winter	25 - 50°S	22.30 - 02.00

In summer therefore the range of maintenance moves equatorwards which is consistent with the apparent (figs. 5.9 - 5.12) northwards movement of the depleted region observed at Hobart.

6.3 Soft Electron Fluxes:

6.3.1 Conjugate Fluxes:

It is only fairly recently that the importance of photoelectron fluxes in the exosphere has been

Fig. 6.7 Total influx (after Titheridge 1968) into the night-time ionosphere.

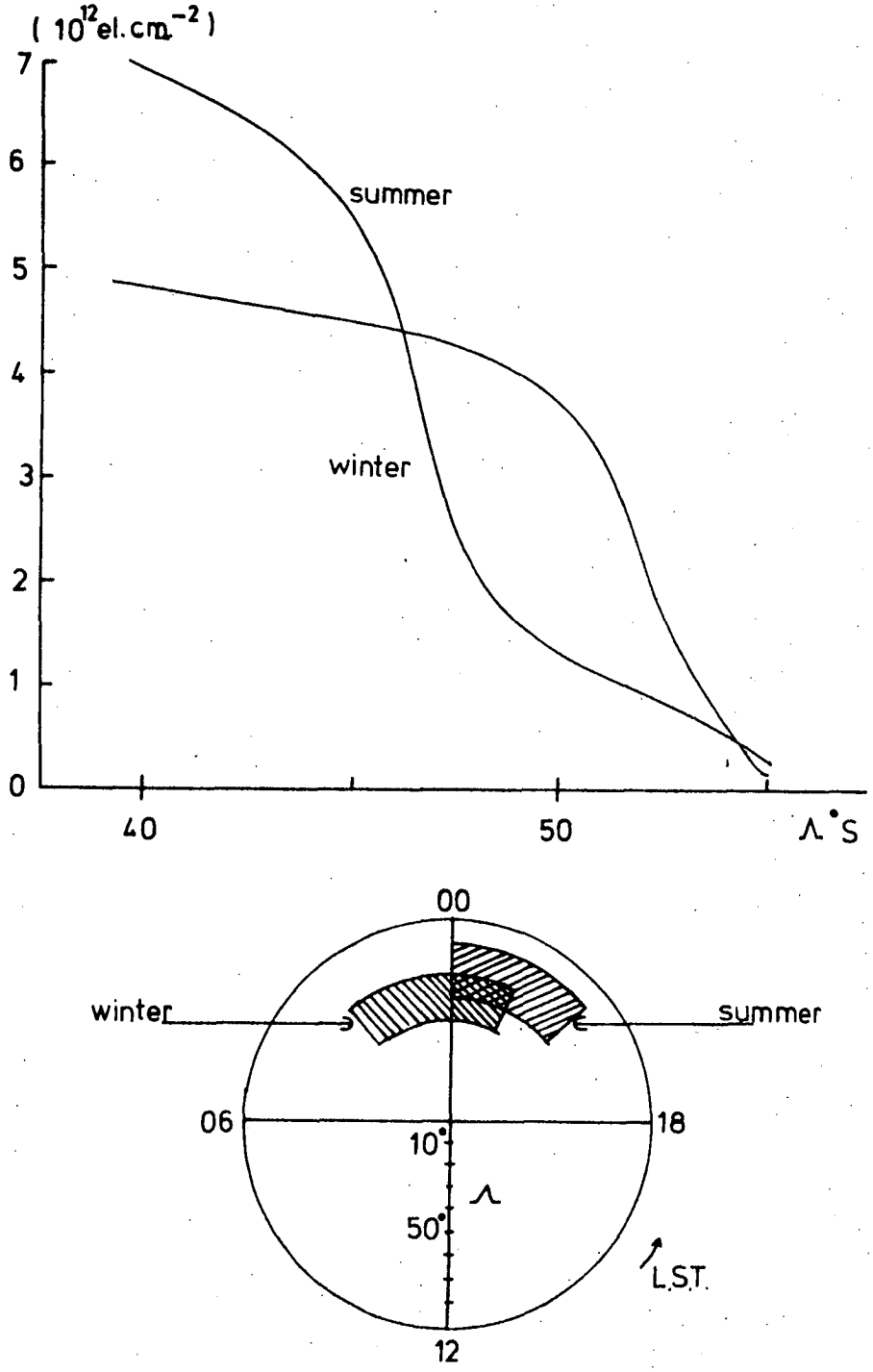

realised (Hanson and Johnson 1961, Hanson 1963). A more complete examination of these fluxes is given in section 9.3 and in this section only the latitude and seasonal effect of the flux is considered. Briefly Hanson (1963) showed that under certain conditions photoelectrons emitted by solar photons from the upper ionosphere can escape into the exosphere and, depending on their energy, pitch-angle and the local magnetic field parameters, they can travel into the conjugate ionosphere. Cole(1965 b) showed that at night at certain seasons and points on the globe the conjugate ionosphere may still be sunlit and thus emitting photoelectrons which could cause increased $O(^1D)$ production in the night ionosphere. The existence of this flux has been confirmed directly (e.g. Rao and Donley 1969; Heikla 1970) and indirectly by the increase in electron temperature which the soft flux causes (Carlson 1965). Now in the previous chapter it was shown that the times when the dissociative recombination of $O(^1D)$ atoms appears to be most inadequate to explain the 6300$\AA$ airglow levels are on winter and equinox early mornings i.e when the trough is most marked. These times however are the ones when the MCP photoelectron flux should be the most significant. Thus qualitatively MCP photoelectron excitation of 6300$\AA$ may be the airglow maintenance mechanism required. To study the effect quantitatively it is necessary to examine the time variance

of the flux magnitude.

Fig. 6.8 shows how the conjugate zenith angle (CZA) changes at 0000 EAST and 0300 EAST for Hobart and Canberra during (southern) winter and the equinoxes. The CZA is $(90^{o} + \alpha)$ where α, the angle of depression, is obtained from

$$\sin,\alpha = -\sin\delta \sin\phi - \cos\delta \cos\phi \cos\tau \quad 6.7$$

where δ is the solar declination, ϕ the geographic latitude of the conjugate point and τ is the hour angle of the sun. The following are the CSZA's for 0000 EAST and 0300 EAST for the 15th of each month.

Table 6.2

Conjugate Solar Zenith Angles (^{o})

EAST	MAR		APR		MAY		JUN		JUL	
	C	H	C	H	C	H	C	H	C	H
0000	129	122	116	109	109	101	104	96	106	98
0300	105	103	95	92	88	84	85	81	86	83

	AUG		SEP	
	C	H	C	H
0000	113	105	125	117
0300	92	89	101	99

where C and H indicate Canberra and Hobart respectively

Now according to work done on the pre-dawn enhancement of 6300Å airglow at Haute Provence (Barbier 1959, Carlson and Weill 1967, Deehr 1969) then for a 10.7 solar flux of 150 $10^{-22} Wm^{-2} Hz^{-1}$, an intensity

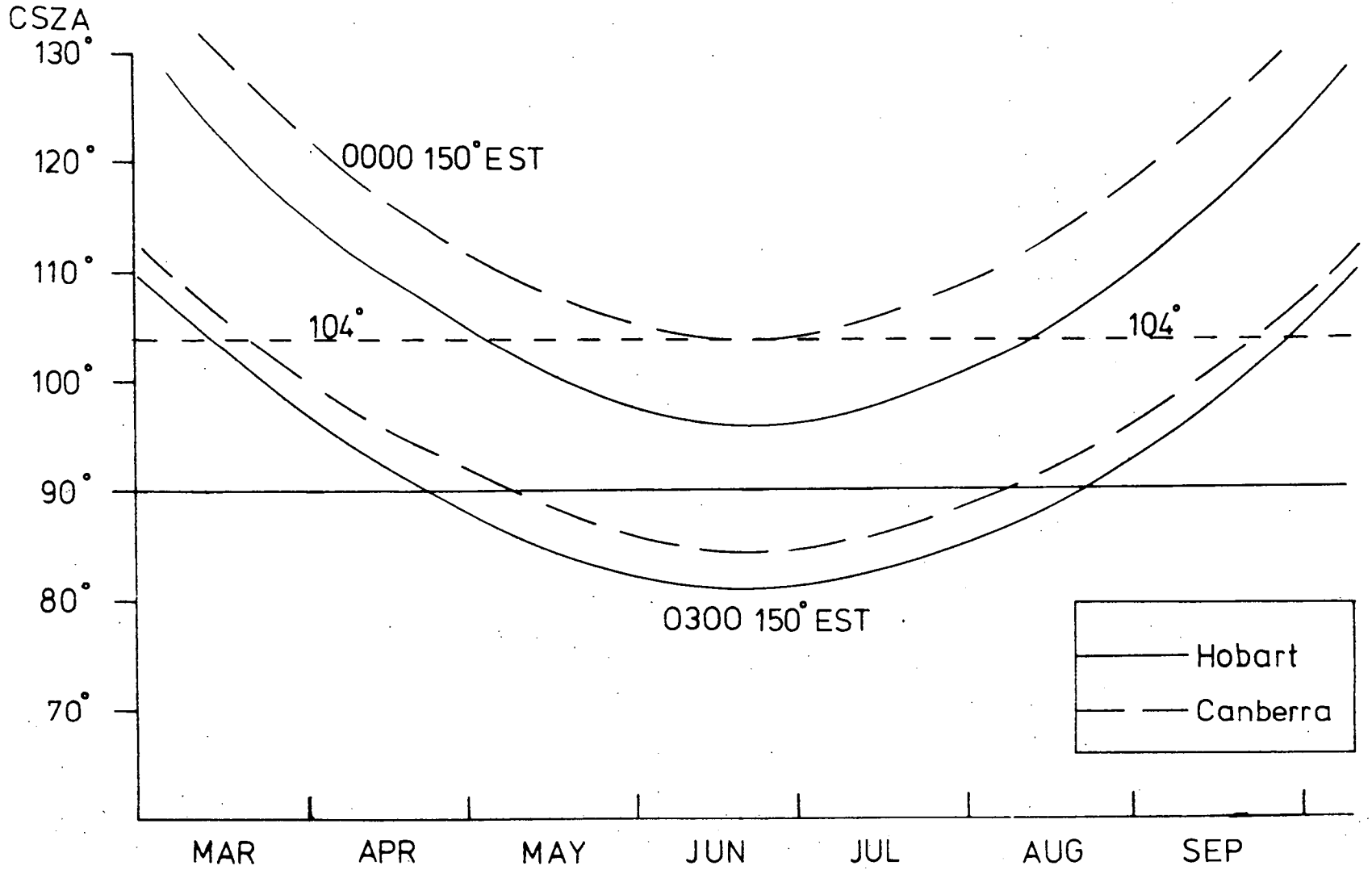

Fig. 6.8 Seasonal variation of the conjugate solar zenith angle.

which is appropriate to winter 1969, then the MCP photoelectrons do not begin to contribute significantly to local 6300Å airglow until a CSZA of 105° is reached. If this is so then from table 6.2 no conjugate fluxes are significant at 0000 EAST in March, April, late August and September. Yet it has been shown in the previous chapter that the midlatitude ionospheric trough is usually well developed in these months at midnight. From the calculations of section 5.4.2 it appeared that the ratio of ionospheric recombination at Hobart to that at Canberra at midnight for these months lay between 1 : 2 and 1 : 4. This it seems that MCP fluxes alone cannot be responsible for the 6300Å maintenance in the trough. To estimate the role they do play it is necessary to know the photoelectron flux escaping from the conjugate ionosphere and the losses experienced by this flux.

From Carlson and Weill's (1967) calculations it appears that , at low to medium solar activity, the production of photoelectrons increases by a factor of four from a solar zenith angle of 96° to one of 90°. According to Nisbet (1968) the flux escaping at 90° sza , for a 10.7 cm flux of $F_{10.7} = 150 \times 10^{-22}$ (W m^{-2} Hz^{-1}), is 7.7×10^{8} el cm^{-2} sec^{-1}, with an energy flux of 7.78×10^{9} eV cm^{-2} sec^{-1}. If the escape flux varies with SZA in the same way as the

production does, then this implies an escape flux of the order 1.8×10^{8} el cm^{-2} sec^{-1} with a mean energy of about 10 eV. Thus near midnight in May, JJune and July during 1969 a flux of this order would be escaping into the exosphere from Hobart's conjugate point. Some of this is lost in the exosphere, particularly the low energy and for high pitch angle component (see section 9.3.3)but a larger part is either mirrored or backscattered. This has been observed experimentally (Rao and Maier 1970). In section 9.3.3 it will be shown that only about 50% of the initial flux will penetrate into the ionosphere at Hobart. Thus at midnight in winter a conjugate flux of order 1×10^{8} el cm^{-2} sec^{-1}, with mean energy 10 eV, is arriving at Hobart. Now the amount of 6300Å airglow this soft flux will produce is given by equation 9.16 and depends on the model atmosphere and ionosphere used. Using the winter ionosphere of Appendix C and the CIRA model 5 for O_2 and N_2 profiles this equation gives for the midnight winter mean hmF2 of 380 km, a maximum of 8.1R of 6300Å airglow. Clearly, whilst not insignificant, this is not enough to maintain the airglow levels in the trough.

6.3.2 Van Allen fluxes

It is well known that the precipitation of charged particles from the Van Allen trapping zones increases strongly with latitude beyond L = 3 ($\Lambda = 55^{\circ}$) even at times of low magnetic activity (O'Brien 1964). At more active periods the precipitated flux grows very greatly, largely due to an increase in the trapped radiation and not due just to an increase in precipitation (O'Brien 1964, Hess 1968). This region, $\Lambda \geqslant 55^{\circ}$, of course includes the midlatitude ionospheric trough and it is possible therefore that the 6300Å airglow maintenance in this region is caused by direct $O(^1D)$ excitation by this cis-auroral zone precipitation. Unfortunately, low energy electron measurements are difficult to make and interpret, although techniques have improved considerably in recent years. Amongst the early works of interest are the IMP I and II measurements of Serbu and associates (Serbu 1964, Serbu and Maier 1965). Fig. 6.9a is taken from Serbu 1964 and shows measurements of electron flux density near the equatorial plane as measured by a retarding potential analyser. The 5 to 10 eV spectrum is of particular interest because it shows that this flux increases sharply beyond a distance of about 3 earth radii.

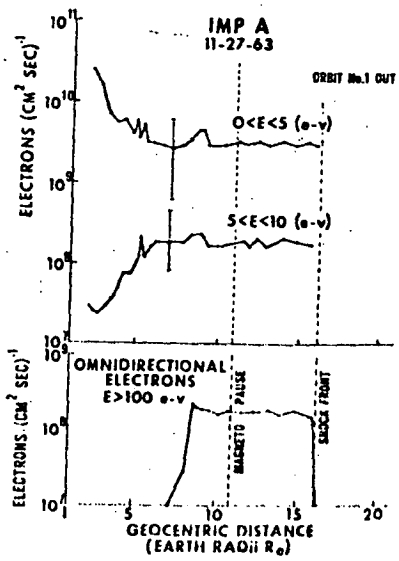

Fig. 6.9(a) Soft electron flux variation with distance from earth: (after Serbu 1965).

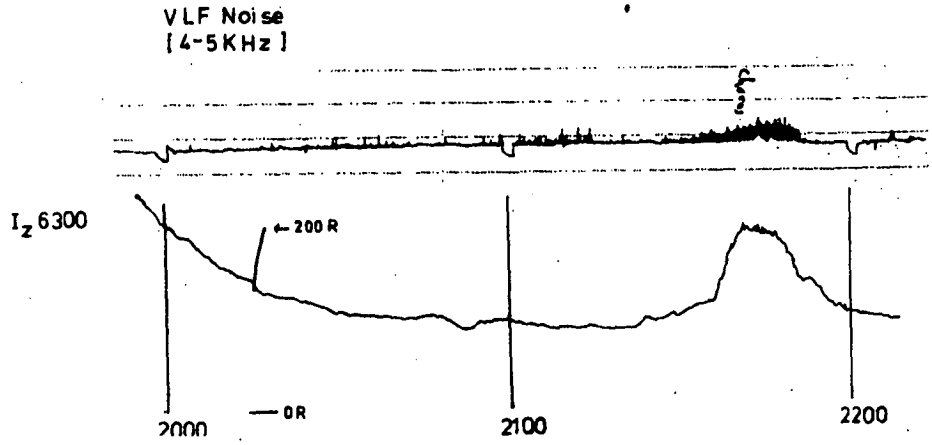

Fig. 6.9(b) Correlated 6300Å enhancement with chorus-type burst of VLF noise.

If this flux were precipitating then these electrons would significantly excite $O(^1D)$ beyond L = 3. Assuming the flux is isotropic at the equator then the fraction which reaches the ionosphere at 350 km is given by:

$$\frac{N_{350}}{N_{eq}} = \arcsin \frac{B_{eq}}{B_{350}} \quad \frac{\pi}{2} \qquad 6.8$$

where N and B are the flux density and magnetic field intensity respectively; the subscripts 350 and eq are the values at 350 km and at the equatorial plane along the same line of force. For Hobart this ratio is 0.0265 so that only 2.65% of the equatorial flux reaches the F-region. Now the actual flux reaching the F-region is given by:

$$N'_{350} = N_{eq} \times 0.0265 \times A \qquad 6.9$$

$$(\text{el cm}^{-2} \text{ sec}^{-1})$$

where A is the area in cm^2 of a tube of force whose cross-sectional area is 1 cm^2 at 350 km. Using 6.9 and putting $N_{eq} = 2 \times 10^8$ cm^{-2} sec^{-1} (after Serbu 1965) this gives, for L = 3, a value of $N'_{350} = 1.27 \times 10^8$ cm^{-2} sec^{-1} of electrons in the 5 - 10 eV region. This flux would produce 10 - 20R of 6300Å airglow depending on ionospheric conditions.

The essential assumption in the above is that the flux at the equatorial plane is isotropic. If there were no injection or acceleration of fresh electrons then the trapped flux would rapidly lose

all of its low pitch angle electrons and no precipitation would occur. This is the usual situation in the inner trapping zone (Van Allen 1966) and it is believed that the same holds for these low energy electrons at L = 3, at least at magnetic quiet. One reason for this is that continuous precipitation of this flux would imply an energy loss to the ambient electrons of the order 10^9 eV cm^{-2} sec^{-1}. According to Evans (1967a, 1967b), however, a flux of this magnitude is only required for T maintenance at L = 3 in winter when it is well accounted for by conjugate point photoelectrons. The small residual summer energy flux is completely accounted for by conduction of heat stored in the tube of force (Geisler and Bowhill 1965, Nagy et al 1970). Besides this other low energy electron satellite measurements show little precipitation at L = 3 (Kazachevskaya and Koryagin 1969; Burch 1968; Rees 1969; Schield and Frank 1970). One exception to this are the measurements of Knudsen (1968a) which show areas at low latitudes where large and continuous precipitation of soft electrons occur. These areas are near 'anomolies' in the geomagnetic field where the weak field allows lower mirror heights, and thus greater loss, than usual. Hobart is not near any anomoly however, and Knudsen's maps show the surrounding region to be one of low precipitation.

Thus at periods of low magnetic activity it is felt that little contribution to the normal red-airglow is made by trapped radiation. However, the Van Allen electrons provide an ideal mechanism to explain the brightenings of I(6300) observed over the whole sky south of $\Lambda = 50^{o}$ on many occasions (e.g. fig5.19) even on quiet nights. It is well known (O'Brien 1965, 1966) that the precipitation of Van Allen electrons increases enormously with local magnetic activity due to an increase in the trapped flux combined with a varying pitch angle distribution. One mechanism that could cause a re-distribution of pitch angles is an instability triggered by VLF emissions (e.g. Roberts 1966). This would explain the coincident bursts of VLF and 6300Å airglow observed by Duncan & Ellis (1959) and occasionally by the present author (fig. 6.9). Also it would explain the tendency for regions of VLF noise to be near the zones of soft electron precipitation as reported by Knudsen 1968b. Clearly this is an important area for future research

6.4 Molecular Concentrations:

6.4.1 Predicted: Static diffusion

Both the Jacchia (1965) and the CIRA (1965) atmospheric models are based on an assumption of static diffusion with fixed boundary conditions. The concentration of the i th species n_i is given by

$$\frac{d\, n_i}{n_i} = - \frac{dz}{H_i} - \frac{dT}{T} (1 + \alpha) \qquad 6.12$$

where T is the temperature a height z and is the thermal diffusion factor. H_i is the local scale height given by:

$$H_i = \frac{k\, T}{M_i\, g} \times 10^{-5} \ (km) \qquad 6.13$$

Where M_i is the mass of the atom/molecule. Jacchia uses the following boundary conditions for evaluating 6.12

At z = 120 km

$$[N_2] = 4.0 \times 10^{11}$$

$$[O_2] = 7.5 \times 10^{10}$$

$$[O] = 7.6 \times 10^{10}$$

$$[H_e] = 3.4 \times 10^{7} \qquad 6.14$$

also he assumes $\alpha = 0$ except for helium where $\alpha = - 0.38$

Now integration of 6 yields

$$\log \frac{n}{n_o} = - \log \frac{T}{T_o} - \int_{120}^{z} \frac{dz}{H} \qquad 6.15$$

where the integration is from the boundary z = 120 km and the subscript 0 refers to values at this height. For convenience the i's have been dropped. It is assumed that $\alpha = 0$.

Knowing the temperature height profiles it is easy to evaluate 6.15 for any height using Simpson's rule. It is easy and more convenient for discussion

to obtain a very good approximation to an analytic solution.

This is possible for Jacchia gives the following close approximation for the neutral temperature profile:

$$T = T_\infty - (T_\infty - T_o) \exp - s\,(z - 120) \qquad 6.16$$

where T_∞ is the exospheric temperature and S is a function of this given by:

$$S = 0.0291 \exp(-x^2/2)$$

$$x = \frac{T_\infty - 800}{750 + 1.722 \times 10^{-4} (T_\infty - 800)^2} \qquad 6.17$$

Thus 6.15 becomes

$$\log \frac{n}{no} = -\log \frac{T}{T_o} - \int_{120}^{z} \frac{dz}{Tg} \frac{M}{K}$$

$$= -\log \frac{T}{T_o} - \frac{M}{k\bar{g}} \int_{120}^{z} \frac{dz}{T} \qquad 6.18$$

where $\bar{g}$ is a constant replacing g which is of course proportional to $(z + R_e)^{-2}$ where R_e is the earth's radius.

Substituting for T in the integral of 6.18 from 6.16 yields.

$$I = \int_{120}^{z} \frac{dz}{T_\infty - (T_\infty - T) \exp -s\,(z - 120)} \qquad 6.19$$

This integral can be easily reduced to standard form and after integration yields

$$I = -\frac{1}{s}\log_e(1-a)\left[\frac{e^{-s(z-120)}}{1-a\,e^{-s(z-120)}}\right] \qquad 6.20$$

where $a = 1 - \frac{T_o}{T_\infty}$

substituting 6.20 back into 6.18 and raising both sides the power of e gives:

$$n = n_o \frac{T_o}{T} \exp\left(-\frac{1}{T_\infty}\frac{m\bar{g}}{k}\frac{1}{s}\right)\left[\log_e(1-a)\left(\frac{e^{-s(z-120)}}{1-a\,e^{-2(z-120)}}\right)\right]$$

$$= n_o \frac{T_c}{T}\left[T_o \frac{e^{-s(z-120)}}{T_\infty - (T_\infty - T_c)^{-s(z-120)}}\right]^{\frac{m\bar{g}}{ks}T} \qquad 6.21$$

Now if $\bar{g}$ is chosen as correct for $z = 200\ k_m$ then 6.21 agrees with Jacchia's model within 2% at F-region heights.

(Note that $\frac{m\bar{g}}{k\,T} = H'$ must be in kilometres if z is)

In the present chapter latitude gradients are being discussed and the constant boundary conditions imply that in 6.21

(i) T_o is not a function of latitude.

(ii) n_o is not a function of latitude.

(iii) T_∞ varies according to equations 5.4 and 5.5 in the previous chapter.

Clearly any increase in T_o or n_o with latitude would

lead to increased neutral densities at a given height which could cause increased recombination in the trough. Similarly an increase in T_∞ with latitude greater than that given in 5.4 and 5.5 would have a similar effect. The magnitude of the required changes are now computed.

From the previous chapter it appeared that in the early morning dissociative recombination was less near $\Lambda = 55^\circ$s, by a factor of 1.5 to 4.0, depending on the season, than at some 10° further north. The 6300Å airglow did not drop across this zone however, which has been shown to be partially due to conjugate point photo-electrons (and possibly thermal excitation). However, at least one third of the airglow in the trough (i.e. south of 55°s) is unaccounted for. If this is due to increased recombination in the trough then the neutral density (or at least the O_2 density) in the emitting region near 300 km must be the order of twice as dense at $\Lambda = 55^\circ$s as $\Lambda = 45^\circ$s.

Using equation 6.21 it is possible to compute the latitude variation of n_o, T_o and T_∞ needed to raise O_2 density by this factor over $\Lambda = 45^\circ$ to $\Lambda = 55^\circ$.

Case (i) T_o constant ; T_∞ constant.

Denoting values at $\Lambda = 45^{\circ}$s and $\Lambda = 55^{\circ}$s by (45) and (55) respectively then the requirement is:

$$n_o(55) = 2\, n_o(45) \qquad 6.22$$

This of course need not occur for all species but only for O_2.

Case (ii) n_o constant ; T_∞ constant

What is required is that z = 300 km

$$n\,(55) = 2\, n\,(45)$$

where $n_o(55) = n_o(45)$

From 6.21 this gives

$$2 = \frac{T_o(55)}{T_o(45)}\left[\frac{T_o(55)}{T_o(45)}\;\frac{1-\left(1-\frac{T_o(45)}{T_\infty}\right)e^{-s\,(z-120)}}{1-\left(1-\frac{T_o(55)}{T_\infty}\right)e^{-s\,(z-120)}}\right]^{\frac{m\bar{g}}{ks\,T}} \qquad 6.23$$

Assuming that $T_\infty = 1050^{\circ}K$, then s = 0.029 (from equation 6.17), and putting $T_o(45) = 355^{\circ}K$ (Jacchia's value) this gives for O_2:

$$\frac{T_o(55)}{T_o(45)} = 1.378 \qquad 6.24$$

i.e. the boundary (z = 120 km) temperature at 55° must be 37.8% higher than at 45° to obtain twice the O_2 density at 300 km at $\Lambda = 55^{\circ}$. This corresponds to

$$T_o(55) = 502^{\circ}K \text{ for } T_o(45) = 355^{\circ}K$$

Case(iii) n_o constant ; T_o constant

the condition n(55) = 2 n(45) at 300 km implies that

$$T_\infty(45)\left[\frac{To\;e^{-s\,(z-120)}}{T_\infty(55)-(T_\infty(55)-T_o)\,e^{-s\,(z-120)}}\right]^{\frac{m\bar{g}}{ks\,T}(55)} =$$

$$2\ T_\infty(55)\left[\frac{T_\infty \qquad e^{-s'(z-120)}}{T_\infty(45) - (T_\infty(45) - T_c)\, e^{-s'(z-120)}}\right]^{\frac{m\bar{g}}{ks'T}} \qquad (45)$$

where it has been assumed that $T\ (z = 300) = T_\infty$

Note also that the s's in the above equation are functions of T_∞ and so are different in each line.

Now if $T_\infty(45) = 1050^\circ K$ then solving 6.5 iteratively give $T_\infty(55) = 1215^\circ K$.

i.e. an increase in T_∞ of $165^\circ K$ over this latitude range will lead to the required increase in recombination.

6.4.2 Predicted : partial mixing

As O_2 is only a minor constituent at 6300Å emission heights then even a slight breakdown of diffusive separation would lead to a large increase in O_2 density at these heights. If only 0.1% of all O_2 molecules between 120 km and 600 km were fully mixed then the O_2 density at 300 km would double. As Jacchia (1964) points out the large day to night temperature variations in the atmosphere have a period which is not much longer than the conduction time in the lower thermosphere, so the assumption of static diffusion is a drastic one.

6.4.3 Experimental concentrations

With reference to the assumption of static diffusion the results of Nicolet and Reber (1966) are interesting. They found on occasions that the density

of N_2 actually increased with height near 600 km. This implies that at these , albeit disturbed , times the atmosphere was well mixed. This occurred near the auroral zone suggesting geomagnetic control over the process. The latitude dependence of neutral densities at F-region heights has been examined by Newton and associates using Explorer 32 data (Newton and Pelz 1969; Newton, Pelz and Holldan 1969; Newton 1969; Newton 1970). They showed that contrary to some earlier evidence (Raetzold and Zschorner 1961, May 1963, 1964) the atmosphere density increases polewards at 350 km. Unfortunately, to date, their work covers only the summer and equinox months. Above 350 km it was found that the ratio of atmospheric density in the latitude range 55°N to 65°N to that at the equator was considerably greater than that predicted by the Jacchia model at night. This effect was greatest between 0000 and 0800 LMT which is the period when the trough is present. They also found a distinct tendency for the largest densities to be found in or near the auroral zone even during magnetically quiet times. In another paper Newton (1970) showed that for the period May - October 1966 there is a strong positive latitudinal gradient of density for latitudes greater than 40°N. He suggested this could be caused by a source of heating near the auroral

zone. Figs. 6.10 and 6.11 are taken from Newton (1970). Fig. 6.10 shows the diurnally averaged results and fig. 6.11 shows the departure from Jacchia (1965) near a geographic latitude of 60°N. Note the tendency for the maximum departure to occur at night; something that does not occur for lower latitudes. Fig. 6.12 is also from Newton (1970) and shows the exospheric temperatures, computed by Jacchia's method, which would explain the observed densities. Note that T_{min} increases rapidly from 800°K to 870°K from 50°N to 60°N. This increase is of the same order as that required in section 6.4.1 (case iii) to explain the airglow gradient in the trough.

Whilst these results of Newton and associates tend to lend support to the suggestion that the trough is a region of increased recombination due to larger than predicted molecular densities complete confirmation cannot be given until winter results are available. The present indications are however, that the trough forms at magnetic quiet because of auroral zone heating causing greater exospheric temperatures than expected. At magnetically disturbed times the neutral atmosphere in the trough becomes more mixed and even greater depletion occurs.

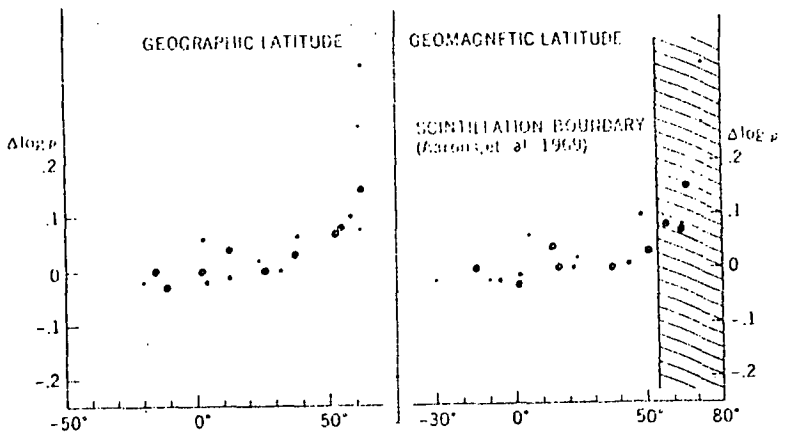

Fig. 6.10 Latitudinal dependence of neutral density (from Newton 1970).

Fig. 6.11 Departure from Jacchia's model for a latitude of 60°N (from Newton and Pelz 1969).

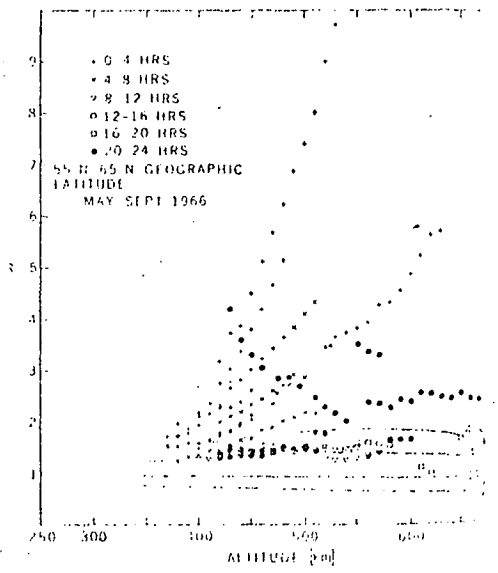

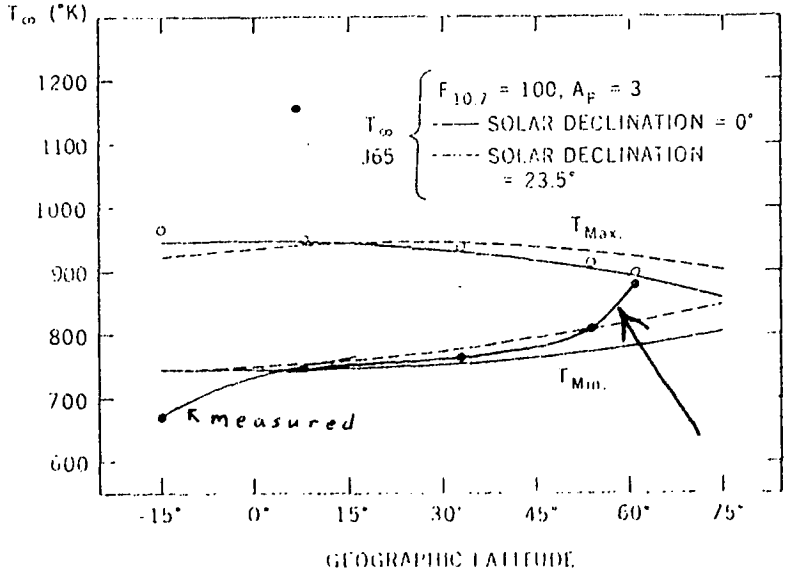

Fig. 6.12 Computed exospheric temperatures. Note the sudden increase in T_{min} near 55° (after Newton 1970).

6.5 Summary

It was found in the previous chapter that the 6300Å airglow intensities remain constant, or increase across the midlatitude ionospheric trough in spite of the apparent large decrease in dissociative recombination in this region. In this chapter several possible explanations have been discussed. Basically it is proposed that the trough is a region of increased recombination due to a partial breakdown of static diffusion and/or a strong gradient in exospheric temperature in the trough, associated with auroral zone heating. This increases the local molecular densities and thus increases the $O(^1D)$ production besides depleting the trough and thus tending to maintain the 6300Å airglow intensities. The formation of the poleward edge of the trough and its diurnal movement are due to the equatorwards movement of the auroral zone during the night. The equatorwards edge forms largely because of the sharp cut-off in maintenance of the F-region by the exospheric ionization reservoir. The trough does not fully develop in summer because of the shortness of the night which causes the region of adequate ionospheric maintenance to move equatorwards and also because the F-region is sunlit longer at higher latitudes. Contributions to the 6300Å airglow are also made in the trough by thermal excitation (only for $\Lambda > 60^\circ$)

and soft electron fluxes. The latter is partly due to conjugate point fluxes (in winter) and for higher latitude the semi-continuous precipitation of trapped electrons. At times of magnetic activity thermal excitation and precipitated electrons become important at lower latitudes. Also at disturbed times the atmosphere becomes more mixed, possibly due to turbulence, and a general increase in 6300Å levels is produced and the trough may form in daylight hours.

Many of the conclusions given above have only been derived qualitatively. This is partly because of the lack of adequate theoretical models, such as in the case of the neutral atmospheres, but also because of the sparsity of data, as in the case of soft electron precipitation. Clearly future experiments must measure more completely the variation of various parameters, such as molecular densities, with geomagnetic latitude over a given longitude range if a more quantitative treatment is to be produced.

Chapter 7: 6300Å AIRGLOW, SUMMER OBSERVATIONS

7.1 Introduction

During the summer of 1966 and 1969 it was found that the 6300Å airglow had a small but regular maximum near local midnight. The typical night-time zenith record for this period showed the usual rapid post-twilight decay until the intensity levelled off near 2300 LMT. Then a gradual monotonic increase occurred until a maximum was reached near 0100 LMT to be followed by a slow decay until the rapid increase due to F-region sunrise. The maximum was of the order of 10R above the 2300 LMT intensity, a rise of some 15%. Although at this time the equipment was not particularly sensitive it was quite clear from the records produced that this maximum was fairly regular and exhibited a similar morphology on different nights. It appeared to be partly under seasonal control as the increase began earlier near the solstice (Nichol 1970 a). This enhancement was called the midnight summer enhancement (MSE).

During the following year (1969-70) the airglow equipment used was more sensitive and the spatial morphology of the MSE and its geomagnetic and ionospheric control was examined in detail. In this

chapter the experimental results are discussed and it is shown that the MSE is caused by increased recombination due to a downward drifting ionosphere. This downward drift could be caused by changes in the neutral wind motion at F-region heights but as the same mechanism appears to be important in producing the winter pre-dawn enhancement (Chapter 8) an examination of this is held over to Chapter 9.

7.2 Optical Observations

7.2.1 The zenith enhancement

Fig. 7.1 shows a plot of 6300A zenith intensity versus local (150°E) time on six nights during the 1968 - 1969 summer. Kp was less than 2+ at all times on these nights and all show the distinctive 'hump' near midnight of the midnight summer enhancement (MSE). The magnitudes of the increases were in the range 7 to 15 R. The mean increase for the 37 quiet summer nights in 1968 - 1969 during which the MSE was clearly observed was 9.32 R. Nights such as 23 January 1969 (fig. 7.1 f) when no decrease occurred before dawn were rare (three nights out of 37). It is of interest to note the similarity in this display of the MSE on nights such as this and the winter pre-dawn enhancements of chapter 8.

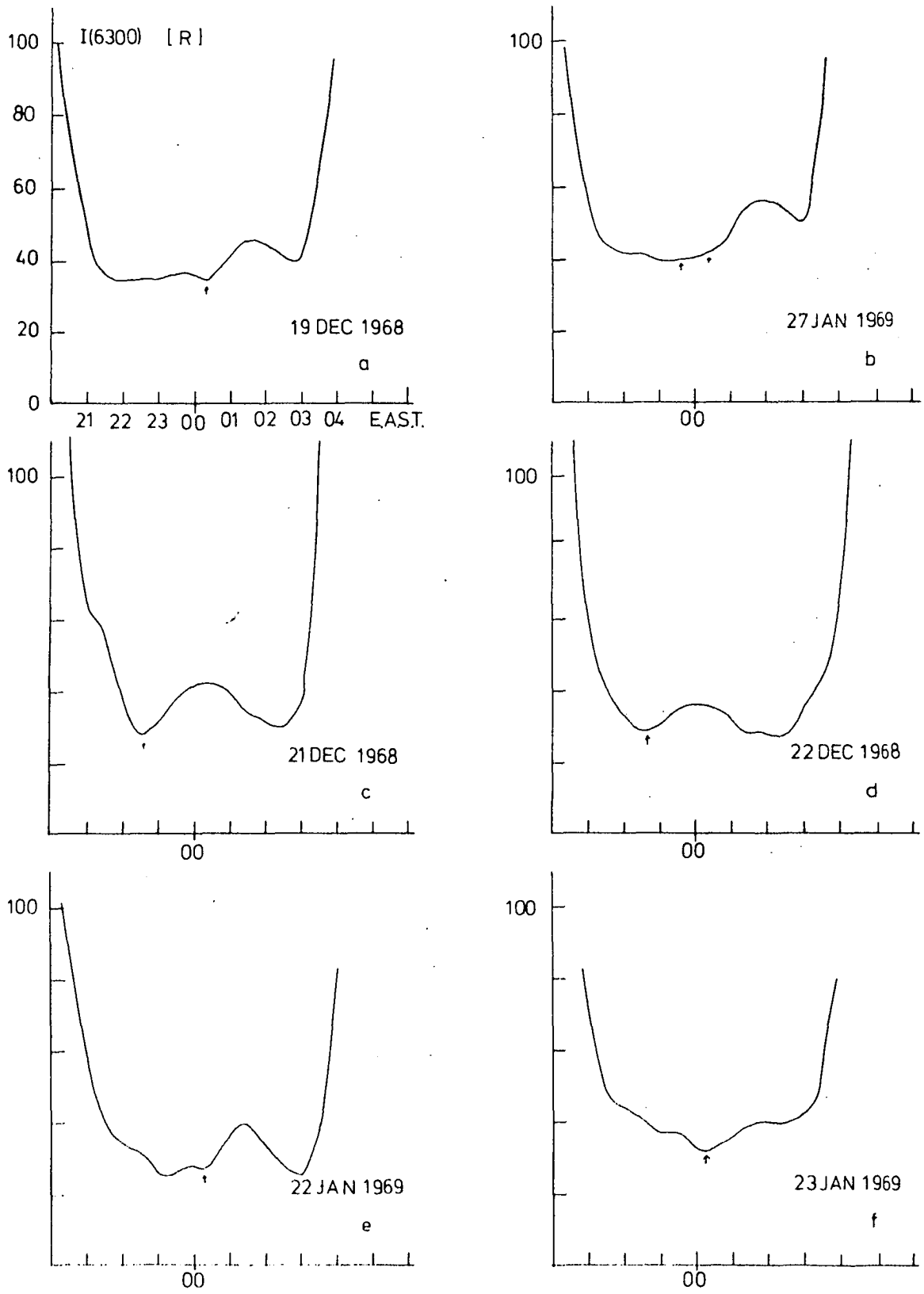

Fig. 7.1 Six examples of midnight summer enhancement.

7.2.2 Latitude variations

Fig. 7.2 shows the intensity variations of I (6300) as obtained from Hobart at points to the north and south (zenith angle 75^{o}) and also the zenith. Their curves are labelled N, S and Z respectively. On all the four nights shown the enhancement occurs to the north: it occurs to the zenith on three nights but only once does it clearly occur to the south. All these nights are quiet geomagnetically. To study this properly it is necessary to have some quantitative measure of the enhancement intensity. For quiet nights (Kp $\leq$ 2o) the following definition for enhancement strength is satisfactory:

$$\Delta I = 1/3 \left[\left(I(t_x) + I(t_x + \tfrac{1}{2}) + I(t_x - \tfrac{1}{2}) \right) - \left(I(t_n) + I(t_n + \tfrac{1}{2}) + I(t_n - \tfrac{1}{2}) \right) \right] \quad 7.1$$

Here t_x is the time of maximum intensity between 0030 and up to 0,5 hours before F-region dawn. Thus $I(t_x + \frac{1}{2})$ is the intensity 0.5 hours after this maximum is reached, and so on. The time t_x cannot fall closer than 0.5 hours to sunrise so as to exclude inflated values of $I(t_x + \frac{1}{2})$ for cases such as in fig. 7.1 f.

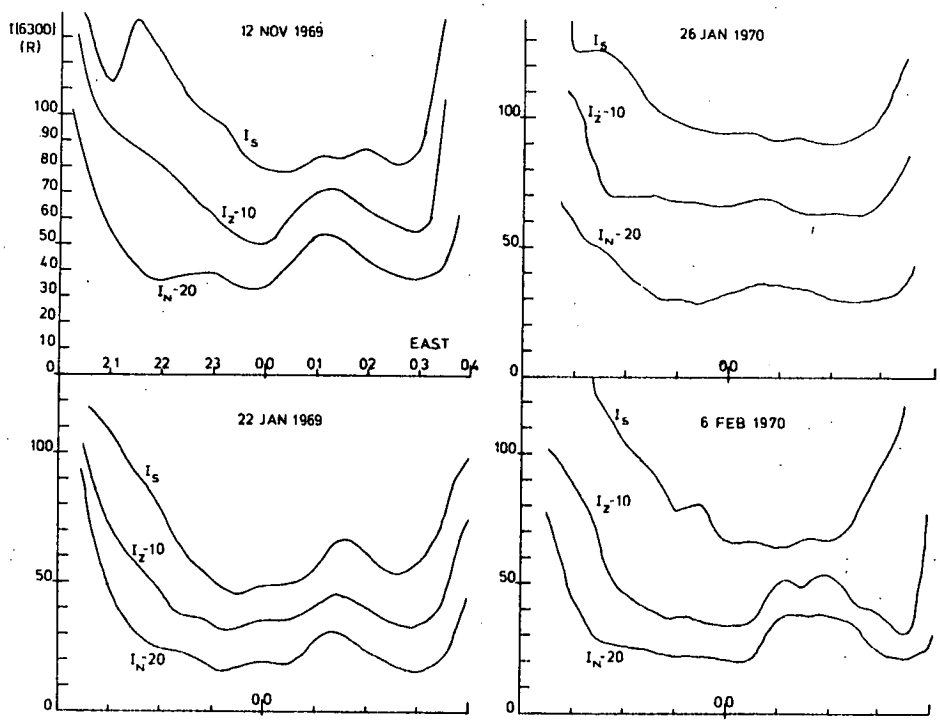

Fig. 7.2 MSE as observed to the north (N), zenith (z) and south (S).

The time t_n is defined as the time of minimum intensity after sunset and before 0030. Values of Δ I could be very misleading on disturbed nights. For on such nights any auroral disturbance would distort Δ I. For this reason only quiet nights are suitable for employing 7.1. On quiet nights large random enhancements of 6300Å can occur at low latitudes; for example see Peterson and Steiger (1966)'s report for Maui (21°N, 156°W). At Hobart however, no such large enhancements on quiet nights have been detected.

Using 7.1 and the 37 quiet nights of 1968 - 1969 the mean magnitudes of the increases in I (6300) are given in the first row of table 7.1:

Table 7.1

	Δ I (south)	Δ I (zenith)	Δ I (north)
Kp $\leq$ 2o	2.3	8.1	12.7
all ΔI>0	10.1	12.8	14.3

It appear that the enhancement is stronger to the north than to the south or zenith. As can be seen from fig. 7.2 the enhancement may not occur to the south or zenith so the weakness of the mean I (south) is partly due to the absence

of the MSE there on some nights. However, even if the mean Δ I's are calculated only for nights in which Δ I is positive in all three positions the Δ I north is still stronger than the other two. This can be seen from the second row of Table 7.1. On individual nights Δ I (south) can be as great as Δ I (north) but usually this is not so. In general:

$$\Delta \text{ I(south)} \quad < \Delta \text{ I (zenith)} \leqslant \Delta \text{ I (north)} \qquad 7.2$$

The MSE is thus stronger at low latitudes and falls off in intensity polewards. The MSE does not have any fixed latitude cut-off but very rarely occurs south of $\Lambda = 60^{\circ}$S. There is a clear tendency for this cut-off to move equatorward with increasing Kp and this will be discussed later.

7.2.3 Onset times

It was reported in Nichol (1970 a) that in the 1968 - 1969 summer the MSE appeared to begin earlier in December than in January or November. From subsequent observations in 1969 - 1970 this result is confirmed. Fig. 7.3 shows a mass plot of onset times and it appears that

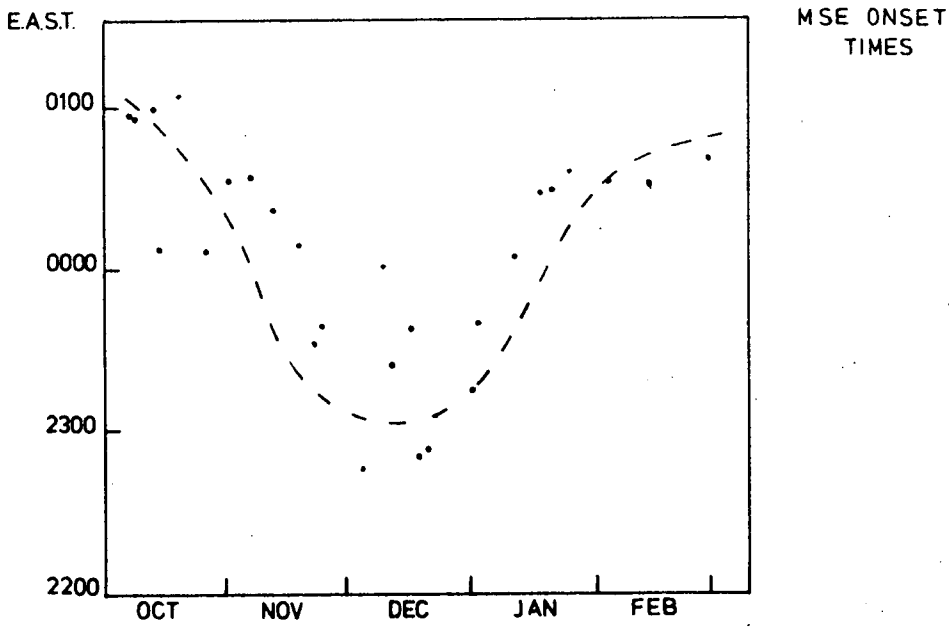

Fig. 7.3 Mass plot of MSE on-set times - note the symmetry about the solstice.

they group fairly symmetrically about the summer solstice. The times shown here are for the northern (75^{o} z.a.) observations because the phenomenon is more consistent there. Note that on many nights the onset time is very similar to that of the previous nights (this can be seen on fig. 7.1). The regularity over a whole month or from one year to the next is not nearly so good. This suggests that there are both long and short time constant controls on the MSE.

7.2.4 All sky morphology $Kp \leq 2o$

Figs. 7.4 and 7.5 show all-sky maps of the MSE for two quiet nights during the 1969 - 1970 summer. On the two nights themselves and on each of the three days which preceded them Kp was less than 8. Note firstly that the results of 7.2.2 hold for these days and that the increase in I (6300) is greatest to the north. The isophotes of intensity move in a more or less east to west direction although they are aligned from NE to SW. This may be caused by the NS gradient which would tend to change a monotonic EW gradient into one like this. However, the discussion of this point is left to chapter 9. The time taken for the peak of MSE to move from the 75^{o} zenith angle to the zenith is about 45 minutes, in both

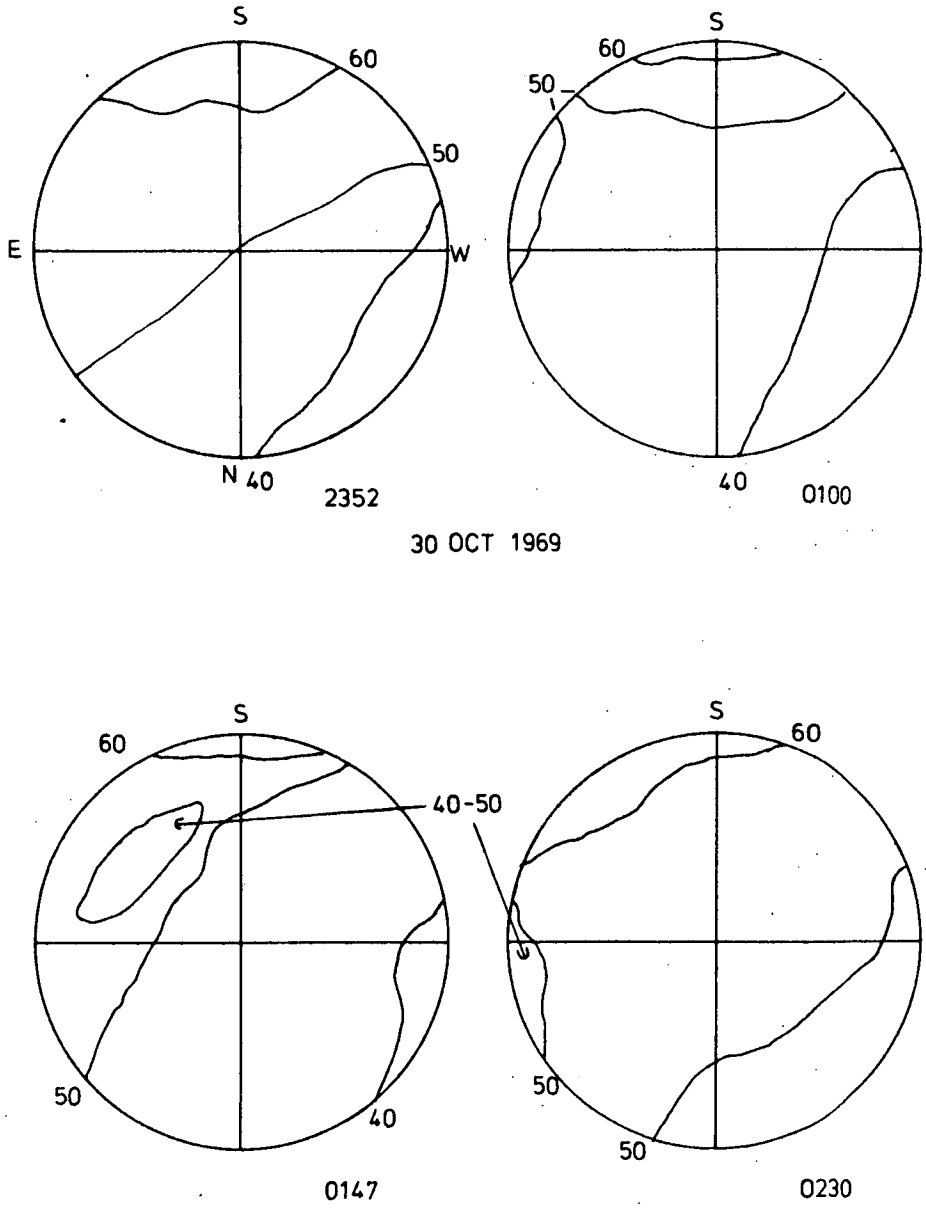

Fig. 7.4 MSE as seen on all sky plot on quiet night.

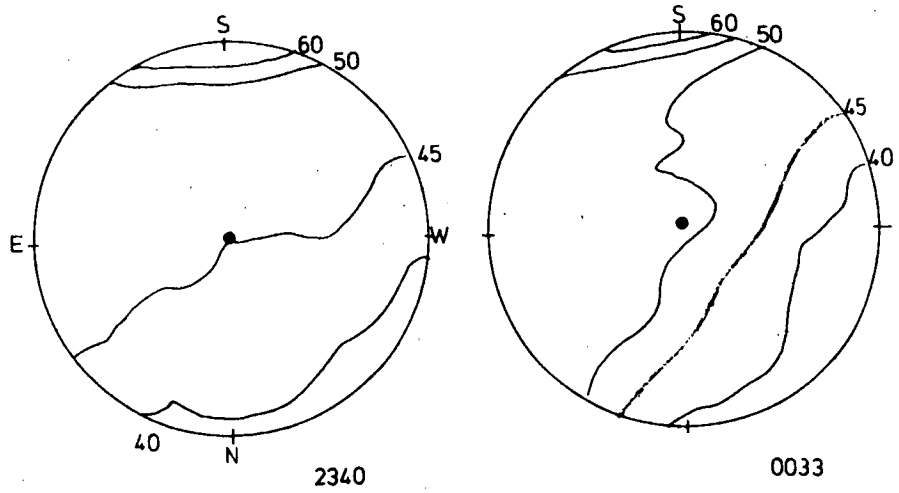

14 NOV 1969

[$\Sigma K_p = 3+$]

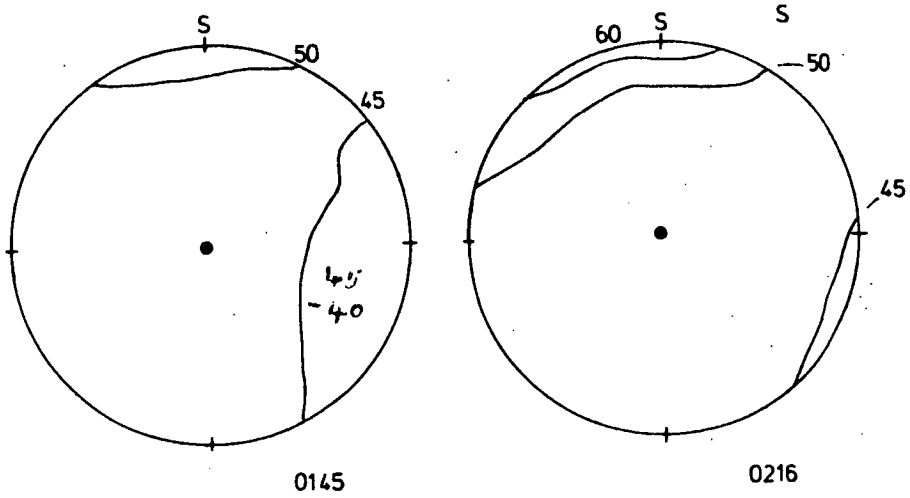

Fig. 7.5 MSE on different quiet night.

figures. This implies that a projection of this peak from an assumed 300 KM level on to the earth's surface would move about 1000 KM in 45 minutes, i.e. at 1333 KM hr. Now the surface rotational speed of the earth (radius R_e) at latitude ϕ) is simply:

$$V_\phi = 2\pi R_E \cos \phi /24 \qquad 7.3$$

which for $\phi = 43^\circ$ yields a velocity of 1250 KM/hr. which agrees well with the above projection's speed. This implies that the MSE is fixed in local time.

7.2.5 All sky morphology Kp > 2o

All the above discussion has been confined to undisturbed days. Any magnetically disturbed day leads to greatly increased 6300Å airglow levels which make the detection of the weak MSE practically impossible. As well as this it is known that 6300Å auroral activity tends to peak near 0100 local time in any case (Sandford 1964). Any effect due to this cannot be satisfactorily distinguished optically from the non-auroral MSE. As discussed in chapter 5 the zenith intensity at Hobart fluctuates strongly even on moderately disturbed nights; this fluctuation is clearly auro-

ral for it correlates well with the intensity to the extreme south. Fig. 7.6 shows such a disturbed night in February 1970. No MSE is apparent to the south or zenith but clearly occurs to the north. This is typical of moderately disturbed days. On very active days no MSE is found even to the extreme north. It thus appears that there is a latitudinal cut-off for the MSE which moves equatorwards at disturbed times.

The latitude cut-off may stay at low latitudes for some days after a disturbed period. Thus in fig. 7.7 which is a quiet day but which follows an active period there is no MSE except to the north. It is known that some of the effects of magnetic storms, such as exospheric heating persist in and near the auroral zone for several days after the storm (Cole 1965a, Cole 1970b). Possibly the increased neutral temperature interferes with the production process of the MSE.

7.3 Ionospheric Observations

7.3.1 Exospheric source of ionization

Fig. 7.8 shows monthly means of F-region critical frquency f_0F2 for various summer

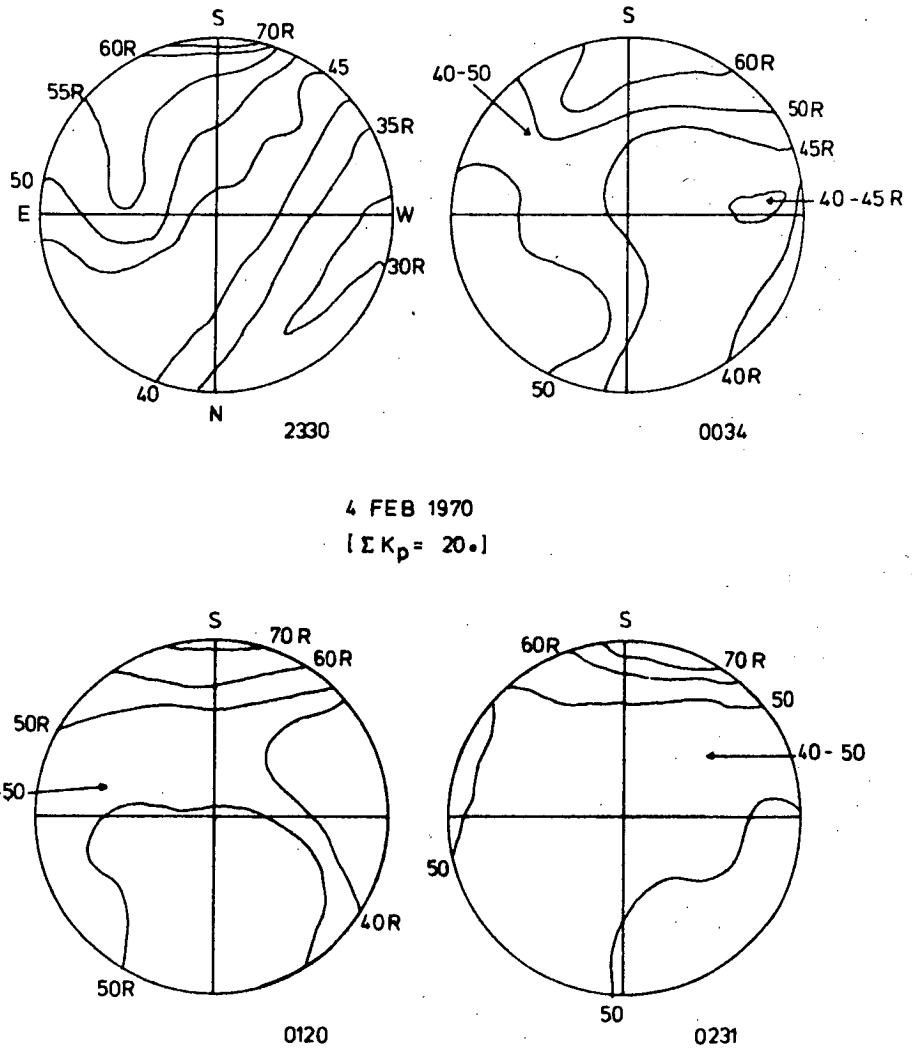

Fig. 7.6 MSE on disturbed night.

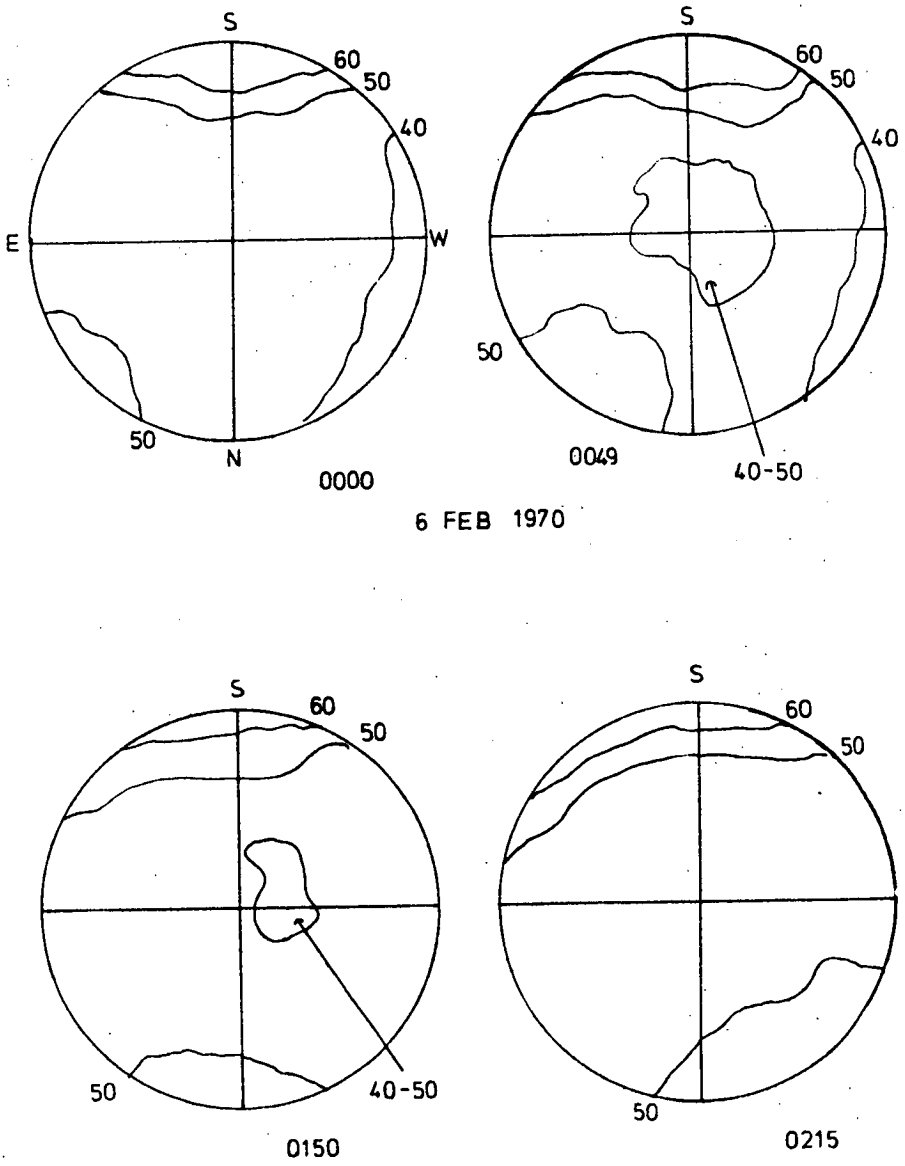

Fig. 7.7 MSE on quiet night but following magnetic storm.

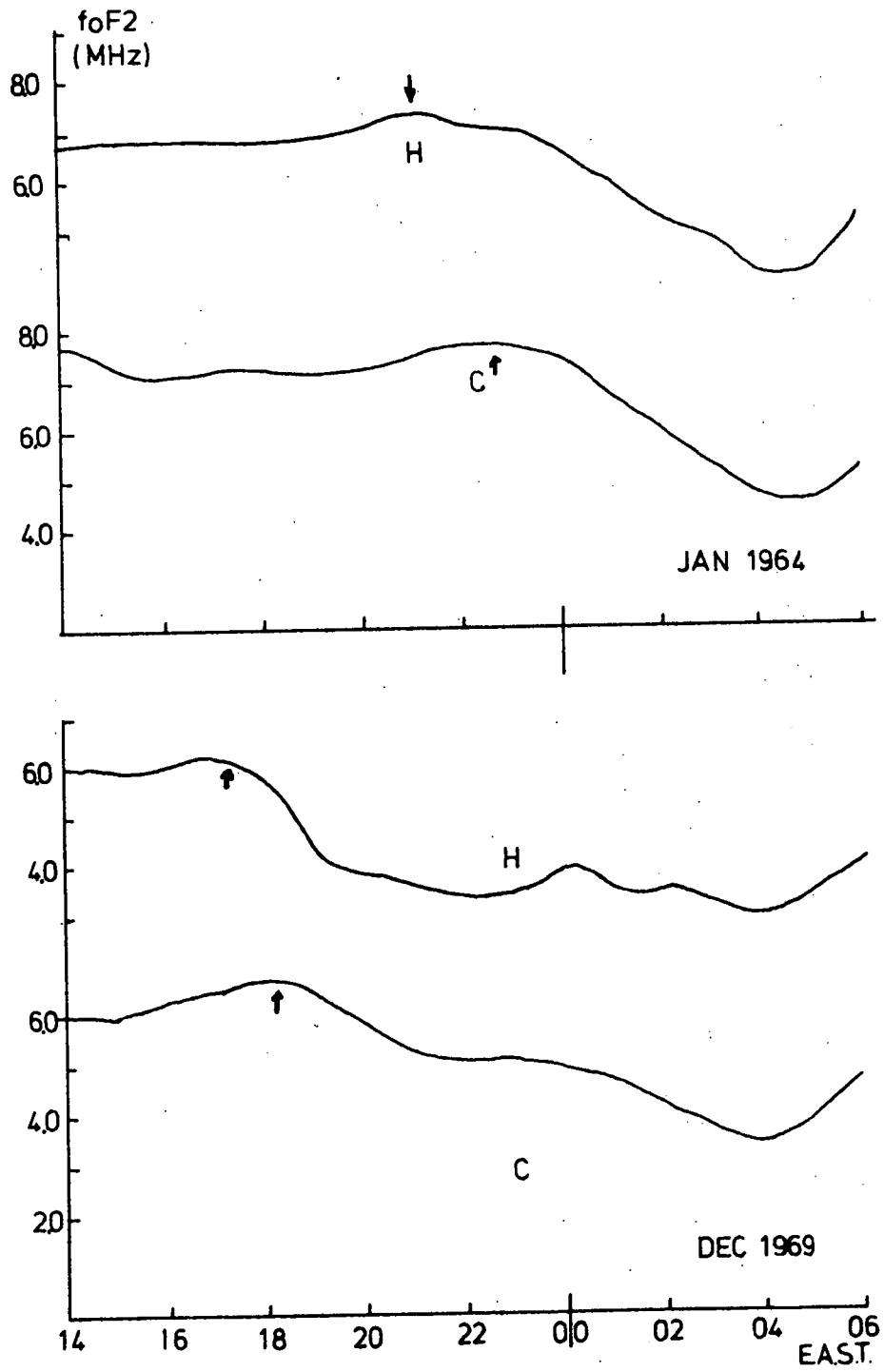

Fig. 7.8 foF2 for various summer months in 1969.

months in 1969 (maximum) at both Hobart and Canberra. All figures show a maximum in f_0F2 just after 98° za sunset. This is most marked at Canberra during solar minimum. It is generally accepted that this increase in peak electron density is caused by an influx of ionization from the ionosphere. Evans (1965 a) concludes from backscatter results at Millstone Hill ($71^\circ W$, $43^\circ N$) that the influx is caused by the large fall in electron temperature which he finds occurs at summer sunset. Titheridge (1968 a and b) however, from total content measurements using Syncom 3, concludes that ambipolar diffusion is not rapid enough to provide the total influx he observes at all seasons above 500 KM. Instead of ambipolar diffusion (which is implicit in Evans' model) he says that a height change in the O^+/H^+ diffusive barrier from near 1000 KM in the day-time to near 500 KM at night can explain the influx. On this model the O^+ ions are compressed into a smaller volume by this change thus leading to the (observed) increase in peak density. Now the behaviour of this influx is in general

very similar to that of the 6300Å MSE.

According to Titheridge:

(i) The influx falls off with increasing latitude (cf. 7.2.2).

(ii) At 42°S it lasts from 2230-0015 LMT.

(iii) The onset is earlier near the solstice (cf. 7.2.3).

However, in spite of this it appears that the influx cannot explain the MSE. Firstly the influx occurs up to 1.5 hours before the MSE does. Secondly the influx is too weak to cause an increase in O ('D) production or at least one lasting two hours According to Titheridge 1968 (b) the total influx below 500 KM at Hobart's latitude is 10^{12} el. cm^{-2} i.e. 1.39×10^{8} cm^{-2} sec^{-1}. However, the total rate of recombination is at least three times this*, so except possibly for a short time near 2200 LT (when f_oF2 increases in fig. 7.8), this influx cannot cause an <u>increase</u> in the recombination rate, merely a decrease in the rate of decay. At lower latitudes where the ionization influx is greater it is possible that the evening increase in f_oF2 is large enough to cause an increase in I (6300).

No such increase seems to have been reported however, probably because the enhancement is lost in twilight effects. It is thus necessary to look elsewhere for the cause of the MSE.

*The typical 6300^{o}A airglow intensity is 50 R on a summer night. If 0.15 photons are produced per recombination then the total recombination rate must be $50 \times 10^{6}/0.15 = 3.3 \times 10^{8}$ cm^{-2} sec^{-1}. If quenching is included this rate is the order of 5.0×10^{8} cm^{-2} sec^{-1}.

7.3.2 The downward ionospheric drift

Fig. 7.9 shows monthly medians of the peak height $h_m(F)$ of the F-region during 1969 for summer months at Hobart and Canberra. There is a downward drift in the ionosphere in all months near mid-night. It seems likely that this drift causes the MSE for of course the increase in ambient O_2 density would lead to increased recombination and thus O('D) production. It is clear from fig.7.9 that the fall is greater at Canberra than at Hobart. Other things being equal this implies that the resulting MSE is greater at Canberra than at Hobart as is observed. Figs. 7.10 and 7.11 show the close correlation observed between -h'(f) and I (6300) on individual nights. In fig. 7.10 I (6300) falls before dawn but h'(f) does not. However it is clear that the electron density is falling fast at this time (fig.7.10) which would tend to reduce the recombination. It must now be shown that the behaviour of the ionosphere is sufficient to explain the observed MSE. This is done below.

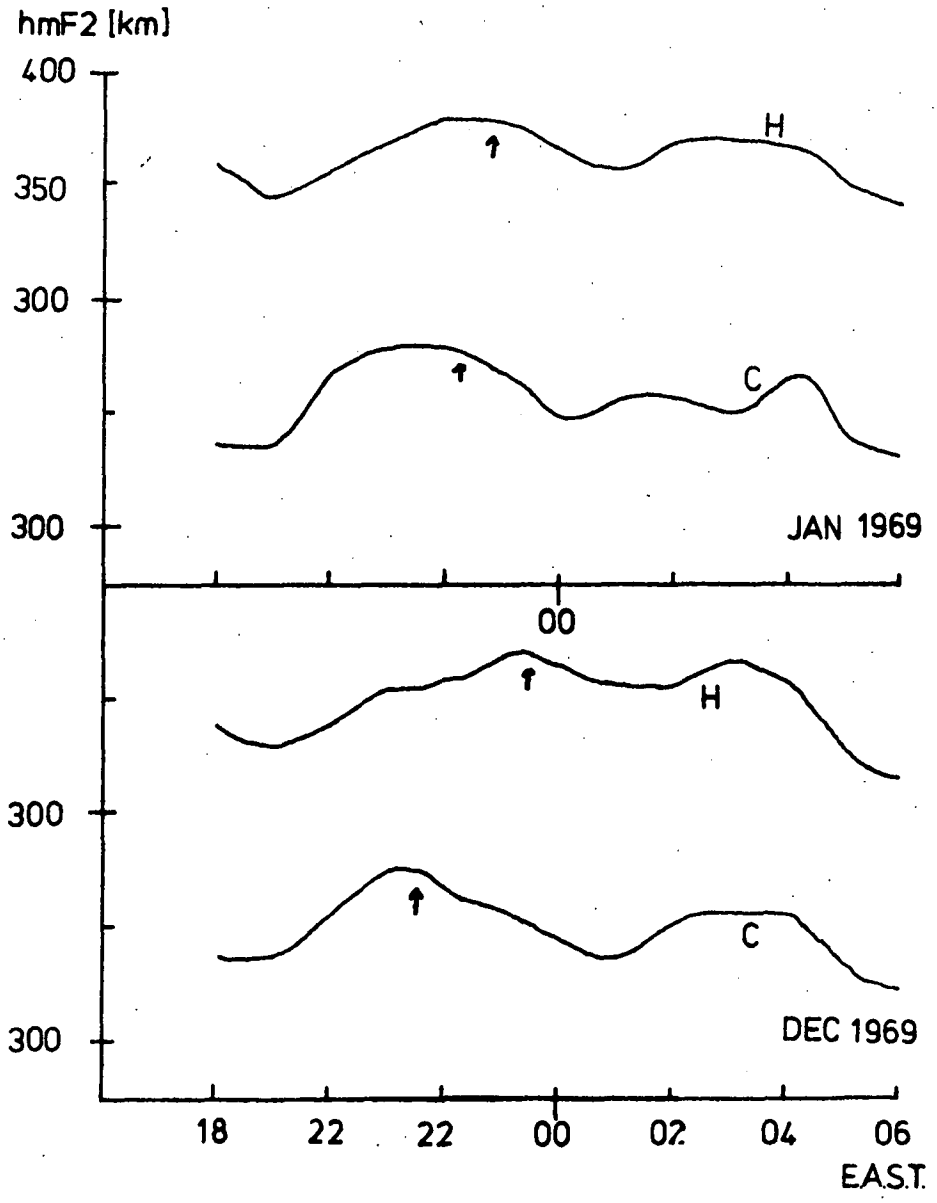

Fig. 7.9 Plots of $h_m F$ versus EAST for Hobart and Canberra in summer.

Fig. 7.10 The midnight enhancement is largely due to a fall in the F region.

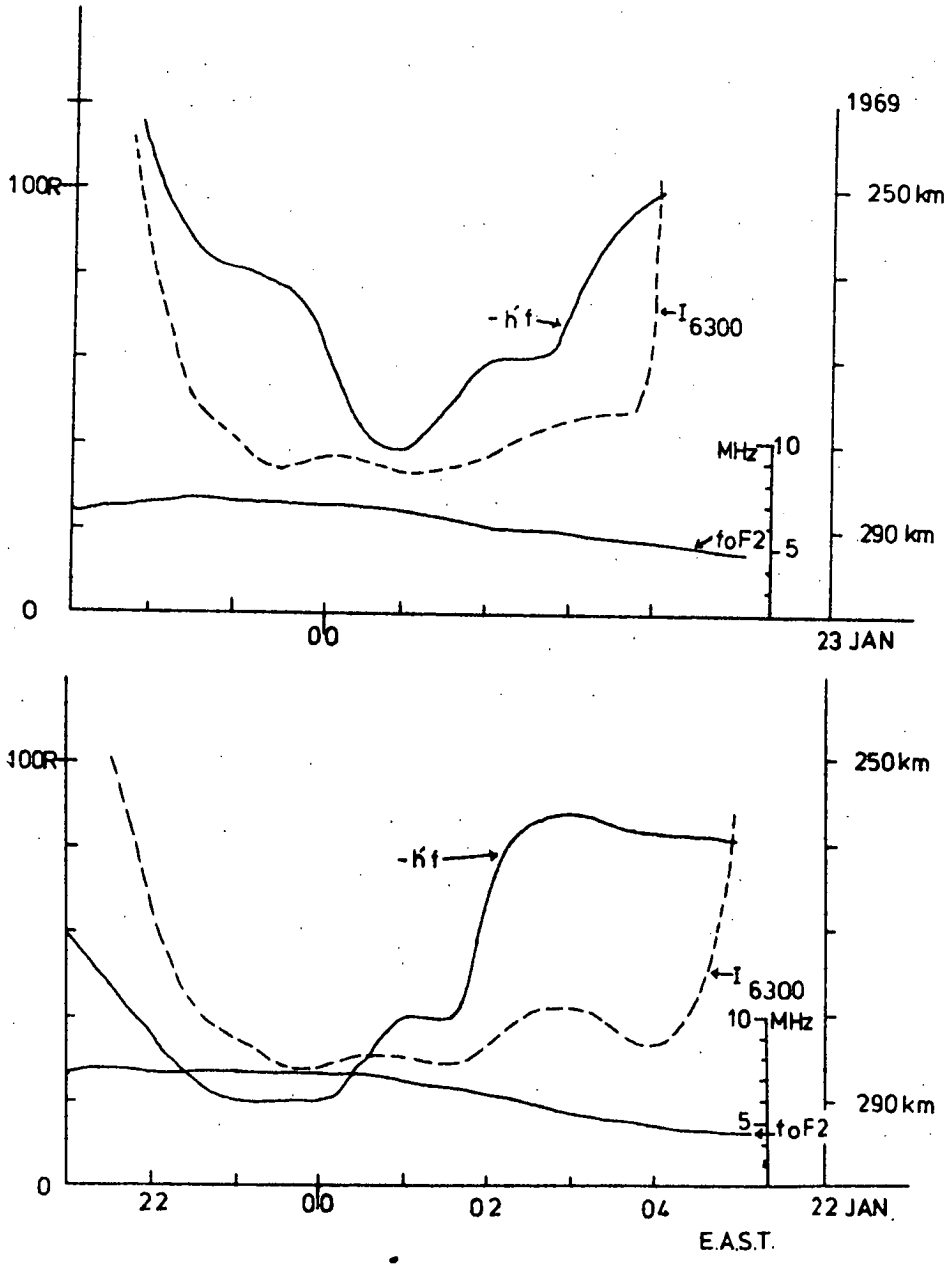

Fig. 7.11 Note that h'f does not fall before dawn (cf. Fig. 7.10).

7.3.3. The downward drift and the M.S.E.

The same procedure to calculate the effect of the increased recombination of I (6300) is adopted here as in chapter 6. Because of the bad sporadic E in summer at Hobart and the lack of topside data the electron profile used is a scaled - up version of that found by N.A.S.A. Flight 11.03 at Wallops Island (Nagy and Walker 1967). The atmosphere used is the CIRA model 6 (10.7 cm flux $F = 175 \times 10^{-22}$ Wm^{-2} Hz). This is used in preference to model 5 (10.7 cm flux $F = 150 \times 10^{-22}$ Wm^{-2} Hz), which for the month to be considered (January 1969) is the 'correct' one, in an attempt to compensate for the increased molecularity of the summer atmosphere at Hobart.

Now denoting the maximum height of the ionosphere's peak as $h_m(t)$ where t is the local time an estimate of this can be obtained by Shimazaki's (1955) formula:

$$h_m = 1490/MUF - 176 \qquad 7.3$$

where MUF is the M(3000)F2 factor routinely obtained from ionograms.

Considering January 1969 then at 2300

LST at Hobart MUF = 270. Using 7.3 this gives $h_m(23)$ = 376 (KM). To estimate the increase in I (6300) produced by the fall in h_m from 2300 to 0100 the mean change in h'(f) from 2300 to 0100 was calculated from the usable ionograms. This fall was 20.5 km.

Thus as

$$h_m \quad h'(f) + \text{constant} \qquad 7.4$$

then $h_m(0100)$ = 355.5 assuming that the MUF factor at 2300 is correct. This round-about approach was adopted because of the earlier expressed reservations about the MUF values as published. Actually for this particular month $h_m(0100)$ estmated from 7.3 is 356.0 km but this is unusual for in most months h'(f) is a much better indicator of height changes (and thus recombination changes) than the MUF factor is.

Thus for January 1969 the median f_oF2 and mean height parameters at 2300 LST and 0100 LST are:

Table 7.2

LST	f_oF2 (MHz)	Ne($\times 10^5$)	h_mF2
2300	7.0	6.07	376.0
0100	6.0	4.47	355.5

where NE is the peak electron density.

From table 7.2 it is seen that although recombination tends to increase between 2300 and 0100 because of the fall there is also a considerable fall in electron density. Also the drop in neutral temperature T_n is quite significant in the CIRA model

Peterson's (1968) formula for volume emissivity of I (6300) as developed in chapter 3 is:

$$E_{63} = \frac{4.56 \times 10^{-12} [O_2] \quad n}{\left(1 + 9 \times 10^{-9} [N_2]\right)(1 + 1.6 \times 10^{-3} [O_2]/n)} \qquad 7.5$$

The electron density and oxygen profiles yield, using 7.5, the height-emissivity curves of fig. 7.13. Integrating these curves gives the total airglow emission in rayleighs as:

$$I\ (t = 2300) = 64.8$$

$$I\ (t = 0100) = 71.9$$

Thus an increase of 7.1 R. This is the same order as that observed at Hobart, although a little on the low side. However, if, as appears likely, the actual fall in T_n between 2300 and 0100 is less than that assumed in CIRA 1965 then the in-

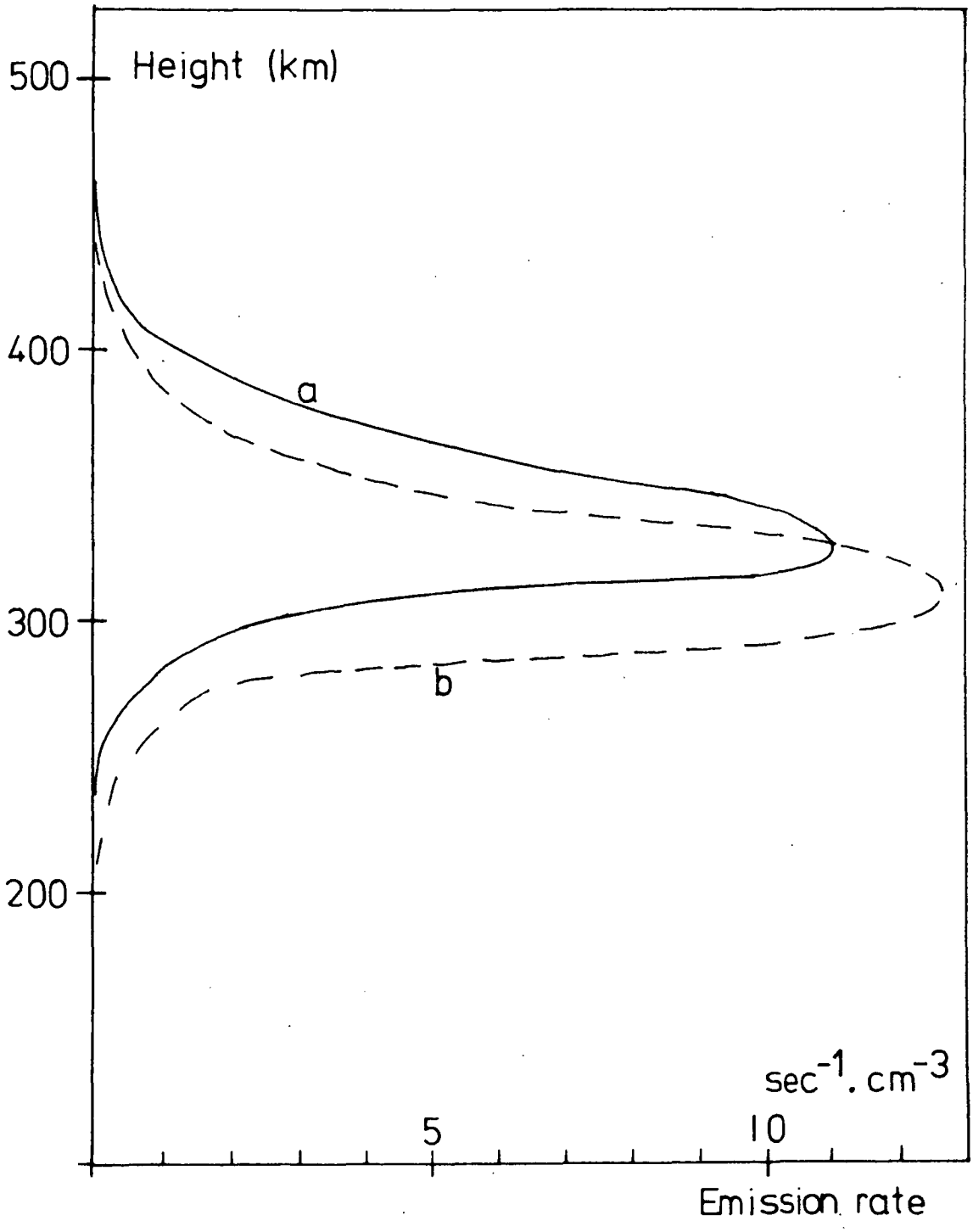

Fig. 7.13 The height-emissivity curves before and After the fall in the ionosphere.

crease could be up to three times as great as this.

However, it appears that an increase in dissociative recombination as produced by a post midnight downward drift in the ionosphere is adequate to explain the MSE.

7.4 Latitude Extent of the MSE

7.4.1 Lower latitude observations of a midnight maximum:

At low latitudes 1 (6300) normally exhibits a maximum near to or after midnight not only in summer but at all seasons (Delsemme and Delsemme 1960: Silverman and Carversle 1966: Barbier 1965: Barbier, Roach and Steiger 1962). At Mt. Abu (25°N, 73°E) Pal and Kulkarni (1968) found an early morning maximum near 0300 LST which like the MSE was well correlated with -h'f. All these maxima are however much greater than the Hobart MSE with increases up to 100 R common.*

*According to Pal (personal communication) the Mt. Abu maximum was much smaller in 1966 than in either 1965 or 1967.
Why this should be is not clear and obviously requires closer study.

However it seems possible, in view of the latitude dependence which the MSE exhibits, that the Hobart enhancement is the weak tail-end of the low latitude enhancement. Prior to the present results the highest latitude station which has reported a mid-night maximum is Sacramento Peak (33°N, 106°W) which has an invarient latitude of $\Lambda = 41^{\circ}$N (Bellew and Silverman 1966).

This maximum does not appear to be as regular as the MSE observed at Hobart but has similar features in that it is stronger to the south (i.e. equatorwards) and anti-correlates with the ionospheric height. However, they find it is stronger on days of high Kp; at Hobart the MSE is not usually detectable on such days. The most obvious explanation of this is that Hobart, because it is much closer to the auroral zone, is subject to large rapid changes in precipitated

electron flux on such days, the effects of which would tend to obscure even a strengthened MSE*. However, as will be shown later there is reason to believe that the mechanism which produces the ionospheric lowering is nullified on such nights near the auroral zone. However, it does appear likely that the Hobart MSE is part of a world-wide lowering of the ionosphere near local mid-night.

*In view of the results of the previous chapter another explanation is the apparent breakdown of diffusive equilibrium at $\Lambda = 55^{\circ}$ but not at $\Lambda = 40^{\circ}$.

7.4.2 F-region fall near midnight

To show how extensive the ionospheric fall in the summer months is, a survey of the published monthly median heights for the IPS station near the 150°E meridian has been made. The year considered is 1964 - 1965 which is a solar minimum year but is chosen because of the availability of h'f data in that year. The stations considered are:

Table 7.3

Station	Latitude	Longitude
Port Moresby	9° 25'S	147° 9'E
Townsville	19° 18'S	146° 44'E
Brisbane	27° 32'S	152° 55'E
Canberra	35° 19'S	149° 0'E
Hobart	42° 55'S	147° 19'E

Figs. 7.14, 7.15, 7.16 use h'f data to show on a geographic latitude - local standard time display where the ionosphere is drifting downwards, i.e. where recombination tends to increase. The shaded area represents the time and place where a fall has occurred in h'f from the previous hour. If no change has occurred in h'f from one hour to the

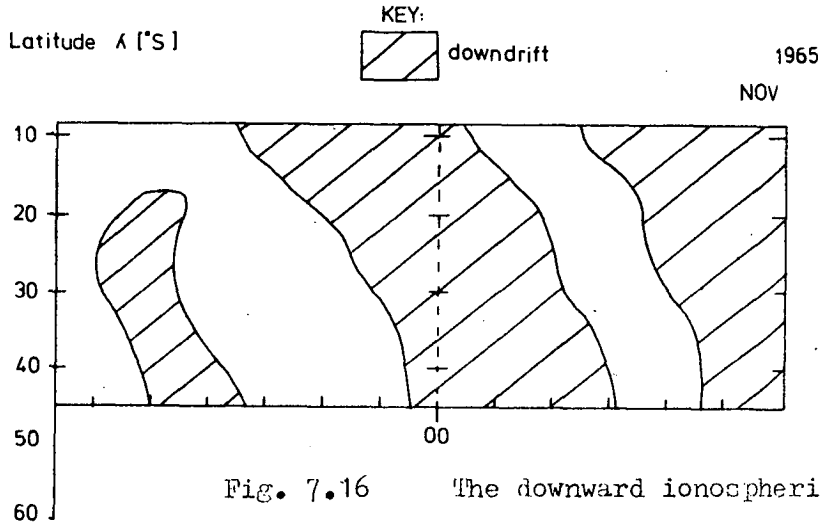

Fig. 7.16 The downward ionospheric drift

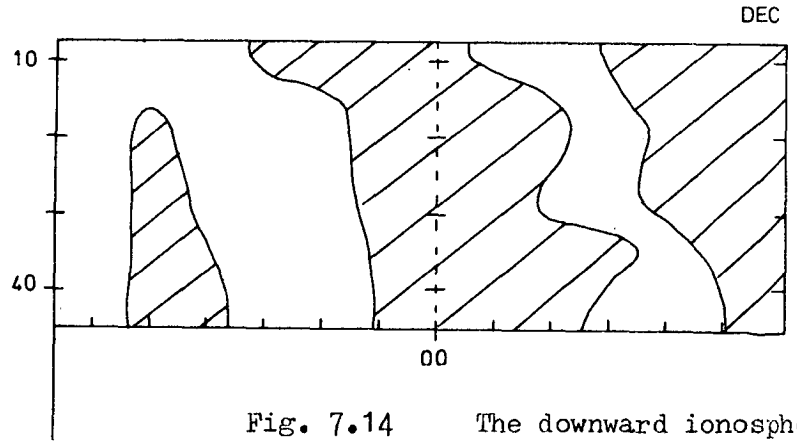

Fig. 7.14 The downward ionospheric drift

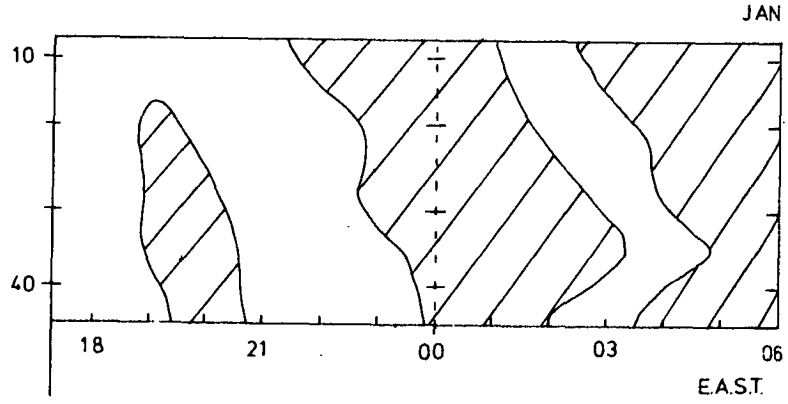

Fig. 7.15 The downward ionospheric drift for January 1965.

next then the area surrounding the second hour is shaded or not shaded according to whether the previous hours were shaded or not shaded. The use of this simple convention results in a remarkably regular and consistent pattern. On all the three months shown it is seen that the ionosphere falls more or less simultaneously from $15^{o}S$ down to at least $43^{o}S$. This is consistent with the E to W movement of the MSE reported in 7.2.4. Note as well that the fall begins earlier in December than in January or February. It thus appears that the spatial morphology of the enhancement is due to a general midnight ionospheric lowering. It must now be shown that the latitude variation of the increase in I (6300) is consistent with the magnitude of the fall.

To do this $h_{m}F2$ as determined by the M(3000)F2 data for January 1969 is used.* This for all five stations is shown in fig. 7.17. From the published $f_{o}F2$'s the behaviour of the airglow on a median night can be calculated

*Because of previously stated reasons h'f data is used at Hobart.

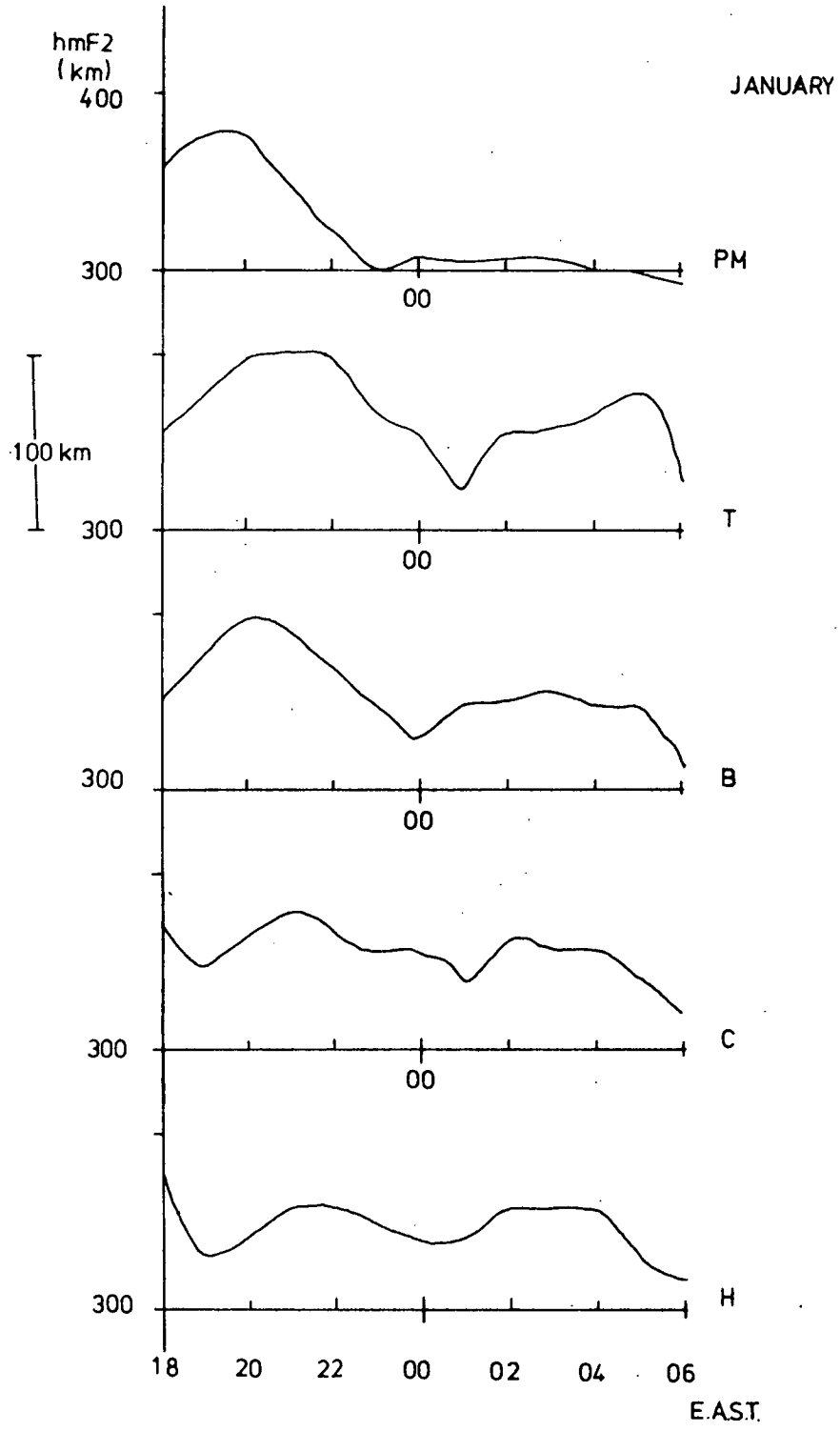

Fig. 7.17 $h_M F2$ for January 1969.

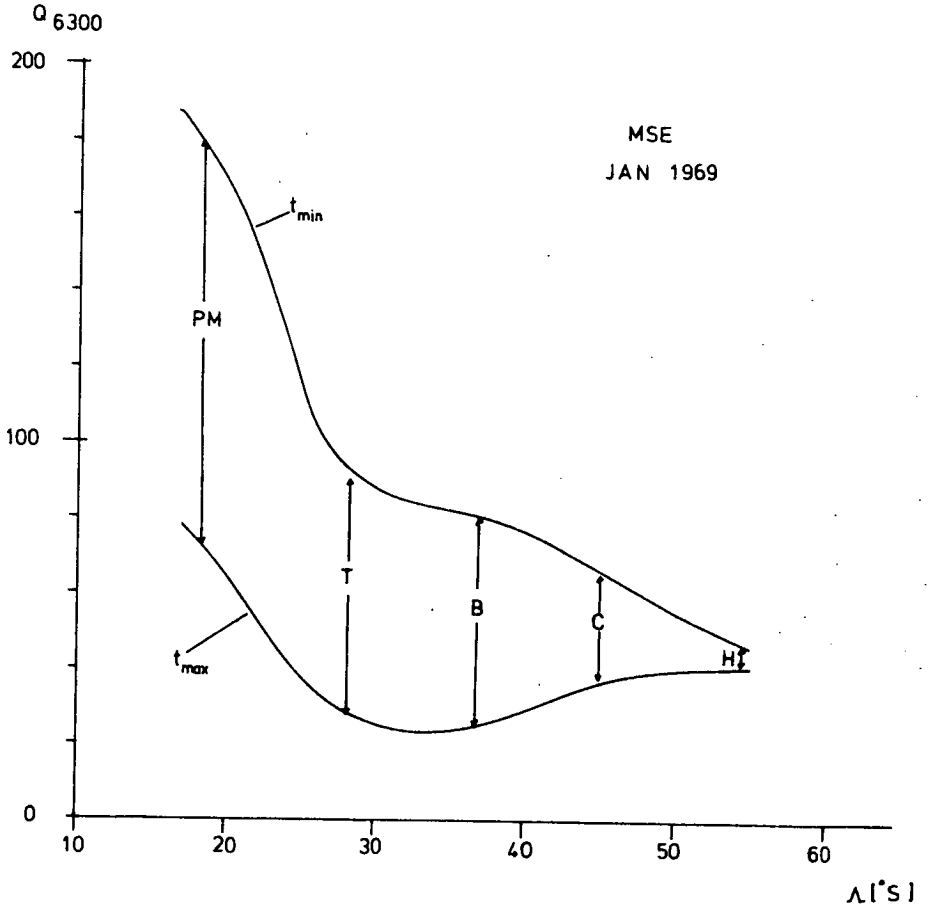

Fig. 7.18 The fall off of the MSE with latitude.

using 7.5 and Jacchia and Slowey's (1967) model atmosphere. This is shown in fig. 7.18. The fall off in the enhancement with latitude is very clear and thus it seems that the world-wide drop in F-region near local mid-night can explain both the Hobart observations and those at lower latitudes.

7.5 CONCLUDING REMARKS

There are still a number of anomolies to explain concerning the MSE. Firstly Bellew and Silverman (1966) suggest that their mid-night maximum only occurs at solar maximum, whereas from section 7.4 above it seems that the MSE should still occur at solar minimum.

Also the Mt. Abu observations of Pal and Kulkarni (1968) suggest a later maximum at low latitudes than is suggested by figs. 7.14 and 7.16. Furthermore, the low latitude maximum appears to occur at all seasons. This suggests that a MSE type enhancement should still occur in winter at Hobart. This will be examined in the next chapter and the previous points raised will be discussed in chapter 9.

Chapter 8: OI AIRGLOW - WINTER AND EQUINOX

8.1 Introduction

Some aspects of the winter and equinox behaviour of the 6300Å airglow have already been discussed in chapters 5 and 6. These concerned the production of $O(^1D)$ atoms during the presence of the midlatitude ionospheric trough. The purpose of the present chapter is essentially to examine the temporal control of those mechanisms. It is known that at many midlatitude stations an enhancement of the red-line occurs in the early morning on most winter nights. This is such that from a minimum near midnight the intensity (I(6300) increases monotonically up to dawn. This phenomenon, which is known as the 'pre-dawn enhancement of 6300Å airglow' (called PDE hereafter) has been much examined in recent years. One of the main reasons for this interest has been the growing awareness of the importance of conjugate point influences on the local ionosphere. In this case it has been thought that the PDE arises from photoelectrons emitted in the sunlit conjugate F-region and which travel along the field to the local ionosphere. Although it has already been necessary to invoke this mechanism to explain part of the 6300Å airglow levels in the trough at Hobart it appears from the present study (Nichol, 1970(b)) that

this mechanism alone is not responsible for the PDE; a conclusion reached independently by Noxon and Johanson (1970) at Boston (Λ = 55.4°N) and S haeffer at Adelaide (Λ = 46.2°S) (personal communication (1971))*. The main conclusions reached by this study are that the onset of the PDE is, for 95% of nights, controlled by a local increase in dissociative recombination of O_2^+. However, later on in the PDE the effects of increasing photo-electron flux become more important. The increase in recombination is mainly due to a fall in the height of the F-region and it is proposed that this is due to the same mechanism as that producing the midnight summer enhancement (chapter 7). The differences between the pre-dawn enhancement and the midnight summer enhancement are thus due almost entirely to the absence of conjugate fluxes in summer. This is discussed in detail in chapter 9.

8.2 Historial review

Elvey and Farsworth (1942) were the first to report the existence of a slow post-midnight rise in 6300Å airglow during winter nights. This commenced too early to be caused by any sunrise effects and its origin was unknown. The spatial morphology of the phenomenon was examined in France by Dufay and Tcheng Mao-Lin (1946) and in detail by Barbier (1959, 1961).

* Now published in Shaeffer (1971)

Barbier said that the enhancement moved across the sky from a SSW direction as a 'sub-polar sheet' and it led to a pre-dawn enhancement of the order of 100R, (see fig. 8.1). It was not until Cole's (1965) suggestion that the enhancement was related to magnetic conjugate point (MCP) sunrise that any viable explanation was produced. Cole's theory was based on the work of Hanson (1963) who found that under certain conditions photo-electrons can escape from a sunlit ionosphere into the exosphere where they would be conducted into the conjugate ionosphere by the magnetic field (see fig. 8.2). For certain places on the globe this conjugate ionosphere could still be in darkness (during local winter) and Cole suggested that heat loss to the ambient electrons by this MCP photoelectrons could raise the electron temperature sufficiently to excite the $O(^1D)$ atoms thermally. That such an increase in local T_e does occur at conjugate (F-region) sunrise had been shown by Carlson (1965) at Arecibo ($\Lambda = 19.2^{\circ}N$) and more recently by Evans and Gastman at Millstone Hill (1968) ($\Lambda = 55.4^{\circ}N$). However, the temperature increase at Saint-Santin de Maurs ($\Lambda = 39.5^{\circ}$ N) observed by Duboin et al (1968) was not great enough (a maximum T_e of $1900^{\circ}K$) to account for the 50R PDE they observed simultaneously. Duboin et al

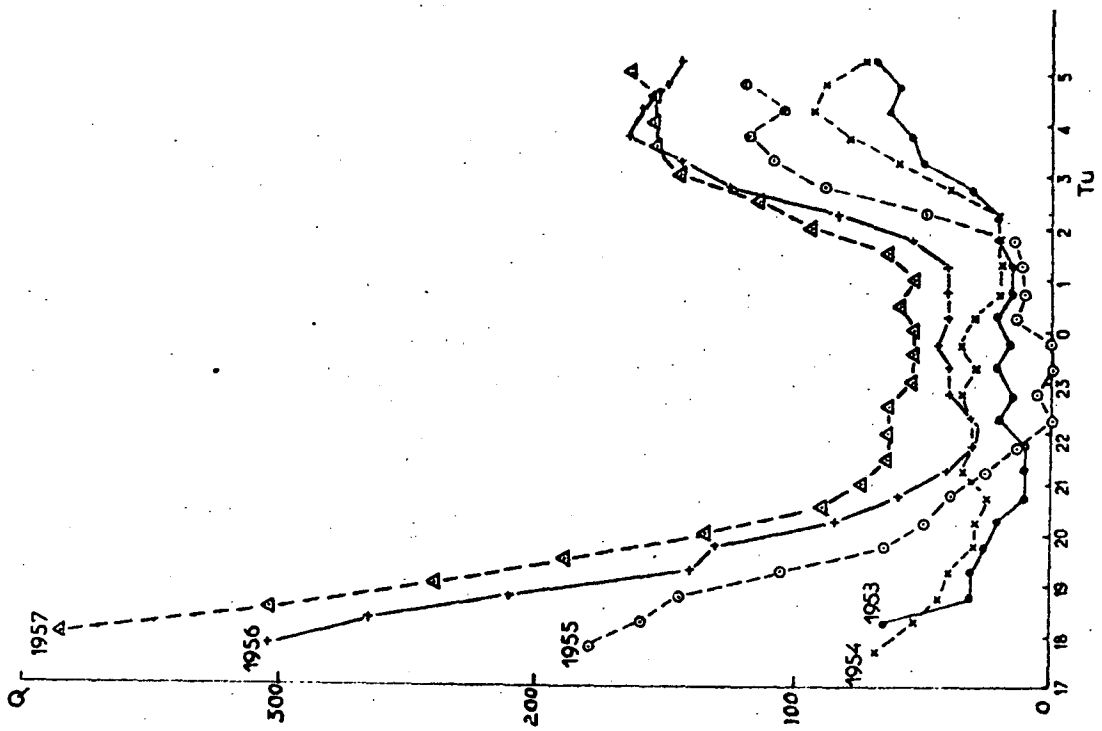

Fig. 8.1 The winter pre-dawn enhancement at Haute-Provence (from Barbier 1959).

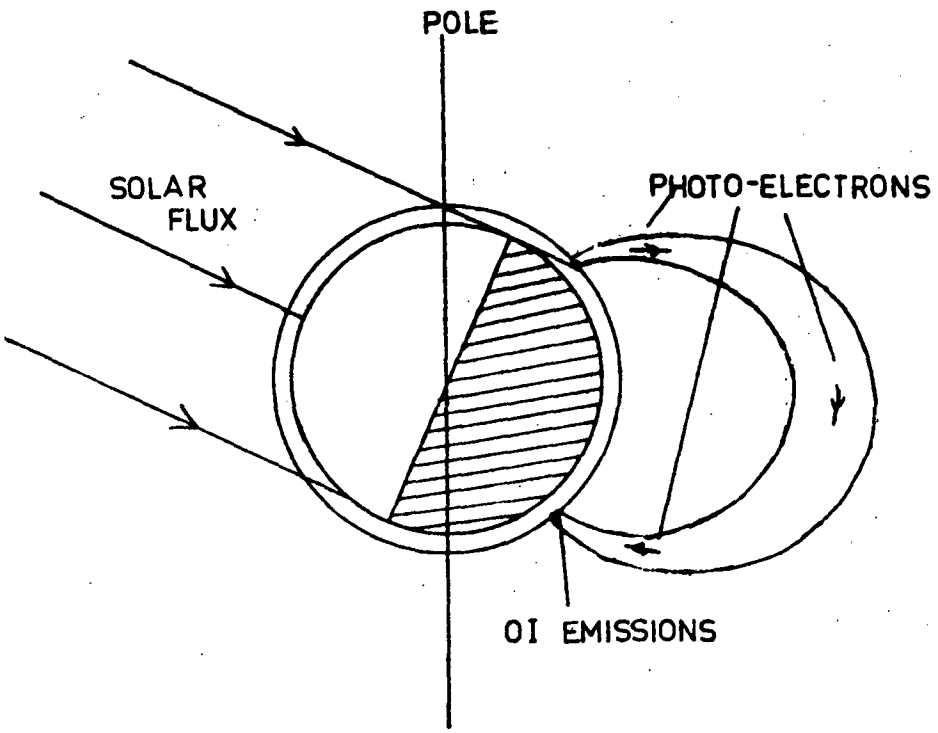

Fig. 8.2 The mechanism invoked by Cole (1965a) to explain the P.D.E.

proposed that direct collisions with OI atoms could explain the 6300Å increase. In situ observations in the exosphere of escaping conjugate photo-electrons has suggested that fluxes of the order 2×10^8 cm^{-2} sec^{-1} (5 - 15eV) should arrive in the darkened ionosphere (Rao and Maier 1970, Heikla 1970, Rao and Donley 1969). This is sufficient to explain the observed enhancement of 6300Å airglow by direct excitation and so it appeared that the PDE was fully explained. However, as will be shown below the PDE is a much more complicated phenomenon than this.

8.3. Airglow Observations

8.3.1 Intensity of PDE

Fig 8.3 shows plots of 6300Å zenith intensity versus local standard time for six typical nights in 1969. The increase in intensity for the minimum up to local F-region dawn was in the range 20 to 60R. For 21 days in June, July and August 1969 on which a PDE was observed its mean value was 39.3R with a standard deviation of 8.6R. For individual enhancements there was no obvious correlation of the increase in intensity and the concurrent solar flux (10.7 cm) levels. Smith (1969) in Great Britain also found no obvious correlation for individual days during 1965-1967. On the other hand

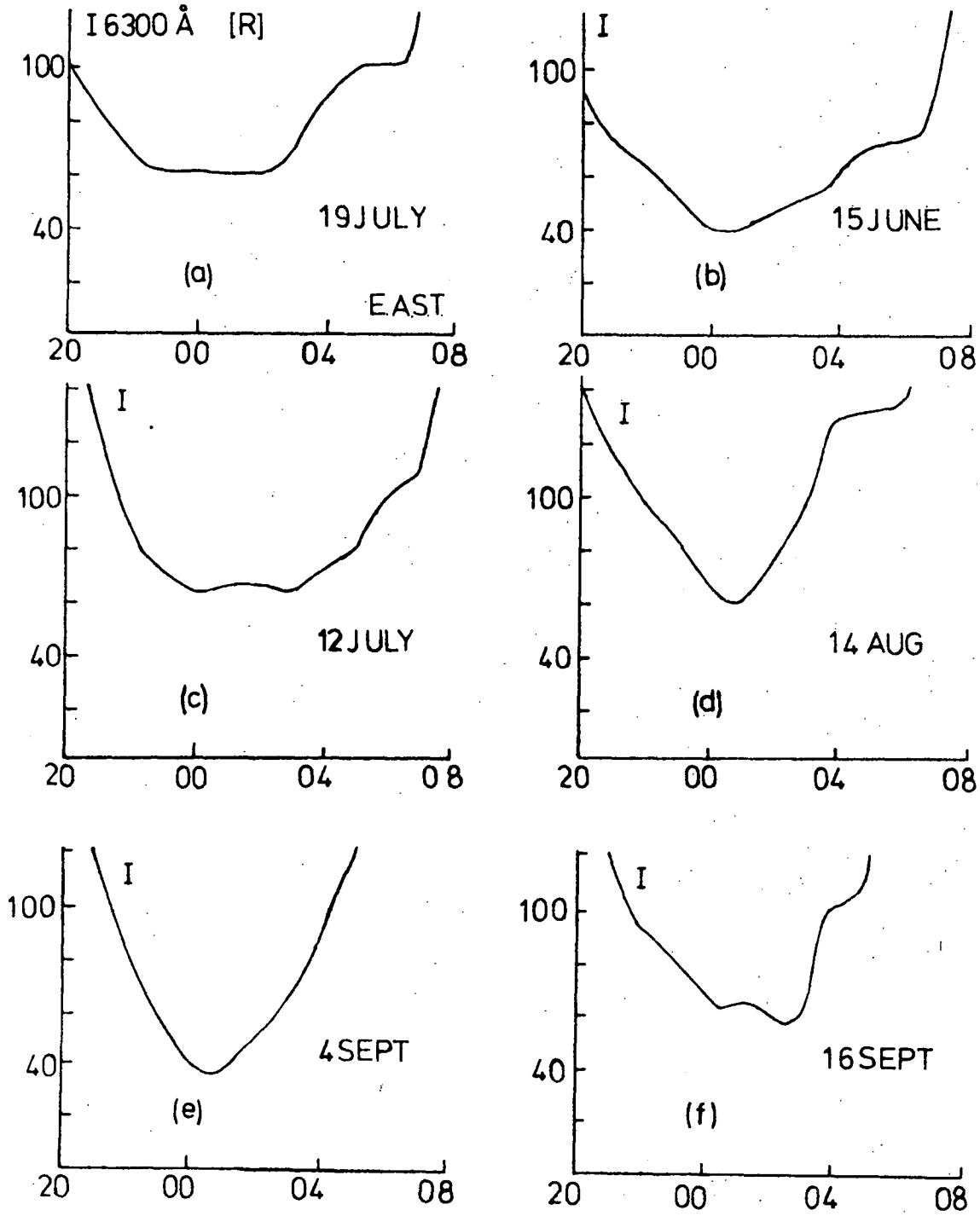

Fig. 8.3 Typical observations of the P.D.E. at Hobart in 1969.

Deehr (1969) using data obtained over a whole solar cycle found that the intensity of the PDE increased monotonically with solar flux. For very high solar flux there was some indication (fig. 8.4) of a plateau being reached in the magnitude of the PDE at Haute Provence. This figure was drawn using mean data and it may be that data averaged over a whole solar cycle is needed before this relationship shows up. This discrepancy between mean behaviour and individual 'events' is a problem which commonly occurs in airglow physics and its solution is essential before a complete understanding of the subject is obtainable. Now the mean value of the enhancement at Hobart given above is considerably less than that expected at Haute Provence for a similar solar flux (from fig. 8..4 this is 120R compared with the 39.3R observed at Hobart). This difference may reflect the longer field line at Hobart and also the different field strengths but in view of the complicated nature of the PDE at Hobart there are other factors involved and these will be discussed later in more detail.

8.3.2 Onset Times

Nearly every night during March to September recorded in 1968-1970 exhibited some sort of pre-dawn enhancement of the 6300Å airglow. The

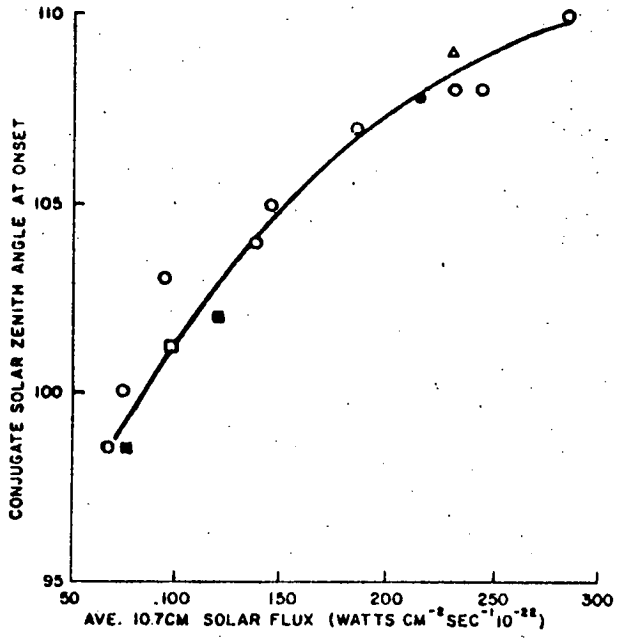

FIG. 2

The relationship of the 10.7 cm solar flux (Ottowa) to the conjugate solar zenith angle at the time of photoelectron onset at several stations: ○ Haute Provence, □ Townsville, Δ Fritz Peak, ● Camden, and ■ Arecibo.

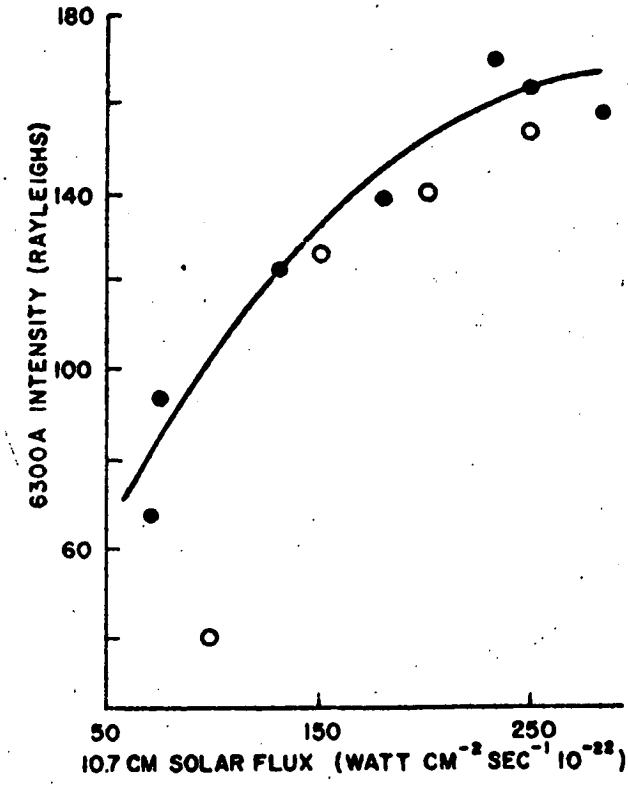

FIG. 3

The 6300 Å plateau intensity observed towards the celestial pole from Haute Provence versus the 10.7 cm. solar flux averaged during the periods of observation.

Fig. 8.4 The variation of the P.D.E. with solar flux.

only exceptions were nights on which auroral displays occurred and there is reason to believe (8.4 below) that a PDE occurs even on these nights, but that it is masked by the strong fluctuating auroral/airglow intensities. Fig. 8.5 shows a mass plot of zenith onset times of the PDE for nights in 1969. Because of bad weather no observations were possible in April. The most obvious feature of this plot is the erraticness of the onset times. In July for examaple this varied from 0033 to 0455 EAST. However, as in the case of the midnight summer enhancement there was a distinct tendency for the onset to be fairly constant over two or three nights but be very erratic over a longer period. For example on the 13th, 14th and 15th August, 1969 the PDE began at 0107, 0103 and 0112 EAST respectively yet only five days earlier on the 8th it did not begin until 0410 EAST. This suggests that both long and short period controls exist in PDE production.

Clearly from fig. 8.5 there is no obvious systematic variation of onset time with solar declination. This is hard to explain on a basis of conjugate point photo-electron emission even after allowing for differing solar fluxes. This can be seen from the following table of PDE's for various

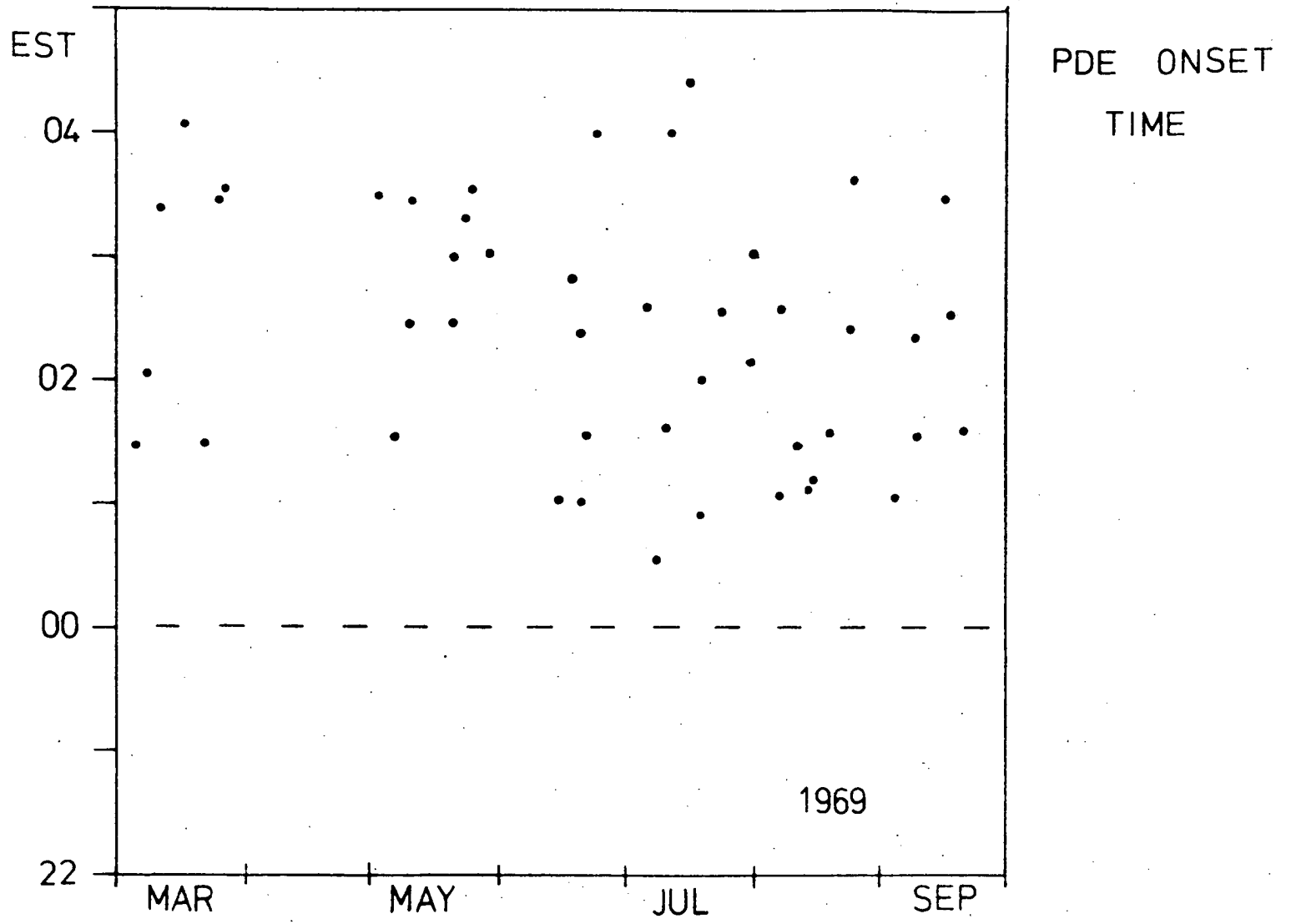

Fig. 8.5 Mass plot of onset times of the P.D.E. in 1969.

days in July and September 1969. For each zenith onset time the corresponding conjugate solar zenith angle (CSZA) is given.

Table 8.1

	actual		predicted
Date	Onset	CSZA	Onset
12/6/69	0110	95°	2331
12/7/69	0312	86°	2331
10/8/69	0120	104°	0130
4/9/69	0112	118°	0245

The actual onset time varies from a CSZA of 8 ° to one of 118° yet on these two days the solar flux levels are very similar. Also shown are the 'predicted' onset times based on Carlson & Weill's (1969) data. The predicted onset times shown are either the time at which the predicted onset angle is reached or, for nights when the CSZA is always less than this angle, the time of maximum CSZA is given. The differences between the above predicted and actual onset times are very marked and are representative of the usual situation at Hobart. On only one of the days in Table 8.1 does the PDE begin within 30 minutes of the predicted time; during 1969 only seven days (out of 53) were these close to the predicted times. Of these four

occurred near the equinoxes (two in March, two in September) and the other three in August. However, the PDE was usually between two and five hours late near the solstice but near the equinox could be up to two hours early. It appears therefore that generally the photo-electron theory of PDE generation is inadequate to explain the onset times even if allowances are made for any increased losses along the longer field line and the difference in field strengths and mirror heights at Hobart compared with, say, Haute Provence. It will be shown later that the days in August on which the PDE began near the "correct" CSZA were no different morphologically from the days in June or July when the PDE was very 'late'. It is very likely that the 'correctness' of these onset-times in August was just coincidence.

8.3.3 Spatial Morphology

From the onset times discussed above several types of nights may be distinguished temporally; these are when, with respect to the predicted onset time, the PDE is:

(i) late to very late; on approximately 75% of nights in 1969 the PDE was between one and five hours late.

(ii) on time, within $\pm$ 30 minutes; anticipating

the later findings these may be separated into type A nights near the equinox in September and late March and type B in August and early May (also late April, 1970) About 10% of nights were in these categories in 1969.

(iii) early by at least 30 minutes; about 15% of nights were in this category. All occurred near the equinoxes. Representative examples of these nights are shown on all-sky isophote charts in figs. 8.6, 8.7, 8.8 and 8.9. These displays are 'real distance projections', as discussed in chapter 4, assuming an emission of 300 km. The nights and the types of PDE they represent are:

Table 7.2

Date	(night of)	Temporal type	Fig.
July, 1969	15th	(i)	8.6
Sept. 1969	16th	(ii)A	8.7
Aug. 1969	15th	(ii)B	8.8
Sept. 1969	3rd	(iii)	8.9

Fig. 8.5 is an example of the most common type of night i.e. where the PDE is late (in this case about four hours late). Near midnight the isophotes to the north are aligned fairly well with the contours of constant CSZA which are also shown

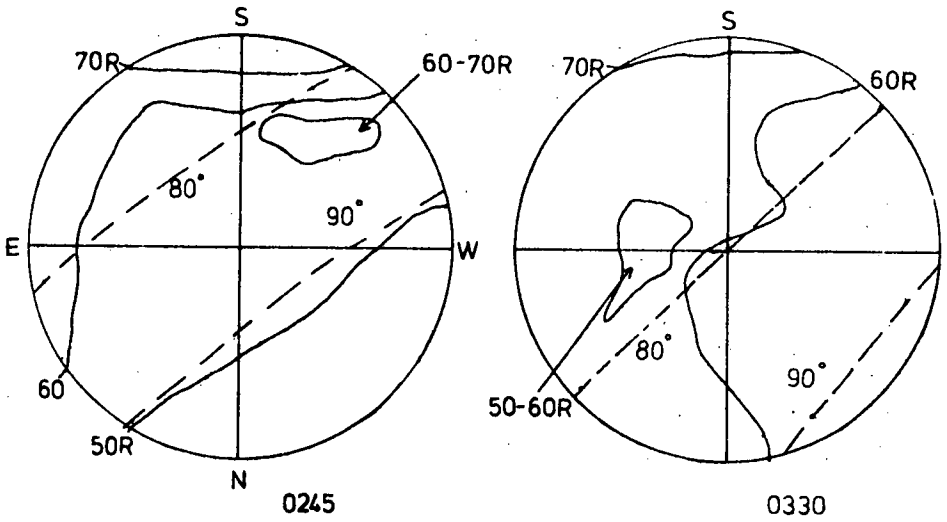

11 JULY 1969
(E.A.S.T.)

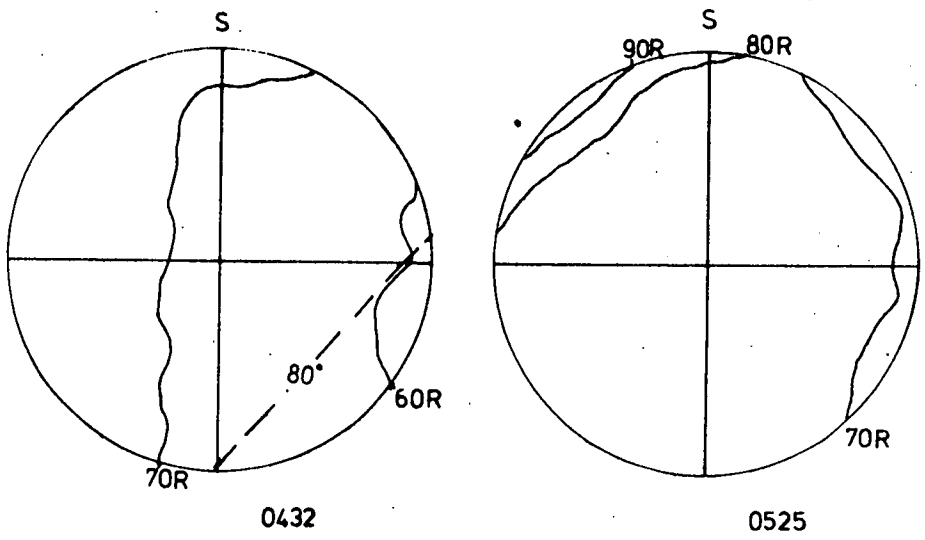

Fig. 8.6 Example of most common type of P.D.E.

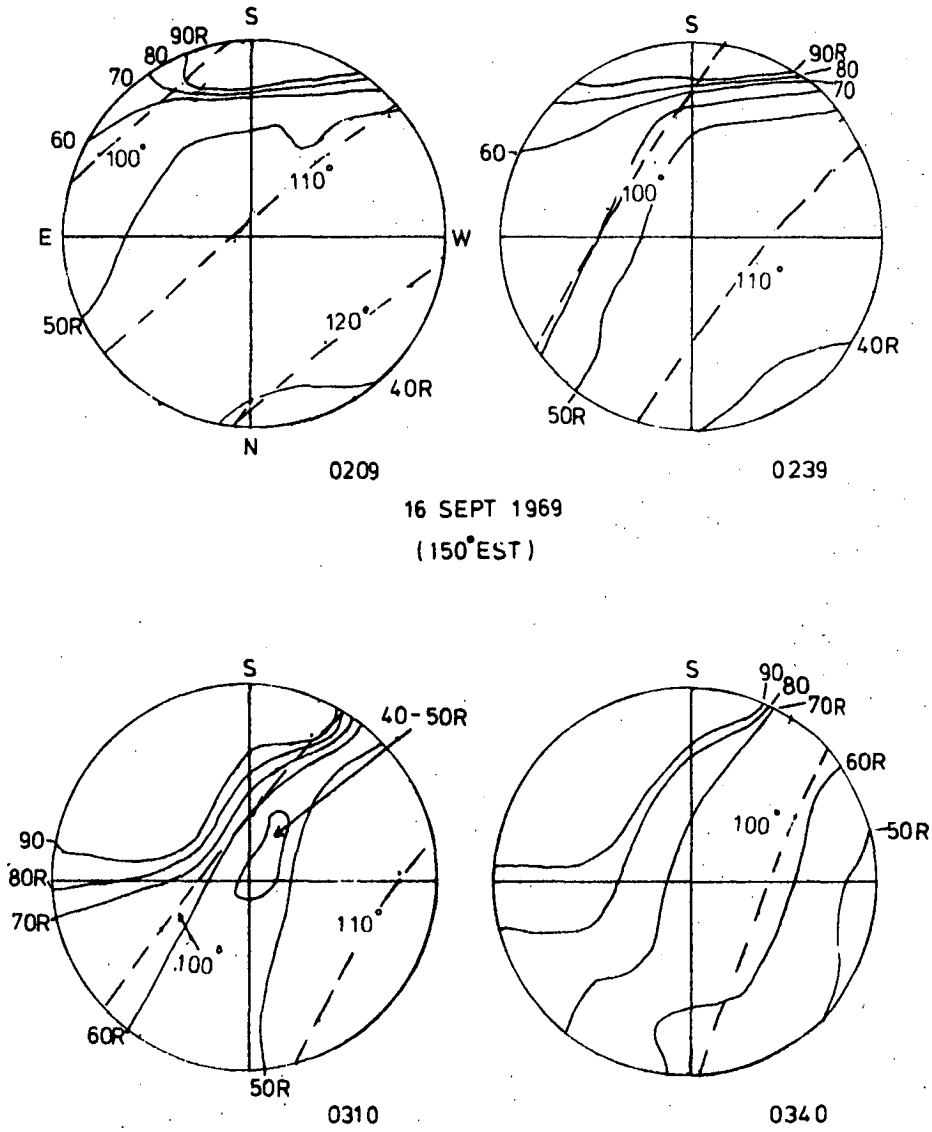

Fig. 8.7 A P.D.E. which commenced when expected and appears to be caused entirely by MCP fluxes.

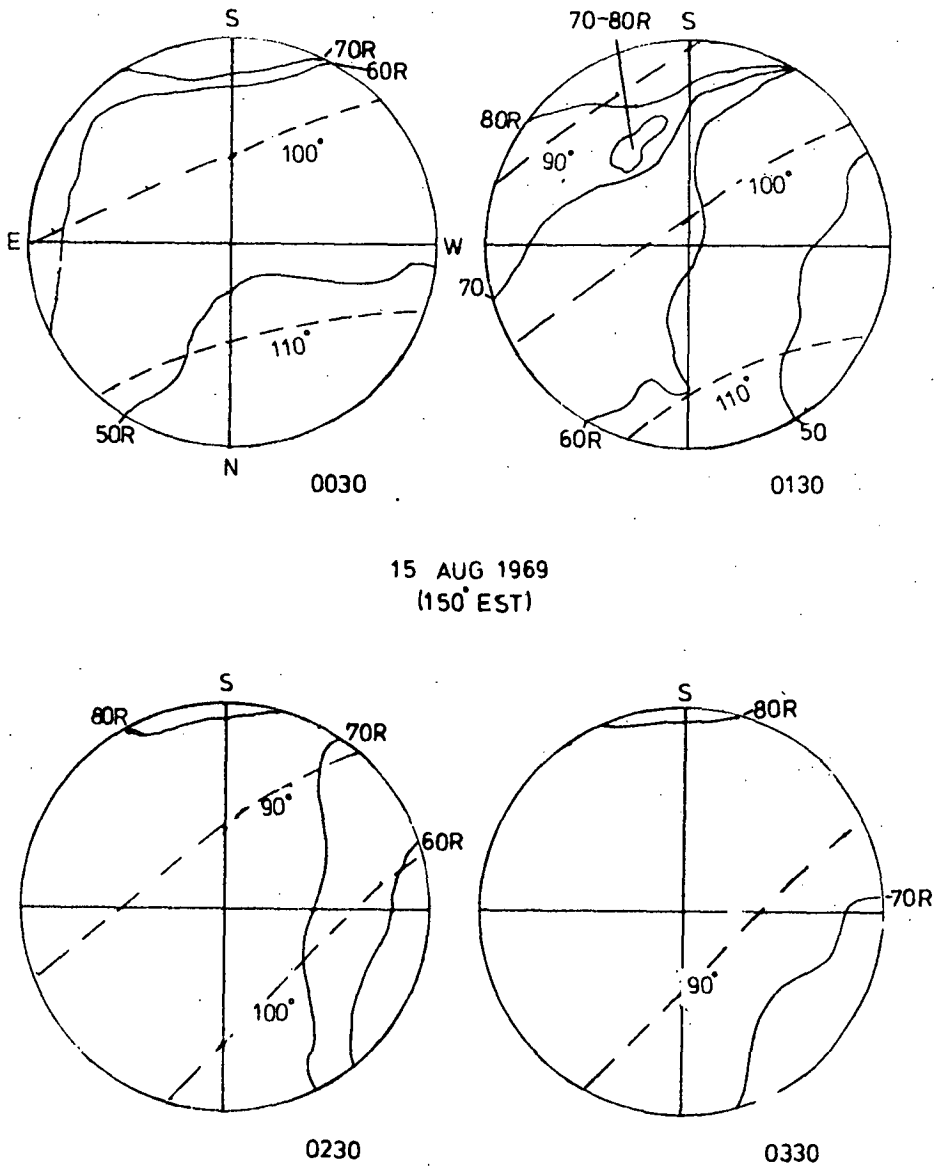

Fig. 8.8 This began when expected but is similar to Fig. 8.6

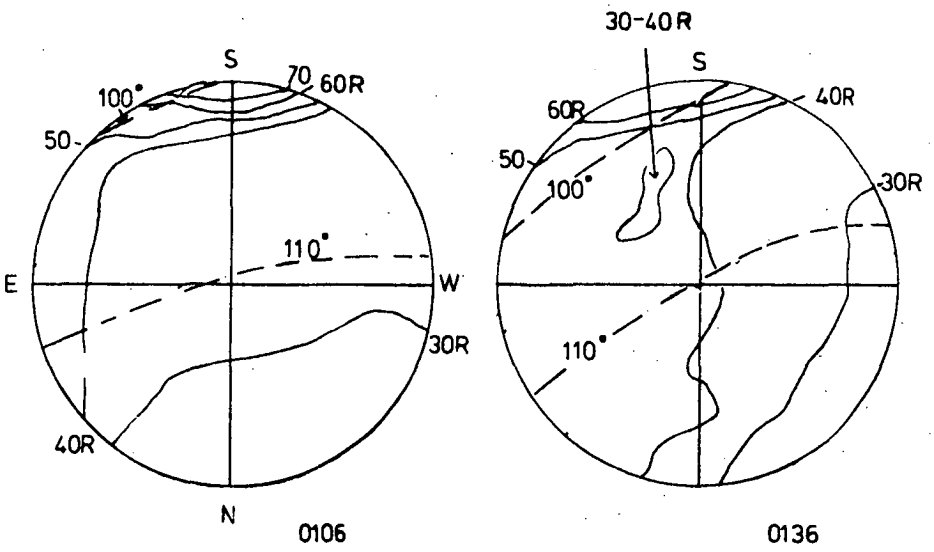

3 SEPT 1969
(150° EST)

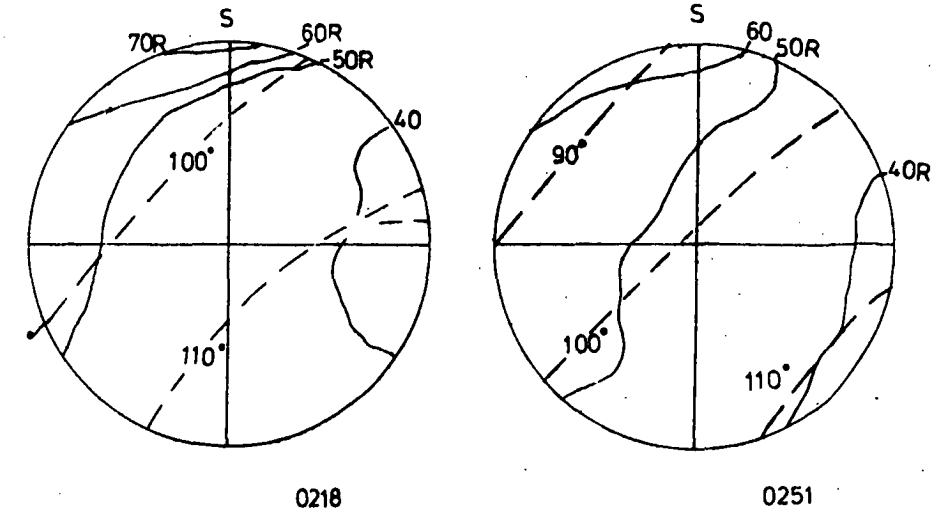

Fig. 8.9 This P.D.E. began very early and is similar to Fig. 8.6

on these figures. As found in chapter 6 this is typical of quiet winter nights. As the night progresses there is some variation in the extreme southern enhancement which, as discussed earlier, leads to some changes in the zenith intensity of the 6300Å line. In this case however, it is estimated that only about 5R is contributed to the zenith intensity by the cis-auroral soft electron flux, so these flux variations are not very important in changing the zenith intensities. Now durin the course of this night the isophotes to the north, swing around to match the changing constant CSZA contours. However, there is no <u>increase</u> in in I(6300) to the zenith between 0000 and 0400 EAST so it seems that there must be a general fall in $O(^1D)$ production by non-conjugate electron processes (possibly due to a fall in recombination of O_2^+) to compensate for the increase in photo-electron fluxes during this period.* The overall effect has kept the 6300Å intensity constant while maintaining alignment of isophotes and CSZA contours. This general fall in recombination must take place over

* Either this or else the efficiency of the photo-electron excitation is dropping; for example by increased back-scattering.

much of the sky except possibly to the extreme south. After 0400 in fig. 8.6 the PDE appears rapidly to the south east and moves at about 1300 m sec^{-1} across the sky in a more or less E-W direction. This speed is close to the rotational speed of the earth at this latitude and the general movement is very similar to that of the midnight summer enhancement (section 5.3). After the PDE front has passed overhead the isophotes align themselves up again with the constant CSZA contours; the contours of CSZA however, are aligned with isophotes some 20R greater than those with which they were aligned before the PDE arrived. It seems therefore that the PDE increase is initially due to some local, non-conjugate effect which moves E-W across the sky but later in the PDE the conjugate effects take over once again.

Fig. 8.7 is one of the rare nights when the PDE arrived close to the expected time. This night appears to be an example of a 'classical' mid-latitude PDE where the isophotes generally align with contours of constant CSZA at all times in the PDE except in the south. The 'southern enhancement' is quite strong on this night probably due to the after effects of a geomagnetic storm 3 days before.

Fig. 8.8 shows one night in the middle of August where the PDE commenced near its expected time

of 0100 EAST. However, it is a very different night from the previous one considered and the PDE moves in an E-W direction and it is not until later in the morning that it aligns with contours of constant CSZA. In fact this night is very similar to that of fig. 8.5 with obvious non-conjugate effects present. It was found that the other nights in August on which the PDE began near 0100 EAST were of a similar kind whereas nights such as in fig. 8.7 above only occurred in middle to late September and late March in 1969. It appears therefore that for some reason the PDE only occurs as expected from the unmodified conjugate photo-electron theory near the equinoxes, and it is just coincidence that the PDE begins near its expected time on some nights in August.

Nights such as fig. 8.9 where the PDE begins well before the necessary CSZA is reached occurred in early September 1969 and April 1970 (no 1969 April records were obtained). From fig. 8.9 the PDE is seen to move in from the east very much as in figs. 8.6 and 8.8. After the sun has risen in the conjugate F-region the isophotes move around from a N-S alignment to a more NE-SW one which is similar to the contours of constant CSZA.

To summarize the above all-sky observations of the PDE it appears that the PDE consists of two

differing effects, one local and the other conjugate. The two however, do not seem to be completely independent because only very rarely does the conjugate effect occur without the local one taking place first. The next step is obviously to examine the behaviour of the night-time ionosphere during the PDE.

8.4 Ionospheric Observations

8.4.1 Winter Morning Ionization Influx

It has already been shown in chapters 5 and 6 that there occurs an influx of ionization, presumably from the exosphere, early on winter mornings at all Australian latitudes. This influx which is associated with ionospheric and exospheric cooling (Evans, 1965b) commences near local midnight and as it raises both the peak electron density Ne and the sub-peak total content T_s it should also raise the recombination rate and hence the 6300Å intensity. However, the influx is latitude dependent (Titheridge 1968) and at Hobart at solar maximum is not usually very significant. However, for points to the north of Hobart, but still within the 6300Å field of view, the influx can be considerable. For example for June 1969 at Canberra the monthly media Ne increased from 1.61 x 10^5 el cm^{-3} at 2300 EAST to 2.54 x 10^5 el cm^{-3} at 0400 EAST; an increase of 58%. On the other hand at Hobart the change over the same time interval was only

from 0.97×10^5 el cm^{-3} to 1.12×10^5 el cm^{-3} an increase of 15%. From Wright's (1960) work it appears that T_s is roughly proportional to Ne at any one station, so it may be assumed that the sub-peak content is increased by about 58% at Canberra and by 15% at Hobart over this time. From the real-height analysis done on Canberra ionograms this was found to be true for nights exhibiting this influx. If there were no change in the shape or height of the F-region and no change in exospheric temperature, then the dissociative recombination would increase by the same amounts. A similar increase in $O(^1D)$ concentration and thus 6300Å airglow intensity, would be expected.

Clearly this influx whilst it could contribute to the PDE at Hobart cannot be a major cause of the PDE there. This is because the PDE is at least as strong at Hobart as at Canberra yet the increase expected from the influx is four times as great at Canberra. Furthermore on many days on which PDE occurs there is no influx at Hobart. This can be seen from Fig. 8.8 which is a plot of the (percentage) early morning increase in Ne for each day in three winter months in 1969 for both Hobart and Canberra. Although the influx occurs every night (Titheridge 1968b) the peak density does not increase during the influx except for a limited period near the solstice.

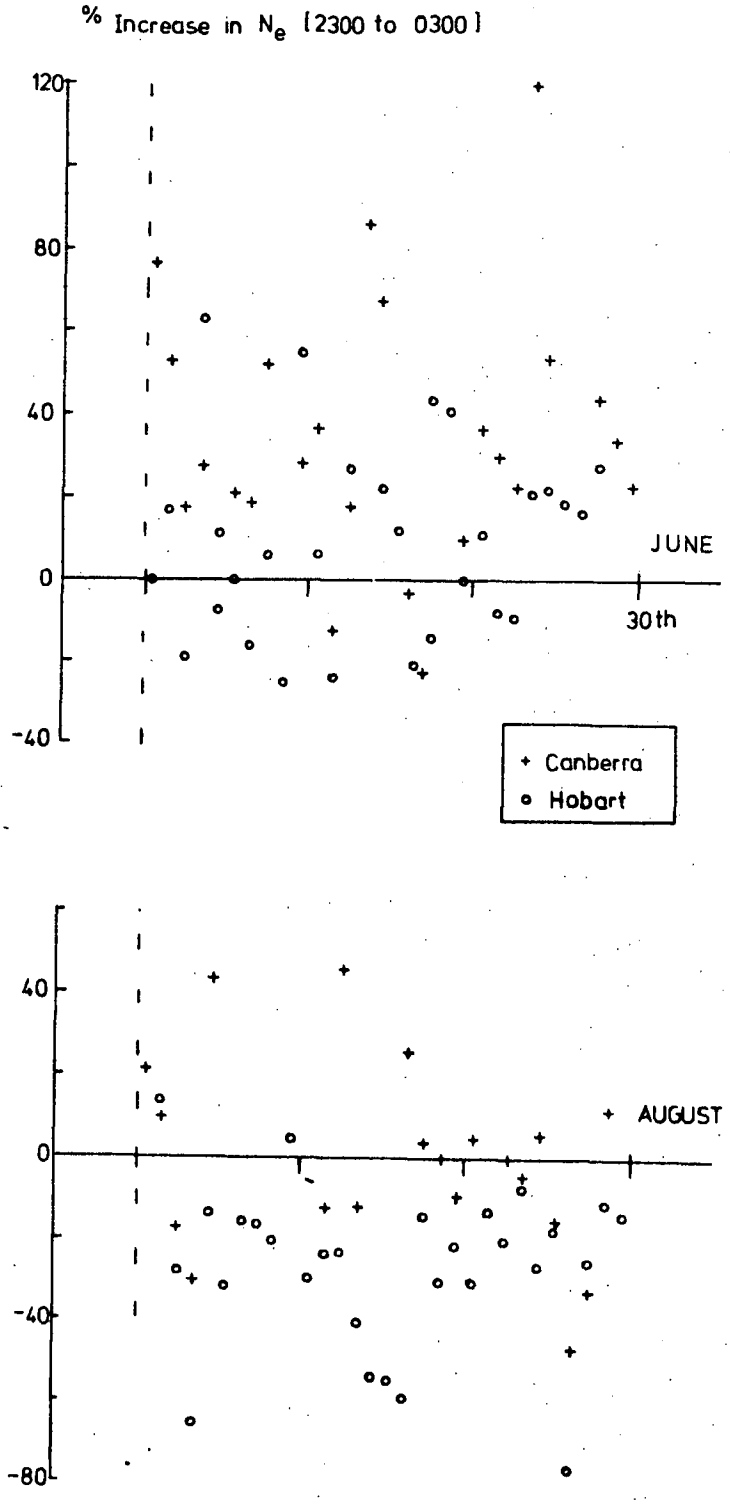

Fig. 8.10 The increase in Ne due to the ionospheric influx in various winter months.

Obviously an enhancement of 6300Å airglow due to this influx can occur only during this period. Using the published (IPS series D, 1969) ionospheric data the percentage increase in Ne is obtained by:

$$P(N) = 100 \left\{ \left[\frac{f(04)}{f(23)} \right]^2 - 1 \right\} \quad 8.1$$

where f(t) is the published value of foF2 at the time.

These values of P(N) can be thought of roughly as the increase in I(6300) due to recombination that would occur over this time interval provided all other ionospheric parameters were constant. Thus for July 1969 the mean airglow level at Canberra near midnight was of the order of 30R. Assuming, as seems likely, that nearly all this is due to recombination then an enhancement of 10R would occur on most nights due to the influx.

This is a significant fraction of the total PDE observed (order of 30R). On the other hand for Hobart at best an enhancement of 3R would result from the influx on a typical night. Exact calculations of the importance of this mechanism using observed and model electron density height profiles are given in the next chapter but even on the basis of the above figures the following statement may be made.

At Canberra near the winter solstice a

significant contribution to the PDE may be made by the observed post-midnight influx of ionization. On the other hand at Hobart the contribution by this source is usually insignificant.

According to Titheridge (1968) the influx commences at about the same time over the latitude range 35^{o}S to 45^{o}S (geographic) so any increase in recombination would lead to a 6300$\overset{o}{A}$ enhancement which would appear to move in from the east. However, because of the weakness of this increase at Hobart this cannot be the cause of north-south aligned isophotes (e.g. Fig. 8.7) during much of the PDE.

8.4.2 F-Region Drift

Fig. 8.11 shows a plot of the mean quiet night-time values of the F-region virtual height h'f for the months of May, July, August and September 1969. To obtain these h'f was measured at half-hourly intervals on nights where Kp was always less that 2+ and the monthly mean was then calculated. The reasons for excluding days of greater magnetic activity were firstly that the airglow data being considered was only obtained on quiet days and secondly on disturbed days h'f can be extremely high and the inclusion of such days in the mean value of h'f can lead to very misleading figures for the mean.

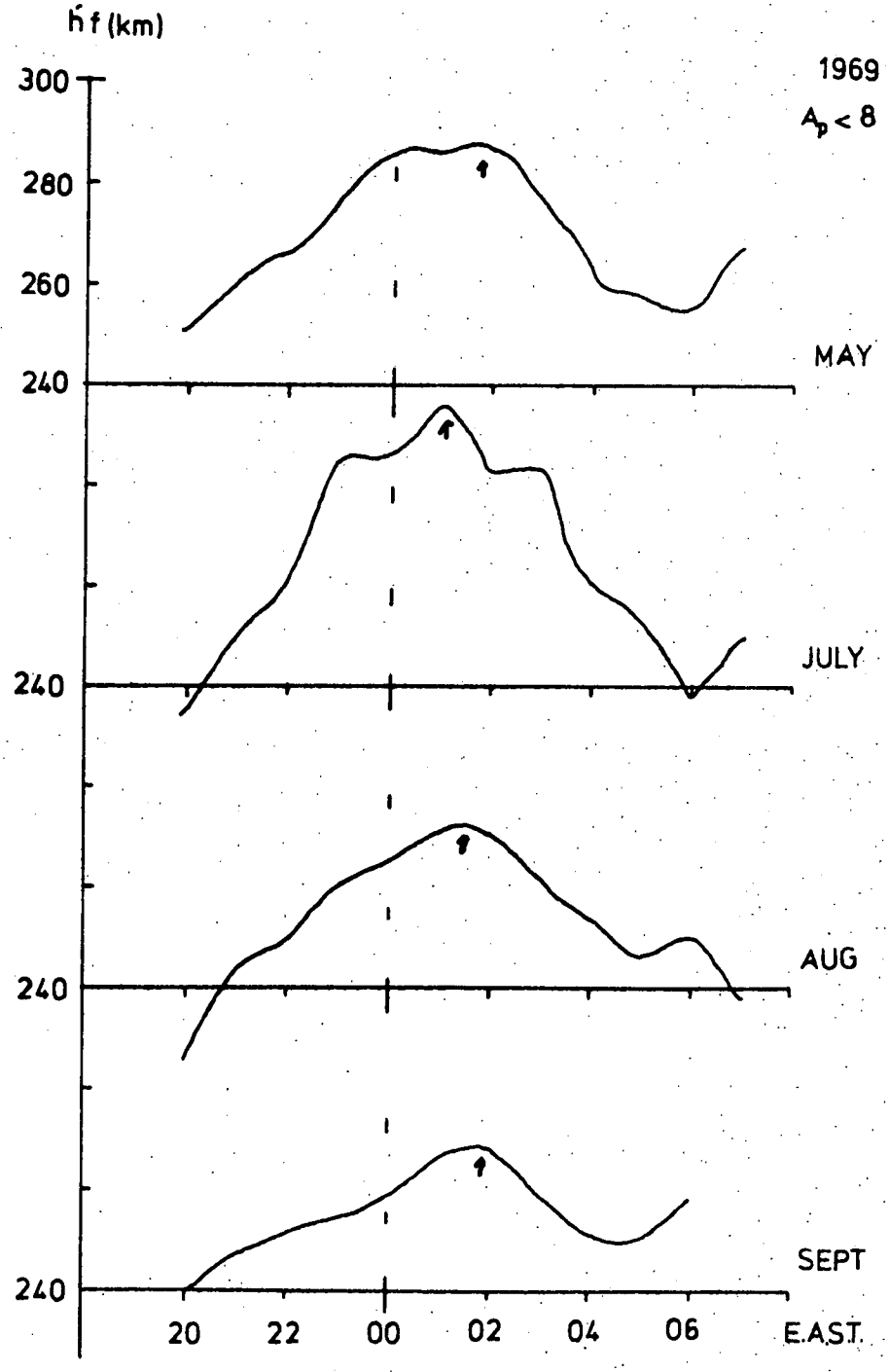

Fig. 8.11 The fall of the F-region on quiet nights is very marked.

From the mean data it appears that during these months the night ionosphere drifts upwards up to 0300, after which it begins to drift downwards. The downward movement results in the ionosphere apparently falling about 30km from 0300 LST up to local F-region. If the fall in virtual height represents a real fall in the F-region then the increased combination due to the fall will be very large.

Figs. 8.12 - 8.14 show plots of the latitude local time extent of the post midnight downward drift (shaded). This was obtained from h'f data for 1965 in a similar way to the summer drifts reported in the previous chapter (sections 7.3.2 and 7.3.3). In fact these figures are very similar to figs. 7.14-7.16 suggesting that the winter and summer drifts have the same origin. It should be noted that the data used in obtaining these two sets of figures are for solar minimum but that h'f data from the 1957-58 solar maximum shows a similar morphology. In section 8.3 it was noted that the isophotes of the pre-dawn enhancement moved across the sky in an EW direction but were initially aligned NE-SW. There is however, only a slight suggestion of a NE-SW alignment of the 'maximum upward drift' front on figs. 8.12 - 8.14. This however, is probably explained by the fact that

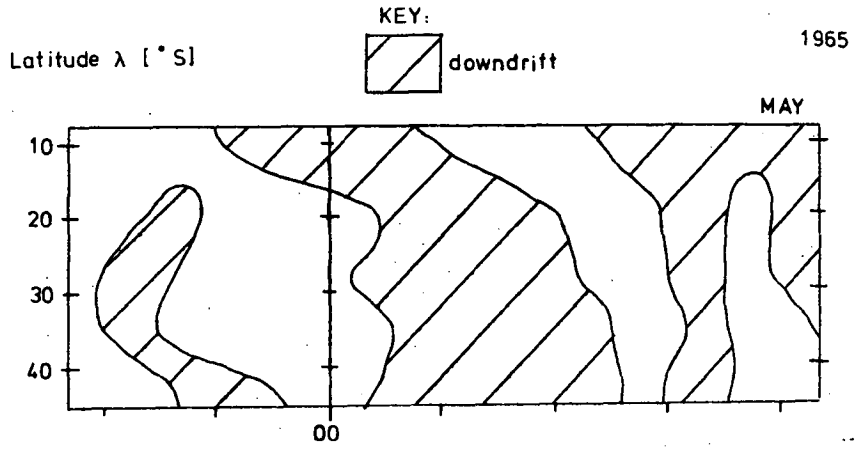

Fig. 8.12 The latitude extent of the downdrift is apparent in this month.

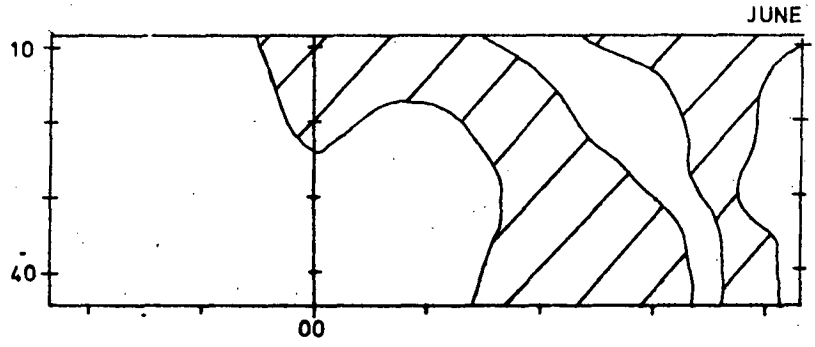

Fig. 8.13 F-region downdrift.

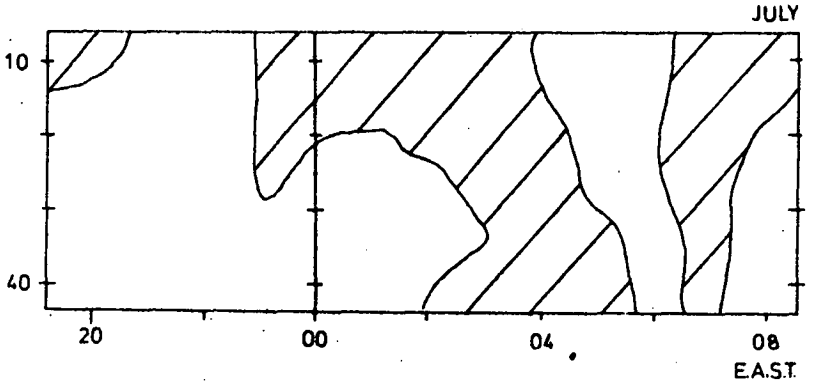

Fig. 8.14 F-region downdrift.

h'f values are only taken every hour whereas the PDE front moves across half the sky in this time, i.e. the temporal resolution of figs. 8.12 - 8.14 is not sufficient to show adequately the downward drift fronts' spatial morphology over the part of the sky observable from Hobart.

Using the ionosphere of Appendix C, suitably scaled, and the following parameters from the downward drift then the mean increase in I(6300) for the winter months at Hobart is given by integrating the Peterson et al (1966) emission rate equation of chapter 2 (2.21). The predicted increases in I(6300) due to the mean fall in various months in 1969 are:

Table 8.3

	km		10^4		
Month	h_x	h_n	N_x	N_n	I (6)
MAY	350	331	10.41	11.90	34.5
JULY	356	323	8.31	10.41	50.7
SEPT	355	329	12.63	10.41	18.2

Where h_x and h_n are the maximum and minimum heights obtained by the F-region peak after midnight but before dawn calculated as in section 7.3.3, N_x and N_n are the peak electron densities prevailing at these times. I (6) is the computed increase in

I(6300 based on the CIRA models 6 caused by this fall

I's are quite comparable to the observed increases suggesting that this ionospheric fall is adequate to explain this part of the PDE. It must however, be emphasised that in view of the difficulties associated with real height determination and also the doubts raised about the static diffusion models that these values are order of magnitude estimates only.

8.4.3 Individual nights

Plots of I(6300) versus - h'f and foF2 are shown for four typical nights in figs. 8.15 - 8.19. In all, except for fig. 8.19, I(6300), is clearly well correlated with - h'f. In section 8.3.3 it was mentioned that the night of 16th September 1969 (fig. 8.18) was one of the very few nights which appeared to be of the 'classical' (i.e. conjugate electron flux) type of pre-dawn enhancements. It will be noted from fig. 8.19 that the electron density in the early morning was very low on this night. The other nights however, all exhibit the midnight increase in recombination due to the fall of the F-region. However, it can be seen from figs. 8.15-8.18 that just before 300 km dawn the recombination should fall because of the rapidly falling electron density.

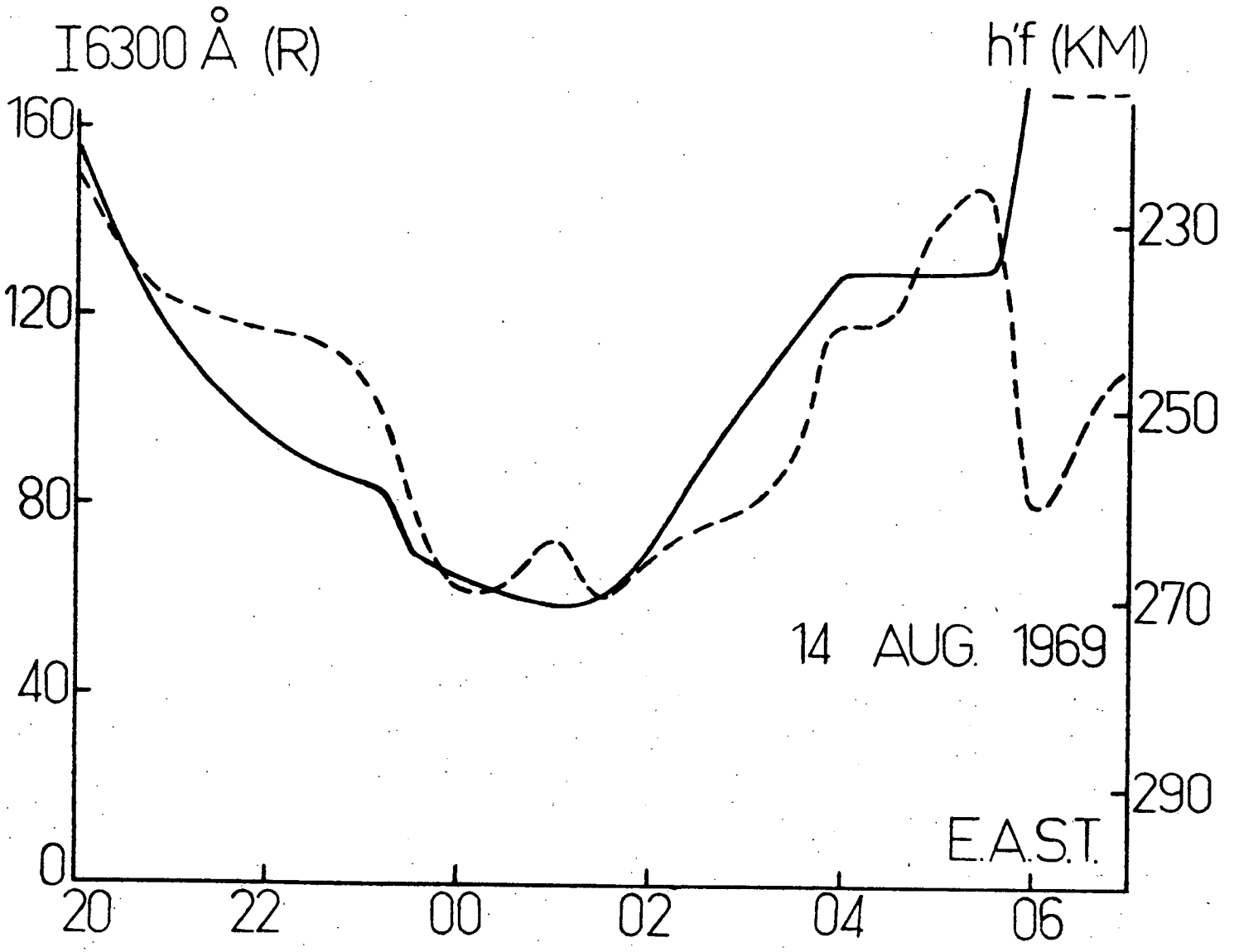

Fig. 8.15 The PDE is well correlated with the ionospheric downdrift.

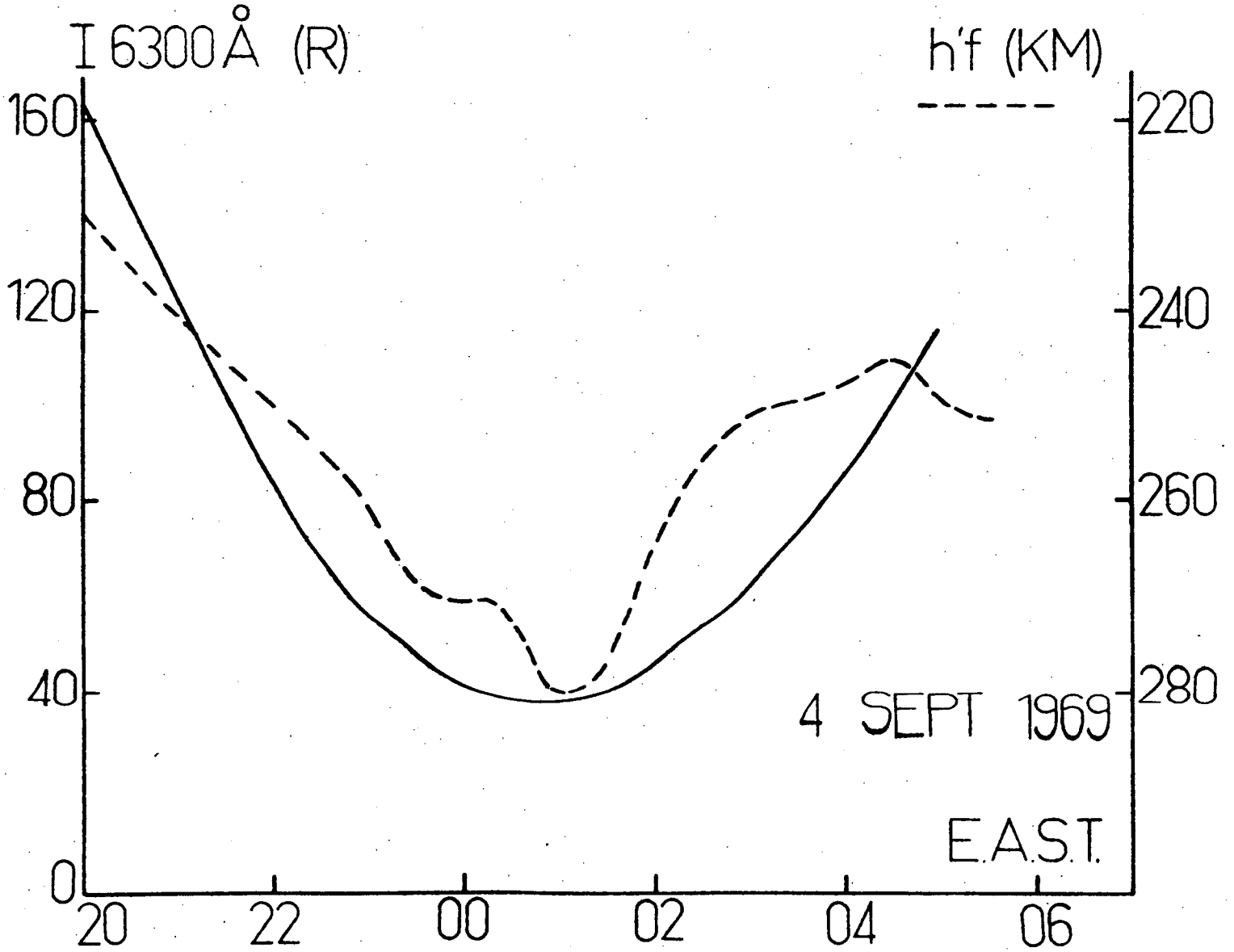

Fig. 8.17 -h'f and I(6300) are well correlated.

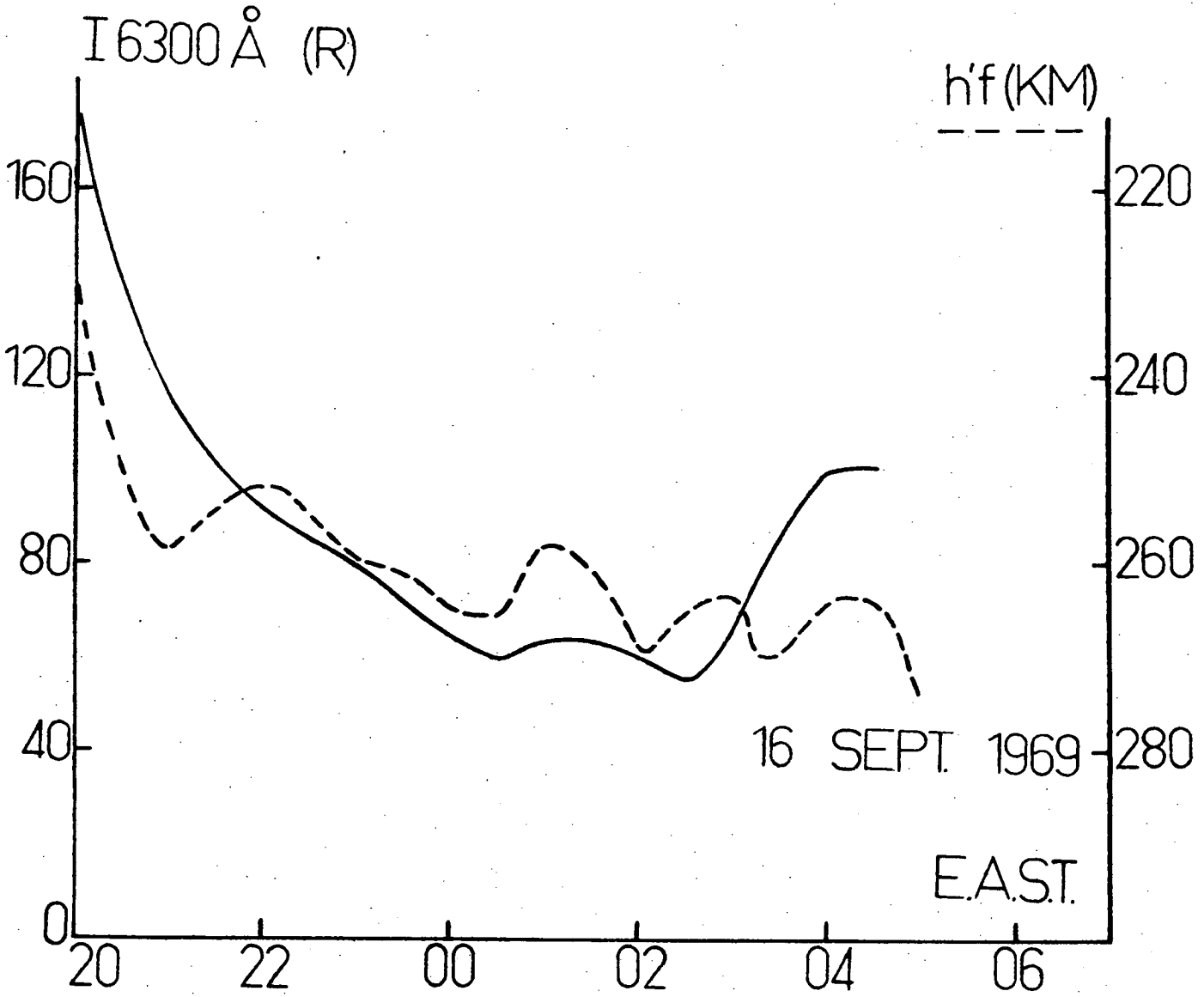

Fig. 8.18 The PDE is not caused by any downdrift.

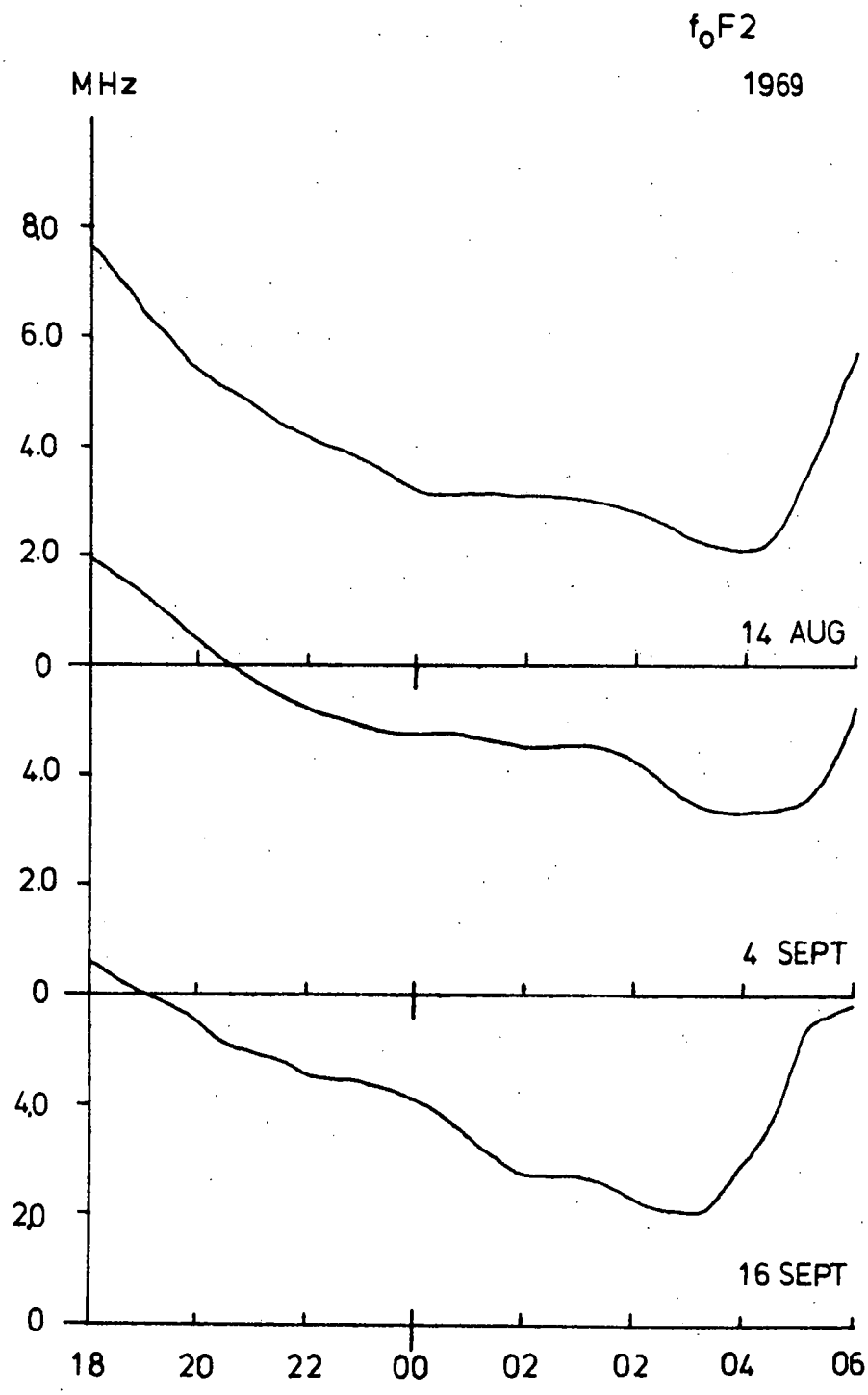

Fig. 8.19 The variation of f_0F2 on the nights of the four previous figures.

In spite of this the airglow intensity continues to increase. This situation contrasts with the summer nights where I(6300) falls off before dawn when the recombination falls. The obvious explanation for this behaviour is that this time the magnetic conjugate point fluxes have become important enough to counter the fall in recombination. This idea is borne out by the better alignment of the isophotes and contours of equal CSZA reported at this time (figs. 8.5 - 8.8).

The need for a non-recombination source of 6300$\mathring{A}$ photons during the early morning can also be seen by computing the increase in the airglow intensity caused by recombination (I(REC)) from the time just before the PDE commences to the time just before local 105^{o} dawn. This increase, which is usually negative, can then be compared with the observed increase in I(6300). The difference $\left[I(OBS) - I(REC) \right]$ is then a least lower bound estimate of the non-recombination component of the terminal stage of the PDE. Table 8.4 shows the results of calculations carried out along these lines for 1969.

Table 8.4

Month	Δ I (REC)	Δ I (OBS)	Δ I
JUNE	- 0.3	33.7	34.0
JULY	+ 6.3	38.8	32.5
SEPT	-20.2	27.2	47.4

The I (OBS)'s are the mean observed increases for all nights in the month on which data was available; the I (REC)'s are calculated for the mean parameters of these nights using equation 7.5. The differences, Δ I , are of the same order as the maximum increases in recombination observed during the PDE. Once again it should be emphasised that these figures are only order of magnitude estimates; however, it appears that the contribution by the photoelectron fluxes is of the order of 35R. This compares with the 20R estimated by Noxon and Johansen (1970) for Boston in winter 1967.

8.5 Summary

The pre-dawn enhancement of 6300Å airglow seems to be largely controlled by the post-midnight downward drift of the ionosphere. This, by increasing the dissociative recombination of O_2^+, causes an increase in I(6300). A similar downward drift occurs in summer leading to the midnight summer enhancement. In winter and at certain latitudes in summer a contribution to

this increase in recombination is made by a midnight influx of ionization; this effect is most important between Λ = 30 and 40° where it will cause an increase of the order of 10R in I(6300). In the summer the total recombination drops off again before dawn causing the 'hump' shaped MSE; but in winter, even though a similar fall-off occurs, the presence of a soft flux of conjugate point photoelectrons causes I(6300) not to decrease during this period. Both these mechanisms, i.e. MCP electron excitation and the post midnight increase in recombination, contribute about 30R to the enhancement.

Chapter 9 NEUTRAL WINDS, PHOTOELECTRONS AND 6300Å AIRGLOW

9.1. Introduction

Due to the continuously changing upper atmosphere neutral temperatures and pressures, global horizontal pressure gradients are set up in the thermosphere. These gradients lead to a global system of neutral winds which, because of the fairly constant solar flux, is quite regular in its behaviour. These neutral winds interact with the ionized layers and cause a regular rise and fall of the F-region. Essentially this occurs because whilst neutral particles can move in any direction the geomagnetic field severely limits the movement of charged particles except in the direction of the field. In this chapter it is proposed that this thermospheric wind system is the prime factor in controlling the onset of both the midnight summer enhancement (MSE) and the pre-dawn enhancement (PDE) of the 6300Å line. In winter and the equinoxes photo-electrons from the sunlit magnetically conjugate hemisphere are also important in exciting $O(^1D)$ atoms by collisional impact. It will be shown that the contributions to the total 6300Å intensity by both the above processes are not entirely independent.

9.2 Neutral Winds

9.2.1 Review

Because of effects of solar heating on the earth mass movements of the atmosphere occur at thermospheric heights, (Deb 1953). Computations of the resulting global system of neutral winds have been made by several authors such as King and associates (King 1964; King and Kohl 1965; King and Kohl 1967; King, Kohl and Eccles 1968), Geisler (1966, 1967) and Challinor (1969). These theoretical models are largely based on the model atmospheres of Jacchia (1965) which are empirically derived from satellite drag analyses such as King - Hele (1964). Now the diurnal ionospheric drifts, such as those reported in the previous two chapters, can be explained in terms of changes in neutral wind direction (e.g. King, Kohl and Pratt 1967) but attempts have also been made to explain these drifts by ionospheric electric fields (e.g. Stubbe 1964, Vasseur 1966). An examination of the relative importance of these two effects has been made by Stubbe and Chandra (1970) who conclude that the measured electric field (2 V KM^{-1}) is insufficient to have much influence on the F-region.

Accordingly only the neutral wind models are considered in this chapter and in particular the simple model of King and Kohl (1967) which is shown to be adequate to explain the observed airglow morphology.

9.2.2. Wind velocities and 6300Å enhancements

If the atmospheric density is denoted by ρ then according to King and Kohl (1967) the following forces (per unit mass) are important in determining the wind velocity $\underline{u}$:

(i) The 'driving force' obtained from the pressure p as $(-\frac{1}{\rho}\ \text{grad}\ p)$

(ii) The coriolis force $2\rho(\underline{u} \times \underline{w})$ where $\underline{w}$ is the earth's angular velocity

(iii) the viscous force $\rho\mu\frac{\partial^2 u}{\partial h^2}$ where μ is the co-efficient of viscosity and h the height of the layer

(iv) The inertial force $\rho\left(\frac{\partial \underline{u}}{\partial t} + \underline{u}\ (\text{div}\ \underline{u})\right)$ Kohl and King conclude that the second term in the bracket may be ignored.

(v) The ion drag is determined from:

$$\rho\,\nu_n\,(\underline{u} - \underline{u}_i) = \rho\,\nu_i\,\frac{N_i}{N_n}\,(\underline{u} - u_i) \qquad 9.1$$

where ν_n is the collision frequency of a neutral particle with all ions; ν_i is the

collision frequency of an ion with all neutral particles; $\underline{u}_i$ is the ion velocity; N_i the ion concentration and N_n the neutral concentration.

The last term , the ion drag, is the one responsible for changing the height of the F-region and because, in the absence of electric fields, ions can only move in the direction of the magnetic field the ion velocity is related to the wind velocity by:

$$\underline{u}_i = (\underline{u} \cdot \underline{t})\ \underline{t} \qquad 9.2$$

where $\underline{t}$ is a unit vector in the direction of the field. The wind velocity is obtainable by solving the equation of motion.

$$\frac{\partial \underline{u}}{\partial t} - \mu \frac{\partial^2 \underline{u}}{\partial h^2} - 2(\underline{u} \times \underline{w}) + \nu_i \frac{N_i}{N_n}(\underline{u} - (\underline{u} \cdot \underline{t})\ \underline{t}) = -\frac{1}{\rho} \text{grad } p + \underline{g} \qquad 9.3$$

This equation was solved numerically for the N - S (x) components and the E - W (y) component of $\underline{u}$ by computer.

The vertical (z) component of the wind was assumed to be zero. (For a discussion of the values of μ and the ion height profile see Kohl and King (1967)). To evaluate the global wind velocity distribution Kohl and King made a number of

simplifications (see their section 4) but for the present purposes the most significant was the assumption that the height of the F-region peak, h_mF2, the peak electron density, Ne, and the electron scale height at the peak, H_m, are all independent of local time and latitude. These are clearly drastic simplifications because of course Ne falls off rapidly in the midlatitude trough; also H_m increases with latitude and the winds themselves change h_mF2. It is rather remarkable, therefore, how well this model can explain the 6300Å enhancements' morphologies. Fig. 9.1 is taken from Kohl and King (1967) and shows the wind velocities on a geographic latitude - local time display for the following condition:

$$Ne = 3 \times 10^5 \text{ cm}^{-3}$$

$$h_mF2 = 300 \text{ km}$$

$$H_m = 60 \text{ km}$$

Equinox conditions - northern hemisphere.

These conditions are quite appropriate to the night-time ionosphere at midlatitudes during 1969 - 1970.

Now it will be remembered from the previous two chapters that although the two enhancements discussed moved in an E - W direction the isophotes were aligned along a NE - SW front. In

Fig. 9.2 The effects of magnetic declination and the convergence of time meridans.

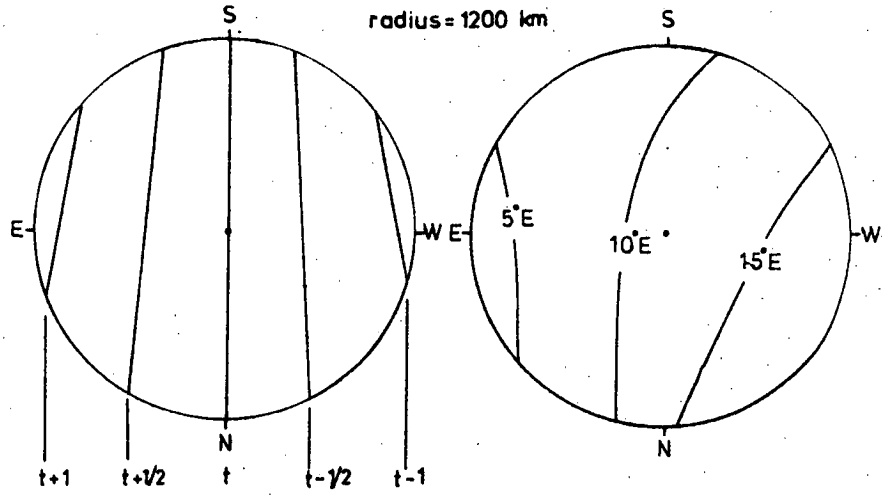

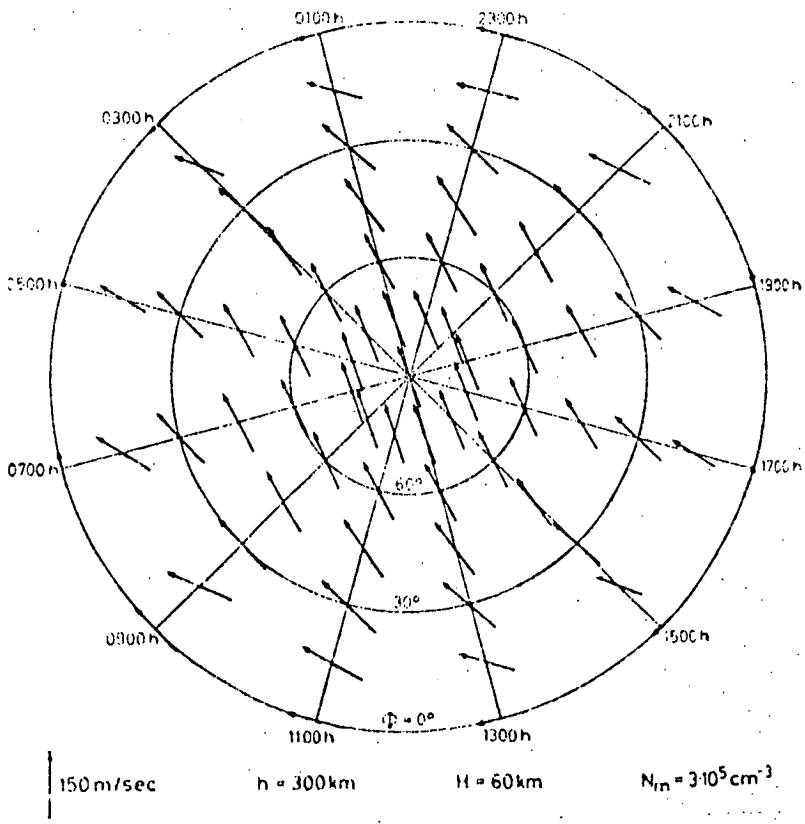

Fig. 9.1 Global winds from Kohl and King 1967.

winter this alignment can be partly attributed to the increase in conjugate solar zenith angle with latitude; however this alignment still occurs when no conjugate flux can be present, as in summer or on certain nights at the equinoxes. Moreover as has been shown both enhancements appear to be initiated by ionospheric lowering, even at times when conjugate fluxes should be significant. Now the maximum upward drift of the ionosphere occurs when the component of the wind velocity in the direction of the magnetic field maximises. This from 9.2 occurs when $\underline{u} \cdot \underline{t}$ is a maximum. From fig. 9.1 it is seen that this maximum occurs at about 0300 LMT when the wind is blowing towards the equator. However the time when this occurs is earlierat high latitudes. This partly explains the NE - SW isophote alignment; for the maximum upward drift, and hence minimum recombination, occurs earlier towards the south of Hobart than to the north. This is because the coriolis force is relatively strong at high latitudes and the inertial force, which oauses the turnover to lag the driving force, is relatively strong at low latitudes. The less dense the ionosphere the more marked is this effect. Before calculating the importance of this effect near Hobart it should be noted that there

are other factors which tend to lead to earlier drift reversals to the south of Hobart; these are:

(i) The magnetic declination becomes more easterly with latitude southward along the 150° meridian. The upward drift thus maximises earlier to the south of Hobart than to the north. The difference between latitude ϕ = 55°s and ϕ = 35°s at λ = 150° E due to this effect is of the order of an hour which is very significant.

(ii) The distance between lines of longitude becomes less with latitude ($\propto \cos\phi$). The effect of this is to make an enhancement which is fixed in local time to be visible earlier to the south of Hobart than to the north. The enhancement to the south would move more slowly than that to the north and would vanish later. There is some evidence for this occurring in the MSE plots of figs. 7.7 - 7.8.

Both these two effects are illustrated in fig. 9.2 where a 1200 km radius of view is assumed.

Now assuming the values of Ne, h_mF2 and H_m given above, equation 9.3 has been solved to give

the wind components in the direction of the magnetic field declination for ϕ = 30, 45 and 50° S on the 150° E meridian. These points approximately represent the extreme north, zenith and extreme south of the 6300Å airglow field at Hobart. The point of maximum updrift is shown by the arrows in 9.3. These times are:

Table 9.1

Longitude = 150° E

Latitude =	Time of maximum updrift
30° S	0224
45° S	0124
60° S	0036

Fig. 9.4 shows the movement of the points of maximum updrift on a 'real range' display centred at Hobart. This compares well, except to the extreme south, with the isophote displays of the enhancements given in the previous chapters. Fig. 9.5 shows the movements of the 50R isophote on one night in the equinox. It thus appears that much of the PDE and the MSE are explicable by the regular diurnal variation in the neutral winds. However, there can be no doubt from chapter 8 that conjugate point effects are also important in winter.

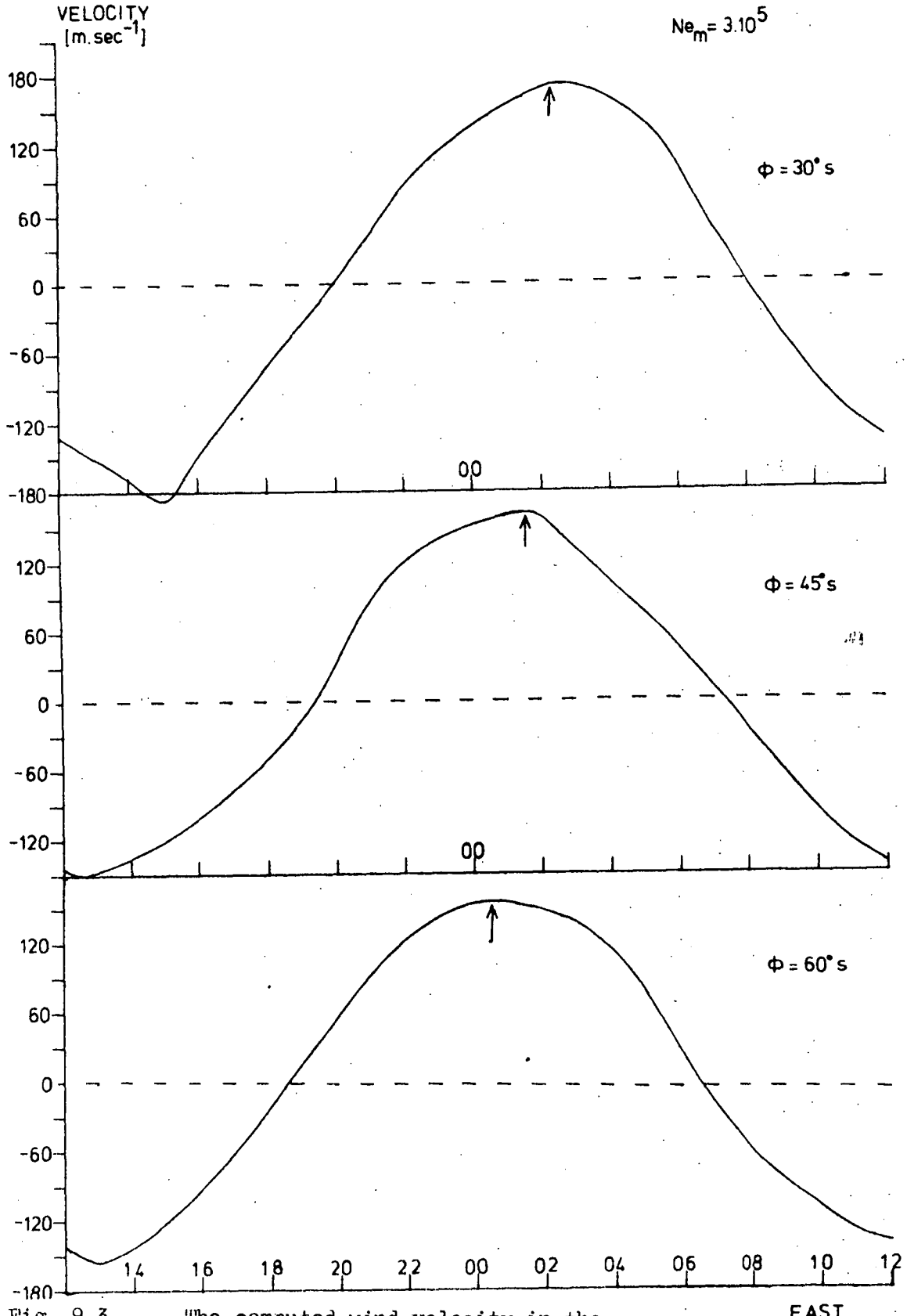

Fig. 9.3 The computed wind velocity in the direction of the horizontal component of the field.

Fig. 9.4 The movement of points of maximum upward drift as observed from Hobart.

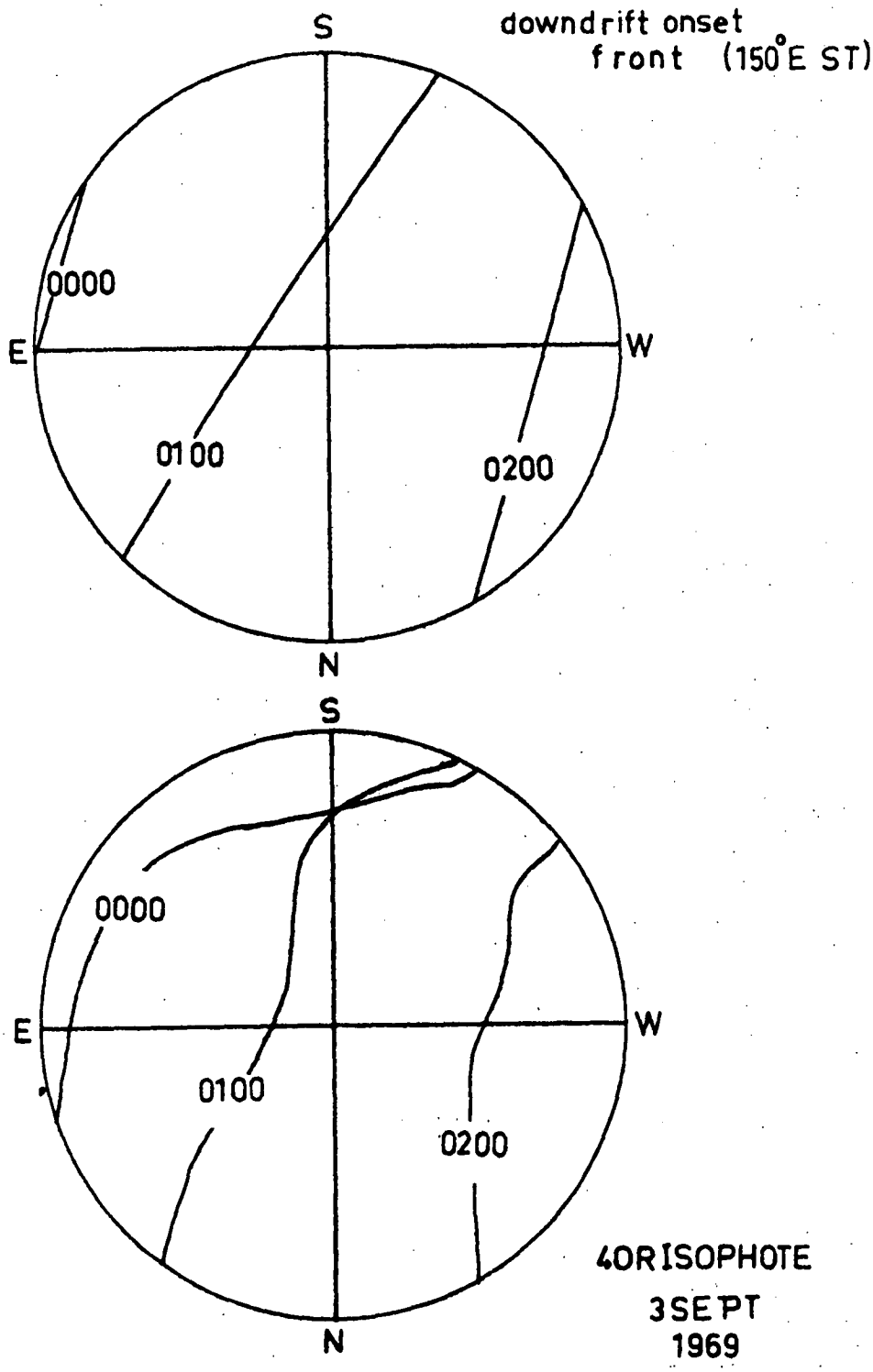

Fig. 9.5 The 5OR isophote movement on one night in 1969. This is quite similar to Fig. 9.4

The magnitudes of the conjugate photoelectron fluxes that are needed to generate the observed 6300Å airglow are calculated below.

9.3 Low Energy (Conjugate) Fluxes

9.3.1 Ionospheric losses

The exact determination of the loss rate of low energy electrons in the ionosphere is complex and it appears no full solution is as yet available. In this section the various loss mechanisms are examined and an approximate solution is obtained. The basic difficulty, as Walker and Rees (1968) point out, is caused by the fact that electron scattering by the ambient plasma is important, not only because of the energy loss involved, but also because it reduces the depth of penetration of the incident electron into the ionosphere. As will be shown the amount of OI airglow generated by electron impact is critically dependent on the height at which the incident energy is lost.

Now because most of the photoelectrons are in the 5 to 15eV range (e.g. Nisbet 1968, Rao and Maier 1970) then ionization losses are ignored.* The other processes involved are:

* The lowest energy thresholds available are 12.1, 13.6 and 15.6 eV which are for the $^2\pi_g$ state of O_2^+, the ^4S state of O^+ and the $^2\Sigma_g$ state of N_2^+ respectively.

(i) Energy loss by ambient electron scattering

The Butler and Buckingham (1962) formula for this mechanism gives the electron loss rate as a function of distance s as:

$$\frac{dE}{ds} = - \frac{5.01 \ 10^{-13}}{(T_e/1000)^{1/2}} \frac{1}{E^{1/2}} F(\varkappa) \log_e n \quad (eV\ cm^{-1}) \qquad 9.4$$

where T_e is the ambient electron temperature, E the electron energy and where

$$F(\varkappa) = \frac{1}{\varkappa} \int_0^{\varkappa} \exp(-x^2)\, dx - 2\exp(-x^2),$$

where $\varkappa = \frac{3.41\ E}{T_e/1000}$

For ionospheric conditions formula 9.4 is usually reduced to the asymptotic forumla:

$$\frac{dE}{ds} = - \frac{1.95 \ 10^{-12}}{E} n \qquad 9.5$$

The equivalent time rate of loss is:

$$\frac{dE}{dt} = 1.16 \ 10^{-4} \ n \ E^{-\frac{1}{2}} \quad (eV\ sec^{-1}) \qquad 9.6$$

Above 300 km this loss mechanism is by far the most significant. This leads to preferential heating of the electrons and thus causes the (observed) high electron temperatures in this region (Evans 1967 a.b.).

(ii) Inelastic collisions with neutrals

Suppose the m th neutral species is initially in the state i and the concentration of this

state is $[i]$. Then if the cross-section for excitation of the j th state by electron collision is $Q_{ij}(v)$, where v is the velocity of the electrons, then the time rate of energy loss is:

$$\left(\frac{dE}{dt}\right)_m = \sum_j v\,[i]\,Q_{ij}\,E_{ij} \qquad 9.7$$

where E_{ij} is the energy required to induce the $i \to j$ transition. For all neutrals the total loss rate by inelastic collisions is:

$$\left(\frac{dE}{dt}\right)_{ie} = \sum_i \sum_j v\,[i]\,Q_{ij}\,E_{ij} \qquad 9.8$$

Of the many possible transitions involving N_2, O_2 and O only the $^3P - {}^2D$ and $^1D - {}^2S$ transitions of O are significant for electrons in the 5 - 15 ev range.

(iii) Other mechanisms

For electrons in the energy range considered, the energy rate of loss by elastic scattering from ions and neutrals is not significant (Dalgarno et al 1963; Nisbet 1968). Of the other processes discussed by Dalgarno et al (1963) only vibrational excitation of N_2 could be significant, and then only for $E < 6$ ev. Even at $E = 6$ ev this process is an order of magnitude weaker than excitation of OI metastable states ((ii) above) and is not considered here.

9.3.2 6300Å photon production

To simplify the problem of evaluating the fraction of the incident photoelectron's energy which is available for $O(^1D)$ production Walker and Rees (1968) considered the ionosphere and atmosphere to be effectively homogeneous above 400 km. For present purposes this method is adopted but the height of homogeneity is lowered. This must be lowered because the ionospheres typical of Hobart (Appendix C) are much less dense than the SAR - arc ionosphere considered by Walker and Rees. The implications of this are that, for the same hmF2, the electrons will penetrate further at Hobart and thus excite more $O(^1D)$. This may be seen by examining the range of a photoelectron with initial energy E_o (at 800 km) which is travelling parallel to the field of declination ; then the range R is given (in km) by:

$$|R| = 10^{-5} \int_o^{E_o} \frac{ds}{\left(\frac{dE}{ds}\right)} \qquad 9.9$$

If the neutrals are ignored then from 9.5 and 9.9

$$R = 10^{-5} \int_o^{E_o} \frac{E}{1.95 \; 10^{-12} n} \, dE \qquad 9.10$$

$$= \frac{2.60 \; 10^6}{n} \; E_o^2$$

where $\bar{n}$ is the mean electron density between 800 km and h_o, the height (km) at which $E \rightarrow 0$. This height is given by:

$$h_o = 1000 - R \sin \phi \qquad 9.11$$

Now $$\bar{n} = \int_{h_o}^{800} \frac{n}{1000 - h_o} \, dh \qquad 9.12$$

From 9.10, 9.11 and 9.12

$$R = \int_{h_o}^{800} n \, dh \; / \; \bar{n} \sin \phi \qquad 9.13$$

$$= 2.60 \times 10^6 \; E_o^2 \; / \; \bar{n}$$

Thus knowing E_o and sin it is then possible to find h_o such that 9.13 is satisfied.

For Walker and Rees' ionosphere equation 9.13 is satisfied for 5 - 15 eV electrons for h_o of about 400 km which is the height of homogeneity they chose. However, for the winter and equinox Appendix C ionospheres and E_o = 15 eV no h_o can be found to satisfy 9.13. This, in the absence of the neutrals, would imply that the 15 eV electrons would pass through the F-region! Of course scattering and neutral losses would prevent this but it has been thus assumed that the electrons penetrate down to 360 km which is near the F-region peak. Accordingly this height is chosen as the onset of homogeneity. Table 9.2 shows the mean (homogeneous) densities of O_2, N_2, O and the mean electron

density for hmF2 = 360 km (assuming the CIRA 1965 model for $\bar{F}_{10.7} = 150$ is appropriate).

Table 9.2.

Species	mean density 360 - 800 km
O_2	$4.23 \quad 10^4$
N_2	$9.74 \quad 10^5$
O	$1.79 \quad 10^7$
e^- (equinox)	$3.08 \quad 10^4$
e^- (winter)	$1.92 \quad 10^4$

Now if the energy loss rate (cm^{-1}) of the electron in producing $O(^1D)$ atoms is $\left(\frac{dE}{ds}\right)_D$ then the amount of energy available for $O(^1D)$ excitation is:

$$E_D = \int_o^{E_o} \left[\left(\frac{dE}{ds}\right)_D \Big/ \left(\frac{dE}{ds}\right) \right] dE \qquad 9.14$$

Where $\left(\frac{dE}{ds}\right)$ is the total loss rate.

For electrons in the energy range considered Q_{pp} is $\approx 1.5 \quad 10^{-17} \quad cm^{-2}$ (see fig. 2.3) and thus from 9.8

$$\left(\frac{dE}{ds}\right)_D = 2.94 \quad 10^{-17} \quad [O]$$

Thus from 9.14 and 9.5

$$E_D \approx \int_o^{E_o} \frac{2.94 \times 10^{-17} \quad [O]}{2.94 \quad 10^{-17}[O] + \frac{1.95 \times 10^{-12}}{E} n} dE$$

i.e. $$= - \frac{\bar{n}}{[\bar{O}]} \quad 6.64 \quad 10^4 \log_e \frac{E_o \quad \bar{O}}{n \quad 6.64 \times 10^4} + 1$$

9.15

where $[\bar{O}]$ is the mean concentration of OI from table 9.2.

Solving 9.15 for the winter and equinox ionospheres, the value of (eV) for various E_o's is given in table 9.3.

Table 9.3

E_o (eV)		5	10	15
E (ev)	Equinox	0.109	0.435	0.982
	Winter	0.175	0.699	1.577

The difference between equinox and winter nights is quite marked. In chapter 8 it was remarked that the few nights near the equinoxes which had 'classical' pre-dawn enhancements had very depleted ionospheres and thus the MCP photoelectrons would excite $O(^1D)$ more efficiently on such nights.

Now the effects of scattering in reducing penetration of the soft electrons has been ignored and the estimates of Table 9.3 are likely to be two or three times too great; thus reducing them by two thirds and taking into account N quenching gives the following estimates of the number of 6300Å photons produced by each electron.

Table 9.4

	E_o	5	10	15
photons/el	Equinox	0.0177	0.0700	0.1581
	Winter	0.0282	0.1124	0.2542

It was found in chapter 8 that about 35R of the terminal IDE appeared to be excited by conjugate point photoelectrons. This would be excited by the following flux of monoenergetic electrons of zero pitch angle.

Table 9.5

Eo (ev)	5	10	15
Equinox	19.75	5.000	2.211
Flux at 800 km (10^8 el cm^{-2} sec^{-1})			
Winter	12.40	3.107	1.372

Of course the actual flux would not be monoenergetic but would have an energy spectrum dependent on the solar zenith angle (Tohomasatu et al 1964; Nisbet 1968; Shawhan et al 1970) but these calculations show that a flux of the order 3×10^8 el cm^{-2} sec^{-1} of 10 eV electrons is required. The total energy flux this implies is very similar to that estimated by Evans (1967 a) to be present on winter mornings at Millstone Hill. To compare these estimates with satellite observations of photoelectron fluxes it is necessary to estimate the exospheric losses of the electrons.

9.3.3 Emitted flux

The estimates of (arriving) fluxes in table 9.5 above must be corrected for exospheric

losses before estimates of the flux actually emitted from the sunlit ionosphere can be made. The correction involves two estimates; firstly losses due to collisions with the exospheric plasma and secondly a reduction in the arrival flux by backscattering, mirroring and possibly electric field repulsion from the dark ionosphere.

Taking the second point first it is easily shown that if the photoelectron flux is emitted isotropically upwards at 300 km at Hobart's conjugate then due to the 0.08 gauss greater magnetic intensity at 300 km at Hobart (Cole and Thomas 1968) then about 10% of this flux is mirrored back to the conjugate from above 800 km at Hobart. Catchpole (1967) has drawn attention to the problem of charge build-up due to photoelectron emission. This would lead to an electric field opposed to the motion of photoelectrons from the sunlit ionspere. Current thinking (Chandra and Stubbe 1970) appears to be that thermal electrons diffuse into the exosphere from the ionosphere to prevent this happening.

Measurements of photoelectron fluxes show they appear to undergo significant backscattering and mirroring (Rao and Maier 1970); perhaps up to 50%

According to Nisbet (1968) the energy degradation of a photoelectron of initial energy E and pitch angle α after travelling distance along a field line is:

$$E = \left[E_0^{\,2} - \frac{3.9 \times 10^{-12}}{\cos \alpha} \int n \, dl \right]^{\frac{1}{2}} \qquad 9.16$$

putting $\int n \, dl = 5 \times 10^{12}$ el cm^{-2} between 800 km heights for $\lambda = 55^{\circ}$ then an electron with $\alpha = 0$ which arrives with energy 5, 10 or 15 eV must have had initially an energy of 6.7, 11.2 or 15.6 eV respectively. Note that low energy and high pitch angle electrons are filtered out in transit.

From these rough estimates it appears that the fluxes of table 9 must be increased by a factor of the order 2 to represent the initial emitted fluxes. These fluxes then agree well with both computed (Fontheim et al 1966, Duboin et al 1969) and observed photoelectron fluxes (Rao and Donely 1969).

9.3.4 F-region height and soft electron degredation

In the previous section it was mentioned that charge neutrality in the dark ionosphere may be preserved by the upward diffusion of electrons into the exosphere. This is in effect an upward ionospheric drift which will lead to some reduction

in dissociative recombination. It is tempting to postulate that this mechanism leads to the observed later down drift onset in winter than summer. However, in view of the inadequate theoretical understanding of this process no estimations are possible of the significance of the mechanism. Also because of the tendency (section 7.2) for onset times of the summer night downward drift to be earlier near the solstice it appears that neutral wind effects are also involved.

A more tractable link between F-region height and soft electron flux is seen in section 9.3.2. That is the number of 6300Å photons produced per recombination depends strongly on the ratio of O to n. Equation 9.15 for the F-region can be approximated well by:

$$E = 0.75 \times 10^{-5} \left[\bar{O} \right] E^2 / \bar{n} \qquad 9.17$$

Clearly from 9.17 more of the photoelectron's energy is available for $O(^1D)$ excitation if the ratio $\left[\bar{O} \right] / \bar{n}$ is high. Thus in the early morning near 0400 LMT in winter, when the ionosphere is depleted and the F-region low, this ratio becomes high compared to the pre-midnight period, say, when the opposite is true. Therefore photoelectrons arriving at dusk do not contribute as much 6300Å production as the same flux arriving

before dawn. To see this more quantitatively consider a flux of 10 eV electrons which penetrate down to hmF2. Using the following mean parameters for winter and equinox 1969 at Hobart then the equation can be solved to give the amount of energy each photoelectron loses to $O(^1D)$ excitation at 0000 EAST and 0500 EAST:

Table 9.7

	$hmF2_1$ (km)	Ne_1 (10^5/el cm^{-3})	$hmF2_2$	Ne_2	E_1 (ev)	E_2
equinox	356	2.512	338	0.714	0.149	0.602
winter	338	0.840	313	1.041	0.704	1.510

where the subscript 1 refers to values at midnight and 2 to values at 0500 LST. In deriving table 9.7 the mean values, $[\bar{O}]$ and $[\bar{N}_2]$, have been evaluated from hmF2 to 800 km and similarly the mean $\bar{n}$ is taken over this range. It should be remembered that the actual E_D's will be less than these estimates by at least half if the effects of scattering are included. However, the trend is clear i.e. photoelectrons are of the order of twice as efficient in exciting $O(^1D)$ after the ionosphere has fallen than before. It is believed that evidence that this is so is given by the all sky charts of the previous chapter In section 8·3·3 it was noted that after the onset of the PDE (i.e. the downward drift of the F-region) then the lines of constant conjugate solar zenith angle (CSZA) were aligned with isophotes some 10R

greater than before the ionospheric fall. This could well be caused by the present mechanism for it was shown in chapter 8 that about 10R of the 6300Å emission at midnight in winter is caused by MCP photoelectrons. Thus after the ionospheric fall the same flux would excite about twice as many $O(^1D)$ atoms as before; i.e. an extra 10R.

It was mentioned in Nichol (1970 b) that there was a tendency for the whole sky to level-off in intensity just before dawn. It was suggested that this could be caused by a cut-off in the emitting mechanism for photoelectrons. Nisbet 1968 proposes that the photoelectron production does actually fall-off for zenith angles less than 90°. This conclusion is supported by the all-sky maps such as figs. 8.6 which show that the levelling-off only occurs for CSZA's less than 90°.

9.4 Summary

It has been shown that the major controlling factor of the pre-dawn enhancement of 6300Å airglow is a postmidnight increase in recombination of O_2^+ believed to be brought about by changes in ionospheric drifts. These F-region drifts are caused by the diurnal temperature variations in the thermosphere leading to neutral atmosphere winds. The effects of magnetic conjugate

point photoelectrons are not very significant until after the ionosphere has fallen. The only exception to this is when the ionosphere is exceptionally depleted, as occurs after magnetic storms. This situation appears to hold over at least the southern part of the 150°E line of longitude (Nichol 1970 b and Shaeffer 1971) and also over North America (Noxon and Johannson 1970). It should also be noted that earlier observations carried out at Camden N.S.W. (Λ = 36°S) by Armstrong (1969) could be explained by the same mechanisms. The midnight summer enhancement noted at Hobart (Nichol 1970a) should be observable at stations with a similar geomagnetic latitude. The situation over Northern Europe is less clear but it appears that few authors there have attempted to compare I(6300) during the PDE with h'f records. The author feels that if this is done a similar picture will emerge to that in Southern Australia and North America.

Finally the latitude cut-off observed by Bennett (1969) and discussed by Cogger and Shepherd (1969), Torr and Torr (1969) and Deehr (1969 b) does not appear from the present work to be an absolute limit. The neutral winds maximise in effect near 45° geographic latitude so increases in I(6300) due to an

ionospheric fall will be smaller at higher latitudes. Besides this there is little change in MCP flux during the night at latitudes where the CSZA is always less than 90^{o}. However, it seems from the Hobart observations that a more critical point is the intensity of the fluctuations of the quasi-permanent auroral zone enhancement which tends to mask out the PDE or MSE in this region.

Chapter 10 CONCLUDING REMARKS

10.1 General

One of the major findings of this thesis is that estimates of dissociative recombination based on generally accepted atmospheric models are too low to explain the observed 6300Å airglow intensities within the midlatitude ionospheric trough (Chapter 5). It is shown how a partial departure from diffusive equilibrium within the trough can largely explain the observed intensities and as well partly explain the formation of the trough; the remainder of the airglow and the lack of maintenance of the trough region are explained by conjugate point photoelectrons. Some contribution, certainly on disturbed days, to the soft electron flux comes from the precipitation of trapped very low-energy Van Allen electrons. It is shown how these processes can cause the trough to move in the way it does (Chapter 6).

Another important finding is the influence of neutral atmosphere winds on 6300Å airglow (Chapter 9). In particular they explain the midnight summer enhancement (Chapter 7) found at Hobart and lower latitudes and partially explain the pre-dawn enhancement (Chapter 8); a phenomenon which has long been puzzling. The remainder of the PDE appears to be due

to conjugate point photo-electrons and a small contribution from downward diffusing exospheric electrons.

10.1 Suggestions for further work

Firstly the findings of chapters 5 and 6 suggest that revised model atmospheres are needed in the region of the trough, particularly for the molecular concentrations. Using the revised model to estimate 6300Å intensities within and equatorwards of the trough provides a simple test for its validity.

Another obvious application of the results of this thesis is in the study of neutral atmosphere winds. Because of the wide field of observation of 6300Å photometers a detailed study of the movement of the midnight summer enhancement, and to a lesser extent the pre-dawn enhancement, should disclose the controlling factors, other than solar heating, on the wind system. Similarly interferometer work along the lines of that carried out by Armstrong (1969) should be extended to the summer for the same reason.

If the conclusions of chapter 6 are correct and the large scale enhancements of I(6300) in the cis-auroral zone are due to Van Allen precipitation then clearly ground based 6300Å

photometers in conjunction with satellite flux measurements will give extensive information on the geomagnetic and other controls on this precipitation.

Acknowledgements

The author wishes to acknowledge the great help and encouragement of his supervisor Prof. G.R.A. Ellis throughout this project.

Also to be thanked is Prof. K.D. Cole for useful discussion at various stages of the project and who first suggested the suitability of Tasmania for red-airglow studies.

The Ionospheric Prediction service kindly lent the ionograms for Hobart and Canberra used in this study.

Dr. M.D. Waterworth designed the lenses used in the photometer.

The author has held a Department of Supply Postgraduate Studentship throughout most of the study.

APPENDIX A

Ionospheric data from the following I.P.S. stations was used in various parts of this thesis:

Station	:	latitude (geographic)	longtitude (geographic)
Port Moresby	:	9° 25'S	147° 9'E
Townsville	:	19° 18'S	146° 44'E
Brisbane	:	27° 32'S	152° 55'E
Woomera	:	30° 48'S	136° 18'E
Salisbury	:	34° 42'S	138° 36'E
Canberra	:	35° 19'S	149° 0'E
Hobart	:	42° 55'S	147° 19'E

APPENDIX B

SYMBOL TABLE

The symbols used in this thesis are defined in the text and a complete list is given here. Some symbols for example α, have different meanings in different chapters. This has been done to follow established nomenclature practice and it should not cause any confusion within the context of each chapter.

A	entry pupil area of photometer
A_λ	Einstein co-efficient
α	angle of solar depression
α	diffusion co-efficient
α	pitch angle
α_i	rate co-efficient
B	Barbier co-efficient
B	magnetic induction
γ_i	rate co-efficient
$\Delta\lambda_o$	bandwidth of filter
δ	solar declination
E	electron energy
E_A	astronomical component of airglow intensity
E_{OH}	hydroxyl component of airglow intensity
$E_{\lambda\ (z)}$	emission rate of line λ at height z
E_{ij}	energy difference between state i and j
e	electron charge

F_{ij}	volume-time rate of i → j transitions
f(v)	velocity distribution
H_M	scale height of species of molecular weight M
h	Planck's constant
h_n	maximum height reached by F-region
h_x	minimum height reached by F-region
I (λ)	measured intensity of line λ
I*(6300)	contribution to I(6300) by electron impact
[i]	concentration of ith species (n_i in chap. 6)
θ	zenith angle
k	Boltzmann's constant
L_i	loss rate of atoms in state i
ℓ	distance along field line
Λ	invarient geomagnetic latitude
λ	wavelength
M_i	molecular weight of ith species
m	electron mass
MUF	M (3000)F2 factor
μ	viscosity co-efficient
N	photon count
Ne	peak electron density
N_ℓ	electron flux at distance ℓ
n	electron density
ν_i, ν_n	collisional frequencies for ions (i) and neutral (n)

P_i	production rate of ith species
p	neutral atmospheric pressure
Q_{ij}	cross-section for $i \rightarrow j$ transition
$Q(\lambda)$	computed intensity of line λ
R	range of electron
R_E	radius of earth
R_z	Zurich sunspot number
ρ	atmospheric density
S_{ij}	rate co-efficient of $i \rightarrow j$ transition
$S(\lambda)$	intensity of standard source
T_e	electron temperature
$T_i(\lambda)$	transmissivity
T_n	neutral temperature
T_∞	exospheric (neutral) temperature
T_o	minimum T_∞
τ	solar hour angle
ϕ	geographic latitude
ϕ	magnetic declination
V	voltage output
$\underline{v}(i)$	velocity of ith species
Z	Van Rhijn co-efficient
z	height above ground
Ω	solid angle of view
Ω_{ij}	collision strength

APPENDIX C

The following ionospheres are computed using Titheridge's (1967) overlapping polynomial method from early morning quiet period ionograms. The topside extension is from Evans's (1967a) measurements at Millstone Hill. It is assumed that the shapes of the ionospheres do not change with any rise or fall in h'f. The decay is assumed to be that of Chapman α - layer

(10^4 el cm^{-3})

height (KM)	electron density summer	equinox	winter
200	0.03	0.02	0.02
240	1.31	0.93	0.79
280	10.42	7.62	4.93
320	11.37	8.05	5.27
360	10.03	6.80	4.60
400	7.88	4.98	3.79
440	5.56	3.23	2.87
480	3.97	1.84	1.92
520	2.51	1.18	1.32
560	1.77	0.96	1.11
600	1.02	0.70	0.87

REFERENCES

C. W. Allen, J. Atmos. Terr. Phys., 4, 53, 1953

S. -I. Akasofu, J. Atmos. Terr. Phys., 19, 19. 1960

A. J. Angstrom, Pogg. Ann. 137, 161, 1869

Z. A. Anzari, J. Atmos. Terr. Phys., 25, 210, 1963

P. R. Arendt & H. Soicher, Nature, 204, 983, 1964

E. B. Armstrong, Planet Space Sci., 17, 957, 1969

P. M. Banks & A. F. Nagy,
J. Geophys. Res., 75, 1902, 1970

D. Barbier, Ann. Geophys., 15, 179, 1959

D. Barbier, Ann. Geophys., 17, 3. 1961

D. Barbier, p. 401 in Res. in Geophysics. I,
ed. Odishaw, MIT, 1964

D. Barbier, F. E. Roach, & T. R. Steiger,
J. Res., 660, 145, 1962

D. Barbier & J. Glaume,
Planet. Space Sci., 9, 133, 1962

Barish & Wiley 1970

D. R. Bates & H. S. W. Massey,
Proce. Roy. Soc. A187, 216, 1946

W. Bellew & S. Silverman,
Planet Space Sci., 14, 407, 1966

W. H. Bellchambers, D. W. Barclay
and. W. R. Piggot,
Ionospheric Obs. R. Soc. IGY
Expedition Halley Bay II p. 179 1962

R. T. Bennet, J. Geophys. Res., 74, 381, 1969

P. J. Bowen, R. L. F. Boyd, W. J. Raitt
& A. P. Wilmore,
Proc. Roy. Soc. A281, 504, 1964

G. C. Bowman, Planet Space Sci., 17, 777, 1969

L. H. Brace & B. M. Reddy,
J. Geophys. Res., 70, 5793, 1965

L. H. Brace, B. M. Reddy
& H. G. Mayr,
J. Geophys. Res. 72, 265, 1967

J. L. Burch, J. Geophys. Res., 73, 3585, 1968

S. T. Butler, & A.D.Buckingham, Phys. Rev., 126, 1, 1962

H. C. Carlson, J.Geophys, Res., 71, 195, 1966

H. C. Carlson & G.M.Weill, Ann. Geophys., 23, 269, 1967

E. H. Carmen & B.P.Kilfoyle, J. Geophys. Res., 68, 5605, 1964

D.L.Carpenter, J.Geophys, Res., 71, 693, 1966

J.R.Catchpole, J.Atmos. Terr.Phys., 29, 819, 1967

R.A.Challinor, Planet. Space Sci., 17, 1097, 1969

J.W.Chamberlain, Physics of the Aurora & Airglow Academic Press, 1961

J.W.Chamberlain & C.A.Smith, J. Geophys. Res., 64, 611, 1959

K.L.Chan & L.Colin, Proc. IEEE, 57, 990, 1969

S.Chandra, B.E.Troy, J.L.Donley & R.E. Bourdeau; J. Geophys. Res., 75, 3867, 1970

C.I.R.A. Cospar Reference Atmospheres, 1965

S.Chapman, Proc. Phys. Soc. (London) 43, 26, 1931

K.D.Cole, J. Geophys. Res., 70, 1689, 1965

K.D.Cole, Ann. Geophys., 21, 156, 1965

K.D.Cole, Ann. Geophys, 26, 187, 1970

K.D.Cole, J. Geophys. Res., 75, 4216, 1970

K.D.Cole, & J.Thomas, Planet, Space Sci, 16, 1357, 1968

L.L.Cogger & G.G.Shepherd, Planet, Space Sci., 17, 1857, 1969

L.P.Cox & J.V.Evans, J. Geophys. Res., 75, 627, 1970

A.Dalgarno, M.B.McElroy & R.J. Moffet, Planet, Space Sci., 11, 463, 1963

A.Dalgarno,M.B.McElroy & J.C.G.Walker, Planet. Space Sci., 1967

A.Dalgarno & T.C.Deggers, Planet. Space Sci., 16, 125, 1968

A.Dalgarno & J.C.G.Walker, J. Atmos. Sci., 21, 463, 1964

S.Deb J. Atmos. Terr. Phys., 4, 28, 1953

C.S.Deehr, Ann. Geophys., 25, 881, 1969

C.S.Deehr, Ann. Geophys., 25, 867, 1969

A.Delsemme & D.Delsemme, Ann. Geophys., 16, 507, 1960

W.B.DeMore & O.F.Roper, Astrophys. J., 139, 1381, 1964

T.M.Donahue, Planet. Space Sci., 14, 33, 1965

M.L.Duboin, G.Lejeune, M.Petit & G.Weill; J. Atmos. Terr. Phys., 30, 299, 1968

J. Dufoy & Tcheng Mao-Lin, Ann. Geophys., 2, 189, 1946

R.A.Duncan, J. Geophys. Res., 67, 1823, 1962

R.A.Duncan & G.R.Ellis, Nature, 183, 1618, 1959

R.B.Dunn & E.R.Monring, J. Opt. Soc. Am., 45, 899, 1955

R.H.Eather, J. Geophys. Res., 74, 153, 1969

R.H.Eather & F.Jacka, Aust. J. Physics, 241, 1966

C.T.Elvey & A.H. Farnsworth, Astrophys. J, 96, 451, 1942

G.R.A. Ellis, Planet. Space Sci., 1, 253, 1959

G.R.A. Ellis & P.A.Hamilton, Astrophys. J, 143, 227, 1966

J.V.Evans, J. Geophys. Res., 70, 4331, 1965(a)

J.V.Evans, J. Geophys. Res., 70, 4365, 1965(b)

J.V.Evans, Planet. Space Sci., 15, 1387, 1967(a)

J.V.Evans, Planet, Space Sci., 15, 1557, 1967(b)

J.V.Evans & I.J.Gastman, J. Geophys. Res., 75, 807, 1970

I. Filosofo,J.A.Greenspan & C.M.Groom, Appl. Optics 4, 215, 1965

J.A.Findlay,P.L.Dyson,L.H.Brace,A.J.Z.Muda, & W.E.Radford, J. Geophys. Res., 74, 3705, 1970

E.G.Fontheim,A.E.Beutler & A.F.Nagy, Ann. Geophys., 24, 489, 1968

R.L.Gattinger, Ann. Geophys., 25, 825, 1969

R.H.Garstang, Month. Not. Roy. Astro. Soc., 111, 115, 1951

J.E.Geisler, J. Atmos. Terr. Phys., 28, 703, 1966

J.E.Geisler, J. Atmos. Terr. Phys., 29, 1469, 1967

J.E.Geisler & S.A.Bowhill, J. Geophys. Res., 70, 4365, 1965

W.B. Hanson, Space Research III North - Holland 173, 1963

W.B. Hanson & F.J.Johnson, Mem. Soc. R. Sci., Liege 4, 390, 1961

I. Harris & W. Priester, J. Atmos. Sci., 19, 4, 1962

W.J.Heikla, Nature, 225, 369, 1970

J.R.Herman & S.Chandra, Planet. Space Sci., 17, 815, 1969

W.N.Hess, in The Radiation Belt and Magnetosphere, Blaisdell, 1968

B.G.Hunt, J. Geophys. Res., 71, 1385, 1966

D.M.Hunten, A.Vallance Jones, C.D. Ellyett & E.C. McLauchlan, J. Atmos. Terr. Phys., 26, 67, 1964

I.P.S. of Australia, Series D, 1965 - 1970

I.P.S. of Australia, Series H, 1969

L.G. Jacchia, Smithsonian Astrophys. Obs. Spec. Rept. 170, 1964

L.G. Jacchia, Space Res. V, 1152, 1965

L.G. Jacchia & J.Slowey, Smithsonian Astrophys. Obs. Spec. Rept. 242, 1967

H.Kamiyama, J. Geomagnet. Geoelec., 14, 58, 1962

T.V.Kazachvskaya & A.I.Koryagin, Cosmic Res., 7, 855, 1969

G.A.M.King, J. Atmos. Terr. Phys., 32, 209, 1970.

J.W.King, H.Kohl & R.Pratt, J. Atmos. Terr. Phys., 29, 1045, 1967

D.G.King-Hele, Planet. Space Sci., 11, 261, 1963

W.C.Knudsen, J. Geophys. Res., 73, 841, 1968

W.C.Knudsen, J. Geophys. Res., 73, 6384, 1968

H.Kohl & J.W.King, J. Atmos. Terr. Phys., 29, 1045, 1967

L. Liszka, J. Atmos. Terr. Phys., 29, 1243, 1967

K.K-Mahajan & L.H.Brace, J. Geophys, Res., 74, 5099, 1969

F. Mariani, J. Geophys. Res., 69, 556, 1964

D.F.Martyn, J. Geophys. Res., 64, 2178, 1959

B.R.May, Planet. Space Sci., 11, 1273, 1963

B.R.May, Planet, Space Sci., 12, 1179, 1964

D.B.Muldrew, J. Geophys. Res., 70, 2635, 1965

Nagy & Banks 1970

A.F.Nagy & J.C.G.Walker, Planet. Space. Sci., 15, 95, 1967

A.F.Nagy, E.G.Fontheim, R.S.Slolarski & A.E.Beutler, J. Geophys. Res., 74, 4667, 1969

K.V.S.K. Nathen & M.J.Seaton, Nature, 209, 1966

G.L.Nehms, Space Res., IV 437,1964

G.P.Newton, J. Geophys. Res., 75, 5510,1970

G.P.Newton & D.T.Pelz, J. Geophys. Res., 74, 4169,1969

G.P.Newton,D.T.Pelz & H. Volland, J. Geophys. Res., 74, 183, 1969

D.G.Nichol, Aust. J. of Phys, 23, 109, 1970(a)

D.G.Nichol, Planet. Space Sci., 18,1335, 1970(b)

D.G.Nichol, Nature, 229, 13, 1971(a)

D.G.Nichol, Planet, Space Sci., in press 1971(b)

M. Nicolet, Smithsonian Astrophys. Obs. Spec. Rep. 75, 1962

J.S.Nisbet, J. Atmos. Terr. Phys. 30, 1257, 1968

J.F. Noxon, J. Chem. Phys., 52, 1852, 1970

J.F.Noxon & A.E.Johanson, Planet. Space Sci., 18, 1367, 1970

B.J.O'Brien, J. Geophys. Res., 69, 13, 1964

B.J.O'Brien, in Radiation Trapped in the Earth's Magnetic Field., p.321f, (ed. Mc Cormac), D. Reidel 1966

S.R.Pal & P.V.Kulkarni, Ann. Geophys., 24, 399, 1968

V.L.Peterson, Ann. Geophys., 24, 101, 1968

V.L.Peterson & T.E.Van Zandt, Planet. Space Sci., 17, 1725, 1969

V.L.Peterson & W.R.Steiger, J. Geophys.Res., 71, 2267, 1966

V.L.Peterson, T.E.Van Zandt & R.B.Norton, J. Geophys. Res., 71, 2255, 1965

H.K.Paetzold & H.Zschorner, Space Research II, 958, 1961

B.C.Rao & J.L.Donley, J. Geophys. Res., 74, 1715, 1969

B.C.Rao & E.J.Maier, J. Geophys. Res., 75, 816, 1970

B.C.Rao & Maier, J. Geophys. Res., 75, 816, 1970

R.G.Rastogi, J. Geophys. Res., 65, 585, 1960

J.A.Ratcliffe & K.Weekes, Physics of the Upper Atmosphere, pp.377, Academic Press, 1960

J.A.Ratcliffe, J. Atmos. Terr. Phys. 8, 260, 1956

C.A.Reber & M.Nicolet, Planet. Space Sci., 13, 617, 1965

M.H.Rees, Space Sci., Rev., 10, 413, 1969

H.Rishbeth, J.Atmos. Terr. Phys. 29, 225, 1967

F.E.Roach & A.B.Meinel, Astrophys. J., 122, 530, 1955

C.S.Roberts, 403, Radiation Trapped in the Earth's Magnetic Field, D. Reidel, 1966

B.P.Sandford, J. Atmos. Terr. Phys., 26, 749, 1964

B.P.Sandford, J. Atmos. Terr. Phys., 30, 1921, 1968

M.A.Shield & L.A.Frank, Univ. of Iowa Rep. 69 - 46, 1969

R.C.Schaeffer, submitted to J. Atmos. Terr. Phys., 1971

M.J.Seaton, Proc. Roy. Soc (London) A218, 400, 1953

M.J.Seaton, in The Airglow & Aurora Pergamon Press, 1955

M.J.Seaton, Astrophys. J., 127, 67, 1958

G.P. Serbu, Space Research V 564, 1965

G.P. Serbu & E.J.R.Maier, J. Geophys. Res., 71, 3755, 1966

G.P. Serbu & Maier, NASA Report T M - x -6381, 1970

S.D. Shawhan,L.P.Block & G.C.Falthammer, J. Atmos. Terr. Phys., 32, 1885, 1970

G.W.Sharp, J. Geophy. Res., 71, 1345, 1966

T. Shimazaki, J. Radio Res. Lab. Japan, 2, 85, 1955

Silverman & Carversle, J. Geophys, Res., 66, 323, 1961

R.W.Smith, Planet. Space Sci., 17, 879, 1969

K.Smith, B.J.W.Henry & P.G.Burke, Phys, Rev., 147, 21, 1966

K.Smith, B.J.W.Henry & P.G.Burke, Phys, Rev., 157, 51, 1967

G.W.Stanley, J. Geophys. Res., 71, 1345, 1966

A.I.Stewart, PhD Thesis, Queen's Univ.Belfast, 1965

A.I.Stewart, J.Geophys. Res., December, 1970

P.Stubbe & S.Chandra, J.Atmos.Terr. Phys., 32, 1909, 1970

H.A.Taylor,H.C.Brinton&M.W.Pharo, J. Geophys. Res., 73, 961, 1968

T.T.Tomatsu, T.Ogawa & H.Tsuruta, Rep. Ionosph. Space Res. Japan, 19, 482, 1965

J.O. Thomas, M.J.Rycroft,L.Colin & K.L.Chan in Electron Density Profiles in Ionosphere and Exosphere, North - Holland, 1966

J.O.Thomas & A.Y. Sadar, J. Geophys. Res., 69, 4561, 1964

J.E.Titheridge, J. Atmos. Terr. Phys., 30, 1843, 1968(a)

J.E.Titheridge, J. Atmos. Terr. Phys., 30, 1857, 1968(b)

J.E.Titheridge, J. Radio Res., N B S D, 1967

M.R. Torr, Nature, 223, 282, 1969

M.R. Torr & D.G.Torr, J.Geophys. Res., 74, 5187, 1969

D.G. Torr & M.R.Torr, J. Atmos. Terr. Phys., 32, 15, 1970

J.A.Van Allen, C.E.McIlwain & G.H.Ludwig, J. Geophys. Res., 64, 271, 1959

P.J.Van Rhijn, Astrophys. J., 50, 356, 1919

G.Vasseur, J. Atmos. Terr. Phys., 32, 775, 1970

L.Wallace & J.W.Chamberlain, Planet. Space Sci., 2, 60, 1959

J.C.G. Walker & M.H.Rees, Planet Space Sci., 16, 459, 1968

A.P.Willmore, Proc. Roy. Soc., A281, 526, 1964

J.W.Wright, J. Geophys. Res., 65, 185, 1960

J.W.Wright & R.E.McDuffie, J. Radio Res. Lab. Japan 7, 409, 1960

F. Zollner, Pogg. Ann., 141, 574, 1870

These articles have been removed for copyright or proprietary reasons.

Nichol, D.G. 1971. Excitation of 6300Å (OI) airglow by soft electron fluxes, Nature physical science, 229, 13-14.

Nichol, D.G. 1970. A summer-time midnight enchantment of 6300Å airglow, Australian journal of physics, 1970 23, 109-110.

Nichol, D.G. 1970. The pre-dawn enchantment of λ6300Å airglow at higher midlatitudes,Planetary and Space Science, 18, 1335-1347